AD_____

AWARD NUMBER: DAMD17-99-1-9571

TITLE: Molecular Mechanisms of Soft Tissue Regeneration and Bone Formation in Mice: Implications in Fracture Repair and Wound Healing in Humans

PRINCIPAL INVESTIGATOR: Subburaman Mohan, Ph.D.

CONTRACTING ORGANIZATION: Loma Linda Veterans Association for
Research and Education
Loma Linda, California 92357

REPORT DATE: April 2006

TYPE OF REPORT: Annual

PREPARED FOR: U.S. Army Medical Research and Materiel Command
Fort Detrick, Maryland 21702-5012

REPORT DOCUMENTATION PAGE

Form Approved
OMB No. 0704-0188

1. REPORT DATE *(DD-MM-YYYY)*	**2. REPORT TYPE**	**3. DATES COVERED** *(From - To)*
01-04-2006	Annual	1 Oct 2004 – 14 Mar 2006

4. TITLE AND SUBTITLE

Molecular Mechanisms of Soft Tissue Regeneration and Bone Formation in Mice: Implications in Fracture Repair and Wound Healing in Humans

5a. CONTRACT NUMBER

5b. GRANT NUMBER
DAMD17-99-1-9571

5c. PROGRAM ELEMENT NUMBER

6. AUTHOR(S)

Subburaman Mohan, Ph.D.

E-Mail: subburaman.mohan@med.va.gov

5d. PROJECT NUMBER

5e. TASK NUMBER

5f. WORK UNIT NUMBER

7. PERFORMING ORGANIZATION NAME(S) AND ADDRESS(ES)

Loma Linda Veterans Association for
Research and Education
Loma Linda, California 92357

8. PERFORMING ORGANIZATION REPORT NUMBER

9. SPONSORING / MONITORING AGENCY NAME(S) AND ADDRESS(ES)
U.S. Army Medical Research and Materiel Command
Fort Detrick, Maryland 21702-5012

10. SPONSOR/MONITOR'S ACRONYM(S)

11. SPONSOR/MONITOR'S REPORT NUMBER(S)

12. DISTRIBUTION / AVAILABILITY STATEMENT
Approved for Public Release; Distribution Unlimited

13. SUPPLEMENTARY NOTES

14. ABSTRACT

The primary goal of the proposed work is to identify genes which play an anabolic role in bone and soft tissue function and to clarify the function of these genes. Three hypotheses have been proposed: 1) The high bone density gene in chromosome 1 in our CAST/B6 congenic mice can be cloned; 2) Genes that regulate soft- and hard-tissue regeneration can be identified by using appropriate mouse strains that exhibit differences in regeneration; and 3) ENU mutagenesis, applied to our mouse model, will lead to the identity of genes that regulate soft and hard tissue function. During the last funding period, we have proposed several specific objectives for each of the above-mentioned hypotheses. As disclosed in the progress report, we have successfully accomplished all of the specific objectives. Our work during the first year of the funding period has resulted in two manuscripts in press, two published manuscripts, and three abstracts. We believe that the successful accomplishment of the proposed studies will provide a better understanding of the molecular mechanisms involved in hard- and soft-tissue regeneration and will provide a framework for future development of therapies for hard and soft tissue injuries.

15. SUBJECT TERMS
Soft- and hard-tissue regeneration; bone density; gene function; cDNA microarray analysis; congenic mice; QTL analysis; mouse genetics; musculoskeletal genes

16. SECURITY CLASSIFICATION OF:			**17. LIMITATION OF ABSTRACT**	**18. NUMBER OF PAGES**	**19a. NAME OF RESPONSIBLE PERSON**
a. REPORT	**b. ABSTRACT**	**c. THIS PAGE**			**19b. TELEPHONE NUMBER** *(include area code)*
U	U	U	UU	251	USAMRMC

Standard Form 298 (Rev. 8-98)
Prescribed by ANSI Std. Z39.18

Table of Contents

I. General Introduction

The primary goal of the project funded by the U.S. Army is to identify genes which play an anabolic role in bone tissue and soft tissue function, particularly during regeneration, and to clarify the function of these genes. To accomplish this goal, we have proposed 3 technical objectives during the funding period. These 3 Technical Objectives are as follows:

A. Technical Objective 1:

Studies proposed in the first technical objective are designed to employ state-of-the-art molecular biotechniques to identify the gene located in mouse chromosome 1 that is involved in the regulation of peak bone density.

B. Technical Objective 2:

Our second technical objective has been focused on identifying the key genes that are involved in soft tissue repair/regeneration using inbred strains of mice as model systems.

C. Technical Objective 3:

The goal of our third technical objective is to identify and characterize novel genes, using ENU mutagenesis techniques and to elucidate the function of known genes that play a key role in the metabolism of bone and soft tissue.

Our progress for each of the technical objectives is described below. The progress report for each technical objective is organized according to the outline provided by the office of the U.S. Army Medical Research and Material Command.

II. Technical Objectives

TECHNICAL OBJECTIVE 1: TO CLONE THE GENE REGULATING PEAK BONE DENSITY ON CHROMOSOME 1 IN THE CAST/B6 CONGENIC MICE.

Introduction

Our long-term goal in this study is to identify the genes involved in the acquisition of peak bone density and evaluate the functions of those genes. Such genes are particularly relevant to determine both one's risk of fractures resulting from battlefield injury and to corresponding gene therapy treatment for such fractures.

In our studies on the identification of candidate genes regulating peak bone density, we focused on a quantitative trait locus (QTL) that contributes significantly to high bone density on mouse chromosome 1 (Chr. 1) from a cross between C57BL/6J (B6) and CAST/EiJ (CAST) mouse strains. We chose the chromosome 1 QTL for our studies based on the following rationale:

1) It contributes to approximately 40% of the total variation of femur volumetric bone mineral density (vBMD) between CAST and B6 mice;

2) It has a LOD (logarithm of the odds) score of 8, which is the statistically strongest QTL identified from B6 X CAST cross; and

3) It is located in a region syntenic with that of human chromosome 1q21-q23, which has been implicated in peak bone density regulation in humans (Koller et al., 2000 and Ralston, 2002)

B6-Cast congenic mouse lines were generated by transferring CAST Chr. 1 alleles (donor) into the B6 strain (recipient) to confirm the contribution of Chr. 1 QTL on vBMD variation. We found that the bone density of B6-CAST congenic mice containing Chr. 1 QTL from CAST mice was significantly higher than that of B6 mice, confirming that the CAST Chr. 1 QTL contains gene/s that contribute to high bone density in B6 mice (previous report).

In order to further narrow down the size of the Chr. 1 QTL (25cM) to a more manageable size for the screen of candidate genes, we have produced several subcongenic lines containing smaller pieces of the CAST Chr. 1 QTL in B6 mice. Our subcongenic approach not only confirmed the biological activity of the QTL gene in this region, but also further narrowed the size of the QTL within Chr. 1 from 25 cM to approximately 7 cM. If this mouse QTL is homologous to the human QTL on Chr. 1q21-1q25, it follows that the QTL region could be within 2 cM, a size feasible for our proposed studies to identify candidate genes by the various approaches proposed below.

To achieve the goal of identifying the candidate gene in Chr. 1 involved in bone density regulation, we have designed state-of art molecular techniques, which include differences in gene expression, sequence polymorphism, presence of functional motif consistent with bone formation or resorption action in candidate genes, and *in vitro* functional testing of candidate genes.

Our specific objectives during the first 12 months of this continuation grant period are as follows:

Specific objective 1. To prepare more subcongenic mice. We have the sub-congenic mice that carry the 10-15 cM segment from Cast chromosome 1.

In order to identify candidate genes, we will have to shorten the cast segment transferred in the B6 mouse. For this end, we need to cross back this sub-congenic with the wild type B6. The first progeny would be all heterozygotes. The heterozygote animals will then be crossed again with the B6 mice. In theory, the frequency of recombination within a 10cM segment is 10%; every animal from the 10% may produce a different site of recombination. The first generation will be heterozygote for every recombination. Therefore, in order to get homozygotes for 5 recombinations, we need to get one pair for every recombination. The probability of getting one female and one male with the same recombination is 0.5%. This means that if we want to get one pair of mice per recombination, for a total of 5 recombinations, we require a population of up to 2,000 mice.

Specific objective 2. To produce up to 3,000 CAST B6 F2 mice for fine mapping.

Recent studies support this strategy that using larger numbers of F2 mice along with newly available microsatellite markers and SNP markers can lead to the successful fine mapping of the QTL down to approximately 1 cM.

Specific objective 3. If the likely candidate gene is a bone formation gene, we will establish an *in vitro* assay using osteoblast line cells as a model and proliferation, differentiation, or apoptosis as end points.

If the likely candidate gene is a bone resorption gene rather than a bone formation gene, we will establish an *in vitro* assay using a pre-osteoclastic cell line, namely the RAW264.7 cells, as a model and formation and activity of osteoclasts as end points. It may be necessary for us in our functional studies to evaluate osteoclasts derived from CAST mice *in vitro*. If so, we will develop this assay using CAST mouse marrow cells stimulated with RANK ligand and test for osteoclast number by TRAP (Tartrate Resistant Acid Phosphatase) staining. These cells would then be used to evaluate the functional assays described below.

Specific objective 4. To test several candidate genes within the QTL region of the mouse chr. 1 in one or more of our functional assays.

In one such functional assay, the candidate genes in BAC clone are inserted into a viral expression vector to be used for evaluating the effect of these candidate genes on osteoblast line cells.

Specific objective 5. To develop a second functional assay, namely the siRNA technique, which, in many instances, is superior to the antisense technique, as a further functional assay to inhibit gene function.

In this siRNA procedure, we will be knocking out a candidate gene and then observing the *in vitro* phenotype as a consequence

Specific objective 6. To sequence candidate genes identified by fine mapping and or functional assays, such as the BAC clone assay and the siRNA assay and the gene knock-in assay.

Specific objective 7. To begin performing fine mapping of chromosome 17 BMD QTL identified in the MRL/SJL cross which also contributes to the bone strength phenotype.

This will be accomplished by eventually performing phenotype and genotype analysis in approximately 2000 MRL/SJL F2 mice.

Body

Our progress during the last 12 months of this grant period for the specific objectives 1 to 7 is provided below

Specific Objective 1.

Generation of subcongenic line of mice

To prepare additional subcongenic line of mice we have used B6.CAST-1D1mit370-D1mit152, designated as C168-185. For all subcongenic lines, we have used a "C" letter referring to the cast allele, followed by the position (in megabases) of the two markers flanking the donated CAST segment. This congenic line carried the CAST chromosomal region which covered 88.3-101 cM in chromosome 1, the equivalent to 168-185 Mb according to the NCBI database. Additional crosses between the congenic and the B6 progenitor produced new recombinations carrying smaller overlapping segments that were fixed in the four congenic sublines reported herein (**Figure 1**). Each subline was genotyped using the polymorphic markers (Table 1) that encompass the 168-185 Mb region. Databases used to identify the polymorphic markers included the Mouse Genome Informatic database (http://www.informatics.jax.org/) and the NCBI database (www.ncbi.nlm.nih.gov). Twenty-three markers were found in the Jackson mouse database, while two markers were identified by screening CT-repeated sequences within the QTL region through the NCBI database. Then, the primers flanking the dinucleotide repeat sequences were designed and used for PCR analyses. Polymorphism was determined by checking the size differences of the repeated sequences between the B6 and CAST mice.

Primers newly designed in this study:

Mg4718-F: 5'-GCA TTT TGA TCC CTT ATA ATA CA-3'
Mg4718-R: 5'-GTG GAA GAC CCT TGA ATG G-3'
Mg4723-F: 5'-GCA TAG CCA ACA AAA GAA ATC TAA TG-3'
Mg4723-R: 5'-GCA GTG TAG CTC AGT GGT AGA TCA C-3'

After each cross, the progenies were genotyped as follows. Extraction of genomic DNA from tail snips was performed following the Gentra PurGene protocol (PUREGENE Tissue kit,

Par#D-7000A). Genotyping of individual mouse DNA was accomplished using two methods: 1) We amplified genomic regions of interest by polymerase chain reaction (PCR) using oligonucleotide primer pairs from Integrated DNA Technologies (Coralville, IA, USA). PCR products were separated by electrophoreses on 20-cm polyacrylamide gels, stained with ethidium bromide, and photographed under UV light. Photographs were scored twice and ambiguous genotypes were reamplified. 2) We also used fluorescently end-labeled primers to amplify genomic regions of interest. Using labeled primers, the sizes of the fluorescently-labeled PCR products were directly determined by the ABI PRISM 377 GeneScan Analyzer. PCR products from B6, CAST and their F1 hybrids were used as standards to identify the mouse genotypes.

In order to narrow down the size of the BMD QTLs in chromosome 1,we have generated more subcongenic lines of mice by further backcrossing C168-185 several times with the B6 control mice; we generated three more subcongenic lines of mice: C168-176, C175-185 and C178-185 (**Figure 1**). Genotyping as well as phenotypic analyses were performed as described above.

Phenotypic characterization

Based on data from previous studies (Beamer et al., 1999) that showed rapid acquisition of vBMD peaked at approximately 16 weeks, resulting in significant higher vBMD values in the CAST females compared to the B6 females, we chose this time point as the age at which to measure our phenotypes. We analyzed 8-13 female mice from the B6 line and from each congenic subline at 16 weeks of age. Body weights were recorded at necropsy. Bones collected were stored in 1 x PBS buffer supplemented with 0.05% sodium azide. Their lengths were measured with digital calipers (Stoelting, Wood Dale, IL, USA). Then, isolated femurs were assessed using the peripheral quantitative computed tomography (pQCT) system from Stratec XCT-RESEARCH (Norland Medical System, Fort Atkinson, WI, USA), operating at a resolution of 0.07 mm. The bone scans were analyzed with an outer threshold of 630 mg/cm^3 to determine bone area/total volume. This threshold was selected to yield values for total bone areas that are consistent with bone histomorphometric derived values. A second analysis was carried out with a threshold set at 230 mg/cm^3 to determine mineral content. Isolated femurs were scanned at nine locations symmetrically located around the midpoint, 11% of the femur length apart and covering the entire length. The vBMD was calculated by dividing total mineral content by the associated total volume. Femur vBMD as well as periosteal circumference, endosteal circumference, and cortical thickness were evaluated at the mid-diaphysis region of the femurs (average of slices 4 and 5). Analyses of the scans were performed using manufacturer-supplied software program (Stratec Medizintechnik GMBH Bone Density Software, version 5.40C). The sublines of mice that were genetically homozygous cast/cast at chromosome 1 segments were homozygous for B6 at more than 99% of the remaining genome (Shultz et al., 2003). Therefore, femoral vBMD variations observed within congenic sublines generated in this study were attributed to a CAST donated segment.

Femur vBMD and other related bone parameters were evaluated at the mid-diaphysis region of the femur using pQCT for the four congenic sublines newly generated as well as for the parental C168-185 subline and for two other subcongenic lines previously identified, along with age- and gender-matched B6. **Figure 2** shows the relative change in various phenotypes introduced by CAST donated regions compared with B6 control mice. All the sublines, which carried overlapping CAST segments from the region 100-185 Mb of the centromere, exhibited a significantly greater vBMD compared to the B6 mice, except subline C168-172 (**Figure 2A**).

The vBMD change for various subcongenic lines were +12.0% for C100-169, +5.0% for C133-165, +9.0% for C168-185, +8.6% for C169-185, +6.3% for C168-179, and +10.6% for C172-185. When these data are superimposed on the genetic map shown in **Figure 1**, there is evidence for the presence of two separates genetic loci that control the vBMD variation; one located within 133-165 Mb (BMD1-1), and the second located within 172-179 Mb (BMD1-2).

Because CAST progenitor mice are considerably smaller than the B6 mice (-64% compared to B6 mice, data not shown), we evaluated the body weights of these congenic sublines to determine if a body weight phenotype co-segregates with mid-diaphyseal vBMD. **Figure 2B** shows that sublines carrying cast alleles from the BMD1-1 locus exhibited significantly smaller body weight compared to B6 (6-9%), while sublines which covered the BMD1-2 locus exhibited significantly greater body weight compared to B6 mice (6-8%), except the C172-185 subline, which didn't show any difference with B6 control mice. Furthermore, overall correlation (**Table 2**) between body weight and vBMD among the 7 sublines was positive ($r=+0.5$; $p=0.12$), but did not reach statistical significance. Moreover, the adjustment for body weight or femur length did not affect the significance of femoral vBMD change. This provided evidence that body weight is not responsible for the vBMD variation introduced by CAST donated segments. **Fig. 2B** shows that there were no significant changes in femur length among the seven sublines.

Other bone parameters such as endosteal circumference (EC), periosteal circumference (PC), and cortical thickness (CT), were analyzed to determine if other phenotypes co-segregated with the vBMD phenotype or could account for the changes in femoral vBMD. The two sublines which carried cast alleles underlying BMD1-1 locus as well as two sublines from BMD1-2 locus (C168-179 and C172-185) showed significantly smaller EC compared to B6 control mice (**Figure 2C**); EC from C100-169 and C133-165 were 7% and 2.2% smaller than B6 mice, respectively, and EC from C168-179 and C172-185 were 2.5 and 4% smaller than B6 control mice, respectively. No significant difference in EC was found in sublines C168-185, and C169-185 but after adjustment for body weight and femur length, their EC became significantly different than B6 mice, Among the seven subcongenic lines, there was a significant negative correlation between the changes of vBMD and EC ($r=-0.67$, $p=0.024$).

With respect to PC, the sublines C168-185, and C169-185 showed significantly greater PC (3-4%, **Figure 2C**). However, after adjustment for body weight and femur length, they lost the significant difference with B6 control mice. While subline C168-172 showed significantly smaller PC and EC compared to B6 control mice, the significance was lost after adjustment for body weight and femur length, which suggests the presence of a genetic locus associated with body weight and bone size at 168-172 Mb from the centromere.

A change in vBMD can be explained on the basis of change in CT and/or material BMD. In our study, sublines showing a higher vBMD exhibited significantly greater CT compared to the B6 mice (4-9%) (**Fig. 2C**) and, when tested for correlation, a strong correlation was found between vBMD change and CT among the seven sublines ($r=0.97$; $p=0.0001$) (**Table 2**). Thus, a change in cortical thickness, rather than cortical material density properties, appears to mainly drive the QTL changes in vBMD observed in our congenic sublines.

For the three new sublines of mice, the effect of the CAST-donated region was to increase femur BMD (**Figure 3A**). The C168-176 subline showed an 8% increase of femur vBMD compared to the B6 control mice, while the C175-185 and C178-185 exhibited a 6% increase of vBMD compared to control mice. Therefore, by superimposing the CAST chromosomal regions carried by the new subline C168-176 with the C168-172, which doesn't

show any significant difference of BMD with the B6 control mice, we eliminated the genes in the region 168-172. We then narrowed down the BMD1-2 to 172-176 Mb. Furthermore, the fact that the C175-185 and C178-185 showed significant differences with B6 control mice provided evidence for the presence of a third BMD locus at 178-185 Mb chromosomal region. No difference in body or femur length was exhibited by the new subline of mice (**Figure 3B**), which confirms that the BMD phenotype is not related to body size genes.

Specific Objective 2.

We have proposed to produce additional F2 mice in the event that we could not fine map the chromosomal location of the BMD QTL region to less than 1-2 cM using additional markers and the congenic approach. To narrow down the chromosomal location of a QTL by linkage study, two strategies are commonly used: 1) use additional markers; and 2) use additional F2 mice. Because of our success to fine map the chromosomal location by using additional markers and by producing new subcongenic line of mice, we eliminated the necessity to produce additional F2 mice.

The data from the seven subcongenic lines discussed above provided evidence for the presence of two BMD QTLs within the initial BMD QTL in chromosome 1. To determine whether fine mapping will confirm the presence of the two BMD loci, we started by genotyping 565 B6.CAST F2 female mice; we have used 29 markers instead of the 7 previously used (Beamer et al., 1999). The number of markers was increased in order to detect and evaluate the effect of more potential recombinations within the major QTL region and initiate the screen for BMD candidate genes. Therefore, interval mapping using MapQTL 4.0 to identify the linkage between polymorphic markers and femur total BMD within the F2 female mice showed two peaks/QTLs significantly associated with femoral vBMD (**Fig. 4**), which confirmed the presence of more than one BMD QTL in this region. Therefore, we shifted the focus to identify BMD candidate gene within the two loci identified above.

Specific objective 3.

Duffy (Dfy) blood group gene was reported at last year's annual report as a BMD candidate gene. This gene was highly expressed in the C168-185 subline and is located at 173.2 Mb from the centromere in chromosome 1 (according to NCBI database). Before starting functional studies, we have performed Real Time PCR to evaluate the expression of this gene in the two newly generated subcongenic lines of mice: C168-179, which exhibits a high BMD phenotype, and C168-172, which does not show a BMD phenotype. Table 3 shows the expression level of the Dfy gene in the femur without bone marrow from the two subcongenic mice and from B6 mice. For each strain, we used 5-6 replicates and 18S was used as a control gene. Dfy gene expression was elevated 12-fold in the bones of the C168-179 subline compared to the B6 control mice. In contrast, no difference in Dfy gene expression was found between C168-172 subline and the B6 control mice. Thus, the C168-179 subline was used in functional study to determine the role of Dfy in BMD variation.

Dfy antigen receptor for chemokines binds a variety of CXC and CC chemokines, in particular, the CC chemokines monocyte chemotactic protein-1 (MCP-1; CCL2), MIP-1 alpha, RANTES, CCL5, the CXC chemokines interleukine-8 (IL-8, CXCL8), (Neote et al., 1994 and Luo et al., 1997), which have been reported to be potent osteoclastogenic factors (Fuller et al., 1995, Bendre et al., 2003, Barill-Nion and Bataille., 2003 and Day et al., 2004). Based on these

data, we hypothesized that Dfy protein acts to regulate formation and /or activity of osteoclasts. Thus, to test this hypothesis, we proceeded as follows:

Bone marrow cells were obtained from femurs isolated from 6 week-old female B6 and C168-179 subline mice. Femurs were dissected, the ends of the bones were cut, and the marrow was flushed out using a 2 ml syringe and transferred into 15 ml falcon tubes. Bone marrow cells were dispersed by repeated aspiration of the cell preparation containing Dulbecco's modified Eagle's medium (DMEM) supplemented with 10% heat-inactivated fetal bovine serum (FBS). Cells were seeded in 10-cm petri dishes and incubated at 37^{o}C in a humidifier incubator with 5% CO_2. After 24 hours, all nonadherent bone marrow cells (NABMC) were transferred to new 50 ml falcon tubes, and then were counted with hemocytometer. Cells were then spun down, and supernatant was removed. The pellet was resuspended in DMEM supplemented with 10% FBS at a density of 8 x 10^5 cells/ml. Cells were then seeded into 24-well plates at a density of 2 x 10^5 cells/well and treated with soluble RANKL (100ng/ml) and murine colony-stimulating factor (MCSF, 100ng/ml).The cultures were maintained for up to 10 days and re-fed twice a week. After 10 days of treatment, the adherent osteoclasts were rinsed with phosphate-buffered saline (PBS), fixed with Citrate (4%)/acetone (60%), and then stained with, per well, 500 µl of freshly prepared TRAP staining solution containing naphthol-AS-BI phosphoric acid in *N*,*N*-dimethylformamide, acetate buffer, sodium tartrate (100 mM) and Fast Garnet GBC salt. After staining, the solution was aspirated and replaced with 500 µl of PBS. The TRAP-positive (pink/purple), multinucleated (MNC) osteoclasts were visualized and counted under light microscopy and only cells with more than two nuclei were considered. We found that the C168-179 subline showed a 70% decrease of TRAP-positive MNC compared to B6 control mice (**Figure 5**), which supports the hypothesis that the Dfy protein synthesized in C168-179 pre-osteoclasts inhibits osteoclastogenesis.

Specific objective 4.

Since the subcongenic mice which exhibit a high femoral vBMD compared to B6 control mice have shown a reduced number of differentiated osteoclast cells, and the Real Time PCR showed no expression of Dfy gene in osteoblast cells, we decided to perform our functional study on pre-osteoclast cells instead of osteoblast cells.

Specific objective 5.

If Dfy protein is involved in the regulation of osteoclastogenesis, then bone marrow cells from C168-179 should lead to impaired formation of mature osteoclasts. We therefore tested this possibility.

To knock down the gene expression an siRNA approach is commonly used. However, the use of the siRNA approach to knock down a gene of interest has not been validated in osteoclast cell culture. As an alternative approach, we used bone marrow from Dfy-knockout mice (Dfy-KO) as these mice has no functional Dfy protein and become available to us through our collaborator Dr. Chaudhuri from Kimball Research Institute of the New York Blood Center. To investigate the role of Dfy gene in regulating bone accretion, we examined the phenotype of Dfy-KO mice with that of age-gender matched wild type progenitors. Body weight as well as femur length were similar for the two strains (**Figure 6**), while total femur vBMD was increased in Dfy-KO mice compared to wild type control mice. The trabecular volume was significantly reduced compared to wild type mice, while endosteal circumference was slightly decreased and no change in periosteal circumference, which resembles the phenotype of the C168-179 subline,

and confirms the involvement of the Dfy gene in BMD variation. Therefore, since the C168-179 subline showed a high expression of the Dfy gene and exhibited a high femur vBMD, this suggests that the SNPs in Dfy coding regions (previous report) alter the function of the protein which by feedback enhances the expression of this gene. Thus in order to determine if the Dfy protein affects osteoclastogenesis, we treated non-adherent bone marrow cells from Dfy wild type and from Dfy-knockout mice with RANKL (100ng/ml) and MCSF (100ng/ml) as described above. Then after 10 days, the TRAP-positive multinucleated cells (MNC) were counted. KO-Dfy showed 50% decrease of TRAP-positive MNC compared to wild type mice (**Figure 7**), which supports the hypothesis that the Dfy protein is involved in the regulation of osteoclast formation/activity.

In addition, we have treated NABMC with Dfy-Antibody (Dfy-Ab) in the presence of RANKL and M-CSF. After six days of treatment, the multinuclear TRAP-positive cells, the NABMC derived from B6 control mice, showed a significant reduction of the number of TRAP-positive multinucleated cells, with the majority of the cells mononucleated and Trap-positive (**Figure 8**). This provides further evidence that the Dfy protein is involved in osteoclast formation and/or activity, and that the reduced osteoclast formation in the NABMC of CAST mice may be explained on the basis of reduced activity of Dfy protein in CAST mice compared to B6 mice.

We next tried to determine if amino acid changes in the CAST *Dfy* gene lead to an alteration of the chemokine binding to NABMC. We chose MCP-1 as a ligand for the binding studies based on previous findings that MCP-1 bound to the Dfy protein and that MCP-1 regulated osteoclast formation. The specific binding of ^{125}I-MCP-1 to NABMC derived from the C168-179 subcongenic line of mice was significantly reduced (51%, $P<0.001$, **Figure 9**) compared to NABMC derived from B6 control mice. As expected, NABMC derived from *Dfy*-KO mice exhibited significantly lower binding of MCP-1 compared to the B6 control mice (50% of B6. $P<0.001$, **Figure 9**). Based on these data, we proposed a model in which the Dfy protein produced in CAST and C3H inbred mouse strains does not bind chemokines with high affinity, which leads to reduced osteoclast formation and, consequently, reduced bone turn-over.

Specific objective 6.

Fine mapping and the skeletal phenotype of the subcongenic line of mice provided evidence for the presence of at least two loci significantly associated with femoral vBMD within the initial BMD QTL in chromosome 1. Expression profiling of candidate genes at locus BMD1-2 with the high LOD score in B6.CAST F2 populations have been reported in previous reports and the functional assay was discussed above. Thus, we had to screen for candidate genes at the BMD1-1 locus. The Real Time PCR was performed for 11 candidate genes located in the region 160-165 Mb covering the first BMD locus (**Table 4**) using femur without bone marrow. Only Gas5 gene showed significantly higher expression in both C100-169 and C133-165 subcongenic line of mice compared to B6 control mice. Using Real Time PCR, we have found that Gas5 is also expressed in marrow cells as well as in immature and mature osetoblast cells. Sequencing procedures are in progress to determine the SNPs that might be involved in differential Gas5 gene expression in these two sublines of mice.

Specific objective 7.

In our previous studies with the female F2 mice of a cross between MRL/MpJ and SJL/J inbred lines, 9 BMD QTLs were identified (Masinde et al., 2002). Besides the chromosome 1

QTL, the next largest QTL was on chromosome 17. The LOD score for femur BMD was 5.8. It explained 6.7% of the F2 femur BMD variance. The LOD score for total body BMD was 6.3. In addition, this QTL also had a pleiotropic effect on other body and bone size phenotypes. Because of the multi-locus nature of polygenic traits, we hypothesize that besides the chromosome 1 loci, there are additional loci that influence mouse BMD, and the QTL region of chromosome 17 harbors some of these loci. Because of the pleiotropic nature of this QTL on multiple phenotypes, we also hypothesize that the responsible genes are more fundamental than the chromosome 1 QTL genes in the development not only of bone but also of other tissues. They may be turned on very early in the mouse development. Thus, it is very important to identify the loci that are responsible for the chromosome 17 BMD QTL. Therefore, we imitate this study with the ultimate objective of identifying BMD genes on chromosome 17.

Our previous QTL study of the MRL/MpJ and SJL/J cross was done with only female mice (Masinde et al., 2002). The first objective of the current study was to verify that the same QTL on chromosome 17 existed in the male mice of the MRL/Map X SJL/J cross. The second objective was to fine-map this QTL using the male F2 mice. The current study is only the first stage towards identifying chromosome 17 BMD genes. The second stage is to breed additional female F2 mice in MRL/MpJ X SJL/J so that we can perform phenotype and genotype analysis in an approximate total of 2000 MRL X SJL F2 mice. Hopefully, all these steps will significantly narrow down the QTL region on chromosome 17, so that a reduced number of candidate genes can be examined to determined which candidate gene is responsible for the femur and total body BMD QTL on chromosome 17.

The 633 female F2 mice of MRL X SJL were used earlier (Li et al., 2002, Masinde et al., 2002). For this study, four week old mice of inbred strains: MRL/MpJ (MRL), and SJL/J (SJL) were obtained from the Jackson Laboratory (Bar Harbor, Maine). An additional 474 F2 male mice of MRL and SJL were generated at the Animal Research Facility, J.L. Pettis Veterans Administration Memorial Medical Center. A PIXIMUS densitometer (LUNAR Corporation, Madison, WI) was used for the measurement of the whole body BMD on the 7 weeks old live animals. At the same time, body weight was recorded for each animal, after which time the F2 male mice were euthanized. Liver was isolated for DNA extraction. Femurs were isolated from both legs. Femur BMD and other femur parameters were determined from the mid-shaft portion of a single femur (usually right femur) using pQCT (Stratec XCT 960 M, Norland Medical System, Ft. Atkinson, WI).

The method of genotyping were described previously (Li et al. 2002; Masinde et al., 2002). Twenty one chromosome 17 genetic markers were genotyped for the F2 male mice of MRL X SJL (**Table 5**). The average distance between markers was 3.16 Mb or 1.74 cM. This covers the 3.62-66.88 Mb QTL region out of 92 Mb for the entire chromosome 17. Genotype data was analyzed using MapQTL (5.0) (Van Ooijien, 2004). MapQTL's interval mapping option was used. Permutation test of MapQTL was used to obtain the LOD scores for the significant thresholds at 0.05 and 0.01 probability levels. For the whole body parameters such as body BMD and body bone area obtained from PIXIMUS, the size of the animal was an influencing factor. Therefore, these parameters were adjusted by body weight. Simple linear regression analysis was carried out using STATISTICA (Release 7, StatSoft, Inc. Tulsa, OK). The adjusted parameters were the residuals of the linear regression.

Although the male F2 mice of MRL X SJL were much bigger (average weight of 32.11g at 7 weeks of age compared to 24.26g for the females), the interval mapping results show that the same chromosome 17 QTL also existed in the male mice. The LOD score was 4.03 ($P <$

0.01) at the position of 45.70 Mb for femur BMD (**Figure 9, Table 6**). Because the number of male mice in the current study was much smaller (only 474 compared to 633 female mice), this LOD score is comparable to the 5.8 LOD score obtained earlier from the female mice (Masinde et al., 2002). At its peak, this QTL explained about 3.9% of the F2 femur BMD variance. Much high LOD score was obtained for the whole body BMD. The LOD score was 5.66 ($P < 0.01$) (**Figure 9, Table 6**). It explained about 6.1% of the body BMD's F2 variance. It was noticed that there is also a body weight QTL at roughly the same position (47.74 MB) (**Figure 9, Table 6**). The LOD score was 5.08 ($P < 0.01$). Because there is a body weight QTL, and because the whole body BMD is influenced by the size of the animal, we have used the adjusted whole body BMD in the QTL analysis, which had taken body weight out of consideration. Therefore, we can conclude that the body BMD QTL on chromosome 17 is independent of the body weight QTL at the same location. In fact, the LOD scores before and after the body weight adjustment were very similar, again to confirm the finding that the BMD QTL was independent of the body size QTL.

Besides bone density, there were also QTLs for bone size on chromosome 17. The LOD scores of the adjusted body bone area obtained from PIXIMUS, femur length and femur periosteal circumference obtained from pQCT were all significant at $p < 0.05$ level (2.82, 2.84 and 2.50, respectively) (**Table 6**). The peak positions were all around 41 to 46 Mb, very similar to the 46 to 50 Mb positions for femur and body BMD QTL.

In terms of narrowing down the BMD QTL region, we have determined the one LOD interval for femur and body BMD QTL peaks. The one LOD interval for femur BMD spanned 26.31 Mb region centered on 45.70 Mb (**Table 6, Figure 9**). This also covered the one LOD interval for body BMD, which was only 8.10 Mb centered on 49.70 Mb. In other words, we have narrowed the chromosome 17 BMD QTL from 63 Mb (about 32 cM) to just 26 Mb (about 13 cM).

In conclusion, we have confirmed that the chromosome 17 BMD QTL identified by our earlier study in the female F2 mice of MRL X SJL also to be present in the male F2 mice of MRL X SJL. This QTL was also shown to be extreme pleiotropic on bone and body size phenotypes. We believe that the same underlying genes that are responsible for both bone density and bone size QTL on chromosome 17. In addition, we have narrowed this QTL from a 63 Mb region to just 26 (about 13 cM).

Table 1. Genetic and Physical Positions Of Molecular Markers Used in this study

Marker name	Genetic position (cM)	Physical position (Mb)
D1mit370	88.3	168.03
D1mit112	91.3	169.04
D1mit113	93.3	171.86
D1mit149	94.2	172.80
D1mit354	95.8	172.98
D1mit206	95.8	173.13
D1mit355	97.0	173.54
D1mit150	100.0	174.76
D1mit541	97.7	174.60
D1mit357	99.8	175.66
D1mit403	100.0	175.77
D1mit166	100.0	176.60
D1mit359	100.0	177.40
D1mit358	100.0	177.68
D1mit115	99.7	177.80
D1mit315	101.0	178.96
D1mit426	101.0	180.40
D1mit509	101.0	180.87
D1mit151	101.0	181.10
Mg4718	-	182.20
mg4723	-	182.40
D1mit360	101.2	182.50
D1mit152	101.5	184.60
D1mit221	102.0	184.86
D1mit407	101.5	185.82

"-" means that the distance is not available.

Table 2. Correlation among various phenotypes from the seven congenic sublines tested. Significant correlations are shown in bold ($p<0.05$, N=7). Values for all phenotypes were expressed as a percentage difference compared with B6 mice.

	Crt.Thickness	Perios.C	Endos.C	Weight	Femur length
vBMD	**0.97**	0.26	**-0.80**	0.50	0.09
Crt.Thickness	1.00	0.43	**-0.67**	0.62	0.23
Perios.C	0.43	1.00	0.37	**0.77**	0.54
Endos.C	**-0.67**	0.37	1.00	-0.03	0.28
Weight	**0.62**	**0.77**	-0.03	1.00	0.45
Femur length	0.23	0.54	0.28	0.45	1.00

Crt. Thickness, refers to cortical thickness. Perio.C, refers to periosteal circumference. Endo.C, refers to endosteal circumference.

Table 3. Results of Real Time PCR performed for Dfy gene in C168-179, C168-172 sublines and B6 control mice.

Ct	Dfy	18S	ΔCt	ΔΔCt	Fold change
B6	29 ± 0.8	17 ± 0.4	12		
C168-172	29.5 ± 0.5	17.3 ± 0.3	12.2	-0.2	-0.4
C168-179	23 ± 0.5	17 ± 0.5	6	6	12

Ct; represents the number of PCR cycles. ΔCt, is the difference (number of cycle of Dfy gene – number of cycles of the control gene) and ΔΔCt is the difference between ΔCt of B6 and ΔCt of the subcongenic mice.

Table 4. Candidate genes at the region 160-165 Mb from the centromere, with the fold change for the gene that showed significant difference in the expression profile between the high vBMD subcongenic mice and the B6 control mice.

Gene description	**Symbol**	**Fold change if significant**
serine (or cysteine) proteinase inhibitor, clade C (antithrombin), member 1	Serpinc1	ns
growth arrest specific 5	Gas5	9.35*
EST		ns
tumor necrosis factor (ligand) superfamily, member 4	Tnfsf4	ns
paired related homeobox 1	Prrx1	ns
kinesin-associated protein 3	Kifap3	ns
selectin, lymphocyte	Sell	ns
non-metastatic cells 7	Nme7	ns
ATPase, Na+/K+ transporting, beta 1 polypeptide	Atp1b1	ns
Dermatopontin	Dpt	ns
chemokine (C motif) ligand 1	Xcl1	ns

5-6 replicates per line were used for Real Time PCR and only genes that showed difference in the expression between C100-169 subline and B6 are going to be further analyzed. *P<0.001 *vs* B6.

Table 5. Markers used in fine-mapping the BMD QTL in chromosome 17

Number	Name	Distance (Mb)	Distance (cM)
1	D17Mit268	3.619	2.7
2	D17Mit246	7.868	0
3	D17Mit113	11.388	2.2
4	D17Mit61	29.238	6.6
5	D17Mit81	29.510	5.5
6	D17Mit175	30.443	6.6
7	D17Mit214	32.835	9.8
8	D17Mit83	33.453	8.7
9	D17Mit64	37.027	10.9
10	D17Mit176	40.888	12
11	D17Mit269	42.697	26.7
12	D17Mit35	43.700	14.2
13	D17Mit250	45.625	19.7
14	D17Mit68	45.735	19.7
15	D17Mit115	45.740	18.6
16	D17Mit177	46.733	19.7
17	D17Mit270	48.700	32.2
18	D17Mit139	50.841	25.1
19	D17Mit20	55.558	29.5
20	D17Mit152	63.696	32.8
21	D17Mit185	66.877	35

Table 6. Chromosome 17 QTL for body weight and different bone phenotypes in MRL X SJL F2 male mice

Trait	Peak position (Mb)	Nearest marker	LOD score	Significance level	Variance explained (%)	One LOD interval (Mb)
Body weight	47.74	D17Mit270	5.08	0.01	5.3	8.01
Adjusted body BMD	49.70	D17Mit20	5.66	0.01	6.1	8.10
Adjusted body bone area	40.89	D17Mit176	2.82	0.05	2.7	6.66
Femur BMD	45.70	D17Mit115	4.03	0.01	3.9	26.31
Femur length	44.70	D17Mit35	2.84	0.05	2.9	18.39
Femur PC	45.74	D17M115	2.50	0.05	1.6	17.81

Physical distance. NCBI (Mb)	Markers	C178-185	C175-185	C172-185	C169-185	C168-185	C168-179	C168-176	C168-172	C133-165	C100-169	
80.3	D1MIT216	-	-	B	B	B	B	B	B	B	B	
133.2	D1mit30	-	-	B	B	B	B	B	B	B	C	
155.95	D1mit451	-	-	B	B	B	B	B	B	C	C	BMD1-1
156.77	D1Mit14	-	-	B	B	B	B	B	B	C	C	BMD1-1
157.36	D1Mit268	-	-	B	B	B	B	B	B	C	C	BMD1-1
162.33	D1Mit106	-	-	B	B	B	B	B	B	C	C	BMD1-1
165.2	D1Mit453	-	-	B	B	B	B	B	B	B	C	
166.7	D1Mit57	-	-	B	B	B	B	B	B	B	C	
167.3	D1mit145	-	-	B	B	B	B	B	B	B	C	
167.78	D1mit110	B	B	B	B	B	B	B	B	B	C	
168.03	D1mit370	-	-	B	B	B	B	B	B	B	C	
169.04	D1mit112	B	B	B	B	C	C	C	C	B	B	
171.86	D1mit113	B	B	B	C	C	C	C	C	B	B	
172.8	D1mit149	B	B	B	C	C	C	C	B	B	B	BMD1-2
172.98	D1mit354	B	B	C	C	C	C	C	B	B	B	BMD1-2
173.134	D1mit206	B	B	C	C	C	C	C	B	B	B	BMD1-2
173.54	D1mit355	B	B	C	C	C	C	C	B	B	B	BMD1-2
174.76	D1mit150	B	B	C	C	C	C	C	B	B	B	BMD1-2
174.6	D1mit541	B	C	C	C	C	C	C	B	B	B	BMD1-2
175.66	D1mit357	B	C	C	C	C	C	C	B	B	B	BMD1-2
175.77	D1mit403	B	C	C	C	C	C	B	B	B	B	
176.6	D1mit166	B	C	C	C	C	C	B	B	B	B	
177.4	D1mit359	B	C	C	C	C	C	B	B	B	B	
177.68	D1mit358	-	C	C	C	C	C	B	B	B	B	
177.8	D1mit115	B	C	C	C	C	C	B	B	B	B	
178.96	D1mit315	C	C	C	C	C	B	B	B	B	B	BMD1-3
180.4	D1mit426	C	C	C	C	C	B	B	B	B	B	BMD1-3
180.87	D1mit509	C	C	C	C	C	B	B	B	B	B	BMD1-3
181.08	D1MIT151	C	C	C	C	C	B	B	B	B	B	BMD1-3
182.2	Mg4718	C	-	C	C	C	B	B	B	B	B	BMD1-3
182.4	Mg4723	C	C	C	C	C	B	B	B	B	B	BMD1-3
182.51	D1MIT360	C	C	C	C	C	B	B	B	B	B	BMD1-3
184.6	D1mit152	C	C	C	C	C	B	B	B	B	B	BMD1-3
184.86	D1mit221	B	B	B	B	B	B	B	B	B	B	
185.82	D1mit407	B	-	B	B	B	B	B	B	B	B	
187.3	D1mit459	B	-	B	B	B	B	B	B	B	B	
-	D1mit17	B	B	B	B	B	B	B	B	B	B	
192.06	D1MIT511	B	B	B	B	B	B	B	B	B	B	

Figure 1. The regions of CAST chromosome 1 transferred onto B6 background for the seven congenic sublines. The genotyping data for every marker are represented with "B" referring to homozygous *b6/b6*, "C" referring to *cast/cast* and "-" for data not available. The names of the subcongenic lines are at the top. We used a letter "C" followed by the proximal and distal limits of *cast* alleles carried by the congenic sublines in megabases. The purple squares denote the CAST chromosomal regions carried by each congenic subline that exhibits high femoral BMD, while the yellow squares represent the CAST chromosomal region carried by the subcongenic mice which do not show a difference of femoral BMD when compared with B6 control mice. The black squares represent the BMD loci; BMD1-1 and BMD1-2 and BMD1-3.

The polymorphic markers with their physical positions along chromosome 1 are presented at the left.

Figure 2A.

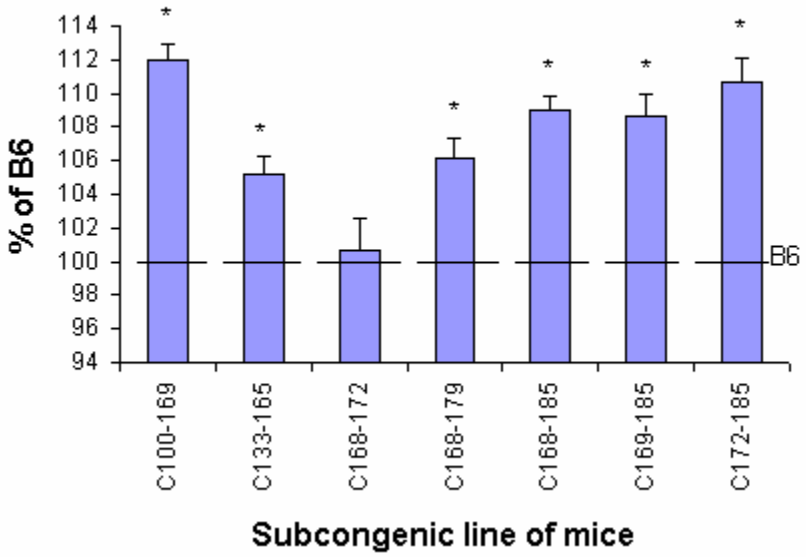

Figure 2B.

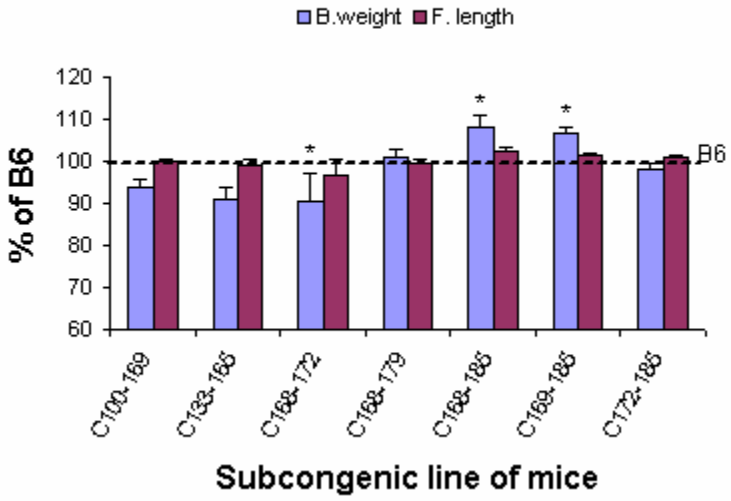

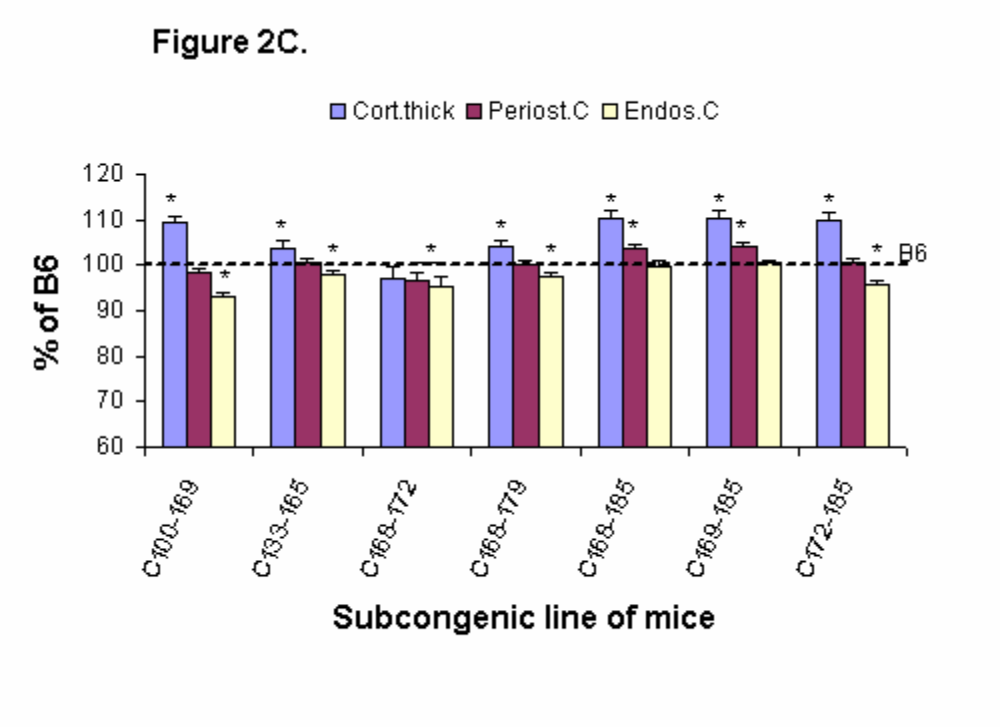

Figure 2. Femoral and body weight data from the seven different subcongenic strains of mice. Data are expressed as a percentage change from B6 and are mean + SEM, n=8-12. significant differences between B6 control mice and subcongenic lines are indicated by an asterix when $P<0.05$. Figure 2A. Mid-diaphysis femur vBMD. Figure 2B. Body weight and femur length. Figure 2C. Mid-diaphysis femur periosteal circumference, endosteal circumference and cortical thickness.

Fig.3A

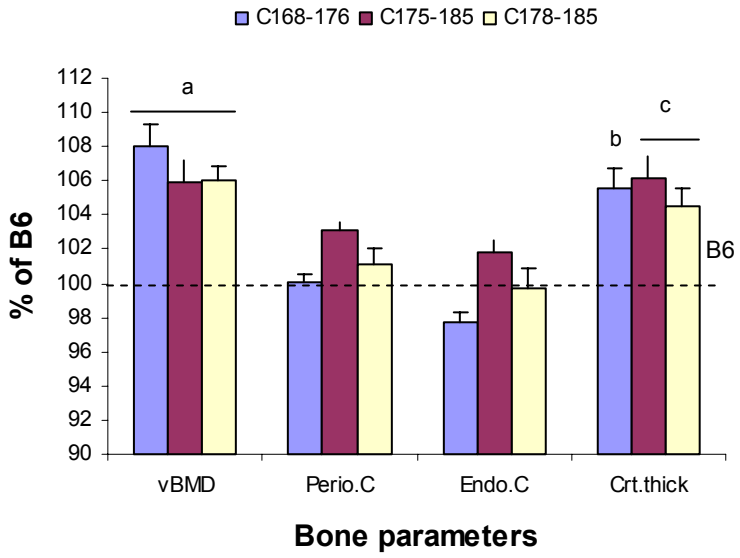

Fig.3B

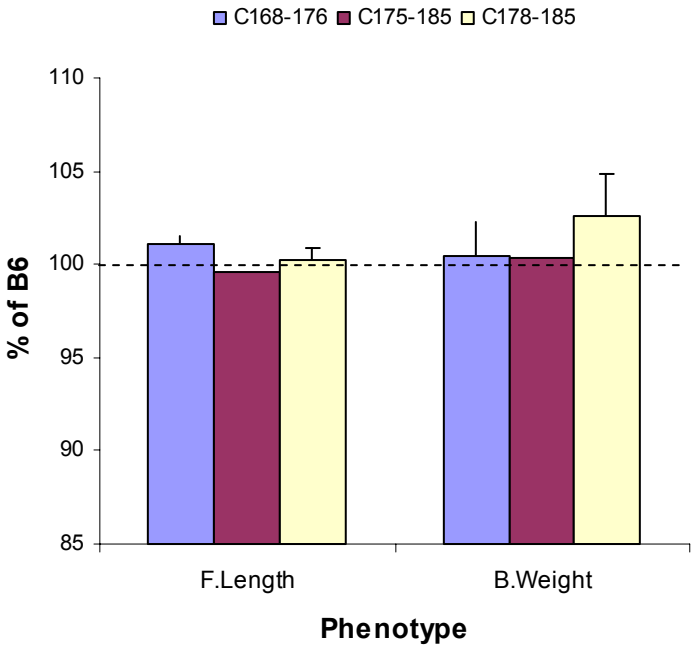

Figure 3. Femoral and body weight data from the three new subcongenic strains of mice. Data are expressed as a percentage change from B6 and are mean + SEM, n=13-17. Significant differences between B6 control mice and subcongenic lines are indicated by lower case letters using *t*-test: [a]P<0.01, [b]0.01<P<0.02, [c]0.02<P<0.05. Figure 3A. Mid-diaphysis femur vBMD, periosteal circumference, endosteal circumference and cortical thickness. Figure 3B. Body weight and femur length.

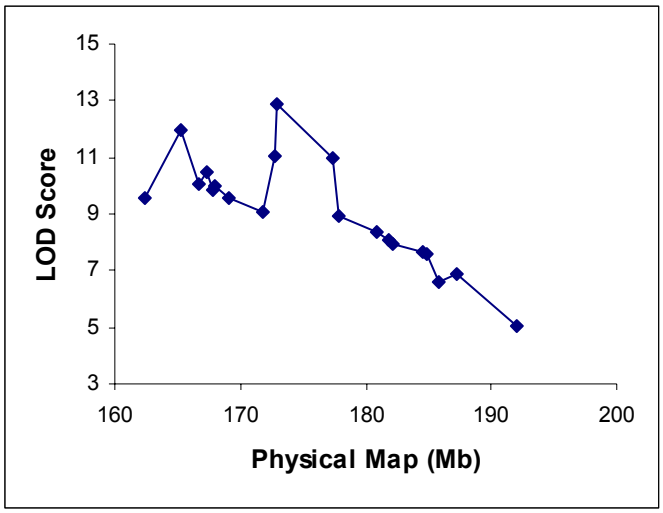

Figure 4. Results of interval maps of chromosome 1 BMD QTL. Statistical analyses are presented as LOD score calculated for molecular markers beginning with the centromeric end on the left and extending toward the telomeric end.

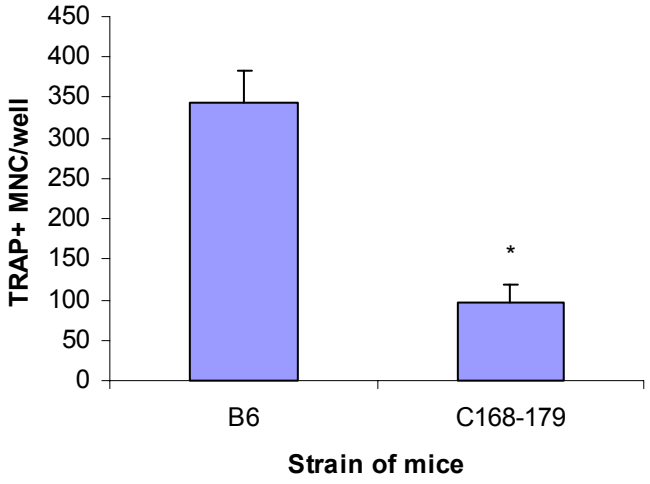

Figure 5. TRAP + multinucleated cell (MNC) formation in nonadherent bone marrow cells treated with RANKL and M-CSF. * $P<0.05$ *vs* B6.

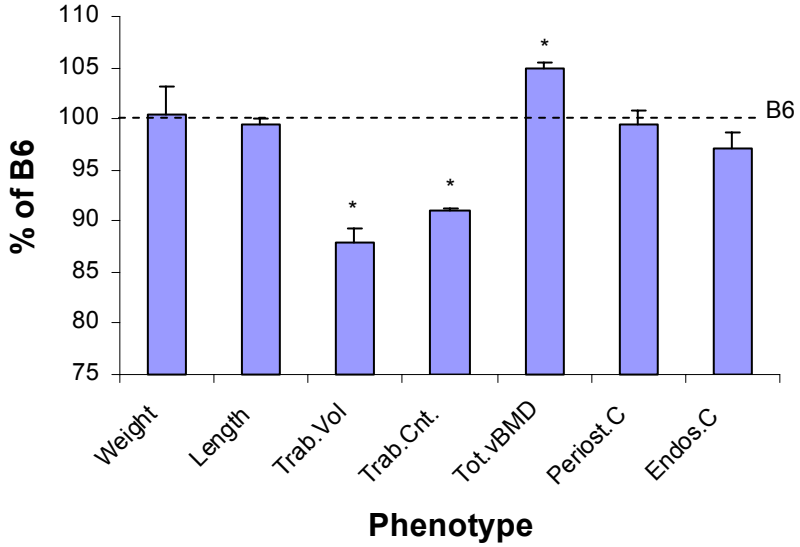

Figure 6. Femoral and body weight data from the Dfy-knockout mice. Data are expressed as a percentage change from the B6 wild type mice and are mean + SEM, n=12-14. significant differences between B6 control mice and subcongenic lines are indicated by $^{*}P<0.05$. Trab. Vol., represents trabecular volume. Trab. Cnt, represents trabecular content. Tot. vBMD, for femur total vBMD. Periso.C, means periosteal circumference and Endo.C., means endosteal circumference

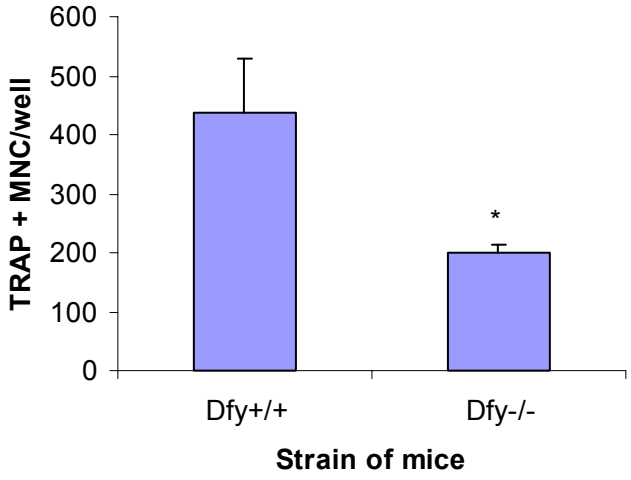

Figure 7. TRAP positive multinucleated cells (MNC) formation from nonadherent bone marrow cells isolated from wild type Dfy+/+ mice and from Dfy knockout mice (-/-) after Treatment with RANKL and M-CSF. **P*<0.05 *vs* Dfy+/+.

Figure 8

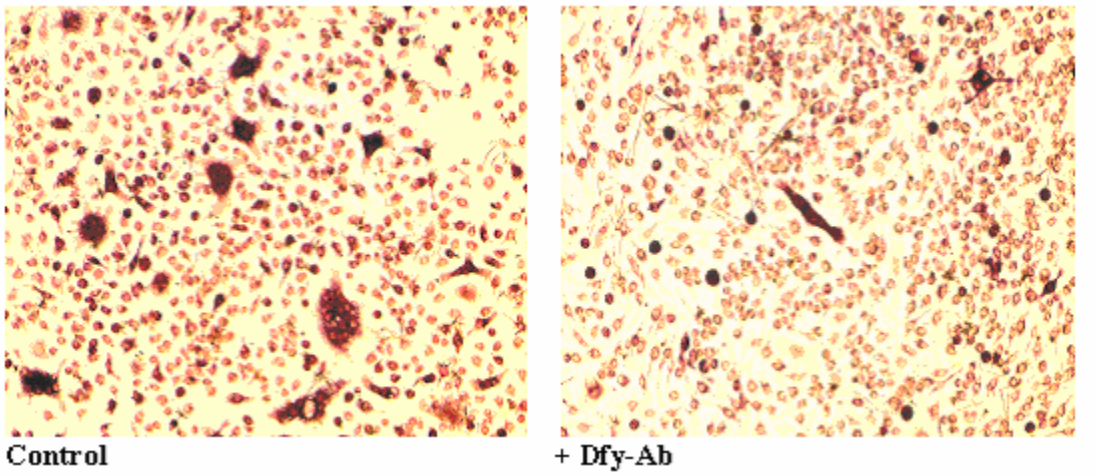

Figure 8. TRAP-stained cells from wild type B6 mice, after six days treatment with Dfy-Ab in presence of RANKL and M-CSF (right panel), the number of TRAP-positive multinucleated cells decreased considerably compared to control cells treated only with RANKL and M-CSF (left panel).

Figure 9

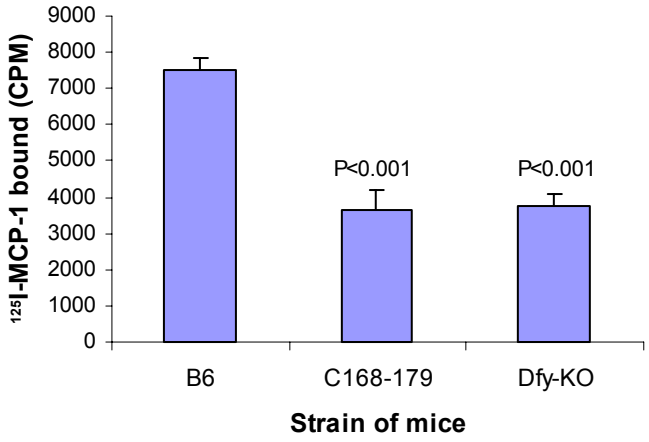

Figure 9. Binding of murine MCP-1. NABMC were incubated at RT in the presence of either only ^{125}I-MCP or in the presence of both labeled and unlabelled MCP-1. The specific binding was expressed as the CPM value in the absence of cold MCP-1 subtracted from the CPM value in the presence of cold MCP-1, n=8-10**.** Groups were compared with Student's t-test.

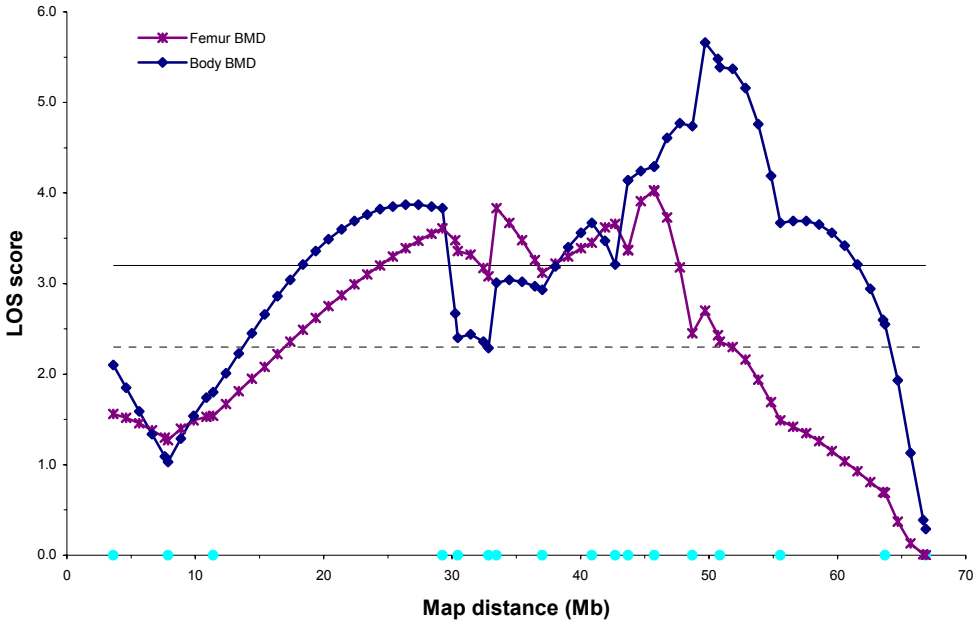

Figure 10. **LOD scores of the chromosome 17 QTL for whole body and femur BMD.** The whole body BMD was adjusted for body weight using the residuals of the simple linear regression analysis. The filled circles on the X-axis indicate genotyped marker positions.

Key Research Accomplishments

- We have generated new B6.CAST subcongenic mice and measured their skeletal phenotype, which provided evidence for the presence of two BMD loci within the initial BMD QTL in chromosome 1.
- We fine mapped the initial BMD QTL in chromosome 1 and confirmed the presence of two BMD loci within this region.
- We optimized the conditions to generate differentiated osteoclast cells from non-adherent bone marrow cells.
- We demonstrated the effect of Dfy gene on osteoclastogenesis.
- We identified a second BMD candidate gene in BMD1-1 locus.
- We generated 474 F2 male mice from the cross MRL x SJL.
- We fine mapped the BMD QTL in chromosome 17 using F2 male mice and confirmed the presence of the BMD QTL within this region

Reportable Outcomes

- **Plenary Poster** presentation at the 27th American Society for Bone and Mineral Research, Sept 23-27, 2005, Nashville, TN.
Title: CAST chromosome 1 QTL is complex and contains three BMD loci and one bone size locus: Evidence from subcongenic lines.
Authors: B. Edderkaoui, D. J. Baylink, W. G. Beamer , K. L. Shultz, N. Dunn, , J. E. Wergedal, S. Mohan.
- **Article in** Journal of Bone and Mineral Research.
Title: Multiple Genetic Loci From CAST/EiJ Chromosome 1 Affect vBMD Either Positively or Negatively in a C57BL/6J Background
Authors: B. Edderkaoui, D. J. Baylink, W. G. Beamer, J. E. Wergedal, N. R. Dunn, K. L. Shultz and S. Mohan.
- **Abstract** 28th American Society for Bone and Mineral Research, September 15-19, 2006 Philadelphia, PA
Title: Identification of Duffy Antigen/Receptor for Chemokine (DARC) as a Chromosome 1 BMD QTL Gene in Mice
Authors: B. Edderkaoui, D. J. Baylink, K. L. Shultz, W. G. Beamer , J. E. Wergedal, R. Porte, A. Chaudhuri and S. Mohan.

Conclusions

1. Identified two BMD loci within the initial BMD QTL in chromosome 1.

2. We demonstrated that the B6-CAST subcongenic mice which exhibit high vBMD, exhibit impaired osteoclast differentiation *in vitro*.

3. Dfy knockout mice exhibit, *in vivo* and *in vitro,* a phenotype similar to that of B6-CAST subcongenic mice, which confirmed the effect of Dfy gene on BMD variation and osteoclastogenesis.

4. We identified a second BMD candidate gene within the initial BMD QTL in chromosome 1.

5. We narrowed down the size of the BMD QTL in chromosome 17 from 63 Mb to 26 Mb.

References

Barille-Nion S, Bataille R. New insights in myeloma-induced osteolysis. Leuk Lymphoma. 44(9):1463-7. Review (2003).

Beamer WG, Shultz KL, Churchill GA, Frankel WN, Baylink DJ, Rosen CJ, Donahue LR Quantitative trait loci for bone density in C57BL/6J and CAST/EiJ inbred mice. Mamm Genome 10:1043-9 (1999).

Beamer WG, Shultz KL, Donahue LR, Churchill GA, Sen S, Wergedal JR, Baylink DJ, Rosen CJ. Quantitative trait loci for femoral and lumbar vertebral bone mineral density in C57BL/6J and C3H/HeJ inbred strains of mice. J Bone Miner Res. 16:1195-206 (2001).

Bendre MS, Montague DC, Peery T, Akel NS, Gaddy D, Suva LJ. Interleukin-8 stimulation of osteoclastogenesis and bone resorption is a mechanism for the increased osteolysis of metastatic bone disease. Bone. 33(1):28-37 (2003).

Cummings SR, Kelsey JL, Nevitt MC, O'Dowd KJ. Epidemiology of osteoporosis and osteoporotic fractures. Epidemiol Rev. 7:178-208 (1985).

Day CJ, Kim MS, Stephens SR, Simcock WE, Aitken CJ, Nicholson GC, Morrison NA. Gene array identification of osteoclast genes: differential inhibition of osteoclastogenesis by cyclosporin A and granulocyte macrophage colony stimulating factor. J Cell Biochem. 91(2):303-15 (2004).

Deng HW, Chen WM, Conway T, Zhou Y, Davies KM, Stegman MR, Deng H, Recker RR. Determination of bone mineral density of the hip and spine in human pedigrees by genetic and life-style factors. Genet Epidemiol. 19:160-77 (2000).

Dequeker J, Nijs J, Verstraeten A, Geusens P, Gevers G. Genetic determinants of bone mineral content at the spine and radius: a twin study. Bone. 8:207-9 (1987)

Fuller K, Owens J, Chambers TJ. The effect of hepatocyte growth factor on the behavior of osteoclasts. Biochem Biophys Res Commun. 212(2):334-40 (1995).

Gueguen R, Jouanny P, Guillemin F, Kuntz C, Pourel J, Siest G. Segregation analysis and variance components analysis of bone mineral density in healthy families. J Bone Miner Res. 10:2017-22 (1995).

Huang QY, Recker RR, Deng HW. Searching for osteoporosis genes in the post-genome era: progress and challenges. Osteoporos Int. 14:701-15 (2003).

Koller DL, Econs MJ, Morin PA, Christian JC, Hui SL, Parry P, Curran ME, Rodriguez LA, Conneally PM, Joslyn G, Peacock M, Johnston CC, Foroud T Genome screen for QTLs contributing to normal variation in bone mineral density and osteoporosis. J Clin Endocrinol Metab 85:3116-20 (2000).

Li X, Mohan S, Gu W, Wergedal J, Baylink DJ. Quantitative assessment of forearm muscle size, forelimb grip strength, forearm bone mineral density, and forearm bone size in determining humerus breaking strength in 10 inbred strains of mice. Calcif Tissue Int. 68:365-9 (2001).

Li X, Masinde G, Gu W, Wergedal J, Mohan S, Baylink DJ. Genetic dissection of femur breaking strength in a large population (MRL/MpJ x SJL/J) of F2 Mice: single QTL effects, epistasis, and pleiotropy. Genomics. 79:734-40 (2002).

Luo H., Chaudhuri A., Johnson KR., Neote V., Zbrzezna Y., He Y., and Pogo AO. Cloning, characterization, and mapping of a murine promiscuous chemokine receptor gene: homolog of the human Dfy gene. Genome Res. 7: 932-941 (1997)

Masinde GL, Li X, Gu W, Wergedal J, Mohan S, Baylink DJ. Quantitative trait loci for bone density in mice: the genes determining total skeletal density and femur density show little overlap in F2 mice. Calcif Tissue Int. 71:421-8 (2002).

Melton LJ 3rd, Kan SH, Frye MA, Wahner HW, O'Fallon WM, Riggs BL. Epidemiology of vertebral fractures in women. Am J Epidemiol. 129:1000-11 (1989).

Neote, K., Mak, J. Y., Kolakowski, L. F., and Schall, T. J. Functional and biochemical analysis of the cloned Dfy antigen: identity with the red blood cell chemokine receptor. Blood 84: 44-52 (1994).

Recker RR, Deng HW. Role of genetics in osteoporosis. Endocrine. 17:55-66 (2002).

Ralston SH. Genetic control of susceptibility to osteoporosis. J Clin Endocrinol Metab 87:2460-6 (2002).

Shultz KL, Donahue LR, Bouxsein ML, Baylink DJ, Rosen CJ, Beamer WG Congenic strains of mice for verification and genetic decomposition of quantitative trait loci for femoral bone mineral density. J Bone Miner Res 18:175-85 (2003).

Slemenda CW, Christian JC, Williams CJ, Norton JA, Johnston CC Jr. Genetic determinants of bone mass in adult women: a reevaluation of the twin model and the potential importance of gene interaction on heritability estimates. J Bone Miner Res. 6:561-7 (1991)

Van Ooijen, JW. MapQTL® 5, Software fore the mapping of quantitative trait loci in experimental populations. Kyazma B.B., Wageningen, Netherlands (2004).

TECHNICAL OBJECTIVE 2: TO IDENTIFY THE KEY GENES THAT ARE INVOLVED IN THE SOFT-TISSUE REPAIR/REGENERATION IN MRL/MPJ AND SJL/J MICE.

Introduction

Clinical treatments resulting in rapid wound healing without scar formation would lead to a better life for patients with various types of injuries, especially those wounded in the battlefield situations. It would also change the life of ordinary people by improving their cosmetic appearance. However, development of novel clinical treatments such as gene therapy would primarily depend on our understanding of the molecular mechanisms that are operating in wound healing and tissue regeneration.

One way to study the molecular mechanisms is to conduct genetic studies in comparable animals. Laboratory animals such as mice provide an economical and controlled environment to do so. It was found recently that the MRL/MpJ mouse strain could heal ear punch hole completely with no scar formation (Clark et al 1998; Heber-Katz, 1999). Our pioneering work in characterizing ear wound repair/regeneration in 20 representatively sampled inbred strains of mice has found that MRL/MpJ and its progenitor strain LG/J healed four times faster than other strains such as Balb/cByJ and SJL/J (Li et al., 2001). The same study also showed that the mouse ear hole healing rate was highly inheritable, with a heritability of 86%. Our QTL (Quantitative Trait Loci) study has identified 10 QTLs for wound healing/soft tissue regeneration in the F2 of a cross between super healer MRL/MpJ (MRL) and poor healer SJL/J (SJL) (Masinde et al, 2001). The largest QTL was on chromosome 9 with a LOD score of 16. It explained 15% of the phenotypic variance in the F2 population of MRL X SJL.

The ultimate goal of the project is to isolate genes that are responsible for the fast-wound healing/soft tissue regeneration phenotype within the identified QTL chromosome regions of the super healer MRL mice, with a priority on chromosome 9. This would be the first major step in our understanding of the molecular mechanisms of wound healing/soft tissue regeneration.

To realize our goal, we propose to use a combination of approaches including in vitro functional assays. In the functional assays, the candidate genes identified in the QTL analysis and in the forms of BAC clones are inserted into a viral expression vector and applied the skin cells such as dermal fibroblast and keratinocytes. The differential expression pattern of these genes will lead to a more likely candidate gene. The specific aims of this grant period was to fine map the chromosome 9 QTL by using both the high density marker mapping and congenic line techniques. In addition, they also include functional testing of the candidate genes identified in the QTL mapping.

Our specific approaches during the first 12 month of this grant period are as follows:

1) To fine map the QTL region on chromosome 9 to less than 1 cM.

2) To develop *in vitro* functional assays to measure the differentiation, proliferation and apoptosis of the keratinocytes and dermal fibroblasts in monolayer culture and the injured ear in organ culture (the latter will be used if the in vitro assays are unsuccessful in the distinguishing the phenotype).

3) To evaluate the likely candidate genes by comparing in vitro the phenotype produced by the MRL alleles compared to SJL allele (if the in vitro phenotype technology does not distinguish the difference between the two mouse strains, we will develop an in vivo model to evaluate candidate gene functions). We will apply either the siRNA assay or the overlapping BAC clone assay for our functional testing.

Body

Our progress in the second year of this grant period for each of Specific Objectives 1 - 3 is summarized below.

Specific Objective 1: To fine map the QTL region on chromosome 9 to less than 1 cM.

a) Produce additional MRL X SJL F2 mice and perform genotype and phenotype analysis.

b) Cross congenic mice (chromosome 9 QTL of MRL transferred to SJL) with SJL mice and generate sub-congenic lines and test phenotype in the sub-congenic lines.

Fine mapping of chromosome 9 QTL.

In the initial analysis, we had 633 female F2 mice from the MRL X SJL cross, and identified 10 QTL on chromosomes, among others, 1, 4, and 9, with the largest on 9 (Masinde et al., 2001). Our last year's report mentioned that we had bred additional F2 mice, and genotyped a total of 15 markers on chromosome 9. A large F2 population and more genetic markers would help to ensure to narrow the QTL region on chromosome 9. Here we report further analysis of the original and additional F2 mice using more genetic markers.

The total number of F2 mice now stands at 1564. This includes the original 633 females, 466 additional females and 465 additional males. The total number of genetic markers genotyped is 23 markers (**Table 1**). These markers cover the 4 to 55 cM or 10 to 101 Mb region of chromosome 9, which is 124 Mb long. Because the peaks of wound healing/soft tissue regeneration QTLs, sth8 and sth9 were localized at 31.7 and 41.5 cM on chromosome 9 (Masinde et al., 2001), it can be seen that the genotyped chromosomal region covers the sth8 and sth9 QTL region.

For fine mapping the soft tissue QTL on chromosome 9, we carried out two analyses, one with MapQTL (Van Ooijen. 2004) and the other with the shrinkage analysis (Wang et al., 2005). Analysis using MapQTL showed that the LOD score was greater than 25 in the analysis of combined F2 (**Figure 1**). This was much higher than the 16 obtained in the original analysis (Masinde et al., 2001). By examining the two LOD score intervals of individual peaks within the chromosome 9 QTL region, we were able to identify four peaks. These four peaks are located in the 60 Mb to 98 Mb (or 30 to 49 cM) region (**Figure 1, Table 2**). The combined length of the two LOD score intervals of the four peaks was only 28.23 Mb, with peak 4 of only 3.28 Mb (**Table 2**). These results indicate that there may be multiple genes (at least one locus under each peak) within this QTL that are responsible for the observed QTL on chromosome 9. In addition, the designation of individual peaks with this QTL would help to prioritize the candidate genes for further study. For example, one might wish to study the candidate genes underneath peak 4, since it is the highest peak within this QTL.

Recently, a Bayesian shrinkage estimation strategy was developed to map multiple QTL (Wang et al., 2005). The Bayesian shrinkage estimation allows marker intervals that contain no

QTL to have estimated effects close to zero, whereas the intervals containing noticeable QTL to have estimates subject to virtually no shrinkage. We analyzed the combined data using this shrinkage analysis (**Figure 2**). Three peaks were identified, corresponding to three of the four identified with MapQTL, with peak 3 as the largest. Under this method, peak 3 defined by marker D9Mit196 at 86.33 Mb and D9Mit9 at 87.62 Mb explained 35.81% of variance in the F2 population (**Table 3**). The summarized length of genomic area directly under the three peaks was only 4.28 Mb compared to the 28.23 Mb from MapQTL, thus significantly narrowing down the chromosome region for further consideration. This would help to prioritize the candidate genes that can be further studied.

In conclusion, we have used a total of 1564 F2 mice of MRL X SJL and 23 markers to map the chromosome 9 QTL. This QTL has been localized on the 68 – 98 Mb region with four peaks defined. The combined length of the two LOD score intervals of these peaks was 28.23 Mb. The shrinkage analysis showed that the summarized genomic length under the QTL effect peaks was only 4.28 Mb. This analysis provided a much shorter chromosomal region where candidate genes need to be examined.

Chromosome 9 congenic analysis.

One way to narrow down the QTL region is to develop congenic strains which contain the desired allele of the QTL. After one or more congenic strains are created, sub-congenic lines can be generated that carry different length fragments of the QTL chromosomal region. Phenotypic analysis of these sub-congenic lines would lead to identification of the exact chromosomal location of the QTL. The objective of our congenic analysis was to develop congenic and sub-congenic lines in the poor healer SJL background that contain the better healing allele of the chromosome 9 QTL from super healer MRL, then evaluating the performance of these congenic lines in the healing phenotype.

In order to develop congenic lines, we first crossed F1 female mice of MRL X SJL back to SJL/J males (recurrent parent). We obtained N2 mice. N2 mice were genotyped using markers specific for the QTL region on chromosome 9 (**Table 1**). N2 heterozygous females that carried the MRL genotype in the QTL region were crossed back to SJL/J males to produce N3 congenics, which were again genotyped using the same markers. This process was repeated for more than 8 generations (N8). The overall proportion of contribution of genome by the non-recurrent parent can be estimated by the formulae of $(1/2)^{(8-1).}$ Thus, the MRL/MpJ genome present at the N8 congenics was only 0.78%. In other words, the genomic composition of an N8 congenic is almost identical to the recurrent SJL/J parent, with the exception of the MRL/MpJ contribution of the selected QTL region.

For phenotypic evaluation in healing, ear punch was done on the 3 weeks old animals of the congenic mice. Ear punch closure measurement was made at days 3, 7, 15, 21, and 25 after the punch was made. Fifteen male and fifteen female mice from each homozygous congenic line plus the MRL and SJL parental lines were used in the phenotype analysis. The methods of both phenotyping and genotyping were described previously (Li et al., 2001; Masinde et al., 2001; Masinde et al., 2005).

As we mentioned in the last year's report, we had already obtained the heterozygous congenic mice at the N8 and N9 generations. These congenic mice carry a MRL chromosome 9 fragment delimited by D9Mit207 (31.7 cM or 60.8 Mb) and D9Mit151 (69.9 cM or 121.5 Mb). It can be seen that this fragment covers the positions of 31.7 and 41.5 cM where the sth8 and sth9 QTLs are located. We have now obtained one homozygous congenic line named 9-1 at the

N8 generation carrying this fragment (Table 4). At the same time, we are making backcross 9-1 to SJL to generate sub-congenic lines that contain parts of the chromosome 9 QTL fragment. We are now breeding to produce pubs for one sub-congenic line named 9-2.

We have finished evaluating the phenotype of the homozygous congenic line 9-1. In male mice, it appears there is a trend of improved healing performance for the congenic animals when compared with the SJL parentals (**Figure 3**). However, in the female animals, there was no such trend (data not shown). The 9-1 line is only one of the several congenic and sub-congenic lines we are evaluating. More congenic lines would provide better proof of performance of the chromosome 9 congenic lines in comparison with the parental strain SJL.

In conclusion, we have created a homozygous congenic line 9-1 at the N8 generation. This congenic line carries the entire chromosome 9 QTL region. In the male mice, it appears that this congenic line healed better than the SJL parentals. Currently, we are evaluating the healing performance of other congenic lines.

Congenics on chromosomes 1 and 4.

As we have mentioned, there are 10 QTLs that were identified in the cross of MRL X SJL (Masinde et al., 2001). Besides the chromosome 9 QTL, which is the largest, the next largest is on chromosome 1. With a LOD score of 7, this QTL explained about 7% of the F2 phenotypic variance. Therefore, it is a very important QTL to study in wound healing/soft tissue regeneration.

The reasons to study the chromosome 4 QTLs are multi-folds. First, like the chromosome 9, chromosome 4 harbors two QTLs for wound healing/soft tissue regeneration: sth3 at 21.9 Mb and sth4 at 50.3 cM (Masinde et al., 2001). With LOD scores of above 6, they each explained about 6% of the phenotypic variance in the F2 of MRL X SJL. They can be considered the third largest QTLs in this cross. Secondly, one of the chromosome 4 QTLs, sth4, is present in multiple crosses. We believe that it is the same as heal8, identified in the MRL X B6 cross, associated with markers D4Mit13 at 71 cM (Blankenhorn et al., 2003) and D4Mit148 at 66.7 cM (Heber-Katz et al., 2004). It was also found as Earheal2, associated with D4Mit170 at 66.6 cM in DBA X 129, with a better healing allele contributed by DBA (Masinde et al., 2005). Our recent analysis with the cross of MRL X CAST also showed that two markers at positions 60 and 66.6 cM on chromosome 4, D4Mit203 and D4Mit170, were also associated with peaks of significant LOD scores (Yu et al., 2005).

The method of developing congenic lines have been described in the previous section. Basically, it involves the crossing and backcrossing of the parental strain (i.e. donor) carrying the better healing allele of the QTL to the other parental strain (i.e. recurrent parent), coupled with selection of the desired DNA fragment from the donor parent. A congenic line is achieved usually at 10^{th} generation when it can be maintained as homozygous line.

For chromosome 1 congenics, we have advanced the crossing to the N4 generation. The congenic fragment from the MRL parent is from 0 to 110 cM on chromosome 1 (**Table 5**). This covers the QTL peak at 49.2 cM. It can be seen that three mice 2F, 3F, and 7F are all heterozygous for the chromosomal region, and can be backcrossed to SJL to advance the congenics to N5.

For chromosome 4 congenics, we have advanced the crossing to the N7 generation. The congenic fragment from the MRL parent is from 8.7 cM to 76.5 cM (**Table 6**). This chromosomal fragment covers both QTLs sth3 at 21.9 cM and sth4 at 50.3 cM. We have one mouse at N7 and 5 mice at N6. We are breeding the N7 mouse to obtain the N8 generation. At

N8, we will intercross the heterozygous males and females to obtain the congenic line with both homozygous male and female animals. Then, from this we will generate more animals for this congenic line, and to perform phenotypic evaluation in comparison with the recurrent parent SJL.

In conclusion, we have obtained N4 congenic for the chromosome 1 QTL and N7 congenics for the chromosome 4 QTLs. We are in the process of generating the N8 homozygous animals for the chromosome 4 QTL. We will be evaluating these congenics for their healing performance.

Specific Objective 2: To develop in vitro functional assays to measure the differentiation, proliferation and apoptosis of keratinocytes and dermal fibroblasts in monolayer culture and the injured year in the organ culture (the latter will be used if the in vitro assays are unsuccessful in distinguishing the phenotypes.

a) For *in vitro* testing of our candidate genes in the above assays, we will develop functional assay in which the candidate genes in the form of overlapping BAC clones are inserted into viral vectors and applied to cells *in vitro* for evaluating the effect of overexpression of candidate genes in our two cell models.

In our preliminary experiments, we isolated the cells from the healing ear tissues from MRL and SJL mouse strains at different time points after injury. The tissues were digested using Type II collagenase and Dispase enzymes and primary cell cultures were established. These cells were used to measure the difference in the proliferation rate. However, we did not find any significant difference in the proliferation rate of cells isolated from healing tissue of MRL and SJL mice. We, therefore, switched our focus to use extracts from healing tissues from MRL and SJL mice to identify potential end points that could be used in our functional evaluation of candidate genes.

Our group and others have shown that scarless wound healing in MRL mice is genetically controlled and involves the expression of a wide variety of genes. Since the gene expression in response to extracellular signals is regulated through the activation of various signal transduction pathways and transcription factors, we investigated the difference in the activation of various transcription factors and signaling pathways in healing tissues of MRL and SJL mice. For these experiments, around 1 mm healing tissues around the ear punch hole were collected from MRL and SJL mice. These tissues were processed for the isolation of nuclear and cytoplasmic extracts using protocols previously described (Kumar, A., and Boriek, A. M., 2003, Kumar et al., 2002, Kumar et al. 2003). Nuclear extracts were used to study the activation of various transcription factors. In brief, nuclear extracts from the control and healing tissues were incubated with set of oligonucleotides consisting consensus sequences for the different proinflammatory transcription factor. Transcription factor-bound oligonucleotides were separated from the unbound oligonucleotides by passing them through a spin column. Transcription factor bound oligonucleotides were then denatured to make them single stranded and used to hybridize with a membrane that contains array of oligonucleotides for these transcription factors. The signal was developed using the reagents and protocols provided by the manufacturer. The results of the transcription factor array are presented in **Figure 4**. The representative data presented shows a drastic increase in the activity of many transcription factors in healing SJL tissue compared to control tissues.

The transcription factor data was analyzed for the fold change in the activity of various transcription factors. A significant increase in the activity of inflammation- associated transcription factors such as AP-1, AP-2, c-Myb, GRE, HNF-4, NF-E2, NF-κB, p53, Stat4 and thyroid hormone receptor (TR) was observed in regenerating SJL mice (**Figure 5**). The activity of many of these pro-inflammatory transcription factors increased to a much smaller extent in the healing tissue of MRL mice compared to SJL mice (data not shown).

Among many transcription factors involved in mediating the immune and inflammatory response, NF-κB is prominent. Since there was higher activation of NF-κB in healing tissue of SJL mice, we compared the activation of NF-κB in MRL and SJL mice using Electrophoretic mobility shift assay (EMSA). For these experiments, the nuclear extracts from control and healing tissues of MRL and SJL mice were prepared by using low salt and high salt buffers. Concentration of proteins was measured using BioRad protein assay reagent. Equal amount of nuclear proteins from different samples was incubated with ^{32}P-labeled oligonucleotides consisting NF-κB consensus sequences. NF-κB/DNA complex was then separated on a 7.5% native polyacrylamide gel electrophoresis. The gels were dried and the DNA-binding activity of NF-κB was quantified using ImageQuant software. Interestingly, we found that the activation of NF-κB was significantly higher in SJL mice compared to MRL mice (**Figure 6**) suggesting increased inflammatory response in SJL mice compared to the MRL mice.

Different combinations of Rel/NF-κB proteins can constitute an active NF-κB heterodimer that binds to specific sequences in DNA (Karin, M. and Delhase, M. 2000, Karin, M. and Lin, A. 2002). To know the constituents of NF-κB complex visualized by EMSA in regenerating SJL tissues, we performed super-shift analysis by a method described previously (Kumar, A., and Boriek, A. M., 2003, Kumar et al. 2003). Nuclear extracts were incubated with antibody to p50, p65, p52, RelB, or c-Rel and then conducted EMSA. Antibody to either p50 or c-Rel subunits of NF-κB shifted the band to a higher molecular weight (**Figure 7**), suggesting that the activated NF-κB complex consisted mainly of p50 and p65 proteins. Irrelevant antibodies such as anti-JNK1 had no effect on the mobility of NF-κB (**Figure 7**).

The activation of NF-κB by inflammatory cytokines such as TNF-α is achieved through the phosphorylation of IκBκ at ser-32 and ser-36 residue followed by its polyubiquitination and degradation (Kumar et al. 2004). The degradation of IκBα leads to the nuclear translocation of NF-κB. We studied whether the activation of NF-κB in regenerating soft tissue in SJL mice was associated with the phosphorylation and degradation of IκBα. The cytoplasmic extracts from control and regenerating SJL tissues were subjected to Western blot analysis, using antibodies that detect phosphorylated IκBα or total IκBα protein. The data presented in **Figure 8A** show that the phosphorylation level of IκBα protein is increased in regenerating soft tissue from the SJL mice. The increased phosphorylation of IκBα was associated with the degradation of IκBα protein (**Figure 8A**).

The degradation of IκBα is preceded by its phosphorylation by IκB kinase (IKK) at ser-32 and ser-36 residue (Kumar et al. 2004). We investigated the activation of IKK in healing ear tissue in SJL mice. The cytoplasmic extracts prepared from regenerating tissue of SJL mice were immunoprecipitated with IKKγ antibody and the kinase activity was determined using GST-IκBα (1-54) as a substrate. A significant increase in the IKK activity was observed in regenerating soft tissue in SJL mice (**Figure 8B**).

We also studied the expression of the genes involved in the activation of NF-κB transcription factor in SJL mice. For these experiments, the RNA was isolated from control and

SJL mice 2 days post-injury. The RNA was converted into cDNA and was used to hybridize with the pathway specific NF-κB array. The data presented here suggest that the expression of several genes involved in the activation of NF-κB signaling pathway were increased in regenerating SJL mice (**Figure 9**). We have thus clearly established that the activation of pro-inflammatory transcription factor NF-κB is prominent in SJL mice and can be a useful functional assay for studying soft tissue regeneration.

b) We will develop siRNA for these cell types.

Since very specific pharmacological and peptide inhibitors of NF-κB are available commercially, we decided to use specific inhibitors of NF-κB to study its involvement in tissue healing in MRL and SJL mice. Specifically, we used NEMO binding peptide (NBD) which inhibits the activation of NF-κB transcription factor by preventing interaction of IKK-γ subunit with IKKα and IKKβ of the IKK complex. Since NF-κB is activated to a greater extent in the poor-healer SJL compared to fast healer MRL, we hypothesize that inhibition of NF-κB should lead to the promotion of wound healing in SJL mice. To test this hypothesis, SJL mice were given i.p. injection of 5mg/kg of body weight, and the healing rates of ear punch hole are being monitored. These experiments are still in progress and we should get data in next 2-3 weeks.

Specific Objective 3.

Work proposed in this Specific Objective will be initiated shortly.

Additional Progress

To confirm the QTL we identified in the MRL X SJL cross, we have also completed genotyping of additional crosses: DBA X 129 and MRL X CAST. One of the inbred lines we used was CAST. CAST is relatively distant genetically from other commonly used strains. To confirm that chromosome 9 QTL also exists in MRL X CAST would demonstrate the presence of this QTL in diverse genetic backgrounds. In addition, there are more polymorphisms available between CAST and MRL. More polymorphic markers between the two strains provide a better opportunity to conduct fine mapping.

Currently, genotyping of both DBA X 129 and MRL X CAST crosses has been completed. Results have been published (Masinde et al., 2005; Yu et al., 2005). In DBA X 129, a totally different cross, there is no super healer. However, DBA healed much better than 129 (**Figure 10**). Genome scan revealed significant QTLs on chromosomes 1, 4, 12, and 18 (**Table 7, Figure 11**). Among these four QTLs, three were contributed by the good healer DBA, while one was contributed by the poor healer 129. The four QTLs named earheal1 to earheal4 explained about 17.1% of the F2 phenotypic variance.

In the MRL X CAST cross, we found that there are two chromosomal regions at 26 cM and 49-61 cM on chromosome 9 that showed significant LOD scores (Yu et al., 2005). These two regions correspond to the soft tissue QTLs sth8 and sth9, respectively, identified in MRL X SJL in our early study (Masinde et al., 2001). Therefore, the chromosome 9 QTL in the MRL X SJL has been confirmed in the cross of MRL X CAST. In addition, we have also identified QTLs on chromosome 4 at 60-66.6 cM positions and chromosome 7 at 53.3 cM position. These are also the same as those named sth4 and sth7 in the MRL X SJL cross (Masinde et al., 2001). By using CAST, we were also able to identify new QTLs that were not present in MRL X SJL. One such example is the chromosome 17 QTL at 22.9 – 45.3 cM (Yu et al., 2005). The high BMD

allele of this QTL was contributed by the CAST parent. This QTL has been previously identified as heal13 in the same cross by another group (Heber-Katz et al., 2004).

The interesting observation in DBA X 129 is that the average healing rates of F1 and F2 were similar to that of the poor healer 129 (**Figure 10**). If we are to examine the healing genes from the good healing point of view, the healing phenotype exhibited a recessive mode of inheritance. This is completely different from the cross of MRL X SJL, where the average healing rates of the F1 and F2 were midway between those of the super healer MRL and the poor healer SJL. In other words, the MRL X SJL showed the additive mode of inheritance. In the other cross, MRL X CAST (Yu et al., 2005), the mode of inheritance was in contrast to DBA X 129. The average healing rates of the F1 and F2 were similar to that of the super healer MRL. Therefore, in MRL X CAST, it is the dominant mode of inherence. Different mode of inheritance in different crosses may reflect the differential consequences of gene interactions in different genetic backgrounds. This warrants further studies, which may help reveal the molecular mechanisms of healing process.

The sth4 on chromosome 4 QTL initially identified in MRL X SJL (Masinde et al., 2001) is also present in our two other crosses, DBA X 129 and MRL X CAST, and another previously published cross MRL X B6 (Blankenhorn et al., 2003). This makes it a very important common QTL. Common QTLs that are present in multiple crosses may be very useful for identification of the underlying genes that are responsible for these QTLs. By constructing the haplotype information (using either SNPs or DNA sequences) of the parental lines involved in these crosses would help pinpoint the exact DNA polymorphisms or mutations that may be responsible for the QTLs.

In order to identify the candidate genes for the Chr 9 QTL regions, we used gene expression analysis, specifically microarray, to screen genes on Chr 9. Our hypothesis is that any candidate genes for wound healing and STR would be expressed differentially between super healer MRL and poor healer SJL. Microarray was carried with two mouse strains, MRL and SJL. The experiment was carried out with 5 female MRL mice and 5 female SJL mice. Three weeks old mice were ear-punched. The punched-out tissue served as the control of each mouse. At day 4 after the ear punch, about 2 mm wide tissues surrounding the ear punch was cut as treatment. RNA was isolated for microarray analysis. We used the Oligator "MEEBO" Mouse Genome Set (illumina, San Diego, CA) for the microarray, which contained 27,784 genes.

Data analysis was carried out using GeneSpring software (Agilent Technologies, Palo Alto, CA). Fold change was the main measure of differential expression between the treatment and the control. Based on our experience, this measure tends to underestimate the difference in gene expression. For example, 1.5 fold change could actually reflect more than 2 fold of difference, the usually cutoff in microarray studies. We tried to use the spike-ins controls to correct this discrepancy in data analysis. The spike-ins were RNA samples with known ratios between C3 and C5, the two dye channels that are used to label the treatment and the control. The median fold change for each of the seven spike-in controls was calculated. Then, the fold change was made linear to percentage change with positive and negative numbers to represent up or down regulation, respectively. Linear regression was then carried out using the input RNA ratio as the dependent variable and the linear percentage change as independent variable. Finally, the regression formulae were used to predict input ratios for the genes on the chip from their linear percentage change calculated from fold change.

We have identified 1,745 genes that were significantly different between the day 4 ear-punch treatment and the day 0 control in either MRL alone, SJL alone or both strains (**Table 8**).

In MRL, 811 genes were significant, with 11 genes greater than 1.5 fold up regulation and 9 greater than 1.5 fold down regulation. In SJL, there were 882 significant genes, 40 and 25 genes in 1.5 fold down and up regulation, respectively. Forty-two genes were up or down regulated at the same time in MRL and SJL, and 10 genes showed mixed pattern of regulation.

Genes with more than 1.5 fold of change are listed in **Table 9**. There were mainly three types of genes that were differentially expressed genes between the treatment and the control, i.e genes induced by soft tissue injury. The first category was genes of small proline-rich proteins. The second category was cell structure-related genes. These included genes for actins, keratins, myosins, procollagens, and tubulins. The third category was genes for the proteases and their inhibitors.

As for the Chr 9 QTL genes, there are 791 known genes between 55 Mb and 124 Mb on Chr 9 as of June 2006 and based on the mouse genome build 36.1 from NCBI. Among these, 491 were on the chip, with 7 genes per Mb. The other 300 genes were not included in the microarray, and could still be involved in wound healing and STR. Out of the 491 genes, 28 were significant (**Table 10**). Two of these genes showed greater than 1.5 fold down regulation (**Table 11**). In terms of expression profiles that fit the criteria of the candidate genes for the Chr 9 QTLs, they should be uniquely differentially expressed in either super MRL or poor healers such as SJL. This differential expression can be in the form of either down or up regulation. These two genes all fit these criteria.

In conclusion, most differentially expressed genes, either in MRL or SJL alone, or in both strains, were related to small-proline proteins, cell structural proteins, and matrix metalloproteinases and their inhibitors. Finally, based on expression patterns in MRL or SJL alone, we have identified 2 candidate genes in the Chr 9 QTL region for further examination.

As we know, no microarray is capable of including every gene of a specific genome. Accordingly, our microarray analysis only covered about half of the candidate genes in the Chr 9 QTL region. Even if some genes were in the microarray, we still needed to confirm the microarray results through alternative means. For this purpose, we conducted real time PCR. We chose 36 candidate genes in the QTL region (**Table 12**). These genes are located within QTL peaks 1 (13 genes), 2 (5 genes), 3 (14 genes), and 4 (4 genes). Some of these genes such as Oaz2 were also included in the microarray. Again, as with the microarray, we used both super healer MRL and poor healer SJL in real time PCR. For each three week old mouse used in the experiment, the ear tissues at day 0 were used as the control, and the day 4 tissues after the ear punch were used as the treatment. We used three mice as three biological replicates for each gene. We carried out three PCR reactions for each mouse RNA sample pair. In other words, we had three technical replicates for each biological replicate. Therefore, we had a total of nine replicates for each treatment/control.

The real time PCR experiments are ongoing. **Table 13** shows some genes for which we have finished all nine replicates and obtained significant results in real time PCR. They showed greater than 2 fold up regulation after the ear punch injury. Most interesting of these were Usp3 at 66.32 Mb under QTL peak 1 and Ccpg1 at 72.78 Mb under QTL peak 2. Usp3 was up regulated 5.87 fold in the MRL injured ear tissues (**Table 13**). However, it was up regulated only modestly 1.75 fold in SJL. Similarly, CCpg1 was up regulated 4.90 fold in MRL and stayed almost the same with 1.13 fold change in SJL. The differential expression patterns of these two genes might explain part of the phenotypic difference between MRL and SJL in ear punch healing, i.e. the part caused by the Chr 9 QTLs. In other words, the Chr 9 QTLs were caused by

the up regulation of these two genes in super healer MRL and almost unchanged regulation in poor healer SJL.

In conclusion, the real time PCR analysis of 36 candidate genes for wound healing and soft tissue regeneration has yielded promising results with several genes showing significant up regulation in both MRL and SJL. Two genes Usp3 and Ccpg1 showed differential expression patterns in MRL and SJL that fitted the criterion of strong candidate for the Chr 9 QTLs.

We have also conducted fine mapping on the chromosome 4 QTLs. The chromosome 4 QTLs have been detected in all the three crosses we have generated in the previous studies (Masinde 2002; 2006; Yu 2005): MRL X SJL, MRL X CAST, and DBA X 129. However, only a few markers were used in each cross. For example, five markers were used in the original study with the MRL X SJL cross (Masinde 2002). We have further mapped this QTL region by genotyping the additional F2 mice of MRL X SJL (474 males and 473 females) we have bred. We have genotyped five additional markers (**Table 14**).

Significant LOD scores were obtained from both the female (**Figure 12A**) and male (**Figure 12B**) mice of the new MRL X SJL. The highest LOD score was 7.42, and occurred between D4Mit31 and D4Mit308 in the females (**Figure 12A**). In the males, the highest LOD score was 5.72, and occurred between D4Mit178 and D4Mit31 (**Figure 12B**). In a separate analysis, we have combined these data with the 633 female mice from the original study (with a total of 1580 mice). The obtained LOD score was 20.02 at the highest peak at 115.07 Mb between D4Mit31 and D4Mit308 (**Figure 12C**). The 2-LOD Interval spanned from 107.07 Mb to 123.07 Mb. The explained phenotypic variance was 7.3%. In conclusion, we have confirmed existence of the chromosome 4 QTLs in the male mice as well as in the additional female mice of MRL X SJL. In order to identify the genes that cause these QTLs, we will further study these QTLs, including using congenic technique.

Table 1. Markers used to map soft tissue QTL on chromosome 9.

Marker	WI Map[a] (cM)	MGI Map [b] (cM)	Physical Dis.[c] (Mb)
D9MIT43	2.2	4	10.09
D9MIT90	7.7	9	32.49
D9MIT229	23	28	49.66
D9MIT71	24	29	50.34
D9MIT207	31.7	33	60.78
D9MIT208	33.9	36	62.49
D9MIT336	33.9	35	65.82
D9MIT263	40.4	42	75.97
D9MIT270	41.5	43	76.45
D9MIT343	41.5	43	80.87
D9MIT133	41.5	43	84.52
D9MIT196	42.6	48	86.33
D9MIT111	42.6	48	86.99
D9MIT9	42.6	48	87.62
D9MIT269	41.5	43	88.38
D9MIT157	43.7	49	89.75
D9MIT308	43.7	49	90.59
D9MIT344	42.6	48	94.22
D9MIT76	43.7	49	95.5
D9MIT35	47	52	98.64
D9MIT114	47	52	98.65
D9MIT355	49.2	49.2	98.66
D9MIT182	53.6	55	101.42

[a] Whitehead Mouse Genetic Map

[b] Mouse Genome Database Genetic Map

[c] Physical distance as of September 20, 2004

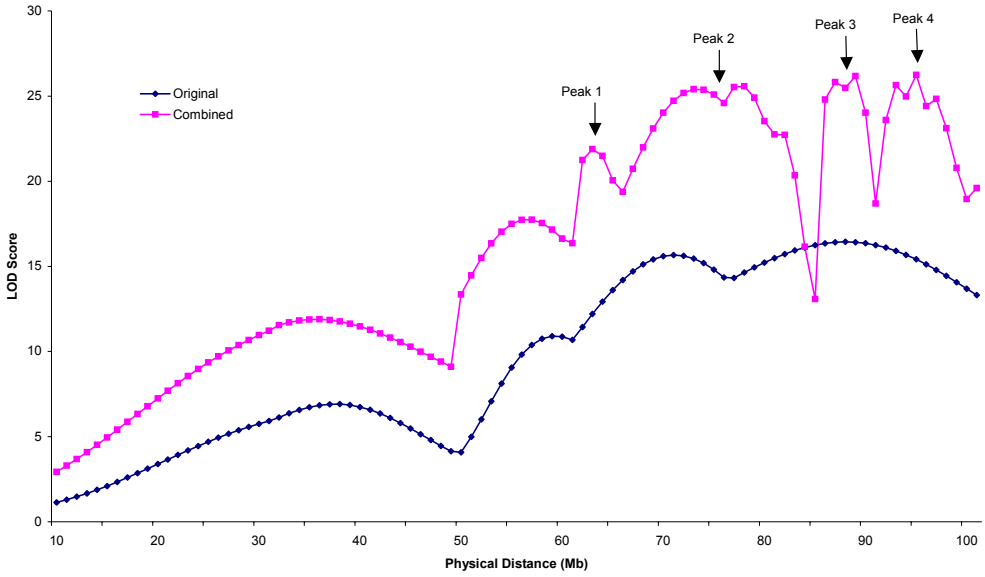

Figure 1. **LOD scores of wound healing/soft tissue regeneration QTL on chromosome 9 in the original 633 female mice (denoted as Original) (Masinde et al., 2001) and 1564 male and female mice (denoted as Combined) of the F2 of MRL X SJL.** Arrows identify four peak positions defined by the two LOD interval.

Table 2. Chromosome 9 QTL peaks determined from the results of MapQTL analysis.

Peak	Position (Mb)	LOD Score	Variance explained (%)	2 LOD interval (Mb) [a]	Interval length (Mb)	Flanking markers
1	63.49	21.88	6.60	60.78 - 65.82	5.04	D9Mit207,D9Mit336
2	78.45	25.58	7.90	68.82 - 84.50	15.68	D9Mit336,D9Mit343
3	89.38	26.18	8.00	85.52 - 89.75	4.23	D9Mit133,D9Mit157
4	95.20	26.25	8.20	94.22 - 97.50	3.28	D9Mit344,D9Mit35

[a] Positions where LOD scores were 2 less than that of peak position.

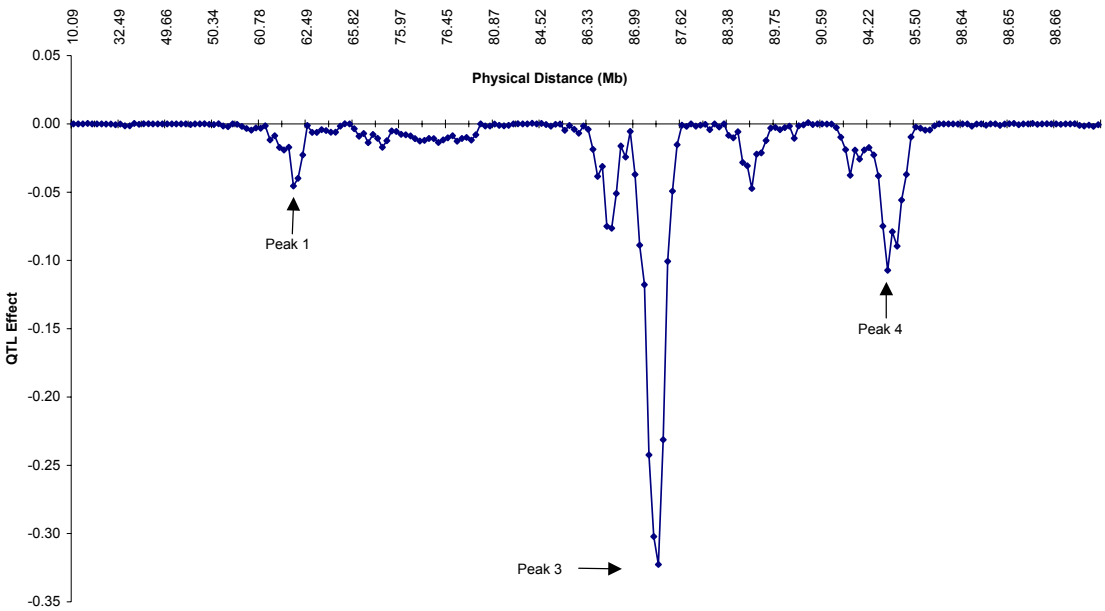

Figure 2. The additive effect of soft tissue regeneration QTL on mouse chromosome 9 using Bayesian shrinkage estimation approach (Wang et al., 2005). Numbers above the graph indicate the marker positions in MegaBase (Mb). Arrows identify three peak positions.

Table 3. Chromosome 9 QTL peaks determined from the results of Shrinkage analysis.

Peak[a]	Position (Mb)	Peak effect	Variance explained (%) [b]	Peak interval (Mb)	Interval length (Mb)	Flanking markers
1	61.98	-0.045	0.71	60.78 - 62.49	1.71	D9Mit207,D9Mit208
3	87.31	-0.323	35.81	86.33 - 87.62	1.29	D9Mit196,D9Mit9
4	94.73	-0.107	3.95	94.22 - 95.50	1.28	D9Mit344,D9Mit76

[a] Peak numbers correspond to those in Table 3.

[b] $=1/2*a^{2}*/V_p$ where a is the effect, and V_p is the phenotypic variance.

Table 4. Genotypes of N8 congenic mice for chromosome 9 markers at different chromosomal positions.

	D9MIT207	D9MIT336	D9MIT263	D9MIT270	D9MIT157	D9MIT35	D9MIT355	D9MIT182	D9MIT347	D9MIT350	D9MIT201	D9MIT151
Congenic	31.7 cM	33.9 cM	40.4 cM	41.5 cM	43.7 cM	47 cM	49.2 cM	53.6 cM	55.7 cM	60.1 cM	63.4 cM	69.9 cM
Line	60.8 Mb	65.8 Mb	76.0 Mb	76.5 Mb	89.8 Mb	98.6 Mb	98.7 Mb	101.4 Mb	103.2 Mb	111.4 Mb	117.4 Mb	121.5 Mb
9-1	M	M	M	M	M	M	M	M	M	M	M	M

M denotes the homozygous genotype for MRL in the SJL background.

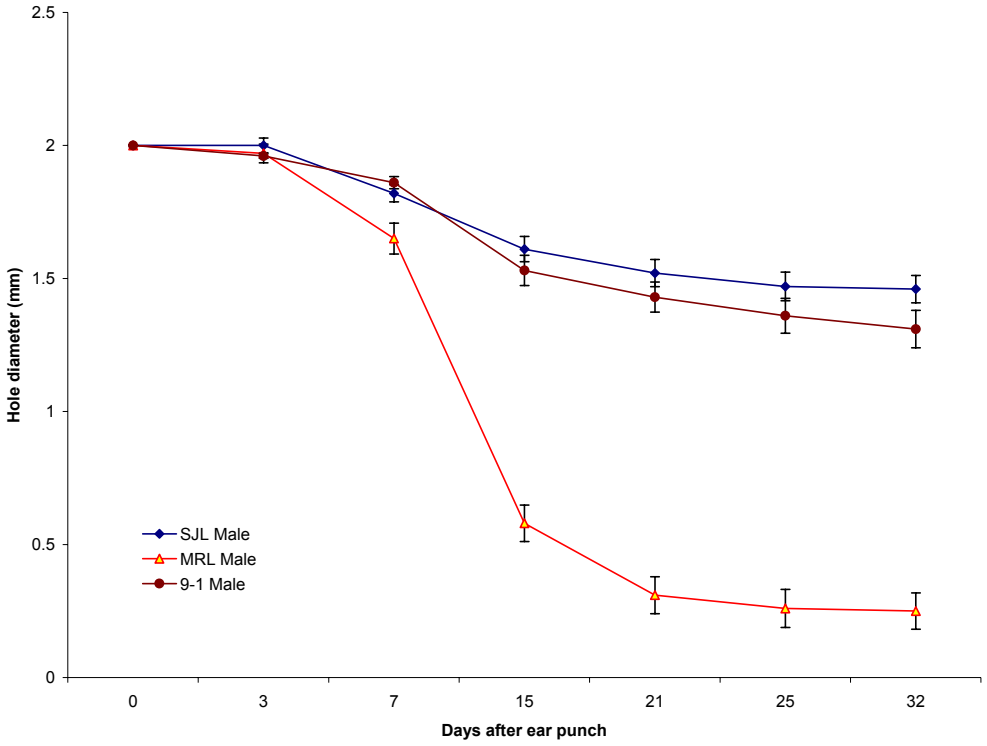

Figure 3. **Ear punch closure healing rate in the male mice of homozygous congenic line 9-1 and the parental MRL and SJL.** Fifteeen animals were in each group. Data values are shown as the Mean±SEM (Standard Error of the Mean). The number of mice was 15 in each group.

Table 5. Genotypes of N4 congenic mice for chromosome 1 markers at different chromosomal positions.

Mouse ID	D1MIT64 0 cM	D1MIT316 3.3 cM	D1MIT231 8.7 cM	D1MIT33 36.1 cM	D1MIT19 37.2 cM	D1MIT216 49.2 cM	D1MIT185 59 cM	D1MIT102 75.4 cM	D1MIT291 103.8 cM	D1MIT17 110.4 cM
N4#2F	H	H	H	H	H	H	H	H	H	H
N4#3F	H	H	H	H	H	H	H	H	H	H
N4#7F	H	H	H	H	H	H	H	H	H	H

H denotes the heterozygous genotype between MRL and SJL.

Table 6. Genotypes of N6 and N7 congenic mice for chromosome 4 markers at different chromosomal positions.

Mouse ID	D4MIT18 8.7 cM	D4MIT196 16.4 cM	D4MIT214 21.9 cM	D4MIT178 30.6 cM	D4MIT31 50.3 cM	D4MIT203 60.1 cM	D4MIT204 61.2 cM	D4MIT170 69.9 cM	D4MIT42 76.5cM
N6#4M	H	H	H	H	H	H	H	H	H
N6#8F	H	H	H	H	H	H	H	H	H
N6#6M	H	H	H	H	H	H	H	H	H
N6#7M	H	H	H	H	H	H	H	H	H
N6#4F	H	H	H	H	H	H	H	H	H
N7#4F	H	H	H	H	H	H	H	H	H

H denotes the heterozygous genotype between MRL and SJL.

Table 7. QTL for fast wound healing detected in DBA x 129 mice population (combined male and female) using MapQTL program.

QTL designation	Marker	Distance (cM)	LOD score	% phenotypic variance explained	Source
earheal1	D1Mit406	101.2	4.1	6.3	129
earheal2	D4Mit170	66.6	2.9	4.3	DBA
earheal3	D12Mit118	45.0	3.1	2.9	DBA
earheal4	D18Mit12	17.0	3.2	3.6	DBA
Total phenotypic variance explained (%)			**17.1**		

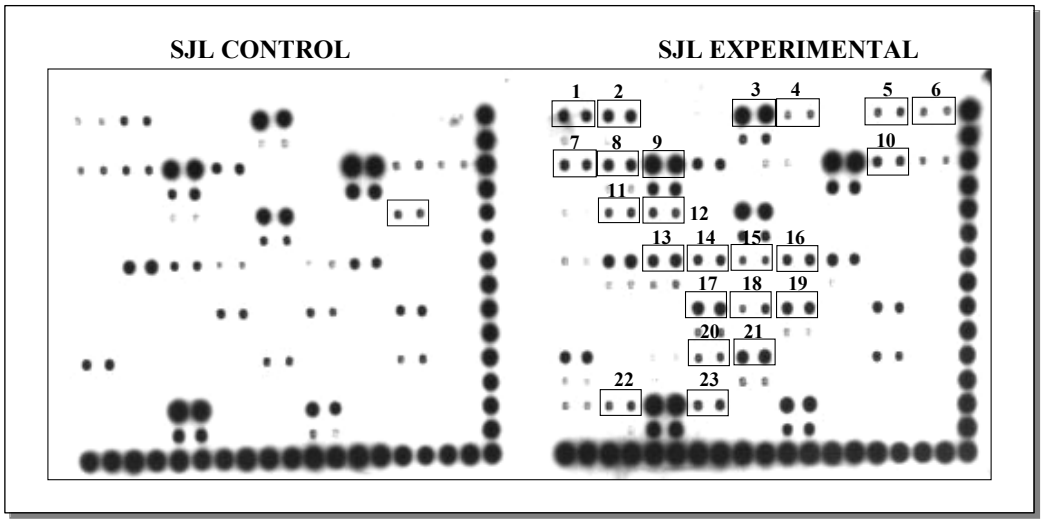

Figure 4. Increased Activation Of Proinflammatory Transcription Factors In SJL Mice. The activity of different proinflammatory transcription factor was measured in control and healing SJL mice. The results presented here show increased activity of several transcription factors in healing SJL mice.

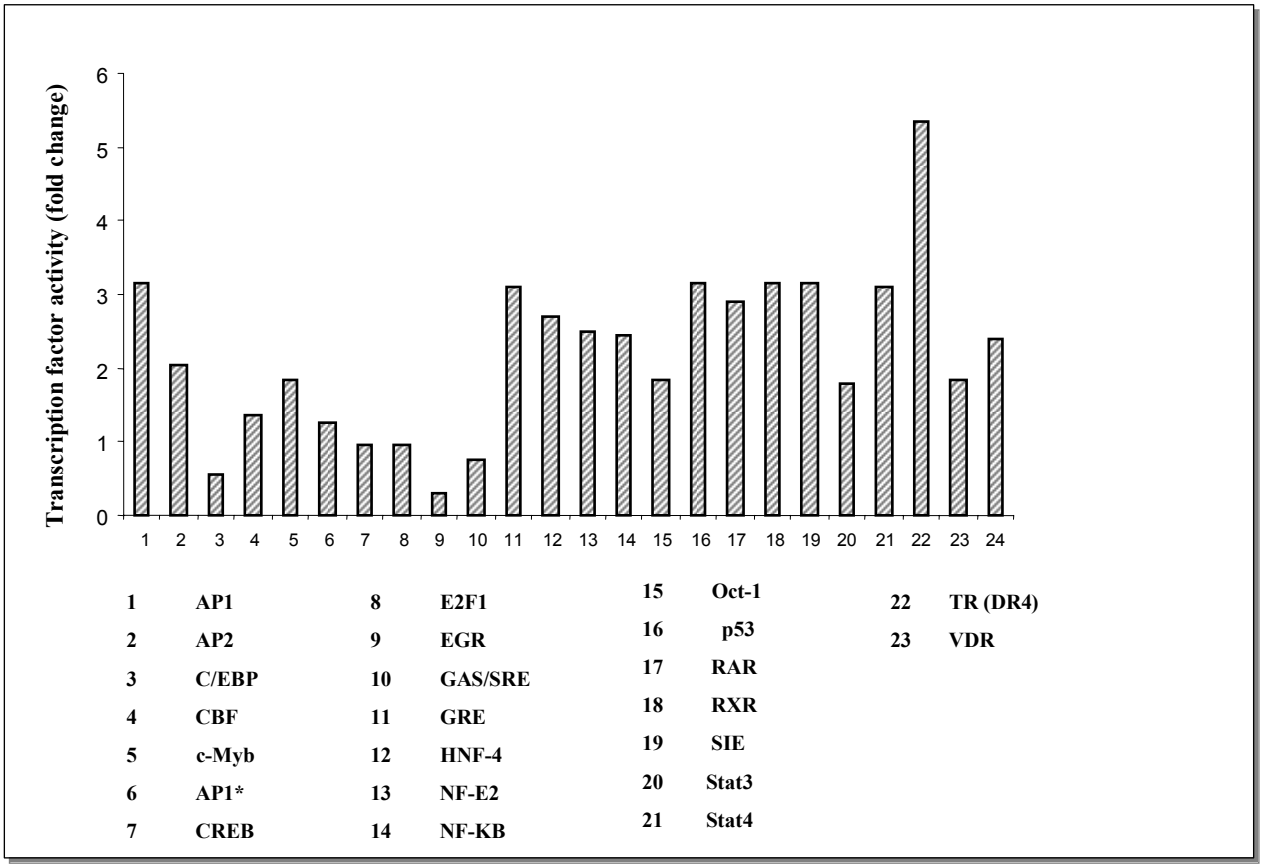

Figure 5. Fold Increase In The Activity Of Different Proinflmmatory Transcription Factors In Healing Tissue Of SJL Mice. Quantification of the array data showed 2-4 fold increase in the activity of indicated transcription factors in healing tissue of SJL mice compared to control tissue.

AP-1, Activator protein-1; AP-2, Activator protein-2; C/EBP, CCAAT/enhancer binding protein; CBF, C-repeat binding factor; CREB, cAMP-response element-binding protein; EGR, early growth response; GRE, glucocorticoid-responsive element:, HNF-4, hepatocyte nuclear factor-4; SIE, sis inducible element; NF-κB; nuclear factor-kappa B; RAR, retinoic acid receptor; TR, thyroid hormone receptor; VDR, vitamin D receptor.

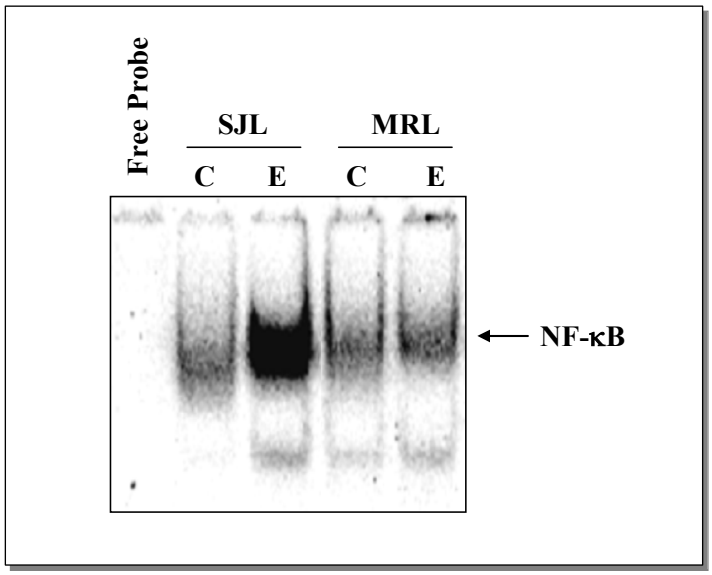

Figure 6. Higher Activation Of NF-κB Transcription Factor In SJL Mice Compared To MRL Mice. DNA binding activity of NF-κB transcription factor in healing tissue measured using EMSA shows higher activity in SJL mice compared to MRL mice.

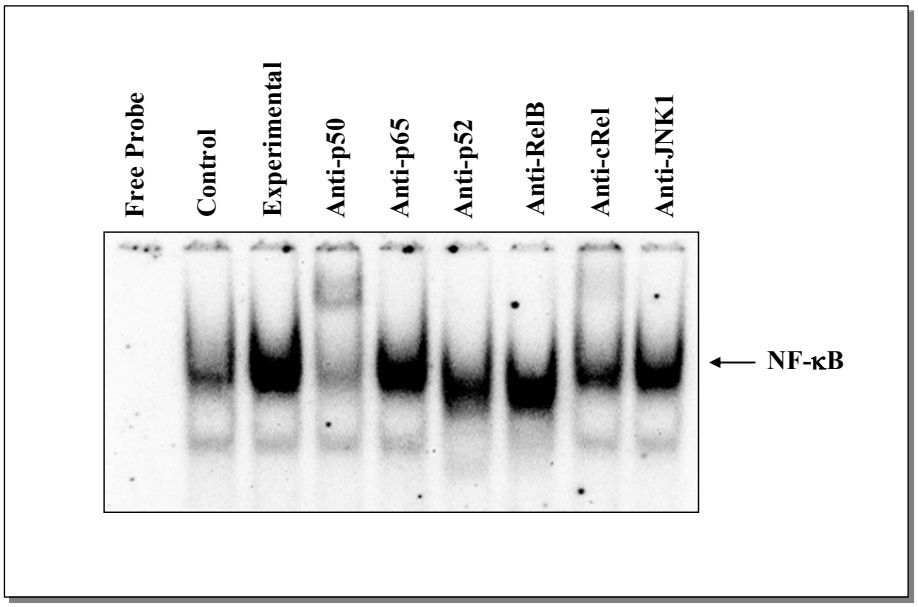

Figure 7. **Activated NF-κB Complex Consist P50 And C-Rel Subunits In Healing SJL Tissues.** Super-shift analysis of NF-κB/DNA complex suggests that activated NF-κB contains p50 and c-Rel subunits in healing tissue of SJL mice

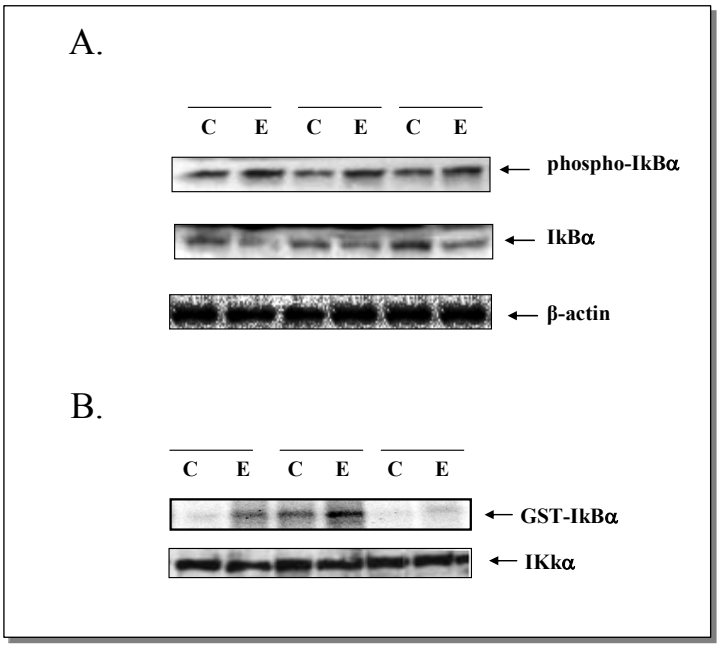

Figure 8. Activation Of NF-κB Involves Phosphorylation And Degrdation Of IKBα Protein. **A**). The tissue lysates form healing mice were subjected to western blot analysis using phosphor-specific or total IκBα antibody. The data shows higher levels of phosphorylated IκBα protein in healing ear tissue compared to control. Total cellular levels of IκBα protein was decreased in healing tissue compared to controls. **B**). Higher enzymatic activity of IKK was observed in healing tissue compared to controls. C, control; E, experimental.

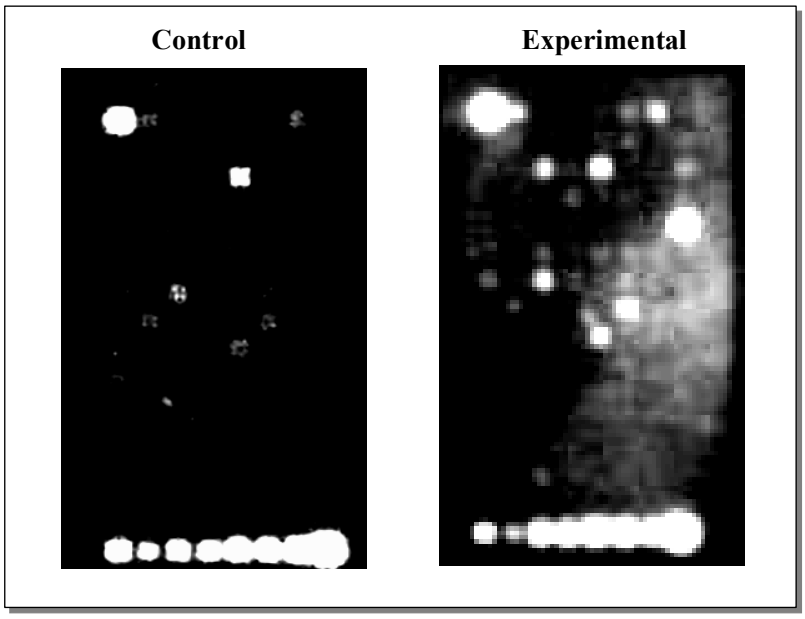

Figure 9. **Increased Expression Of NF-κB Pathway Related Genes In Healing Tissue.** NF-κB pathway specific array analysis revealed increased expression of genes involved in the activation of NF-κB transcription factor in

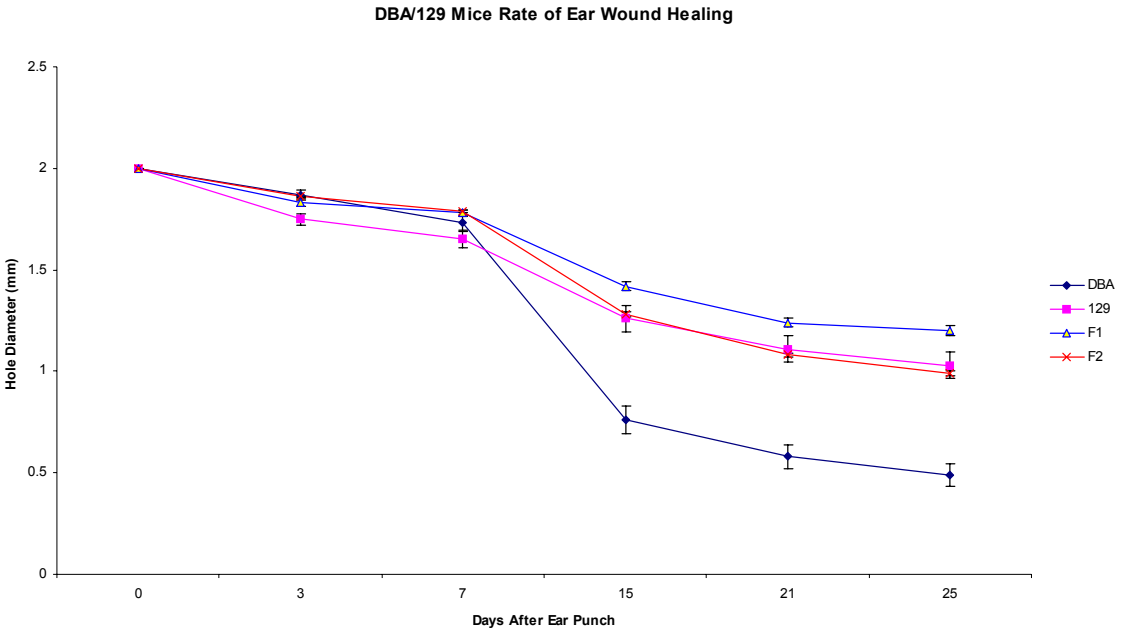

Figure 10. Line graph of the ear punch hole diameter measured from day 0 to day 28 in the DBA and 129 parental strains, and their F1 progenies. DBA (a good healer) heals much faster than 129 (a poor healer), while F1 heals more poorly than the 129.

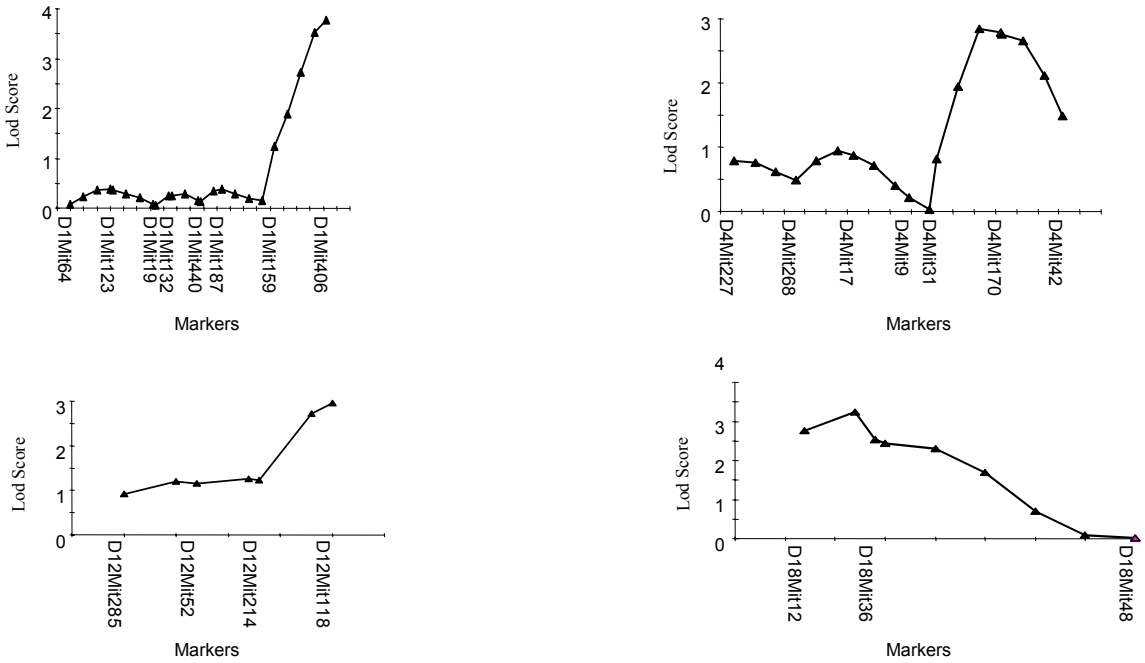

Figure 11. Interval maps for chromosomes 1, 4, 12, and 18 shown to carry QTL for wound healing. The vertical axis shows the LOD scores while the horizontal axis shows the markers from centromeric end of each chromosome on the left extending towards telomeric end on the right.

Table 8. Numbers of genes that are significant in the microarray analysis.

	Fold Change[a]				Total
Regulated	<= 0.67	0.67 - 1.0	1.0 - 1.5	>= 1.5	
MRL only	10	404	386	11	811
SJL only	40	422	395	25	882
Both up or down	6	14	14	8	42
One up one down					10
Total					1745

[a] While "<= *0.67*" and "*0.67 - 1.0*" represent >= 1.5 fold down-regulation and < 1.5 fold down-regulation, respectively, "*1.0 - 1.5*" and ">= *1.5*" represent < 1.5 fold up-regulation and >= 1.5 fold up-regulation.

Table 9. Known genes that are significant, and 1.5 fold up or down-regulated in the MRL vs SJL microarray experiment

Gene Name	Chr	MRL Fold	MRL Adj	SJL Fold	SJL Adj	Gene Description
In both MRL & SJL						
AK084926	1	6.042	15.078	2.396	5.216	RIKEN cDNA C030045D06 gene
BC046809	17	4.061	9.438	3.525	8.519	Bromodomain containing 2
Unc5a	13	3.531	7.929	2.810	6.427	Unc-5 homolog A (C. elegans)
Nfasc	1	2.898	6.126	1.590	2.859	Neurofascin
5430432M24Rik	2	1.956	3.444	1.688	3.145	Mus musculus RIKEN cDNA 5430432M24 gene (5430432M24Rik), transcript variant 2
Fgfr2	7	0.602	-1.160	0.594	-0.867	Mus musculus fibroblast growth factor receptor 2 (Fgfr2), transcript variant 2
Fkbp1a	2	0.260	-7.381	0.367	-3.913	FK506 binding protein 1a
In MRL only						
Mmp16	4	3.688	8.376			Mus musculus matrix metalloproteinase 16
Gabpb1	2	2.256	4.299			Mus musculus GA repeat binding protein, beta 1 (Gabpb1), transcript variant 1
Tnfsf14	17	2.040	3.684			Tumor necrosis factor (ligand) superfamily, member 14
Pira4	7	1.901	3.288			Paired-Ig-like receptor A4
Slc6a2	8	1.875	3.214			Solute carrier family 6 (neurotransmitter transporter, noradrenalin), member 2
AI428936	7	1.563	2.325			Expressed sequence AI428936
D630023O14Rik	1	0.668	-0.693			RIKEN cDNA D630023O14 gene
D030041I09Rik	1	0.661	-0.738			Nicotinamide nucleotide adenylyltransferase 2
Pla2g4a	1	0.652	-0.797			Mus musculus phospholipase A2, group IVA (cytosolic, calcium-dependent)
AW555464	12	0.635	-0.914			Mus musculus expressed sequence AW555464 (AW555464)
Hsd17b12	2	0.620	-1.023			Hydroxysteroid (17-beta) dehydrogenase 12
Rpl23	11	0.620	-1.023			Ribosomal protein L23
Eef2	10	0.610	-1.098			Mus musculus eukaryotic translation elongation factor 2
Dia1	15	0.606	-1.129			Diaphorase 1 (NADH)
AW742319	9	0.509	-2.024			Protein tyrosine phosphatase-like A domain containing 1
Hnrpab	11	0.436	-2.961			Heterogeneous nuclear ribonucleoprotein A/B
In SJL Only						
Postn	3			3570.000	10441.172	Periostin, osteoblast specific factor
Sprr2d	3			3.616	8.785	Small proline-rich protein 2D
Stfa1	16			3.603	8.747	Stefin A1
Stfa3	16			3.025	7.056	Stefin A3
Fa2h	8			2.598	5.807	Fatty acid 2-hydroxylase
AK039445	1			2.597	5.804	Protein phosphatase 1, regulatory (inhibitor) subunit 12B
Aqp4	18			2.311	4.968	Aquaporin 4
IGKV13-73-1	6			2.169	4.552	Mus musculus IgVk go33r pseudogene.
TRGV1	13			2.103	4.359	Mouse T-cell receptor germline gamma chain gene V-region (V108B).
MoV3sS4gp1	8			2.101	4.353	Mammalian orthoreovirus 3 segment S4, complete sequence.
Krt2-6b	15			1.951	3.915	Keratin complex 2, basic, gene 6b
1810007M14Rik	16			1.680	3.122	RIKEN cDNA 1810007M14 gene
D630010B17Rik	15			1.545	2.727	RIKEN cDNA D630010B17 gene
Barx1	13			1.521	2.657	BarH-like homeobox 1
Ctla2a	13			1.516	2.642	Cytotoxic T lymphocyte-associated protein 2 alpha
Baiap1	6			1.506	2.613	Membrane associated guanylate kinase, WW and PDZ domain containing 1, transcript variant 1
AF191028	5			0.663	-0.354	Cysteine endopeptidase, papain-type (XCP2)
Tnnt1	7			0.646	-0.470	Mus musculus troponin T1, skeletal, slow
Myom2	8			0.640	-0.513	Myomesin 2
Ank	15			0.631	-0.578	Mus musculus progressive ankylosis
Pgam2	11			0.614	-0.706	Phosphoglycerate mutase 2
Mylpf	7			0.608	-0.753	Mus musculus myosin light chain, phosphorylatable, fast skeletal muscle

Krt2-17	15	0.607	-0.761	Keratin complex 2, basic, gene 17
Btc	5	0.602	-0.801	Betacellulin, epidermal growth factor family member
Actn2	13	0.592	-0.883	Actinin alpha 2
Cidea	18	0.583	-0.960	Cell death-inducing DNA fragmentation factor, alpha subunit-like effector A
Tnni2	7	0.577	-1.012	Troponin I, skeletal, fast 2
Casp6	3	0.573	-1.047	Mus musculus caspase 6
Eln	5	0.570	-1.074	Elastin
Hrc	7	0.570	-1.074	Histidine rich calcium binding protein
1110020C03Rik	4	0.551	-1.251	RIKEN cDNA 1110020C03 gene
Tcap	11	0.549	-1.270	Titin-cap
3110040M04Rik	1	0.538	-1.379	RIKEN cDNA 3110040M04 gene
BC057690	1	0.534	-1.420	Signal transducer and activator of transcription 1
Tnnc2	2	0.508	-1.700	Troponin C2, fast
Elovl5	9	0.503	-1.758	ELOVL family member 5, elongation of long chain fatty acids (yeast)
3110079O15Rik	1	0.480	-2.036	Mus musculus RIKEN cDNA 3110079O15 gene
Hbb-b1	7	0.480	-2.036	Hemoglobin, beta adult major chain
Scd1	19	0.452	-2.414	Stearoyl-Coenzyme A desaturase 1
Col8a1	16	0.431	-2.729	Procollagen, type VIII, alpha 1
Fhl1	x	0.409	-3.094	Four and a half LIM domains 1
Atp2a1	7	0.375	-3.743	ATPase, Ca++ transporting, cardiac muscle, fast twitch 1
Wif1	10	0.374	-3.763	Wnt inhibitory factor 1

Table 10. Numbers of genes in the QTL region of chromosome 9 that are significant.

	Fold Change[a]				Total
Regulation	<= 0.67	0.67 - 1.0	1.0 - 1.5	>= 1.5	
MRL only	1	8	6	0	15
SJL only	1	4	8	0	13
Both up or down	0	0	0	0	0
Total					28

[a] While "<= *0.67*" and "*0.67 - 1.0*" represent >= 1.5 fold down-regulation and < 1.5 fold down-regulation, respectively, "*1.0 - 1.5*" and ">= *1.5*" represent < 1.5 fold up-regulation and >= 1.5 fold up-regulation.

Table 11. Candidate genes in the Chr 9 QTL region that showed differential expression patterns in two microarray experiments.

Gene Name	Position (Mb)	QTL Peak	Experiments	Strain	Regulation	Description
AW742319	64.784989	1	MRL vs. SJL	MRL	1.5 fold down	Protein tyrosine phosphatase-like A domain containing 1
Elovl5	77.703052	2	MRL vs. SJL	SJL	1.5 fold down	ELOVL family member 5, elongation of long chain fatty acids (yeast)

Table 12. Genes that are tested in real time PCR in the Chr 9 QTL region.

Gene	Start Pos (bp)	Stop Pos (bp)	QTL Peak	Gene Description
Itga11	62475867	62581966	1	integrin, alpha 11
Map2k5	62961776	63175858	1	mitogen activated protein kinase kinase 5
Smad3	63444773	63556000	1	MAD homolog 3 (Drosophila)
Smad6	63751143	63819327	1	MAD homolog 6 (Drosophila)
Map2k1	63983794	64051338	1	mitogen activated protein kinase kinase 1
Rab11a	64514239	64535762	1	RAB11a, member RAS oncogene family
Parp16	65012727	65037224	1	poly (ADP-ribose) polymerase family, member 16
Pdcd7	65144074	65157649	1	programmed cell death protein 7
Rasl12	65196544	65210704	1	RAS-like, family 12
Oaz2	65474596	65488303	1	ornithine decarboxylase antizyme 2
Csnk1g1	65707016	65843020	1	casein kinase 1, gamma 1
Usp3	66315887	66390986	1	ubiquitin specific peptidase 3
Tln2	67017280	67338759	1	talin 2
Foxb1	69556916	69559991	2	forkhead box B1
Ccnb2	70206853	70220718	2	cyclin B2
Aqp9	70909221	70961849	2	aquaporin 9
Ccpg1	72782710	72813123	2	cell cycle progression 1
Gnb5	75097304	75131580	2	guanine nucleotide binding protein, beta 5
Tpbg	85639128	85642507	3	trophoblast glycoprotein
Pgm3	86349194	86368545	3	phosphoglucomutase 3
Rwdd2	86368771	86371614	3	RWD domain containing 2
Mod1	86378094	86492941	3	malic enzyme, supernatant
Prss35	86539561	86554745	3	protease, serine, 35
Snap91	86562350	86678320	3	synaptosomal-associated protein 91
Tbx18	87502145	87529206	3	T-box18
Nt5e	88125533	88169982	3	5' nucleotidase, ecto
Snx14	88174668	88236822	3	sorting nexin 14
Syncrip	88250166	88280101	3	synaptotagmin binding, cytoplasmic RNA interacting protein
Rasgrf1	89707668	89827694	3	RAS protein-specific guanine nucleotide-releasing factor 1
Ctsh	89852402	89873982	3	cathepsin H
Morf4l1	89889562	89912655	3	mortality factor 4 like 1
Adamts7	89961138	89997904	3	a disintegrin-like and metallopeptidase (reprolysin type) with thrombospondin type 1 motif, 7
Atp1b3	96142025	96173651	4	ATPase, Na+/K+ transporting, beta 3 polypeptide
Rnf7	96280289	96327074	4	ring finger protein 7
Rasa2	96351797	96440845	4	RAS p21 protein activator 2
Spsb4	96752834	96827707	4	splA/ryanodine receptor domain and SOCS box containing 4 (alias: SSB4)

Table 13. Candidate genes of the Chr 9 QTLs that showed significant injury-induced regulation in the ear tissues.

Gene	MRL Cont DCt	MRL Exp DCt	MRL DDCt	MRL Fold Change	SJL Cont DCt	SJL Exp DCt	SJL DDCt	SJL Fold Change
Map2k5	13.08	8.78	-4.29	19.8	12.43	9.74	-2.79	8.83
Usp3	8.33	5.78	-2.55	5.87	6.26	5.45	-0.8	1.75
Tln2	10.47	8.57	-1.9	3.74	9.69	7.84	-1.84	3.59
Ccnb2	11.34	7.05	-4.29	19.52	9.65	7.09	-2.56	5.9
Ccpg1	8.27	5.98	-2.29	4.9	6.45	6.28	-0.17	1.13

Note: 'Dct' refers the difference in threshold cycles between target (amplified gene) and reference (internal control gene). We used the GAPDH-1 as the reference. 'DDct' refers the difference between Dct of the day 4 experiment (Exp) and that of the day 0 control (Cont) in each mouse strain.

Table 14. Markers genotyped for the chromosome 4 QTL region for STR in different crosses of inbred mice

Marker	Position (cM)	Position (Mb)	MRL X SJL	MRL X SJL (new)	MRL X CAST	DBA X 129
D4Mit264	1.9	9.32	X	X		
D4Mit227	3.2	9.93			X	X
D4Mit18	5.2	13.94		X		
D4Mit268	17.9	20.68				X
D4Mit196	12.1	39.59		X		
D4Mit214	17.9	45.57	X	X		
D4Mit17	31.4	62.46			X	X
D4Mit178	35.5	66.27	X	X		
D4Mit9	44.5	94.04			X	X
D4Mit31	51.3	106.07	X	X		X
D4Mit308	57.4	123.19		X		
D4Mit203	60.0	128.60			X	
D4Mit204	61.9	132.39	X	X		
D4Mit170	66.6	137.50		X	X	X
D4Mit42	81.0	150.06		X		X
D4Mit256	82.7	153.48			X	

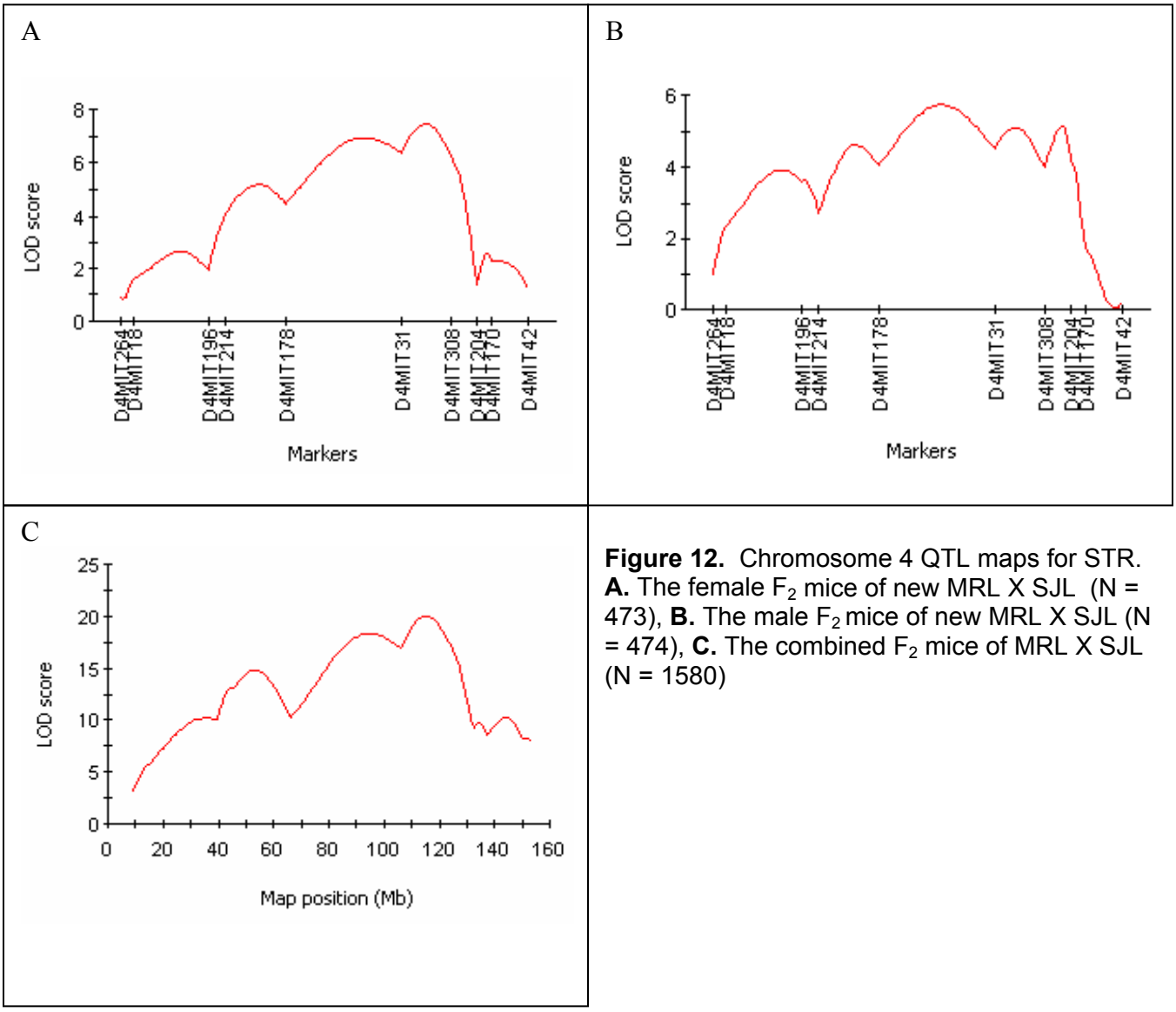

Figure 12. Chromosome 4 QTL maps for STR. **A.** The female F_2 mice of new MRL X SJL (N = 473), **B.** The male F_2 mice of new MRL X SJL (N = 474), **C.** The combined F_2 mice of MRL X SJL (N = 1580)

Key Research Accomplishments

- As part of the high resolution mapping of the chromosome 9 QTL, we have finished genotyping new F2 mice and added additional genetic markers. The combined analysis is now based on 1564 F2 mice (both males and female) and 23 genetic markers.

- We have finished analyzing the high-resolution mapping of the chromosome 9 QTL using both MapQTL and the shrinkage estimation of QTLs. We are in the process of writing the results for publication.

- We have finished the analysis of additional crosses of DBA X 129 and MRL X CAST to confirm the results of the MRL X SJL cross. The results have been published (see the Reportable Outcome section of this report).

- We have obtained a homozygous congenic strain at the N8 generation for the chromosome 9 QTL. This congenic strain carried a MRL chromosome 9 fragment 31.7 cM or 60.78 Mb long in the SJL background. This fragment covers the sth8 and sth9 QTL region on chromosome 9. We are in the process of creating the sub-congenic lines for this congenetic strain.

- We have compared this congenic mouse with parental progenitor strains in post-ear punch healing performance. We have used 15 animals in each group of congenic males and congenic females, in addition to SJL males and SJL females.

- We have advanced the chromosome 1 congenics to the N4 generation. The heterozygous congenic animals contain a chromosome 1 fragment from the MRL parent at 0 to 110 cM positions. This fragment covers the QTL peak at 49.2 cM. We are in the process of creating N5.

- We have advanced the chromosome 4 congenics to the N7 generation. The heterozygous congenic animals carried a chromosome 4 fragment from the MRL parent at 8.7 cM to 76.5 cM positions. This fragment covers both QTLs sth3 at 21.9 cM and sth4 at 50.3 cM. We are in the process of advancing to N8 and generating homozygous congenic strains at the same time.

- We have studied the activation of proinflammatory transcription factors in MRL and SJL strain of mice. Although the activation of many proinflammatory transcription factors was increased in healing ear tissue of MRL and SJL mice, the activation of Nuclear Factor-kappa B (NF-κB) was significantly higher in SJL compared to MRL. Activation of NF-κB can serve as a major end point in the functional studies to test the candidate genes. We are also investigating the effect inhibition of NF-κB on the healing rates in MRL and SJL mice.

- We have used microarray analysis to identify candidate genes for the Chr 9 QTLs. Based on expression patterns in MRL or SJL alone, we have identified 2 candidate genes in the Chr 9 QTL region for further examination.

Reportable Outcomes

Manuscripts

Masinde GL, Li R, Nguyen B, Yu H, Srivastiva AK, Edderkaoui B, Wergedal JE, Baylink DJ, Mohan S. (2006) New quantitative trait loci (QTL) that regulate wound healing in an intercross progeny from DBA/1J and 129X1/SvJ inbred strains of mice. Genomics. Funct Integr Genomics. 6(2):157-63.

Yu H, Mohan S, Masinde GL, Baylink DJ. (2005) Mapping the dominant wound healing and soft tissue regeneration QTL in MRL X CAST. Mammalian Genome. 16(12): 918-24.

Yu H, Baylink DJ, Masinde GL, Li R, Nguyen B, Davidson HM, Xu S, Mohan S. Mouse Chr 9 QTL for Soft Tissue Regeneration: Congenic Analysis and Fine Mapping. Mammalian Genome. Submitted.

Conclusions

1. For the chromosome 9 QTL, sth9, the high resolution mapping indicated that it was localized in a 68 – 98 Mb chromosomal region, with four peaks that could be defined. This indicates multiple loci in this region are responsible for this QTL. The combined length of these four peaks was 28.23 Mb, defined with the two LOD score interval using MapQTL, and only 4.28 Mb with the QTL effect peaks using the shrinkage analysis.

2. With 15 mice in each group, the homozygous congenic mice showed a trend of improvement in healing when compared to the SJL parentals in the male mice. In the female mice, there was no such trend. This might be due to a large biological variation within each group and small sample sizes. Power analysis showed that at least 50 mice are required to show significant difference in this situation.

3. The chromosome 9 QTLs, sth8 and sth9, identified initially in MRL X SJL are now confirmed in the cross MRL X CAST. Significant LOD scores are found at the 26 cM (corresponding to sth8) and 49-61 cM (corresponding to sth9) on chromosome 9 in the MRL X CAST cross. The sth4 QTL on chromosome 4 initially identified in MRL X SJL is present in most other crosses such as MRL X B6, MRL X CAST, and especially in a totally different cross, DBA X 129.

4. The activity of proinflammatory transcription factors such as NF-κB and activator protein-1 (AP-1) is higher in the healing tissue of SJL compared to MRL mice. Difference in the inflammatory response in response to injury in SJL and MRL mice could be responsible, in part, for the difference in wound healing in these two strain of mice.

5. In the microarray study to identify candidate genes for the Chr 9 QTLs, we have found that most differentially expressed genes, either in MRL or SJL alone, or in both strains, were related to small-proline proteins, cell structural proteins, and matrix metalloproteinases and their inhibitors. Based on expression patterns in MRL or SJL alone, we have identified AW7423190 and Elovl5 as candidate genes for the Chr 9 QTLs for further examination.

References

Blankenhorn EP, Troutman S, Clark LD, Zhang XM, Chen P, Heber-Katz E. (2003) Sexually dimorphic genes regulate healing and regeneration in MRL mice. Mamm Genome. 14, 250-60.

Clark LD, Clark RK, Heber-Katz E. (1998) A new murine model for mammalian wound repair and regeneration. Clin Immunol Immunopathol. 88:35-45.

Heber-Katz E. (1999) The regenerating mouse ear. Semin Cell Dev Biol. 10, 415-9.

Heber-Katz E, Leferovich JM, Bedelbaeva K, Gourevitch D. (2004) Spallanzani's mouse: a model of restoration and regeneration. Curr Top Microbiol Immunol. 280, 165-89.

Karin, M., and Delhase, M. The I kappa B kinase (IKK) and NF-kappa B: key elements of proinflammatory signalling. Semin Immunol. 2000 Feb;12(1):85-98. Review.

Karin, M., and Lin, A. NF-kappaB at the crossroads of life and death. Nat Immunol. 2002 Mar;3(3):221-7. Review.

Kumar, A., Takada, Y., Boriek, A. M., and Aggarwal, B. B. Nuclear factor-kappaB: its role in health and disease. J Mol Med. 2004 Jul;82(7):434-48. Epub 2004 Jun 3. Review.

Kumar, A., and Boriek, A. M. Mechanical stress activates the nuclear factor-kappaB pathway in skeletal muscle fibers: a possible role in Duchenne muscular dystrophy.
FASEB J. 2003 Mar;17(3):386-96.

Kumar, A., Chaudhry, I., Reid, M. B., and Boriek, A. M. Distinct signaling pathways are activated in response to mechanical stress applied axially and transversely to skeletal muscle fibers. J Biol Chem. 2002 Nov 29;277(48):46493-503.

Kumar, A., Lnu, S., Malya, R., Barron, D., Moore, J., Corry, D. B., and Boriek, A. M. Mechanical stretch activates nuclear factor-kappaB, activator protein-1, and mitogen-activated protein kinases in lung parenchyma: implications in asthma. FASEB J. 2003 Oct;17(13):1800-11.

Li X, Gu W, Masinde G, Hamilton-Ulland M, Xu S, Mohan S, Baylink DJ. (2001) Genetic control of the rate of wound healing in mice. Heredity. 86, 668-74.

Masinde GL, Li X, Gu W, Davidson H, Mohan S, Baylink DJ. (2001) Identification of wound healing/regeneration quantitative trait loci (QTL) at multiple time points that explain seventy percent of variance in (MRL/MpJ and SJL/J) mice F2 population.
Genome Res. 11, 2027-33.

Masinde, GL, Li R, Nguyen B, Yu H, Srivastiva AK, Edderkaoui B, Wergedal JE, Baylink DJ, Mohan S. 2006. New quantitative trait loci (QTL) that regulate wound healing in an intercross

progeny from DBA/1J and 129X1/SvJ inbred strains of mice. Functional and Integrated Genomics. 6(2):157-63.
Van Ooijen, JW. 2004. MapQTL® 5, Software fore the mapping of quantitative trait loci in experimental populations. Kyazma B.B., Wageningen, Netherlands.

Wang H, Zhang YM, Li X, Masinde GL, Mohan S, Baylink DJ, Xu S. (2005) Bayesian shrinkage estimation of quantitative trait loci parameters. Genetics. 170:465-80.

Yu H, Mohan S, Masinde GL, Baylink DJ. 2005. Mapping the dominant wound healing and soft tissue regeneration QTL in MRL X CAST. Mammalian Genome. 16(12): 918-24.

TECHNICAL OBJECTIVE 3: TO APPLY THE ENU (ETHYL N-NITROSOUREA) MUTAGENESIS TO IDENTIFY NEW GENES THAT REGULATES SOFT- AND HARD-TISSUE REGENERATION IN C3H STRAIN OF MICE.

Introduction

The main goal of Technical Objective-3 is to identify and characterize novel genes or to elucidate the function for known genes that play key role in the soft-tissue regeneration and musculoskeletal phenotypes using the ENU mutagenesis technique in C3H/HeJ (C3H), C57BL/6J (B6), and MRL/MpJ (MRL) mice. Technical Objective 3 was revised for the current grant period; the descriptions of the revised specific objectives are given below.

REVISED SPECIFIC OBJECTIVES

Our specific objectives during the first 12 months of this continuation grant are as follows.

1) To generate mutations by ENU treatment of MRL male and screen mutations by one-generation dominant and two-generation recessive screenings. To accomplish these objectives, we will:

a) Inject three weekly ENU doses of 100 mg/kg to MRL mice to generate founder males;
b) Breed ENU founder males that regain fertility with wild type MRL females;
c) Screen 100 F1 mice generated from ENU-injected males for dominant mutations affecting: i) body weight; ii) body composition; iii) bone density; iv) growth markers; v) hematology; vi) serum & urine chemistries; and vii) soft-tissue regeneration;
d) Breed about 10 randomly selected F1 males with wild type MRL females for recessive screening. All F2 female pups thus generated will be bred back to F1 male. The F3 progeny generated from F2 (female) X ENU founder male will be screened for recessive mutations affecting: i) body weight; ii) body composition; iii) bone density; iv) growth markers; v) hematology; vi) serum & urine chemistries; and vii) soft-tissue regeneration;
e) Confirm selected mutations by backcrossing the affected MRL mice with other wild type strains of mice;
f) Breed approximately 20 lines of previously screened recessive phenodeviants and about approximately 20 dominant phenodeviants with wild type B6, C3H and MRL mice to confirm inheritability of each mutant line and generate additional affected mice for further characterization of the phenotypes; and
g) Maintain a small breeding colony of all interesting phenodeviants that are confirmed for inheritance testing in specific objective 1.f.

2) To determine the chromosomal location of the mutant gene responsible for the selected mutant phenotypes, we will:

a) Select mouse mutant/s for genotyping based on the importance of phenotype and based on the magnitude of change in phenotype induced by ENU mutation;
b) Breed selected mutant C3H, B6 or MRL phenodeviant mice with another inbred strain of mouse (chosen based on the similarity in phenotype with wild type C3H, B6, SJL, or MRL and availability of markers for genotyping) to produce F1 mice;
c) Intercross F1 mice to produce approximately 50-100 F2 mice;

d) Screen F2 progeny for phenotype and extract genomic DNA from ear punch for genotyping;
e) Perform a genome-wide scan using appropriate SNPs and/or polymorphic microsatellite informative markers representing all chromosomes with average length of 5-20 cM;
f) Perform interval mapping using commercially available software and determine the significance level of interval mapping;
g) Identify unique QTL in ENU mutant mice by comparison of all background QTLs in the progenitor strains. For this purpose, we will: 1) breed a non-mutagenized MRL mouse with another inbred strain of mouse (same as used for genotyping described above in item #a) to produce F1 mice; 2) intercross F1 mice to produce approximately 50-100 F2 mice; 3) screen F2 progeny for phenotype and extract genomic DNA from ear punch for genotyping; 4) perform a genome wide scan using appropriate SNPs and/or polymorphic microsatellite informative markers representing all chromosomes with average length of 5-20 cM; and 5) perform interval mapping using commercially available software and determine the significance level of interval mapping.

3) To identify the candidate gene in the chromosomal locus established for the selected mouse mutant in specific objective 2 of year 1, we will:

a) Extract RNA from appropriate tissue of mutant mice and corresponding control mice;
b) Perform in house microarray to identify genes that are differentially expressed in the mutant versus control mice;

Our specific objectives during the final 4 months of this continuation grant are as follows.

1) To continue to generate mutations by ENU treatment of C3H male and screen mutations by one-generation dominant and two-generation recessive screenings (i.e. repeat of studies proposed in specific objective 1 of first 12 months in order to find mouse mutants for phenotypes of interest). To accomplish these objectives we will:

1) To generate mutations by ENU treatment of MRL male and screen mutations by one-generation dominant and two-generation recessive screenings. To accomplish these objectives we will:

a) Inject three weekly ENU doses of 100 mg/kg to MRL mice to generate founder males;
b) Breed ENU founder males that regain fertility with wild type MRL females;
c) Screen 30 F1 mice generated from ENU injected males for dominant mutations affecting: i) body weight; ii) body composition; iii) bone density; iv) growth markers; v) hematology; vi) serum & urine chemistries; and vii) soft-tissue regeneration;
d) Confirm selected mutations by backcrossing the affected MRL mice with other wild type strains of mice;
f) Breed previously screened recessive and dominant phenodeviants with wild type B6 and MRL mice to confirm inheritability of each mutant line and generate additional affected mice for further characterization of the phenotypes;

g) Maintain a small breeding colony of all interesting phenodeviants that are confirmed for inheritance testing in item #1.f.

Body

Although the Specific Objectives were mentioned separately for first 12-months and last 4-months, we report combined progress on the Revised Specific Objectives 1-3 for the full 16-month time period.

SPECIFIC OBJECTIVE 1

The main aim of the **Specific Objective-1** was to generate mutations by ENU treatment and screen 100 mice for skeletal phenotypes caused by dominant mutations and 10 lines of mice for recessive mutations.

In the current reporting period, we have used the MRL/MpJ (MRL) strain of mice for dominant screening. We bred ENU-treated MRL male to wild type MRL females and then screened mice for dominant mutations for soft tissue regeneration, growth, musculoskeletal phenotypes, blood chemistry, and blood hematology phenotypes.

Specific Objective 1a. To generate F1 & F3 mice for dominant and recessive screening, respectively, we injected two batches of 8-10 week old 15 MRL male mice with 3x100 mg/kg of ENU. We observed that MRL mice could tolerate a 3x100 mg dose and regain fertility within 12-22 week post ENU injection. **Table-1** shows data on fertility/sterility period, litter numbers produced, and litter size from ENU injected males. Two batches of male mice were injected with a gap of 3 months to allow a continuous supply of ENU mutagenized MRL for breeding with MRL wild type females. However, first batch of ENU injected mice produced the desired number of F1 mice proposed in this study and hence a second batch was not bred with WT MRL mice.

Specific Objective 1b. We bred each ENU-injected MRL male with two 8-12 week old wild type MRL females, 12-14 weeks after the last ENU injections. The ENU injected male mice typically recovered in 20-25 weeks and produced litters with 2-5 pups/litter. However, the fertile period was brief and only lasted between 12-16 weeks. About 70% males were fertile and 27% males died before recovery of fertility (**Table-1**). Females are checked routinely for pregnancy, and the pregnant mice are removed from mating cages and replaced with fresh females. A maximum of 10 progeny was screened from each founder male, and then the founder male was euthanized.

Specific Objective 1c. The generation and screenings of MRL mice were performed as described in **Figure 1**. During this reporting period, we have generated 33 litters of mice for dominant mutations and have, so far, completed screening of 118 MRL mice. For recessive screening, we bred 10 lines of F1 MRL mice. Both dominant and recessive screen mice were screened for: a) visible abnormalities, b) growth or body weight; c) total body bone density determined by DEXA instrument PIXImus; d) volumetric bone density at tibia determined by peripheral quantitative computed tomography; e) bone formation markers; f) blood chemistry; and g) hematology phenotypes. The main phenotype screens on F1 and F3 offspring were carried out at 10-weeks of age, however, we added a soft-tissue regeneration screen in our dominant screen on 3-week old mice. An abnormality was recognized if a phenotype differs by

2-3 standard deviation (depending on the measurement and population variance) as compared age and sex matched control MRL mice. Since MRL mice are good healers (with almost complete healing of 2mm ear punch in 4-weeks), we anticipated hypomorphic mutations to predominate for STR phenotype. Musculoskeletal measurements that are found to be abnormal are repeated at 16-weeks to confirm the phenotype. For this purpose, we have obtained additional baseline values for age and sex matched MRL mice at 16-weeks of age.

In order to identify outlier mice, it was important to obtain reliable cut-off values from control mice. To achieve this in MRL mice, we collected normal range data from male (n=10) and female (n=10) mice collected during the current reporting period with the exception of hematology data, which was collected from only-35 mice, and we have relied on the Mouse Phenome Database (MPD home page at www.jax.org/phenome) for identifying abnormal hematology values. Those phenotypes that are confirmed after repeat testing at 16-weeks of age are subjected to inheritance-test (IT) or backcross with wild type mice. Because of the significant efforts involved in progeny testing, we have focused on those phenodeviants that had highest differences in phenotypes. A mutation is considered inheritable if the phenotype is recovered in several inherited progeny.

Phenodeviants Identified in Dominant Screening: We have screened 118 new F1 progeny (**Table –2**) for all phenotypes listed in Specific Objective 1c. We continue to observe an unusually high number of mice (>30) that have phenotype differences of 2-3SD, referred to as phenodeviants in our primary screening (performed at 10-weeks). All musculoskeletal phenodeviants (along with few littermates) were retested at 16-weeks to confirm phenotype. Phenotype description of all phenodeviants identified in dominant screen are shown in **Figures 2-5**, which include those mice that are confirmed in retesting and currently bred with wild type MRL mice to confirm heritability of the mutation (described as inheritance test or IT). The phenodeviants observed in the MRL dominant screen could be grouped into three categories, as discussed below.

a) Phenodeviant with reduced soft-tissue regeneration (STR) capacity: As expected, we observed several phenodeviants with reduced soft-tissue regeneration capacity. In wild type MRL mice, a 2 mm ear punch is 80-90% healed in 3-weeks after making the hole, thus, the 99% confidence limits for slow healing after 3-weeks is 1.2 mm. **Figure 2** shows several mice with only 10-30% healing. However, Figure 2 also shows a large variation in STR rate in F1 progeny and it is possible that some of the slow healing mice could be false positive. Consequently, we are only focusing on those phenodeviants that show extreme phenotype. We are currently breeding a few STR phenodeviants with wild type MRL female mice to test heritability.

b) Phenodeviants with abnormal hematological parameters: In the dominant screen, we also included whole blood hematology measurements using Hemavet 950 (Veterinary Multi-species Hematology System with 5 part differential capability from Drew Scientific & Escalon Medical Corp., Wayne, PA), which is designed for mouse hematology measurements. Peripheral blood was drawn (80-100 microliters) by retro-orbital puncture using a Pasteur pipette. Blood was collected in Microtainer brand tubes containing K_2EDTA (Becton Dickinson, Franklin Lakes, NJ) and samples analyzed using a Cell-Dyn 3500R automated veterinary hematology analyzer according to the manufacturer's instructions. The hematological parameters measured

included hematocrit, platelet counts, hemoglobin, WBC, RBC, lymphocytes, neutrophils, mean cell volume etc. We observed several phenodeviants in our primary screen with platelet count, mean cell volume, hematocrit, hemoglobin, monocyte etc. Representative data on hematocrit and blood platelet counts measured at 10-week screen is shown in **Figure 3**. Other parameters screened but not shown in this figure include, hemoglobin, WBC, RBC, lymphocytes, neutrophils, mean cell volume etc. Four phenodeviants were confirmed in the 16-week retesting and two of the phenodeviants survived and currently bred for IT.

c) Phenodeviants with abnormal bone density, bone size, or bone mineral content phenotypes: **Figure 4** shows phenodeviants with abnormal total body bone density measured by DEXA, total body bone mineral content, body weight and volumetric bone density measured by peripheral quantitative tomography (pQCT). So far, we confirmed 5 phenodeviants in our repeat testing at 16-weeks of age. We observed that F1 progeny showed a significant shift in bone area as compared to WT MRL values, and therefore we excluded bone area from our mutation detection.

d) Phenodeviants with abnormal blood chemistry: In the dominant screen, we observed several phenodeviants in our primary screen with abnormal alkaline phosphatase, blood urea nitrogen (BUN), or lipid panel. Representative data on alkaline phosphatase and HDL levels in 116 MRL mice screened at 10-week are shown in **Figure 5**. Three phenodeviants are currently bred for IT.

Specific Objective 1d. The aim of this specific objective was to identify phenodeviants that have a recessive mode of inheritance. Therefore, a three-generation breeding strategy (shown in **Figure 1**) was used to recover recessive mutations in the F3 progeny. To generate F3 mice for the recessive screen, we randomly selected 10 F1 MRL males generated in our dominant screening and bred them with 20-30 wild type MRL females (**Figure 1**). Each F1 male was mated with 2 normal wild type female mice at one time. Once the mating was successful, pregnant mice were separated and placed individually to give birth to F2 littermates. If a F2 litter had 3-4 female mice, they were used to generate F3 progeny. Otherwise, a new WT MRL female was bred until 3-4 F2 females were obtained. Each F2 female was reintroduced for mating with an F1 male to produce at least one litter with minimum 4 pups. The aim was to screen a minimum of three litters from each line.

During the current reporting period, we bred approximately 20 female F2 pups with 6 F1 male (founder male). Three F1 males did not produce any litters and one male was not efficient in mating and hence discontinued. The lower number of mice screened was primarily due to poor breeding performance of the MRL male F1 mice, which are often reproductive for a brief period and did not breed well for the two generation breeding cycle required for recessive screening. We bred 6 lines, and so far, we have screened approximately 24 F3 progeny for recessive mutations (**Table-3**). The screening procedure is similar to that described for dominant mutations in Specific Objective 1c. Our screening strategy involves repeat testing at 16-weeks of all phenodeviants identified in the 10-week screening. Those phenotypes that are confirmed after repeat testing are subjected to inheritance-test (IT) with wild type mice.

Phenodeviants Identified in Recessive Screening: We observed one phenodeviant in our STR screening performed at 35-day post ear punch. This phenodeviant will be further evaluated before introducing it to inheritance testing.

Specific Objective 1e-g. In addition to new phenodeviants identified in the current reporting period, we also continued breeding phenodeviants from the previous year's screens; these phenodeviants are listed in **Tables 4-6.** In the current reporting period, we produced ~1200 mice from inheritance testing of new or previously identified phenodeviants. We bred 42 phenodeviant mice (including both MRL, C3H, and B6) into inheritance testing (**Tables 4-6**) by mating affected male and female mice with wild type MRL, C3H, and B6 mice. Each phenodeviant was mated with 1-2 normal wild type male or female mice. Once the mating was successful, pregnant mice were separated and placed separately to give birth to B2 littermates. If a F1-affected mouse was a female, it was reintroduced for mating to produce 3-5 litters, totaling about 20-25 F2 pups. If the affected mouse was male, 3-5 female mice were mated simultaneously. The inheritance testing (IT) F2 offspring were screened at 10-and 16-weeks of age. A mutation was considered inheritable if the phenotype was recovered in several progeny. The animals were not genotyped at this stage to differentiate mutant from non-mutant genotypes. Thus, phenotype distribution was the only means for separating the mutants from their unaffected littermates. To avoid potential breeding of an un-affected progeny, we bred only extreme scoring mice for generating affected progeny in subsequent breeding. All phenodeviant mice that were bred under inheritance testing in the current grant period are listed in **Tables 4-6**.

To compare the abnormal phenotypes in B6 recessive lines, we have continued to obtain normal data from B6 (n=20), C3H (n=10), and MRL (n=20) mice and updated our previous normal data base of B6 mice to 100 male and 100 female mice; 30 MRL male and 30 MRL female mice; and 60 C3H male and 60 C3H female mice. In addition to musculoskeletal phenotypes, we also obtained bone marker phenotype, blood chemistry phenotypes and hematology phenotypes.

Detailed Phenotypic Characterization of Selective Phenodeviants Identified in Previous Dominant & Recessive Screens

Mutant Line 917M- In our previous ENU screen for dominant musculoskeletal phenotypes using a C57BL/6J (B6) strain of mice, a phenodeviant was discovered which exhibited a highly significant decrease in bone size. Three main parameters that assess bone size, i.e. bone area, bone mineral content (BMC), and periosteal circumference were all significantly lower in affected mice even after adjustment for decreased body weight. Interestingly, the total body bone area phenotype was consistently expressed in males (92% affected), whereas only 6% of females exhibited partial phenotype. We continued to breed this line to generate additional affected mice for further characterization of mutation. Since only 50% of males are supposed to be affected, we have to produce a significantly higher number of animals to obtain affected male progeny. Thus far, we have generated about 60 additional mice, as shown in **Table-5**. We used these male mice to perform bone area measurements in 6-week old mice (**Figure 6**). Since we observed low bone area in 6-week old mice, we have now proposed to evaluate bone area in 3-week old mice to study if changes in bone area are related to sex steroids during puberty. We continue to breed this line and maintain a small colony until identification of mutant gene is completed.

Mutant Line 12184- Line 12.18.4 was generated in a dominant screening of C57BL/6J (B6) strain of mice. The phenodeviant has 10-14% high body weight-adjusted total body bone density and 7-14% high bone mineral content. We bred the phenodeviant with B6 females and generated about 67 progeny in this grant period (**Table-5**). As shown in **Figure 7**, about 50% of IT

progeny were classified as affected. Previously, we have shown that 12184 mutation causes higher total bone density and an increase in periosteal bone perimeter measured by pQCT. At the same time, the endosteal perimeter is not increased. These data suggest that the phenotype could be due to increase periosteal bone formation as well as reduced endocortical bone resorption. To identify if changes in osteoblast cell function could explain higher bone density, we isolated periosteal osteoblasts from 12184 and WT female mice and investigated the cell function by *in-vitro* assays.

Characterization of Osteoblast Cell Function in Mutant12184: To investigate if 12184 mutation could influence osteoblast cell function, we isolated the periosteal osteoblasts from femur and tibiae of normal and 12184 mutant mice and propagated them in culture for *in vitro* phenotypic characterization. In brief, the mice were euthanized with CO_2 and decapitated. Soft tissue was removed from femur and tibia without scraping off the bones so that periosteal cells were not lost at this point. Femur and tibia were placed separately in 50 ml falcon tubes containing sterile PBS, and subsequently in culture dish containing 10 ml of DMEM/antibiotics and the left over muscles were removed from the bones. The periosteal cells were extracted from bone by collagenase digestion for 90 minutes at 37^{o}C. Cells were counted and plated at a density of 10^6 cells per dish and grown with 10% FBS/DMEM/antibiotics. Periosteal osteoblasts at passage 2-3 were used to study cell proliferation, differentiation, and apoptosis. These characteristics cells from mutant mice were compared with cells isolated in identical manner from age-and sex-matched wild type mice. Cell proliferation was studied using (3H)-thymidine incorporation and results were confirmed by uptake of Almar Blue dye during cell proliferation. Cell differentiation was measured by observing changes in the alkaline phosphatase activities using PNPP as substrate. For apoptosis studies, the Homogeneous Caspases Assay from Roche Biochemicals was used which is a fluorimetric assay for the quantitative *in vitro* determination of caspases activity in microplates. Periosteal cells were incubated with DEVD-Rhodamine 110 for 2 h. Upon cleavage of the substrate by activated caspases, fluorescence of the released Rhodamine 110 was measured. Apoptosis results were further confirmed using FACS analysis of isolated cells in presence/absence of 10%FCS.

I. Apoptosis (caspase activity): **Figure 8A** shows the rate of apoptosis, as measured by the caspase activities in periosteal osteoblasts isolated from 10-week old B6 normal and ENU mutant mice. No significant changes were observed in the caspase activities in the cells of mutant mice as compared to those from normal mice (**Figure 8A**).

II. Cell Differentiation: The specific activity of alkaline phosphatase (a marker of osteoblasts differentiation) was estimated in periosteal cells derived from normal and ENU mutant mice (**Figure 8B**). No significant changes were observed in ALP activities of cells from mutant mice as compared to those from wild type mice.

III. Cell Proliferation: **Figure 8C** shows the basal proliferation rates of periosteal osteoblasts isolated from femur and tibiae of 10-week-old normal and ENU mutant B6 female mice. No significant changes were observed in the basal rate of cell proliferation in cells from mutant mice as compared to the normal WT mice (**Figure 8C**).

Measurement of Bone Density Phenotype in 12184 Mice at 6-Week and 1-Year Time Points: In addition, we evaluated bone density in 6-week old mice and also in female mice that are 1-year old. These data are shown in **Figure 9**, and indicate that mutation results in higher bone density at early age and higher bone density is maintained over a period of 1-year.

Mutant Line 12137- Line 12.13.7 was also generated in a dominant screening of C57BL/6J (B6) strain of mice. We bred the phenodeviant with B6 females and generated about 56 progeny in this grant period. The mutants had 10% high body weight, 10-14% high body weight adjusted total body bone density, and 10-25% high body weight adjusted bone mineral content as compared to wild type control mice. As shown in **Figure 14**, about 50% of IT progeny could be classified as affected. Using mice from IT progeny, we performed the following characterizations: 1) measurement of total body bone density between 6-week age and 1-year old mice; 2) ex-vivo pQCT analysis of the excised tibia and femur; 3) osteoblast cell function; and 4) histological examination of bone formation rate and bone resorption rate after dual labeling with tetracycline.

Measurement of Bone Density Phenotype in 12137 Mice at 6-Week and 1-Year Time Points: We evaluated bone density at 6-week old mice and also in female mice that are 1-year old. These data are shown in **Figure 15**, and indicates that mutation results in higher bone density at an early age, and higher bone density is maintained over a period of 1-year.

Characterization of Osteoblast Cell Function of Mutant12137: To study the cellular mechanism of increased bone density in the 12137 mutant, we isolated the periosteal osteoblasts from femur and tibiae of normal and 12137 mutant mice as described above for 12184 mutant mice and propagated them in culture for *in-vitro* phenotypic characterization. The following characteristics were examined:

i) Cell Proliferation: **Figure 16A** shows the basal proliferation rates and proliferation rate when stimulated with calf serum and IGF-I of periosteal osteoblasts isolated from femur and tibiae of 10-week-old normal and ENU mutant B6 female mice. Our preliminary results indicate that the basal proliferation rate appears to be higher in osteoblasts isolated from 12137 mice. In addition, a significantly higher rate of proliferation was observed in osteoblast cells isolated from 12137 mice in the presence of calf serum but not IGF-I (**Figure 16A**). Increased basal proliferation rates in 12137 osteoblast cells were confirmed by alamarBlue dye uptake as shown in **Figure 16B**.

ii) Apoptosis (Caspase activity): **Figure 16C** shows the rate of apoptosis, as measured by the caspase activities in periosteal osteoblasts isolated from 10-week old B6 normal and ENU mutant mice. No significant changes were observed the caspase activities in the cells from mutant mice as compared to those from normal mice (**Figure 16C**).

Histomorphometric measurements to determine cellular mechanism of high bone density phenotype in 12137 mutant mice: We performed histological examination of bone formation rate and bone resorption rate after dual labeling with tetracycline at 14-week and 16-week time points. After second tetracycline injection, femur and tibia were isolated and cleared of surrounding tissues. To measure bone formation and resorption, a location 1 mm proximal to the midshaft was marked on the femur with a pencil. A 5 mm segment of the femur midshaft was cut from the bone starting at the mark and going distally. The samples were fixed in 10% formalin for 4 hours, rinsed in PBS, and then partially decalcified (6 hours) in 10% EDTA in the cold. The samples were infiltrated in glycol methacrylate and embedded vertically with the midshaft end down. The samples were sectioned with a Jung microtome and the first 1 mm of material discarded until the mid point of the shaft was reached. Sections were prepared for analysis by staining for ALP and tartrate resistant acid phosphatase (TRAP). Total ALP and TRAP covered

surfaces were measured using the Osteomeasure system equiped with a digitizing tablet (Osteometrics, Atlanta, GA and color camera (Sony, Japan).

Results of dynamic histological examination of femur midshaft region are shown in **Figure 17**. Bone area at the femur midshaft in 16-week old mutant mice (A) was significantly higher as compared to WT control mice examined in previous grant periods. In addition, endocortical bone formation rate (B & C) at the femur midshaft measured by tetracycline labeling is shown (periosteal bone formation rate was significantly affected). These data suggest that high BMD phenotype in mutant mice appears to be due to increased endocortical bone formation.

Mutant Line Agouti & Low BMD – The agouti mutant was generated in recessive screening of the C3H/HeJ (C3H) strain of mice. The mutant mice showed 8-10% lower total body bone density and bone mineral content. To generate additional F3 mice, we bred the affected male and female phenodeviants, which could be easily identified by agouti coat color, which has a greasy appearance, as shown in **Figure 20**. About 25% of IT progeny were classified as affected. The *in-vivo* DEXA scan of total body bones and tibia shows that bone density was significantly lower in mutant mice as compared to WT control.

Line 10145 – Line 10145 was generated in recessive screening of the C3H/HeJ (C3H) strain of mice. The mutant mice showed 23% high total body bone density and about 17% lower bone area and no changes in bone mineral content. We bred the phenodeviant with C3H females in a three-generation breeding protocol similar to that described in Figure 1 and generated about 30 progeny in this grant period. The *in-vivo* DEXA and pQCT scan of total body bones and tibia shows that bone density was higher in the mutant mice as compared to WT control. However, we observed a shift in total body bone density and volumetric bone density in WT male and female mice, such that the total body BMD in WT mice was similar to those in mutant mice. To confirm this upward shift in BMD, we obtained new male (n=5) and female (n=5) mice from The Jackson Lab in the current reporting period and obtained total body BMD at 10- and 16-weeks of age. We compared this data with data obtained in 2001 and data collected in 2005 was significantly higher (**Figure 34**). Due to this increased BMD in WT mice, which we routinely obtain from The Jackson Laboratory for propagating the 10145 line, we are not characterizing this line any further until this discrepancy is resolved.

Phenodeviant with high bone density B2.4: The phenodeviant (Line 2.4) was identified as a 15-20% high total body bone density and bone mineral content whereas the bone area was largely unaffected. The body weight was about 5-8% higher in the phenodeviant mice, however, the body weight adjusted BMD was 10-12% higher. We generated 118 mice in this grant period for characterization of high bone density phenotype (**Table-4** and **Figure 21**).

Measurement of Bone Density Phenotype in Line 2.4 Mice: We evaluated bone density in 10-week and 16-week old mice and the results are shown in **Figure 21**.

Measurement of Ex-vivo pQCT Bone Density: Total bone density (mg/cm^3) and cortical bone density were measured by pQCT in femur and tibia from 16-week old male and female progeny obtained IT progeny. Nine slices covering the entire length of the bone were scanned, and slices 1 & 9 were excluded from analysis due to large variation. Total bone density of affected 2.4

mice was consistently higher ($p<0.05$) over the entire length of femur as shown with age- and sex-matched wild type (WT) female mice (**Figure 22**). The increase in bone density appears to be associated with increased bone area due to increased periosteal perimeter.

Histomorphometric measurements to determine cellular mechanisms of high bone density phenotype in Line 2.4 mutant mice: We performed histological examination of bone formation rate and bone resorption rate after dual labeling with tetracycline at 14-week and 16-week time points. Bones were processed as described above for mutant 12137.

Results of dynamic histological examination of femur midshaft region are shown in **Figure 23**. Bone area at femur midshaft in 16-week old mutant mice (A) was significantly higher as compared to WT control mice examined in previous grant periods. In addition, bone formation rate measured by dual labeling was increased at both periosteal and endosteal surfaces (**Figure 23**) at femur midshaft. These data suggest that that high BMD phenotype in mutant mice is due to increased bone formation.

Genotyping of Line 2.4 Mutant: Since the phenotype was interesting and we have bred this mutant extensively, we selected this phenodeviant for genotyping to identify chromosomal location of the mutation. In order to identify mutant locus, we bred 2.4 mutant with C3H/HeJ mice to produce approximately 28 F1 mice, which were then bred F1 male with F1 females to produce about 98 female F2 mice. We have completed the phenotype analysis of these F2 mice (representative data on BMC is shown in **Figure 24**) and currently genotyping the F2 mice for QTL analysis.

Phenodeviant with high volumetric bone density Line20: The phenodeviant (Line 20) was identified as a high bone density measured by PIXI. The total body bone density was 10-17% higher in male or female mice as compared to WT mice (**Figure 25**). The high bone density appears to be associated with 9-25% higher bone mineral content as compared to WT control mice, whereas bone area was within only 1-4% different from WT control mice. The body weights of the phenodeviant mice were 6-10% higher, however, the body weight adjusted BMD was also 8-10% higher.

Phenodeviant with blood chemistry phenotypes: We bred two phenodeviants (line 19.4 and Line 3.2) with abnormal lipid levels (total cholesterol, high density cholesterol, and triglycerides) and one phenodeviant (Line 7.2E) with high blood urea nitrogen levels (described in **Table-4**). Representative data on lipid levels for Line 19.4 and Line 3.2 are shown in **Figures 26** and **27**. Some of the F3 progeny appears to be affected with high blood lipid levels, however, these levels were measured in non-fasting blood and could be influenced by food consumption. We are currently collecting additional fasting samples to confirm these lines.

Phenodeviant with Low Alkaline Phosphatase Levels & High Bone Density: We observed one phenodeviant (Line 29.2) where low alkaline phosphatase values (30-40%) in serum were accompanied by higher bone density (+1.8SD units). We bred this phenodeviant and produced >40 mice in this line. Preliminary data on alkaline phosphatase levels is shown in **Figure 28**, which indicates that alkaline phosphatase levels in some mice were>80% lower as compared to littermates. The bone density in these mice was also higher, which would suggest that mutation affects gene(s) that control bone turnover. We are currently generating additional mice to confirm these findings.

Phenodeviant with High Total Body & Volumetric BMD: Earlier, we identified a phenodeviant (Line 5.4) that expressed high total bone density measured by PIXI that correlated with volumetric bone density and cortical thick ness. The cortical thickness was > 3SD units different from the wild type control mice. We generated 50 mice this year and approximately 25% of the F3 mice showed a high BMD phenotype (**Figure 29A**). The correlation with volumetric BMD and cortical thickness is shown in **Figure 29B** & **C**.

We performed e*x-vivo* bone density and bone size measurements in femur and tibia from high bone density mutant Line 5.4. The increased bone density was associated with higher bone area, which appears to be due to lower endosteal circumference in affected 5.4 female mice (**Figure 30**). These data suggest that the phenotype can be explained by decreased bone resorption or increased bone formation at endocortical bone surface.

Phenodeviant with High Total Body & Volumetric BMD: Our last recessive line was a phenodeviant (Line 5.3) that also expressed high total bone density measured by PIXI. We generated >100 mice this year and total body BMD data is shown in **Figure 31A**. The total body bone density showed significant correlation with volumetric BMD and cortical thickness (**Figure 31 B** & **C**). However, the correlation between total body BMD and cortical thickness was slightly weaker than that observed in Line 5.4.

We performed *ex-vivo* bone density and bone size measurements in femur and tibia from high bone density mutant Line 5.3. The increased bone density was associated with higher bone area, which appears to be due to higher periosteal circumference in affected 5.3 female mice (**Figure 32**). However, these data were not conclusive. The Line 5.3 appears to be similar to Line 5.4 and, in the future, we may only continue further characterization of Line 5.4.

Phenodeviant with Slow Soft-Tissue Healing (M1.2d): Our last line was a phenodeviant (Line M1.2d) expressed slow or no healing of a 2 mm ear punch hole in MRL strain of mice. We generated >100 mice during this reporting period and soft-tissue healing data is shown in **Figure 33**. Since the mutation affects tissue healing rate in an MRL background, we explored differential gene expression using microarray in this line, which is described in Specific Objective 3.

Specific Objective 2. The aim of this Specific Objective was to determine the chromosomal location of the mutant gene responsible for the phenotypes in selected mutant. We have proposed to achieve this aim by breeding the mutant mice with a mapping strain of mice to generate F1 mice and then breeding the F1 mice in back-cross or inter-cross breeding scheme to produce 50-100 F2 mice. The F2 mice are phenotyped and genotyped using 40-60 micro satellite markers and linkage analysis is employed to identify chromosomal location of mutation. Our progress on the Specific Objective 2 is discussed below.

Specific objective 2a-d.

We selected two dominant mutant lines, 12137 and 12184, and one recessive mutant line, B2.4, for mapping mutant locus. The rationale for selection of these mutants is based on extensive characterization of mutant phenotype, the robust inheritability of the mutation and the observation that all three mutation causes high bone mineral density. Of these three lines, we

have partially mapped line 12184 in the previous year without any success in identification of significant loci probably due to the low number of F2 mice screened.

Line 12184 Mapping

To identify the chromosomal location of the 12184 mutation, we generated 3 additional F1 mice by mutant B6 mice with C3H. We then intercrossed F1 mice to produce total of 137 B6C3H F2 mice for 12184 mutant (**Table-5**). We have screened all F2 progeny for bone density and size phenotypes at 10-week and at 16-week age as described in our dominant and recessive screen protocol. In addition, we have collected blood from 10-week old mice for biochemical analysis. The bone density phenotype data, which is the main phenotype in both lines, are shown in **Figures 10-14**. We combined data from male and female and performed interval mapping. Comparison of bone density data in mutant F2 mice with wild type F2 mice shows significantly higher bone density in mutant mice, which indicates that mutation is causing the shift in bone density.

Line 12137 Mapping

We generated 8 additional C3HB6 F1 mice by breeding the 12137 male with WT C3H mice. We generated a total of 148 F2 from more than 15 F1 mice for QTL mapping (Table-5). We have screened all F2 progeny for bone density and size phenotypes at 10-week and at 16-week age as described in our dominant and recessive screen protocol. In addition, we have collected blood from 10-week old mice for biochemical analysis. The bone density phenotype data, which is the main phenotype in both lines, is shown in **Figure 19**.

Line 2.4 Mapping

We generated 28 C3HB6 F1 mice by breeding 2.4 male mice with WT C3H mice. We generated a total of 98 F2 female by breeding 28 F1 mice for QTL mapping (**Table-5**). We have screened 92 F2 female progeny for bone density and size phenotypes at 10-week and at 16-week age as described in our dominant and recessive screen protocol. In addition, we have collected blood from 10-week old mice for biochemical analysis. The bone density phenotype data is shown in **Figure 24**.

Specific objective 2e-g

The tail clips were collected from >400 F2 mice from three different intercrosses and genomic DNA was extracted from for genotyping. Genomic DNA was isolated from tail clips using DNAeasy kits (Qiagen) for mouse tissue. DNA samples were quantified and quality determined by measuring their absorbance at 260 nm and 280 nm.

So far, a genome-wide genotyping scan has been completed in the 137 F2 mice using the >50 informative polymorphic markers for mutant 12184 mice. Genotyping was performed by using fluorescent labeled [labeled with FAM (blue), VIC (green), and NED (yellow)] informative markers which were PCR amplified from 60 F2 DNA. Markers were spaced at either end of each chromosome, and in some cases in the middle (for larger chromosomes). We performed approximately >10,000 PCR reactions to achieve genotyping. PCR reactions and running conditions allowed from 4 to 6 microsatellite markers to be multiplexed in a single electrophoretic lane. All 6 reactions were run in a single capillary on the ABI 3100 DNA analyzer. Following electrophoresis on the ABI 3100 DNA Analyzer, Genotyper software macros were used to semi-automatically score the allele calls for all the multiplex pools of every

single F2 mice. The pooled products were analyzed for fragment size on ABI Model 3100 DNA Analyzer and Genescan software was used to size alleles (Applied Biosystems). After an initial scoring by these macros, allele calls were visually checked and edited if necessary. Allele calls and edits were done using Genotyper software (Applied Biosystems) and exported as tab-delimited tables. A table of the calls was generated and the allele sizes converted into respective allele bins for entering into software program.

The interval mapping was performed by the Pseudomarker (obtained from www.jax.org/research/churchill) MAINSCAN program written for the MATLAB (Mathworks Inc., Natick, MA, USA) programming environment. Phenotype data and genotype data were imported into the software in excel comma separated text file format; mice with missing phenotypic and genotypic data were coded as phenotype unknown. Interestingly, one highly significant linkage was observed on chromosome 4, between 58-75 cM with LOD>5.0, as shown in **Figure 12** (A LOD score is the logarithm of odds score, i.e. the logarithm of the likelihood that two loci are linked/likelihood that loci are unlinked. Thus, a LOD score of 2 indicates that odds are 100:1 that a respective genetic region will show linkage to that trait).

To fine map the chromosome 4 locus affecting bone density, we used 11 markers on chromosome 4 (**Figure 13**). We then mapped all F2 mice with additional polymorphic microsatellite markers covering the entire length of chromosome 4 as shown in **Figure 13**. The fine mapping indicated that QTL peak was located between 65 cM and 75 cM region. In addition to data combined from male and female, we performed interval mapping of BMD and BMC traits separately for male and females. The results indicated that only one peak at chromosome 4 influenced bone density (**Table-6**).

Genotyping an interval mapping of lines 12137 and 2.4 is currently under progress.

SPECIFIC OBJECTIVE 3. The aim of this objective was to identify the candidate gene in the chromosomal locus established for the selected mouse mutant in Specific Objective 2 of the year 1. To achieve this, we have proposed to use DNA microarray analysis to investigate if the global gene expression pattern was altered in bone from mutant mice compared with wild type control mice. We selected two mutant mice, a soft tissue regeneration mutant line M1.2d and a bone size mutant line 917M mutant. We selected the 917M line because this mutant has been mapped to a precise chromosomal location. Although, in the previous year we had performed a microarray experiment using RNA from 917M mice. However, we observed that the intensity level of gene expression was low and variance was high, which could lead to identification of many false positive or false negative genes. Therefore, in the current reporting period we repeated the microarray experiments using additional replicates and added analysis of a new mutant line M1.2d.

Specific Objective 3a. To collect RNA from both mutant lines, we have to rely on phenotype distribution because the genotype is not available currently. Consequently, we screened several male progeny from 917M mutant at 10-weeks of age and selected those mice that exhibited Z-score of –2.5 or less. We used four replicates from four affected 917M mice, however, only RNA from only one additional affected mouse was collected in this reporting period. Three samples collected previously were utilized. To collect RNA sample, we sacrificed 917M mice and tibia and femurs were quickly isolated from any attached tissue. The ends of the tibia and femur were cut to flush out bone marrow, which was collected separately. The bones were then flushed with phosphate buffer saline solution. The bone and marrow were then stored at –70^{o}C

in RNALater (Ambion) according to manufacturer's protocol until extracted by pulverizing the bone in liquid nitrogen. Since we proposed to use bones from wild type mice as control, we collected additional tibia and femur from wild type male mice (n=4) exactly as described for mutant mice.

For line M1.2d, we punched a 2 mm hole in each ear of the mutant progeny (shown in **Figure-33**) when mice were 3-weeks old. Four days after the 2 mm ear punch, we collected approximately 0.5 mm of the tissue lining the 2 mm hole from one ear; the other ear was left untouched to monitor rate of healing at 21-days post ear punch. If the untouched ear hole healed after 21-days, the other ear tissue sample collected at 4-day was categorized as unaffected and if healing was significantly reduced (hole size 1.0-2.0) the tissue sample was categorized mutant. Tissue samples from 2-3 mice were pooled to make one replicate. We collected 4 affected and 4 control replicates and then stored at -70^{o}C in RNALater (Ambion) according to manufacturer's protocol until extracted by pulverizing the tissue in liquid nitrogen.

For extraction of total RNA from bone and marrow tissues, the tissue homogenate were prepared in appropriate amount or lysis solution/beta-mecaptoethanaol mixture (20ul/mg) and cells manually lysed with a mortar and pestle. The cellular debris was removed by centrifuging up to 600ul of homogenate through the mini prefiltration column, for 3 minutes at 13000 rpm, and collecting the filtrate. Equal volume of 70% ethanol added to the filtrate, placed on ice for at least 5 minutes, and further purified using spin columns from RNeasy Total RNA Isolation Kit (Qiagen, Chatsworth, CA, USA) according to the manufacturer's instructions. Using the above protocol, we have obtained very high quality RNA from small amounts of tissue (50 milligrams and less).

Before microarray analysis, each sample was evaluated for quality of the RNA by spectrophotometric analysis using Agilent 2100 Bioanalyzer. Concentration of the RNA yield was determined by spectrophotometric analysis using the convention that 1 OD at 260 nm equals 40 ug per ml. The absorbance was checked at 260 and 280 nm for determination of sample concentration and purity. Only samples with A260/A280 ratio close to 2.0 were selected for microarray analysis.

Specific Objective 3b. To perform in-house microarray to identify genes that are differentially expressed in the mutant versus control mice, we analyzed RNA from tibia of 917 and wild type mice together in two replicates. In addition, we analyzed pooled samples from ear tissues of mutant M1.2d. The pooled RNA was reverse transcribed into cDNA, labeled, and hybridized on our in-house microarray, which was created using Corning UltraGaps II glass slides and includes 15,000 mouse genes or uncharacterized expressed sequence tag (EST) clone. To make slides the PCR products were spotted using a Genetix Q-Array2 robotic arrayer. The arrays are also spotted with Amersham Lucidea Universal Scorecard controls to insure correct gene expression values were obtained from each array. The Lucidea Universal ScoreCard is a set of 23 unique microarray controls that can be used with samples from most species and with any microarray platform. The controls are artificial genes that generate pre-determined signal intensities that do not change across samples or experiments. Thus, the microarray analysis is not dependent on relative quantification. The controls generate a calibration curve for determining limits of detection, linear range, and data saturation, and they can be used as universal references for validating and normalizing microarray data. Controls are spotted in duplicate in the first and last PCR plates to insure proper data tracking.

The microarray slides were scanned using a GSI Lumonics ScanArray 4000 scanner. The arrays were scanned at a resolution of 10 microns which corresponds to ~15 pixels in diameter of each of the ~15,000 spots and a spacing of ~5 microns between the spots. The signal intensity of all microarray images was determined using Imagene 5.1 software. This software uses a patented image processing technology to provide quantification of microarray images of high density. Quality control measures include automated flagging of good, marginal and absent spots so that these can be filtered in the expression analysis.

Specific Objective 3c. To identify if any of the differentially expressed genes are located in the chromosomal location of mutant gene, scanned output files were analyzed using GeneSpring software version 4.2.

Before the formal analysis, we used the Scatter plot and the Condition tree features of GeneSpring software to evaluate the microarray chips to determine if they are suitable to be included in the analysis. The Scatter plot shows the data skewness between the Cy3 and Cy5 dyes (i.e. the treatment vs. control) for a particular chip. If there are too many genes highly expressed in one color, but not in the other, this may indicate that there are problems with the labeling process.

To allow for comparison of gene expression, the gene chips were globally scaled to an average intensity of 500. cDNA from each mice was put on two chips and was compared with the two control chips, generating 8 comparison files in total. Significance of differentially expressed genes was calculated by TTEST analysis, with $p<0.05$ as significantly altered gene expression. An average-fold change for the four comparisons of the selected genes was then calculated. We looked at fold change for all differentially expressed genes with $p<0.05$. Using these selection criteria, approximately 50 genes were differentially regulated in the bone from mutant mice compared with control mice. Those genes that are differentially regulated and are located on Chr 1 or 4 are shown in **Table-7**. We are in process of confirming expression levels of selective genes with real time PCR.

In the current reporting period, we have not completed the microarray data analysis of the soft tissue regeneration mutant line M1.2d. Our preliminary analysis indicates several potential candidate genes that are differentially expressed in ear tissue of mutant mice as compared to those from control mice. Detailed analysis of differentially expressed genes in the healing tissue of mutant versus control mice is currently in progress and will be reported in the subsequent report.

Specific Objective 3c. Further understanding the role of the differentially expressed genes in the pathways is critical in microarray studies. For this purpose, we use Gene Ontology to classify genes, to identify the pathways involved in each microarray study. Gene Ontologies are structured, controlled vocabularies that describe gene products in terms of their associated biological processes, cellular components and molecular functions in a species-independent manner. To determine if differentially expressed genes represent a pathway that is controlled by an upstream regulatory gene located in the chromosomal region for mutant gene, we have looked into all differentially expressed genes that could be likely candidate genes. At present, this analysis is preliminary, hence no specific pathway is currently reported.

ENU BREEDING SCHEME

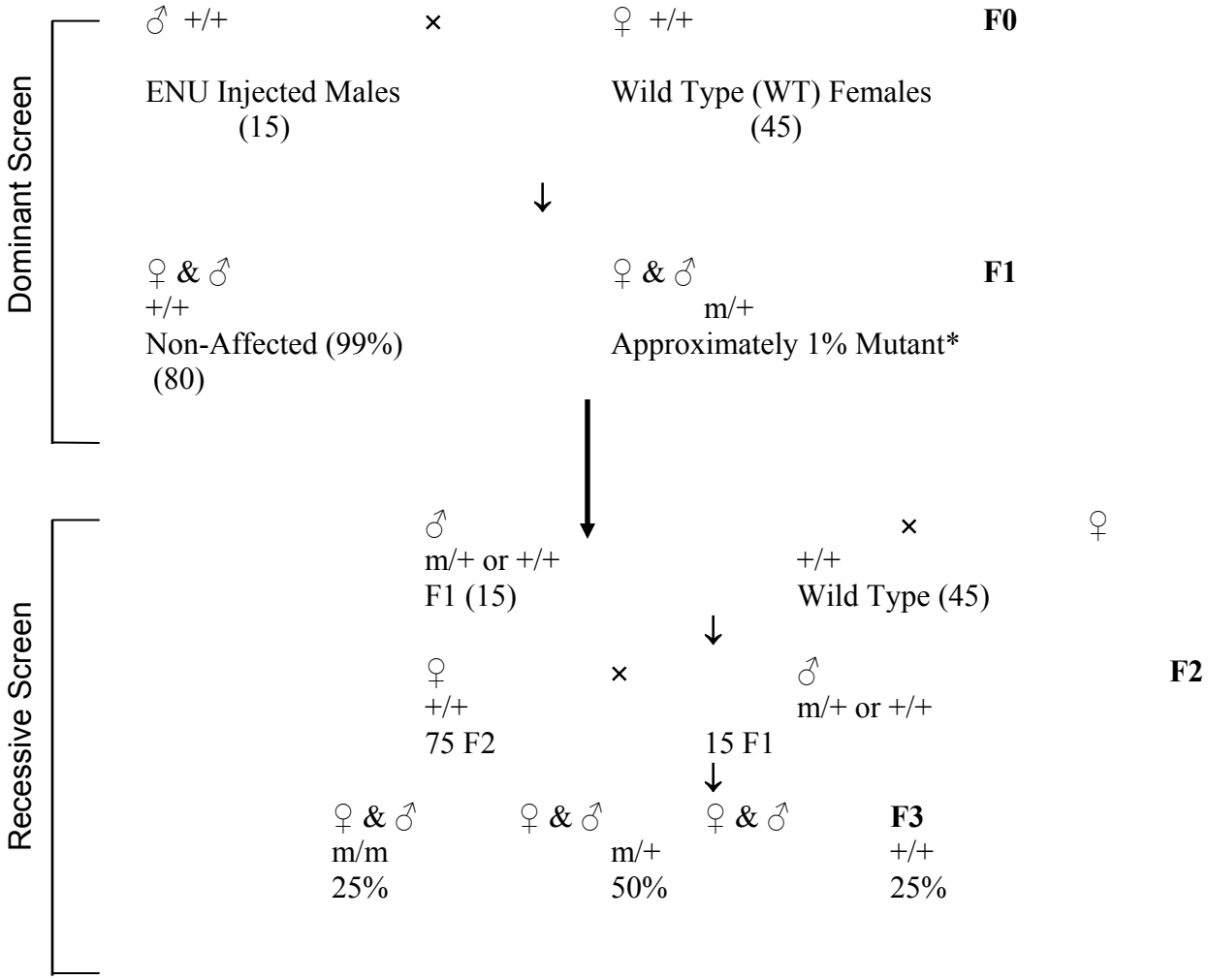

Figure 1. ENU Breeding Scheme. The breeding scheme incorporates dominant and recessive mode of inheritance (using MRL/MpJ mice). The numbers are only an approximate estimate of mice that were bred and progeny generated.

*This estimate is based on previous experience in C3H & B6 strain of mice for musculoskeletal phenotypes.

Table – 1. Response of MRL mouse strain to 3 X 100 mg/kg dosage of ENU.

	MRL/MpJ (MRL)
Percentage of males died before regaining fertility	27%
Average Time Taken by ENU Injected Male to Return to Fertility (Weeks)	21.3
Percent of Males Sterile	27%
Total Number of Litters Produced	33
Total Number of Litters Survived	25
Average Litter size	4.8
Number of Mice Produced for Primary Screening	119

Table – 2. Number of mice tested, phenotypes scored and confirmed in retest, phenodeviants introduced to inheritance testing.

Procedure	Recessive Mode of Inheritance	Dominant Mode of Inheritance
Number of Mice Screened	24	118
Abnormal Phenotypes Identified in Primary Screen	1	>30
Abnormal Phenotypes Confirmed in Secondary Screen	1	25
Phenotypes Introduced to Progeny Testing	1	25
Phenotypes Confirmed in Progeny Testing	Not Yet Completed	Not Yet Completed

Table – 3. Results from breeding of MRL mice for production of F3 mice for recessive screening.

Procedure	Number of Mice
F1 MRL Mice Bred with WT MRL Females to Produce F2 Mice	10
F1 MRL Mice Produced F2 Litters	7
F2 Female Mice Produced	18
F3 Litters Produced	6
Phenotypes Introduced to Progeny Testing	0

Table-4. Number and current status of recessive screen phenodeviants that have been identified in previous grant periods and bred this year to confirm heritability.

No	ID	Phenotype at Repeat Screening or 16-Week Confirmation Screen	Number of F1 & F2 Mice Produced[a]	Number of F3 Mice Screened[b]	Current Status
1	B2.4.C.M	Total Body BMD Z-Score=3.9, Total Body BMC Z-Score=3.0	118	114	**Confirmed**
2	B7.2.E	High Blood Urea Nitrogen (45 mg/dL)	0	18	**Not Confirmed**
3	B24.3	12-17% High Total Body BMD	6	0	**Could Not Breed**
4	B19.4	55-90% High Triglyceride	54	14	**Not Confirmed**
5	B17.2	High FAT Mass Z-Score=6.1, Total Body Bone Area Z-Score=-2.5	19	8	**Not Confirmed**
6	B3.2	20-30% Low Total Cholesterol, HDL, & TG	65	86	**Not Confirmed**
7	B20.3E & F	Total Body BMD Z-Score=2.4 to 3.5, Total Body BMC Z-Score=2.4 to 2.5	71	35	**Partially Confirmed**
8	B9.4.i & k	Total Body BMD Z-Score=2.6-4.2, Total Body BMC Z-Score=3.0-4.1	49	48	**Not Confirmed**
9	B5.4.D	Total Body BMD Z-Score=3.2, Total Body BMC Z-Score=4.2	102	75	**Confirmed**
10	B14.1.E	High FAT Mass Z-Score=4.5	0	5	**Not Confirmed**
11	B15.3.f	Body Weight Z-Score=-5.8 Low IGF-I	64	43	**Not Confirmed**
12	B5.3.f	High Cortical Thickness Z-Score=2.0	169	123	**Partially Confirmed**
13	B22.3	Body Weight Z-Score=-2.5 to –5.6, Low IGF-I	0	0	**Could Not Breed**
14	B29.2	30-40% Low Serum Alkaline Phosphatase and Osteocalcin, Total Body BMD Z-Score=1.8	80	98	**Partially Confirmed**
15	B27.2	Total Body BMD Z-Score=-5.0, Total Body BMC Z-Score=-6.8	46	43	**Testing**
Total			**843**	**710**	

BMD= Bone Mineral Density, BMC= Bone Mineral Content, Z-Score indicates differences in a particular phenotype in terms of SD units from wild type control mice.
[a]Includes mice produced after September 2004.
[a]Includes mice produced before September 2004 but screened after September 2004.

Table-5. Mutant mice strains that have been identified in earlier screens and bred in current grant period for genotyping and detailed characterization of the phenotypes.

No	ID	Phenotype (Strain)	Number of IT Mice Produced	Number of IT Mice Screened	Number of New F1 & F2 Mice Produced for Genotyping
1	9.1.7.B.M	15-20% Low Total Body Bone Area and BMC (B6)	128	104	0
2	12.13.7.E.M	20% High BW & Total Body BMC (B6)	129	100	**156**
3	12.18.4.D.F	16% High Total Body BMD & BMC (B6)	98	105	**184**
4	10.14.5.E.M	High Total Body BMD (C3H)	48	48	0
5	Agouti & Low BMD	Low Total Body BMD (C3H)	19	16	0
6	B2.4.C.M	Total Body BMD Z-Score=3.9, Total Body BMC Z-Score=3.0	129	93	**126**
TOTAL			**551**		**466**

Table-6. Number and status of phenodeviants from MRL dominant screen that have been identified in 2003-2004 screen period and were bred in current grant period to confirm heritability.

No	ID	Phenotype Observed at 16-Week Confirmation Screen	Number of Mice Produced for Inheritance Testing	Current Status
1	M1.2d	STR 1.9 mm, Tibia Midshaft BMD Z-Score=4.2, Trabecular BMD Z-Score=3.7	116	Confirmed
2	M1.9a	STR 1.9 mm	13	Not Confirmed
3	M1.4d	STR 1.7 mm, Tibia Midshaft BMD Z-Score=2.0	1	Could Not Breed[a]
4	M1.4.A	Low Total Body BMC, Z-Score=-3.1	0	Could Not Breed
5	M1.4.B	High Total Body BMC, Z-Score= 2.5, Tibia Midshaft BMD Z-Score=3.8	15	Not Confirmed
6	M1.11b	Low BW Z-Score=-2.1, Total Body BMD Z-Score=-3.7, Total Body BMC Z-Score=-3.1	0	Could Not Breed
7	M1.2.k	High BW Z-Score=2.0, Total Body BMD Z-Score=2.9, Total Body BMC Z-Score=2.4	0	Could Not Breed
8	M1.8.A	High Total Body BMC Z-Score=4.2	0	Could Not Breed
9	M1.8.B	High Total Body BMD Z-Score=3.4, Total Body Bone Area Z-Score=-3.2	3	Could Not Breed
10	M1.9.D	BW Z-Score=3.3, Total Body BMD Z-Score=3.9, Bone Area Z-Score=-5.1	18	Not Confirmed
11	M1.6.A	STR 1.6 mm, High BMD BW Z-Score=3.2, BMD Z-Score=3.7, BMC Z-Score=2.8	0	Could Not Breed
12	M1.9.k	STR 1.1 mm, Total Body BMD Z-Score=3.7, Total Body BMC Z-Score=2.3	0	Could Not Breed
13	M1.5.I	Total Body BMD Z-Score=2.8, Total Body Bone Area Z-Score=-3.1, High Alkaline Phosphatase	16	Partially Confirmed
14	M1.5.k	Total Body BMD Z-Score=3.6, Total Body BMC Z-Score=3.0	0	Could Not Breed
15	M1.2.L	Total Body BMC Z-Score=2.9, Total Body Bone Area Z-Score=2.9	0	Could Not Breed
16	M1.6A	STR 1.6 mm	0	Could Not Breed
17	M1.7A	STR 1.4 mm	15	Not Confirmed
18	M1.14.g	51% High Alkaline Phosphatase	0	Could Not Breed
19	M1.4.F	23% High Blood Triglyceride	0	Could Not Breed
20	M1.14C	Low BMD at Midshaft Tibia Z-Score=-5.8	0	Could Not Breed
21	M1.7.D	STR=1.9	8	Could Not Breed
Total			**205**	

BW= Body Weight, BMD= Bone Mineral Density, BMC= Bone Mineral Content, STR= Soft tissue Regeneration phenotype shown as size of hole in mm (normal values range between 0-5 mm) Z-Score indicates differences in a particular phenotype in terms of SD units from wild type control mice.

[a]A lot of mice could not produce more than one or two litters and therefore we were unable to assess if mutation is inherited or not. A possible reason was that these mice were bred only after secondary screening (when >16-week old) and after 1-2 breeding cycle their productivity declines considerably as they grow older.

Table-7. List of genes that belong to chromosomes 1 and 4 and are significantly up or down regulated in mutant 917 mice as compared to WT control mice.

Gene Name	Normalized Data	Common		Genbank
H3106E12	5.99	Cbfa2t1h	Chr 4	BG072085
H3087D02	5.48		Chr 4	BG070437
H3068H11	2.84		Chr 4	BG068752
H3062A11	2.76		Chr 4	BG068128
H3045G04	2.38		Chr 4	BG066591
H3155F06	2.22		Chr 4	
H3038H06	2.10		Chr 4	BG066098
H3063H09	1.76		Chr 4	BG068298
H3009E04	1.40	2410043F08Rik	Chr 4	BG063619
H3025H09	1.34	Vamp3	Chr 4	BG064970
H3004B04	1.33		Chr 4	BG063189
H3101C12	1.31		Chr 4	BG071628
H3059H05	1.28	Smp1-pending	Chr 4	BG067938
H3065E11	1.14		Chr 4	BG068443
H3106C04	1.11		Chr 4,10,14	BG072059
H3021G02	1.11		Chr 4	BG064599
H3113A04	0.93	Rps6	Chr 4	BG072620
H3016C08	0.93		Chr 4	
H3145H04	0.92	C1qb	Chr 4	BG075320
H3128E03	0.90		Chr 4	
H3131B04	0.90	Scp2	Chr 4	BG074122
H3022H02	0.89		Chr 4,18	
H3115H06	0.88		Chr 13,17,4	
H3055A12	0.81	Prdx1	Chr 4	BG067497
H3099G06	0.50	Tcea3	Chr 4	BG071507
H3144D01	0.13		Chr 8,4	BG075190
H3064E12	3.376		Chr 1	BG068355
H3037G06	2.374		Chr 1	BG065999
H3064B04	2.243		Chr 1	BG068315

H3146F07B	1.909		Chr 1	BG075390
H3124H10A	1.813		Chr 1	
H3146G02	1.539	Cfh	Chr 1	BG075397
H3125B12	1.463		Chr 1	
H3061H05	1.433		Chr 1	BG068111
H3033A06	1.42		Chr 1	BG065593
H3040G11	1.417		Chr 1	
H3019B03	1.402	Soat1	Chr 1	BG064396
H3056C01	1.347	Fmn2	Chr 1	BG067604
H3146C07	1.314		Chr 1	BG075356
H3140F12	1.212		Chr 1,M	BG074900
H3041A10	1.179		Chr 1	BG066276
H3019A11	0.939	Vps4b	Chr 1	BG064392
H3107E08	0.915	C130074G19Rik	Chr 1	BG072168
H3112E01	0.905	Snrpe	Chr 1	BG072573
H3066F01	0.892	Rgs2	Chr 1	BG068533
H3009C06	0.872	Arpc2	Chr 1	BG063604
H3121A10	0.863		Chr 1	
H3113E11	0.862	LOC226519	Chr 1	BG072670
H3124F03	0.856		Chr 1,14	
H3076A07	0.851	2810031L11Rik	Chr 1	BG069483
H3016F11	0.81		Chr 1,11	
H3130F03	0.808		Chr 1,14	
H3039H04B	0.759	Ipo9	Chr 1	BG066182
H3124G10	0.742	Uxs1	Chr 1	BG073697

This list only includes genes that are differentially expressed between mutant 917M mice as compared to WT mice and are located on chromosome 1and 4 where two QTLs regulating bone size were observed.

Table-8. Results of interval mapping of mutant with high bone density (Line 12184).

Phenotype	Phenotype	Chr	cM	LOD Score
Male BMD	4	58.4	3.8	23%
Female BMD	4	68.6	3.2	22%
Male BMC	4	58.4	3.4	21%
Female BMC	4	65.0	1.4	9%
Male ABMD	4	66.6	3.7	21%
Female ABMD	4	69.6	4.6	27%
Male ABMC	4	58.4	4.0	25%
Female ABMC	4	75.6	1.8	15%

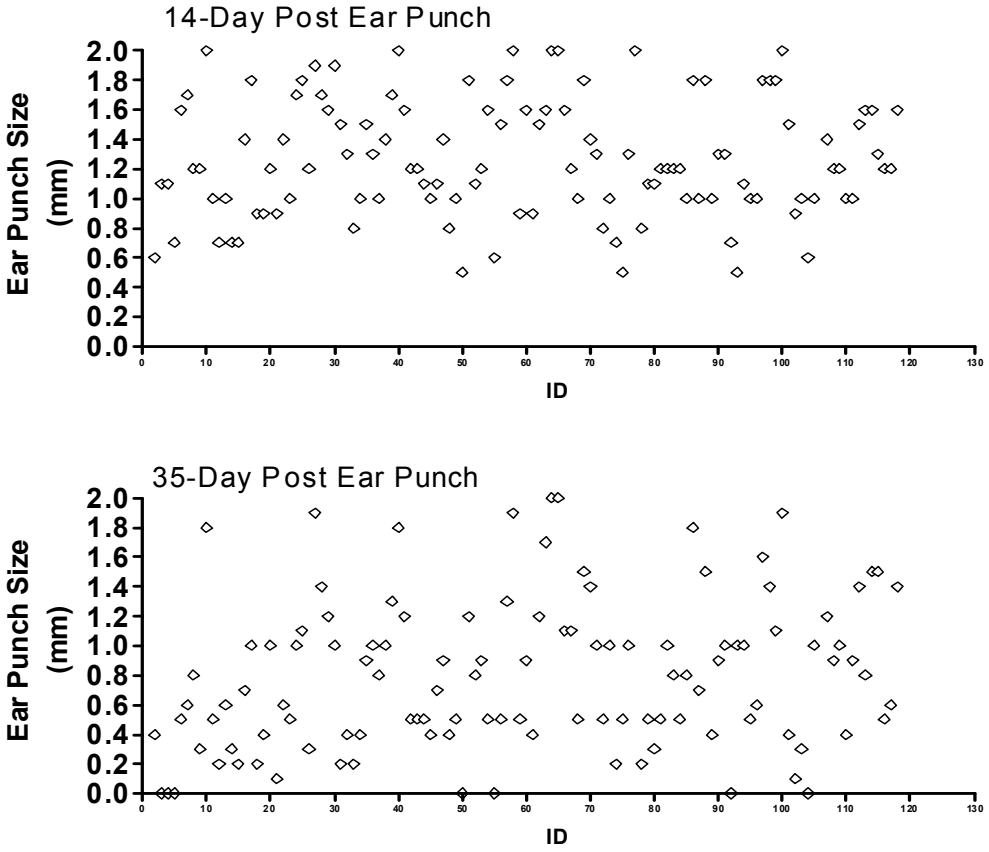

Figure 2. Soft-tissue regeneration screen in MRL mice. Top panel shows average hole size measured at two week after 2-mm ear punch (the cut-off for slow healing is hole size >1.4, based on average healing in wild type MRL mice). Bottom plot shows average healing after 5-weeks there was a large variation in phenotype, however, >75% mice show greater healing 35-days after ear punch compared to 14-day after ear punch. We are currently evaluating several of these mice that heal poorly to test heritability.

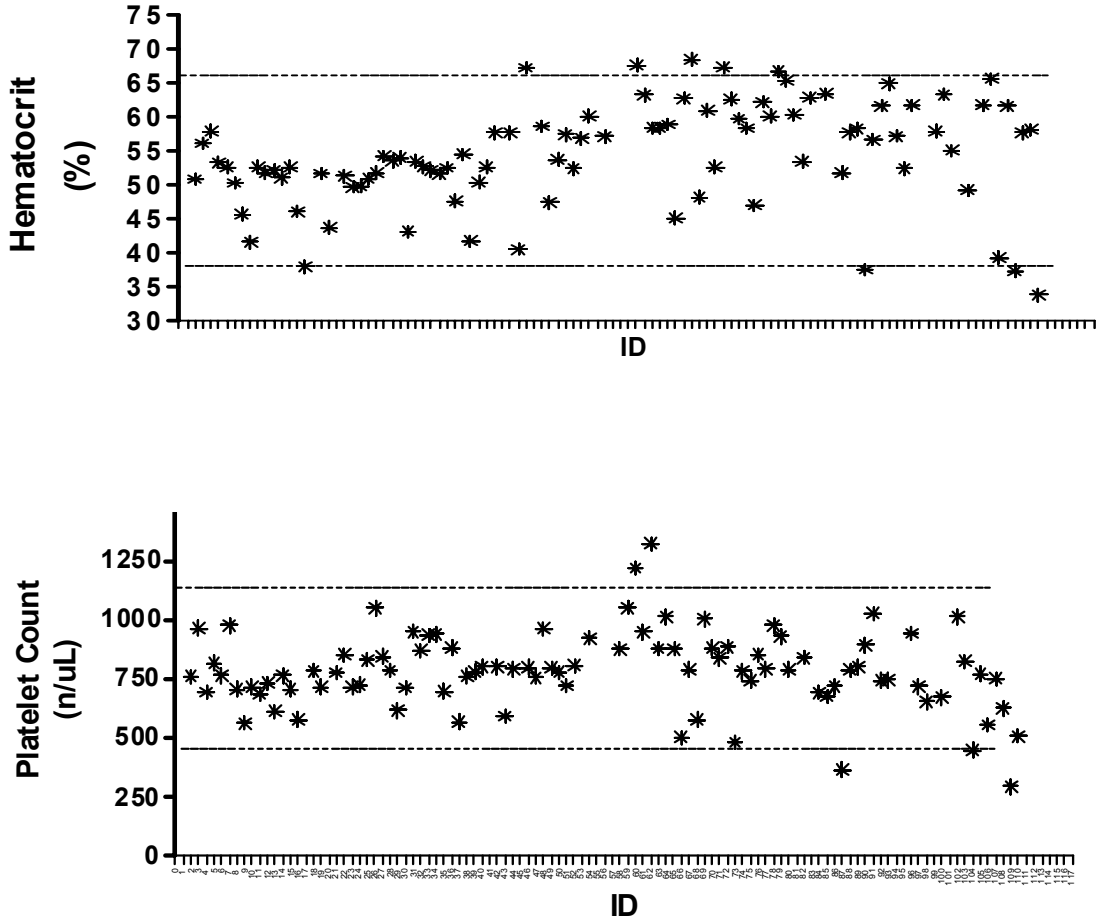

Figure 3. Representative data from screening of hematological parameters in dominant screen in MRL/MpJ mice. Top panel shows average hematocrit and bottom panel shows blood platelet counts measured at 10-week screen. Other parameters screened but not shown in this figure include, hemoglobin, WBC, RBC, lymphocytes, neutrophils, mean cell volume etc. We have arbitrarily set up cut-off values (shown as broken lines) to represent abnormal hematology for identification of phenodeviants.

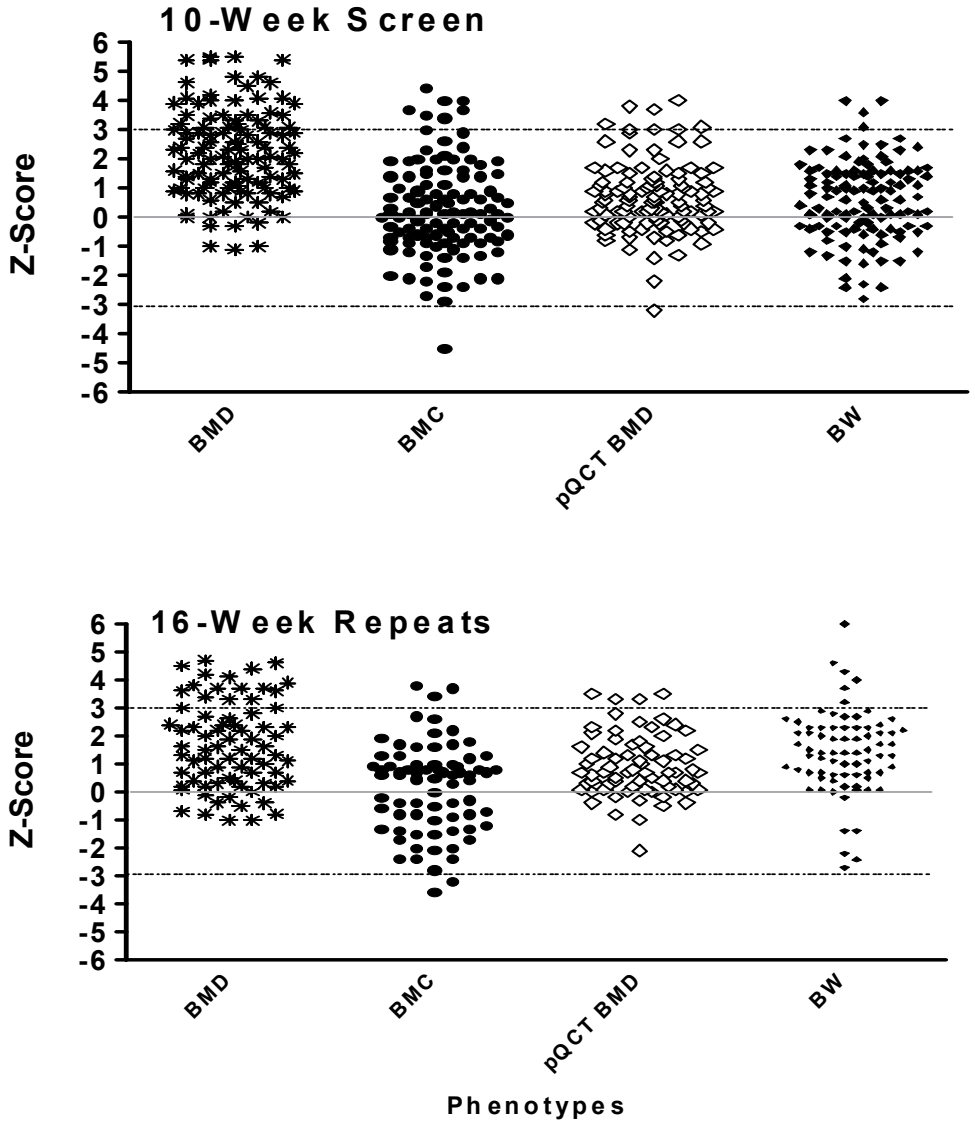

Figure 4. Representative data from various musculoskeletal phenotypes in MRL/MpJ mice measured for dominant screening. Top panel shows Z-scores (represents differences in SD units from mean value of WT mice) phenotypes such as body weight, total body bone density, total body bone mineral content, and body weight adjusted BMD measured at 10-week screening. The bottom panel shows 16-week phenotype of several phenodeviants along with normal littermates. We have used a Z-score of 3 as cutoff for identifying phenodeviant mice because of large number of outliers.

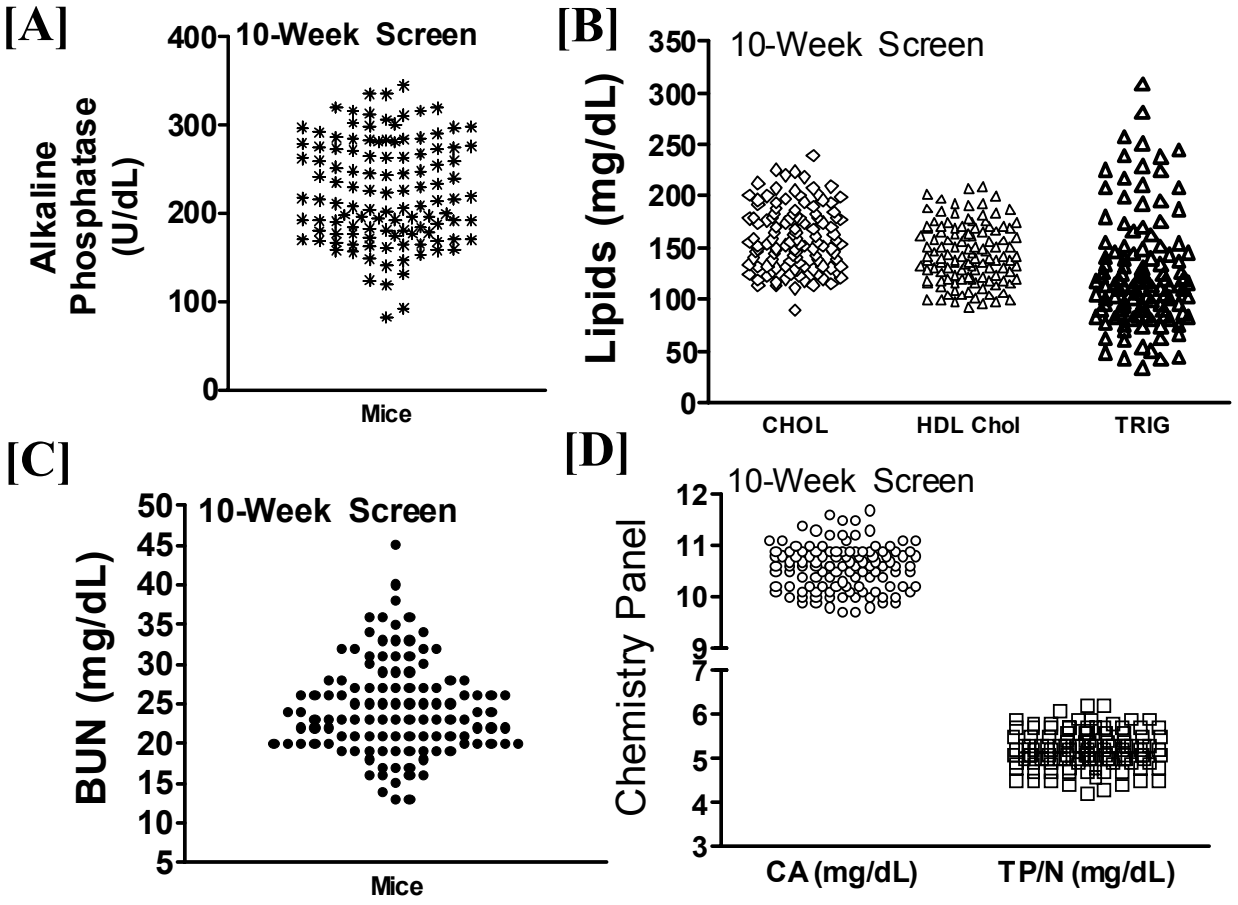

Figure 5. **Representative phenotype data from blood chemistry measurements in the dominant screen.** Representative data on blood chemistry phenotypes such as alkaline phosphatase (A), cholesterol (Chol), HDL cholesterol, triglycerides (TRIG) (B), blood urea nitrogen (BUN) (C), and calcium (CA) and total protein (TP/N) (D) levels are shown for MRL mice screened at 10-week.

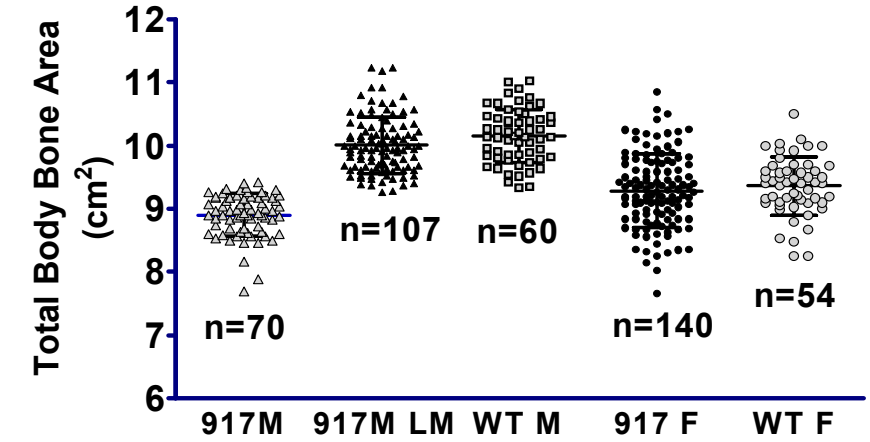

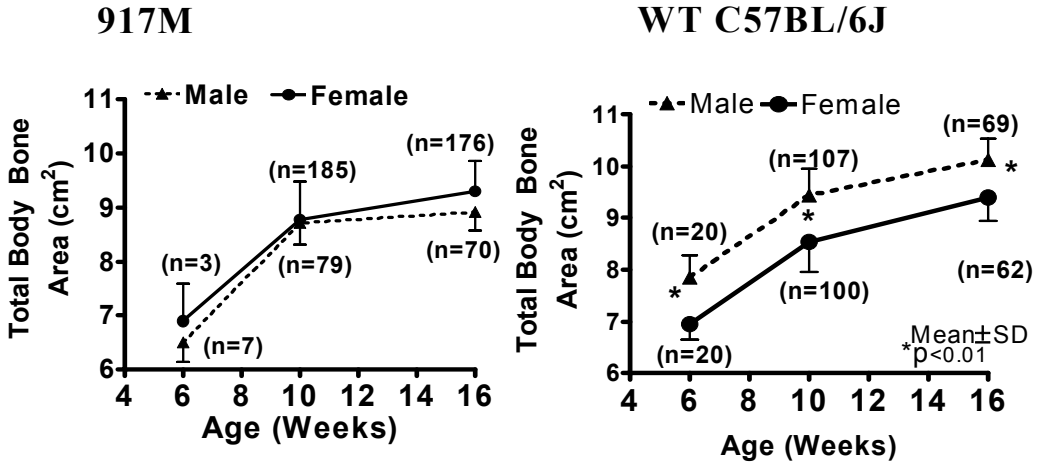

Figure 6. Generation of affected progeny (top panel) for previously identified phenodeviant with reduced bone size (Line 917M). The plot shows that only male mice (approximately 40%) were affected. In this reporting period we generated several new mice for further characterization of the low bone area phenotype. Especially, we screened mice at 6-week age that showed that low bone area phenotype was expressed at this age. We propose to measure bone area in 3-week old mice to identify if changes in bone area occur at puberty.

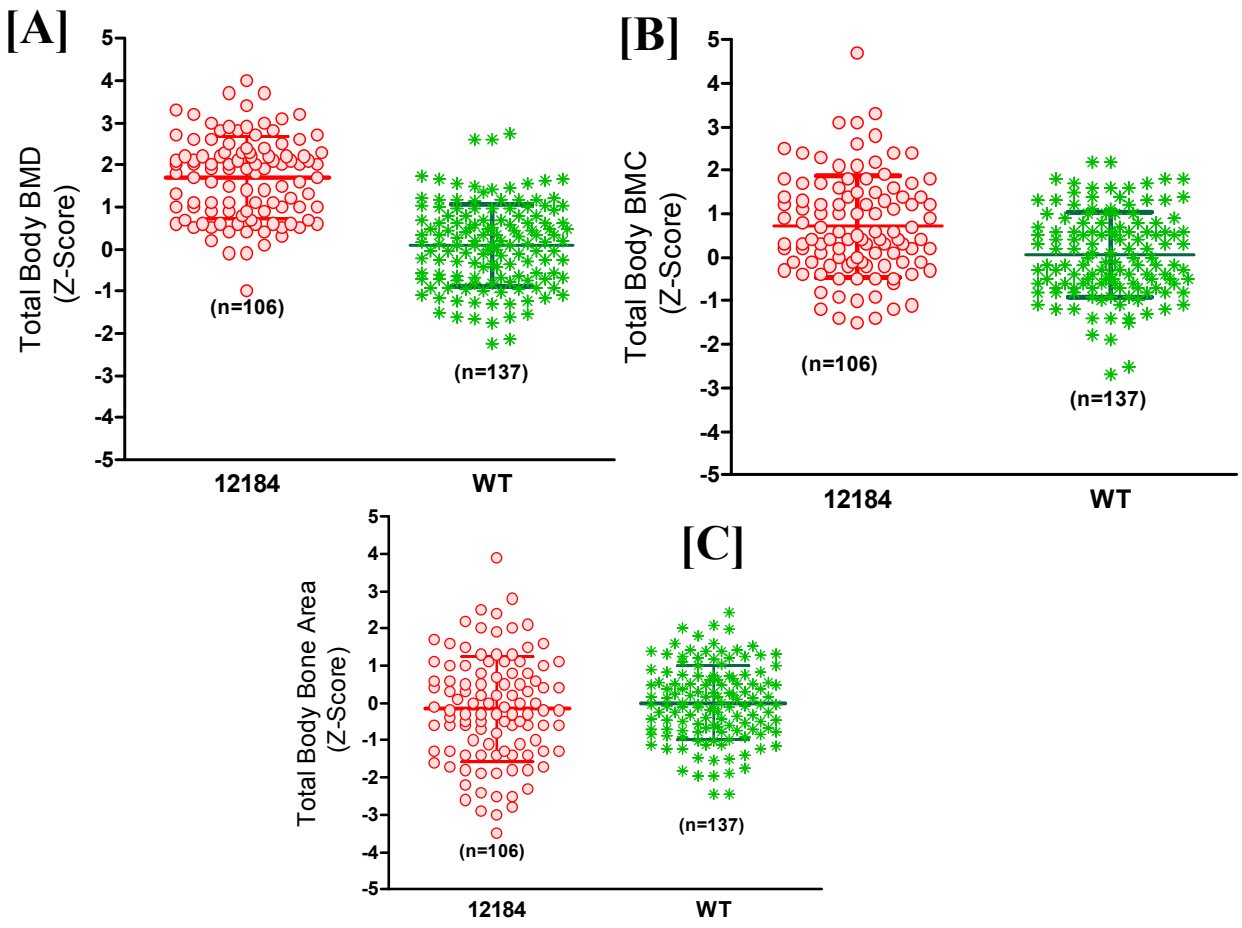

Figure 7. Generation of affected progeny for previously identified phenodeviant with increased bone density (Line 12184). The y-axis represents Z-score for total body bone density (A), bone mineral content (B), and bone area (C). The x-axis includes all IT progeny including the non-affected littermates. The body weight adjusted total body bone density and bone mineral content were 7-10% higher ($p<0.05$) in mutant mice, whereas the bone area was largely unaffected ($p>0.05$). About half of the IT progeny were classified as affected. These data suggest that there is an increase in material bone density in mutant mice. In this reporting period we generated several new mice for further characterization of the bone density phenotype, as shown in subsequent figures.

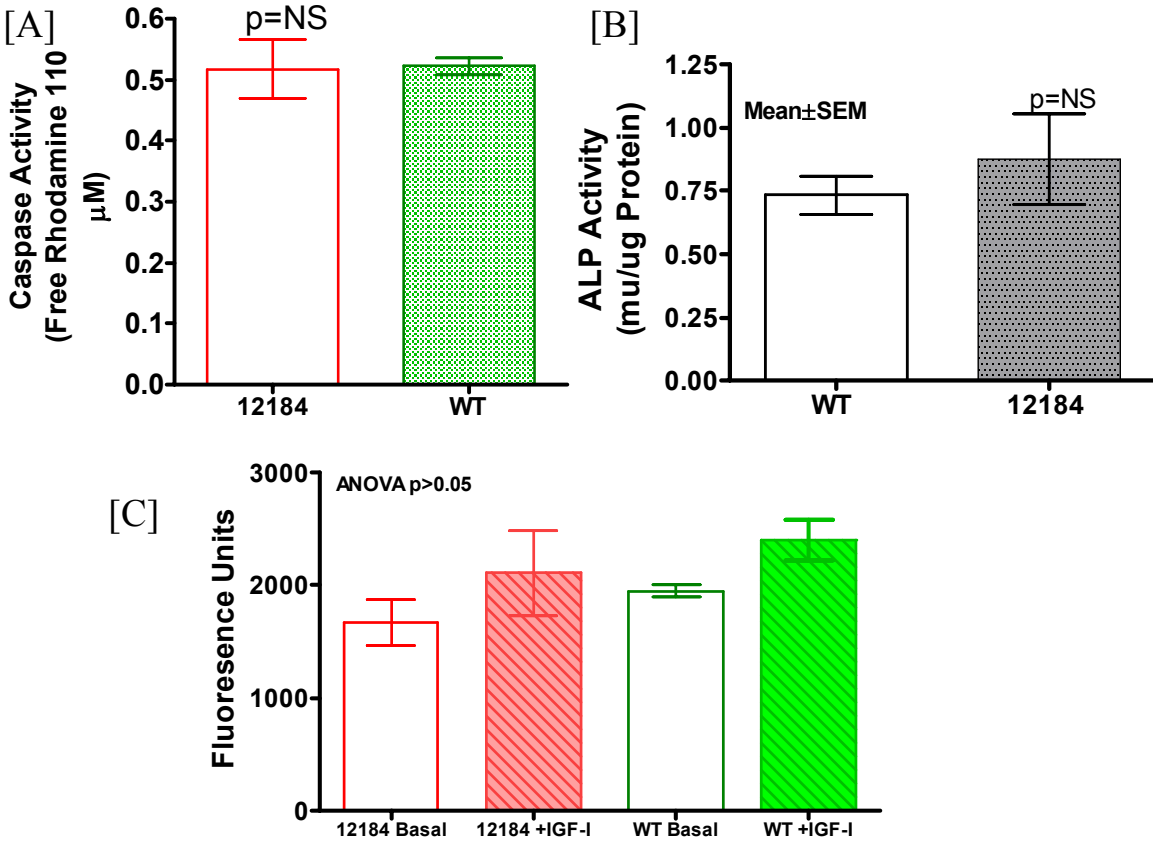

Figure 8. Characterization of periosteal osteoblast phenotype for mutant with increased bone density (Line 12184). Periosteal osteoblasts were isolated from 10-week old female WT and mutant 12184 mice and grown in cultures. Each experiment was performed with cells from three animals and 3-4 wells were used for cell culture for each animal. Data from 2-4 animals were combined and shown as mean values. No significant differences were observed in basal apoptosis (a), differentiation (B), and proliferation (C) levels of cells from 12184 mice as compared to those from WT mice.

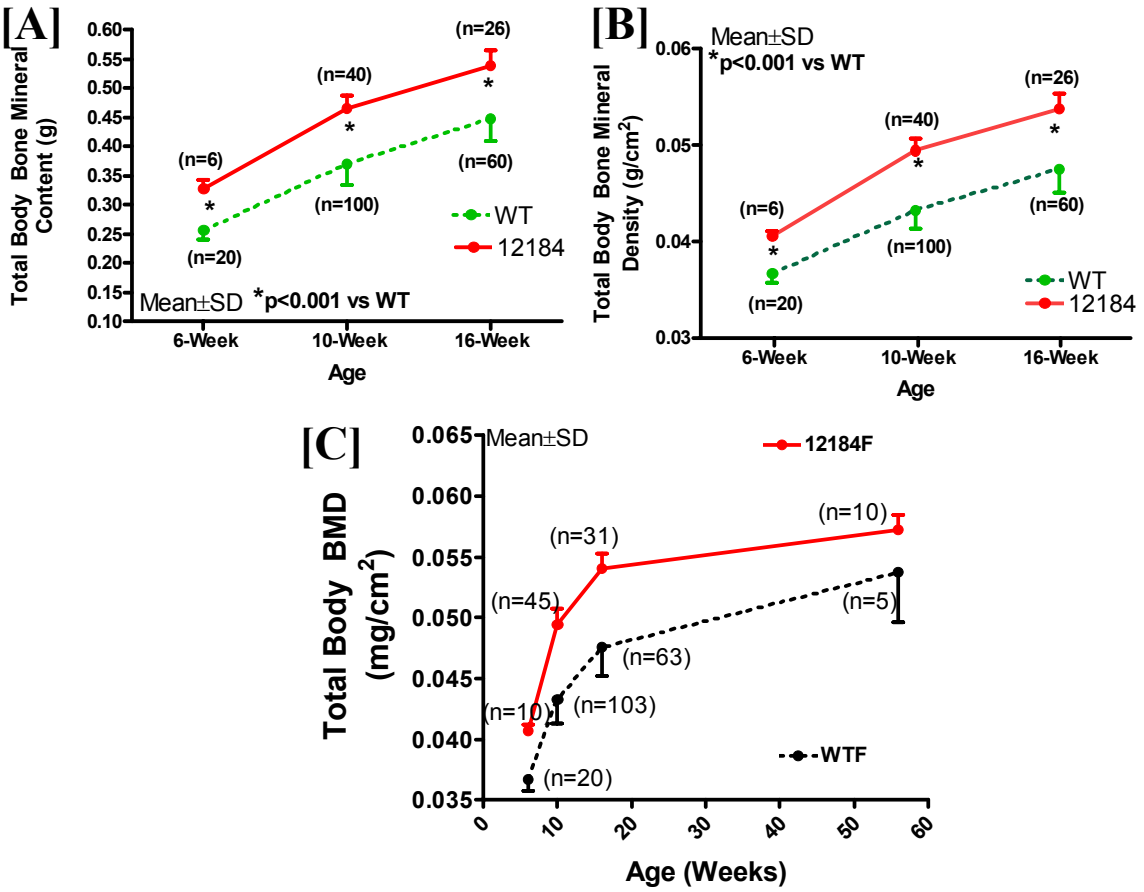

Figure 9. Generation of affected progeny for previously identified phenodeviant with high bone density (Line 12184). In the current reporting period, we generated several new mice, especially, we measured bone density at 6-week and 1-year old mice. The figure shows total body bone density (BMD) and bone mineral content (BMC) for 6-week, 10-week, and 16-week old mutant 12184 and wild type (WT) female mice (A & B). These data suggests that as compared to WT females, increase in BMD in 12184 mutant mice occurred at early age (<6-week) with only slightly higher increases at 10-week and 16-week. These data also suggest that there is an increase in material bone density at very young age. We propose to measure bone density in3-week old mice to identify if changes in BMD occur prior to or during puberty. Furthermore, bone density continues to be higher in mutant female mice that are 1-year old (C).

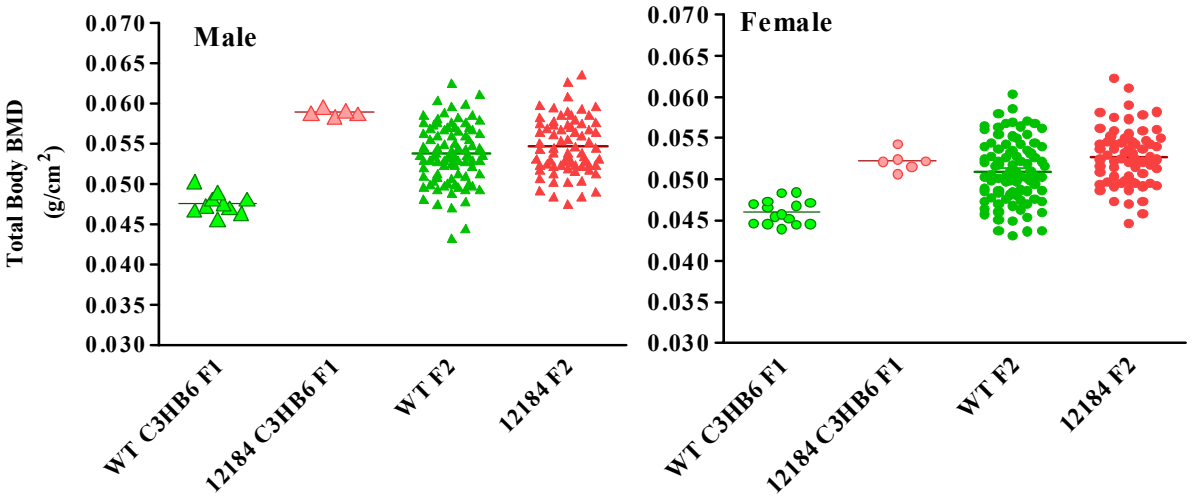

Figure 10. Generation of F1 & F2 progeny for identification of chromosomal location of high bone density mice (Line 12184). In the current reporting period, we generated several new F1 & F2 mice. This figure shows that the high bone density phenotype was robustly expressed in the F1 mice generated from breeding of mutant 12184 (B6) with C3H/HeJ mice.

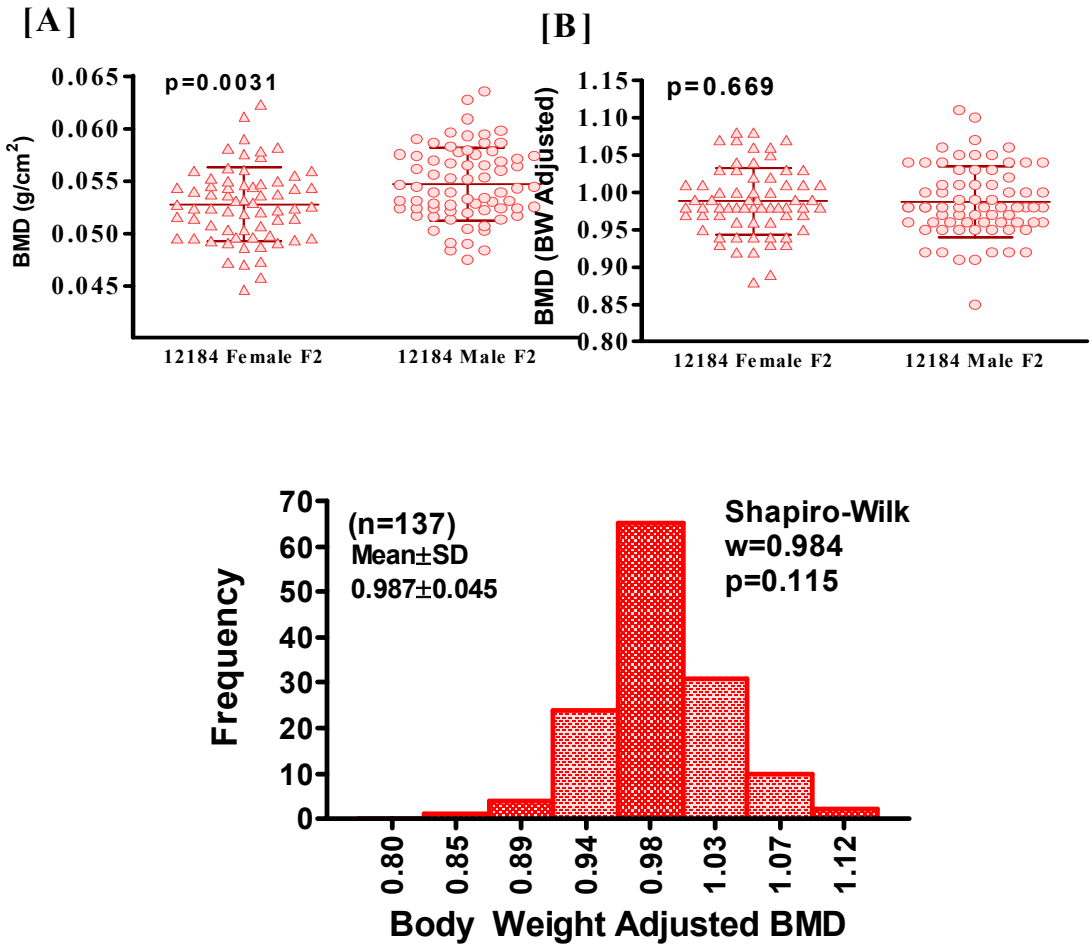

Figure 11. To identify the chromosomal location of high bone density mutant mice, we used body weight adjusted BMD data from F2 male and female progeny (Line 12184). The top panel (A) shows that total body BMD from male and female F2 mice are statistically different, however, body weight adjusted BMD are similar in male and female F2 mice. Hence, data from male and female F2 could be combined for QTL mapping. The bottom panel shows that the body weight adjusted BMD was normally distributed; therefore, interval mapping could be used to identify QTLs affecting BMD.

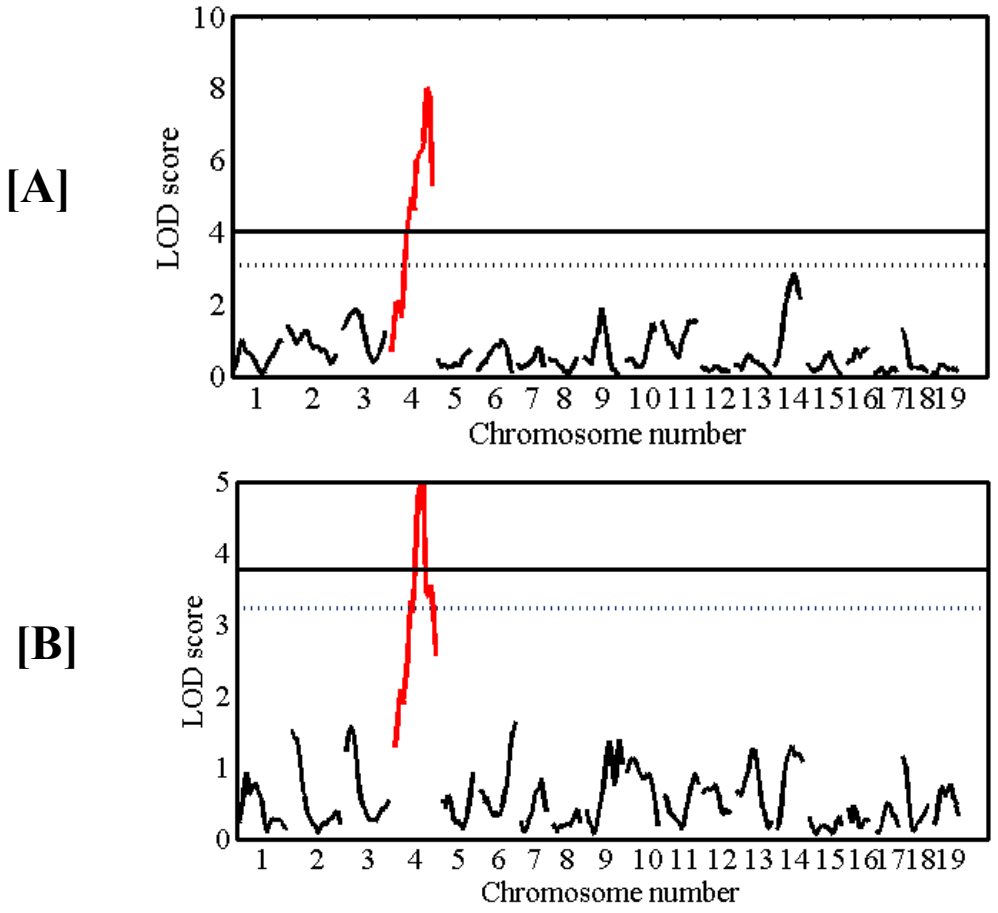

Figure 12. Mapping chromosomal location of ENU mutation exhibiting high bone density (12184). Genome wide main QTL(s) associated with total body bone density (DXA) in 10-week old intercrossed B6C3H F2 male and female mice (n=137) generated from mutant mice. The horizontal lines indicate genome-wide error levels of $p<0.01$ (solid line) and $p<0.05$ (broken line). The interval mapping was performed by Pseudomarker (obtained from www.jax.org/research/churchill) MAINSCAN program written for the MATLAB (Mathworks Inc., Natick, MA, USA) programming environment. Chromosome 4 locus showed a highly significant linkage with bone density and bone mineral content in F2 progeny.

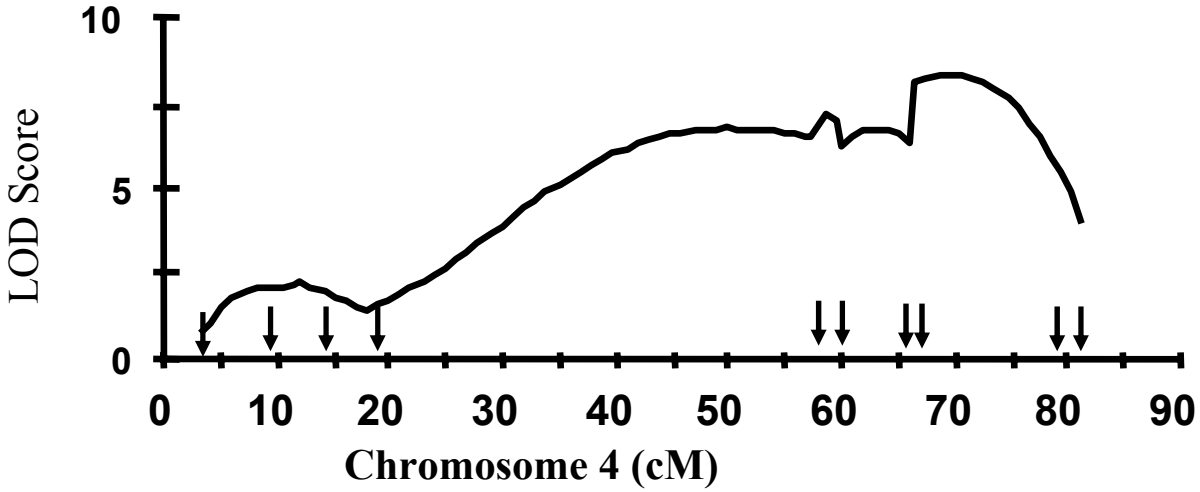

Figure 13. Fine mapping of chromosome 4 locus affecting BMD in 12184 mutant mice. The fine map of chromosome 4 using 11 additional markers confirms peak locus between 65-75 cM that influences BMD. Marker locations are shown by arrow.

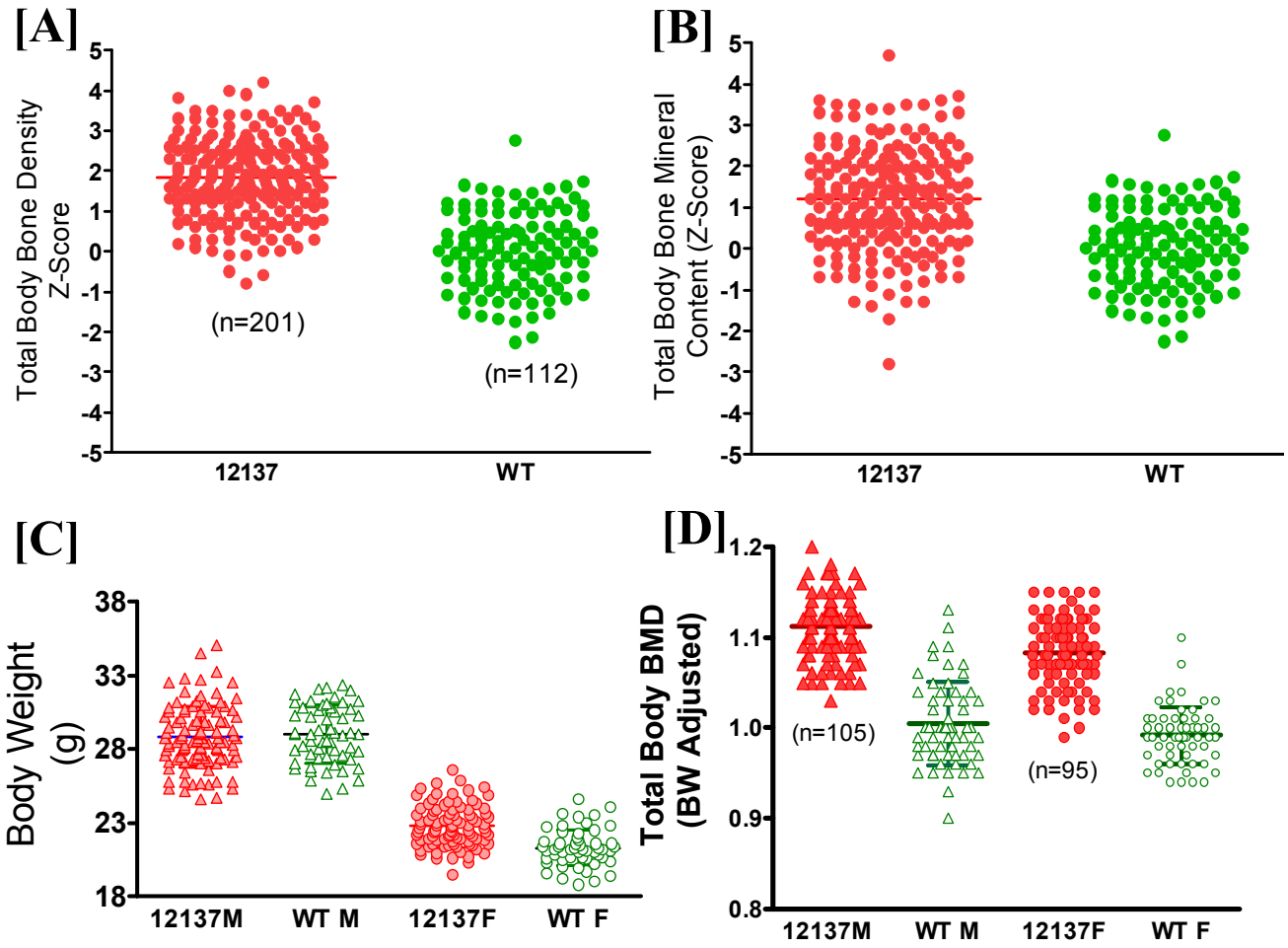

Figure 14. Generation of affected progeny for previously identified phenodeviant with increased bone density (Line 12137). The y-axis represents Z-score for total body bone density (A), bone mineral content (B). The x-axis includes all IT progeny including the non-affected littermates. The body weight adjusted total body bone density and bone mineral content were 8-10% higher ($p<0.05$) in mutant mice. About half of the IT progeny were classified as affected. The body weight were slightly higher in affected 12137 mice (C), however, the increased BMD was more than BW (D).

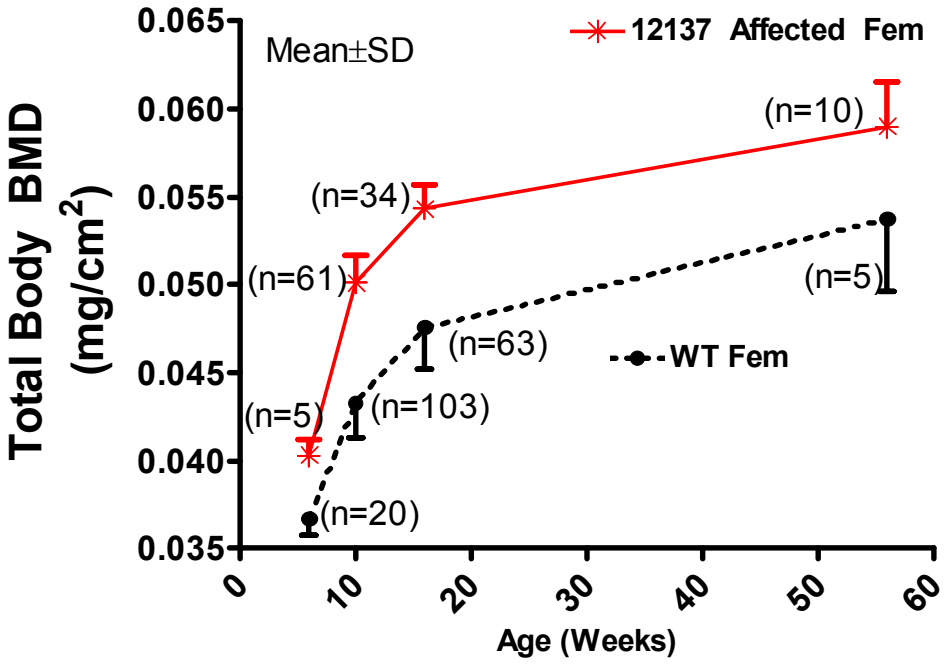

Figure 15. Generation of affected progeny for previously identified phenodeviant with high bone density (Line 12137). In the current reporting period, we generated several new mice. Especially, we measured bone density at 6-week and 1-year old mice. The figure shows total body bone density (BMD) and bone mineral content (BMC) for 6-week, 10-week, and 16-week old mutant 12137 and wild type (WT) female mice (A & B). These data suggests that as compared to WT females, increase in BMD in 12137 mutant mice occurred at early age (<6-week) with only slightly higher increases at 10-week and 16-week. These data also suggest that there is an increase in material bone density at very young age. We propose to measure bone density in3-week old mice to identify if changes in BMD occurr at puberty. Furthermore, bone density continues to be higher in mutant female mice that are 1-year old (C).

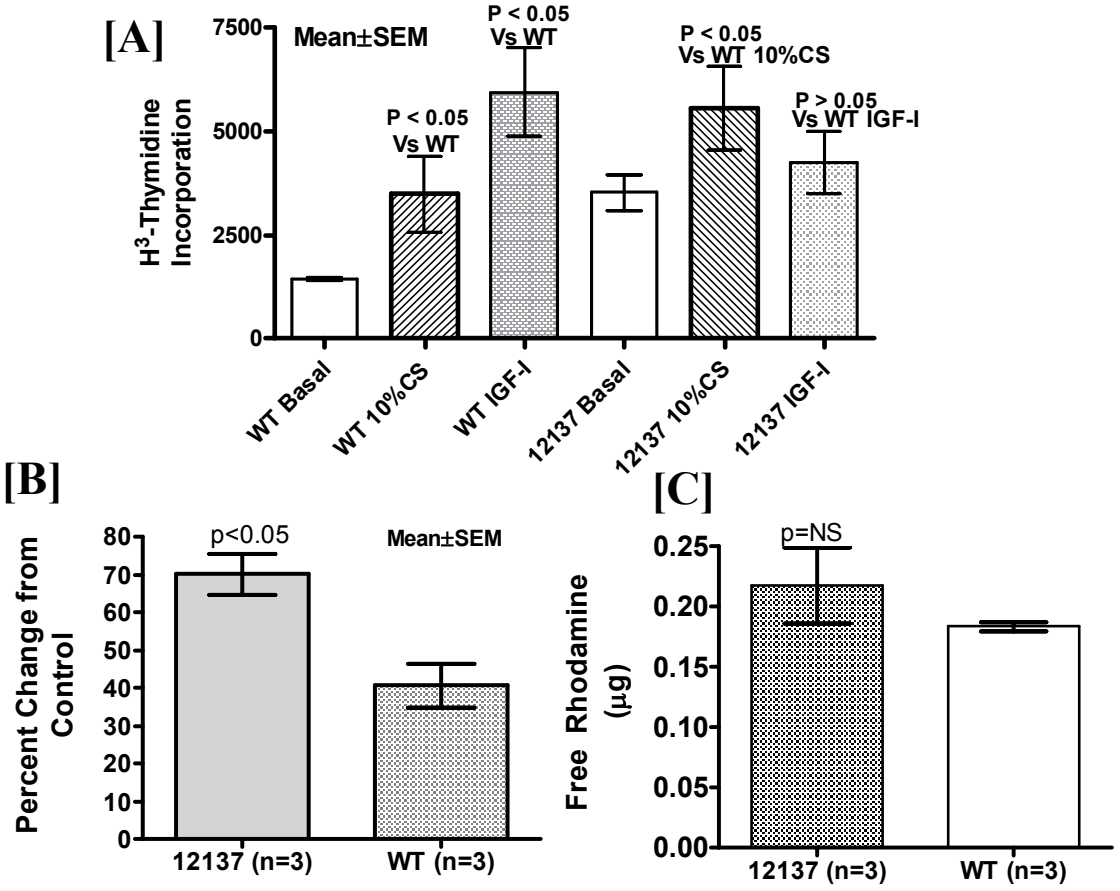

Figure 16. Characterization of periosteal osteoblast phenotype for mutant with increased bone density (Line 12137). Periosteal osteoblasts were isolated from 10-week old female WT and mutant 12137 mice and grown in cultures. Each experiment was performed with cells from 3-4 animals and 3-4 replicates were used for each animal. Data from three animals were combined and shown as mean values. Our preliminary data indicates higher basal proliferation rate measured by thymidine incorporation in osteoblasts from 12137 mice as compared to WT mice (A). There was a higher increase in proliferation in response to calf serum as compared to IGF-I (A). Basal proliferation rate was also higher when Almar Blue dye was used to measure proliferation rate (B), the y-axis shows percent change in fluorescence units as compared to control. No significant differences were observed in basal apoptosis (C) rate in osteoblasts from 12137 mutant mice, as compared to those from WT mice.

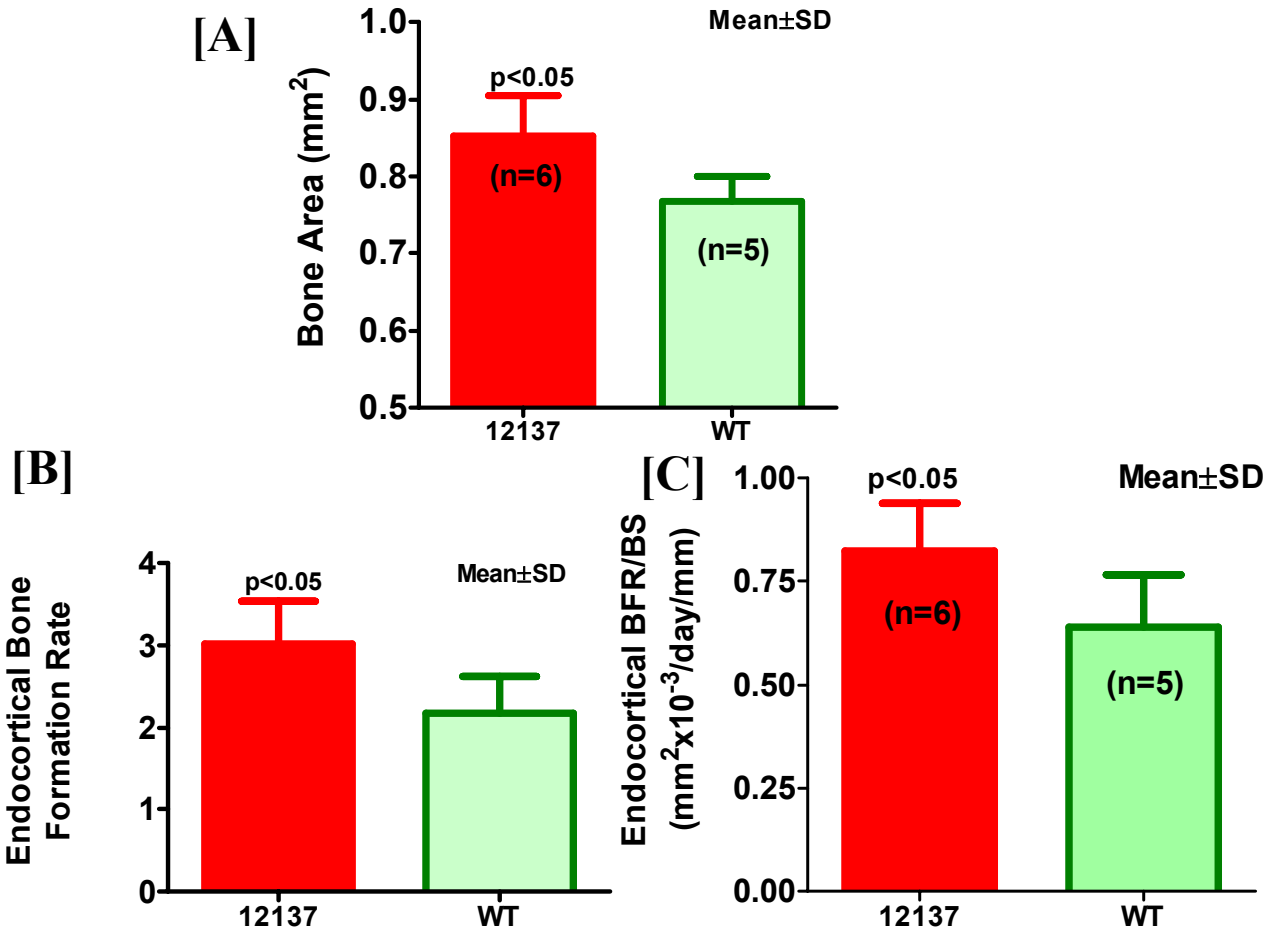

Figure 17. Histomorphometric measurements to determine high bone density phenotype in 12137 mutant mice. Bone area at femur midshaft in 16-week old mutant mice measured by histology (A). Endocortical bone formation rate (B & C) at femur midshaft measured by tetracycline labeling (periosteal bone formation rate was not significantly affected). These data suggests that high BMD phenotype in mutant mice appears to be due to increased endocortical bone formation.

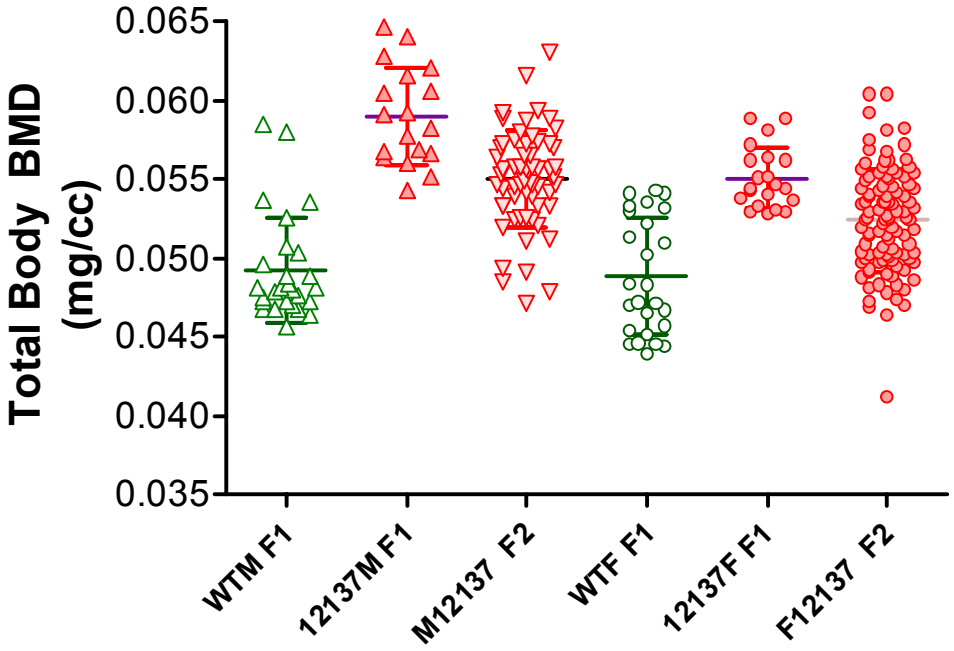

Figure 18. Generation of F1 & F2 progeny for identification of chromosomal location of high bone density mice (Line 12137). All F1 & F2 mice reported for 12137 were generated in the current reporting period. The figure shows that the high bone density phenotype was robustly expressed in the F1 mice generated from breeding of mutant 12184 (B6) with C3H/HeJ mice. The bone densities in 12137 male (12137M F1) and female (12137F F1) were significantly higher by ANOVA, as compared to WT male (WTM) or female (WTF).

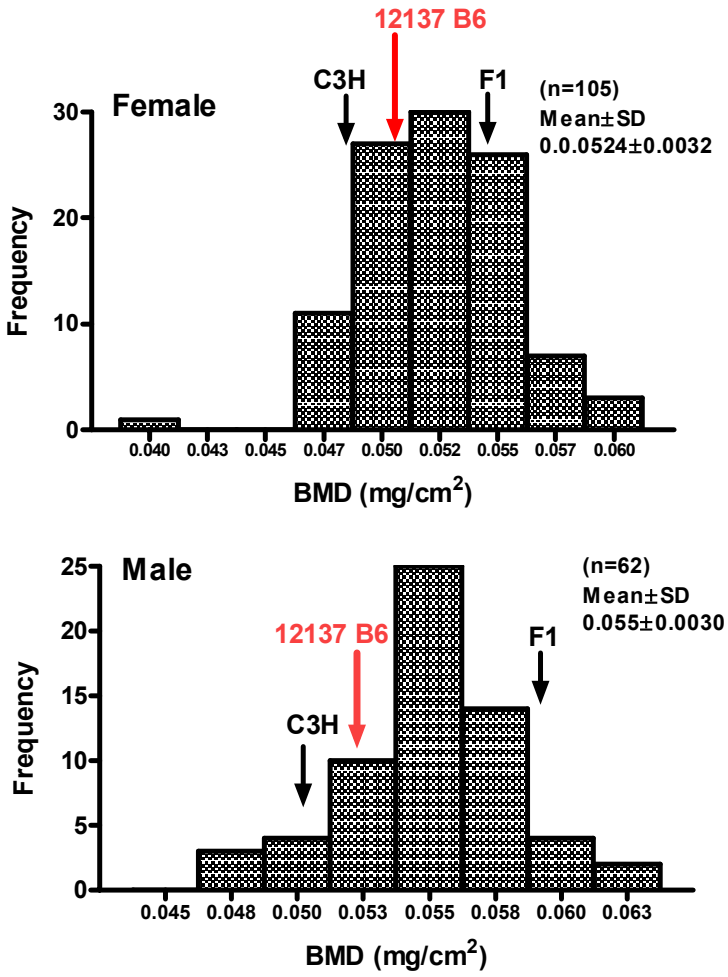

Figure 19. Frequency distribution of total body BMD phenotype in F2 male and female progeny (Line 12137). The BMD data appears to be normally distributed; therefore, interval mapping could be used to identify QTLs affecting BMD. We have completed the phenotype and genotyping of all F2 mice and currently performing the QTL mapping to identify the mutant locus.

Agouti Line
C3H/HeJ background

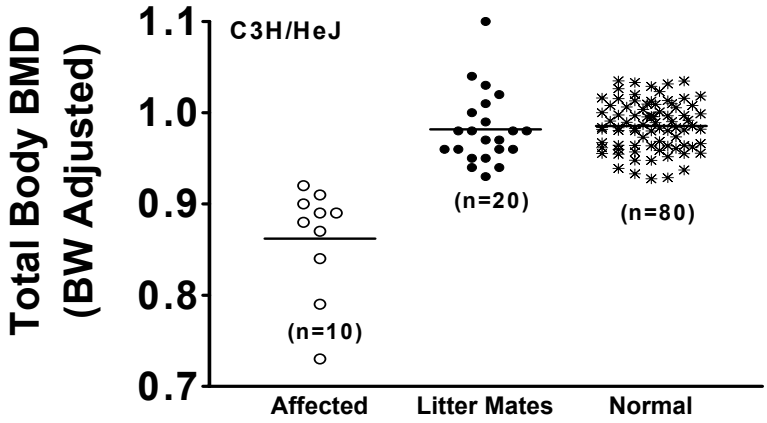

Figure 20. (Top) A yet to be fully characterized mutant mice (left) shown with normal littermate (right), affected mice appears weak (slightly lower body weight) and shows fur with greasy appearance early in development (birth to 6-week age). Adults have hairs with increased yellow pigmentation, and low BMD (bottom). The mutant mice breed less efficiently, however, we have generated some additional mice in this line and continue to breed this line for further characterization.

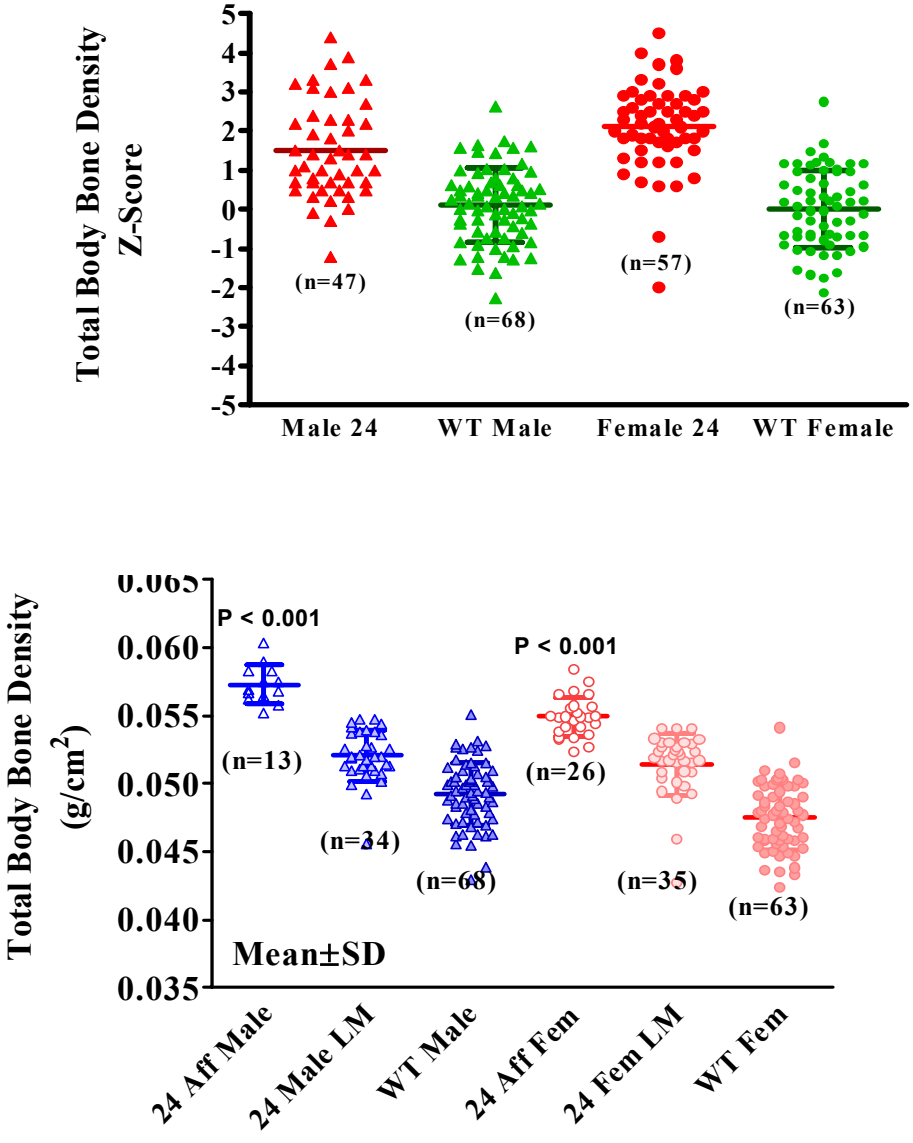

Figure 21. (Top) Z-scores for total body BMD in 16-week old progeny from male and female B2.4.C.M (referred as 2.4 or Line 24 for simplicity) mutant mice. (Bottom) Total body BMD in 16-week old progeny from male and female B24 mutant mice.

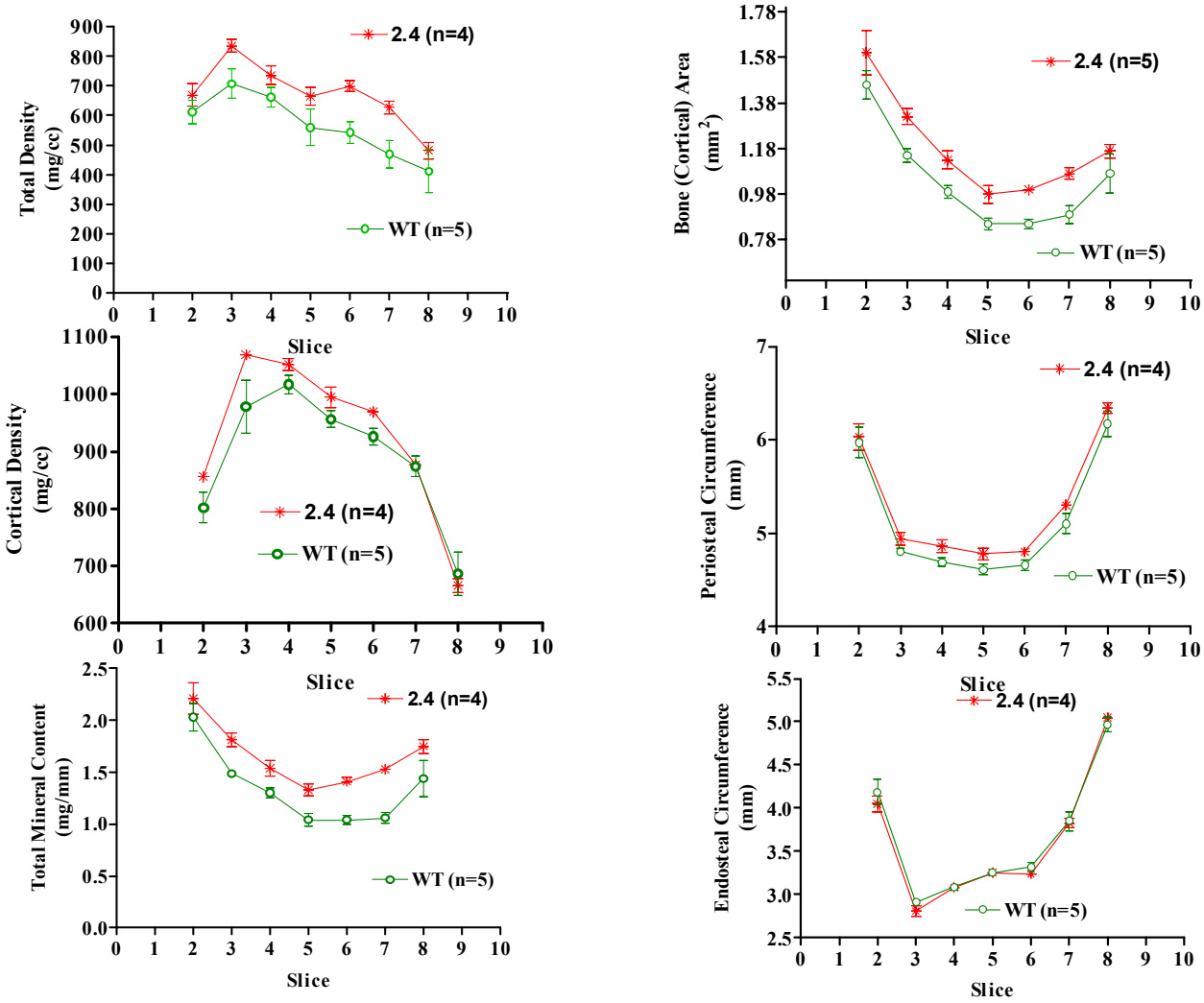

Figure 22. *Ex-vivo* bone area measurements in femur from high bone density mutant identified in B6 dominant screen (Line 2.4). Total bone density (mg/cm^3) and cortical bone density were measured by pQCT in 16-week old female progeny obtained from breeding mutants with WT B6. Nine slices covering entire length of the bone (slices 1 & 9 were excluded due to large variation) were scanned. Total ($p<0.05$) and not cortical bone density of affected 2.4 mice was consistently higher over the entire length of femur as shown with age and sex matched wild type (WT) mice. The increase in bone density appears to be associated with increased bone area probably due to increased periosteal perimeter.

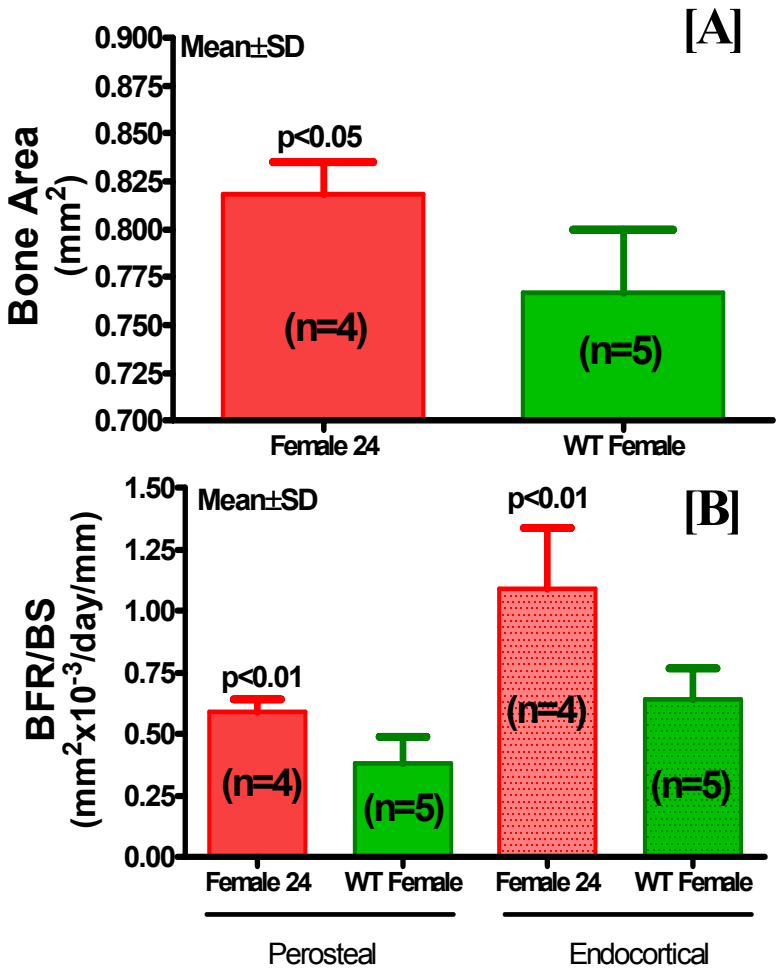

Figure 23. Histomorphometric measurements to determine high bone density phenotype in Line 2.4 mutant mice Bone area at femur midshaft in 16-week old mutant mice measured by histology (A). (B) Bone formation rate at femur midshaft measured by tetracycline labeling. The histology data suggests that high BMD phenotype is due to increased bone formation at both periosteum and endosteum.

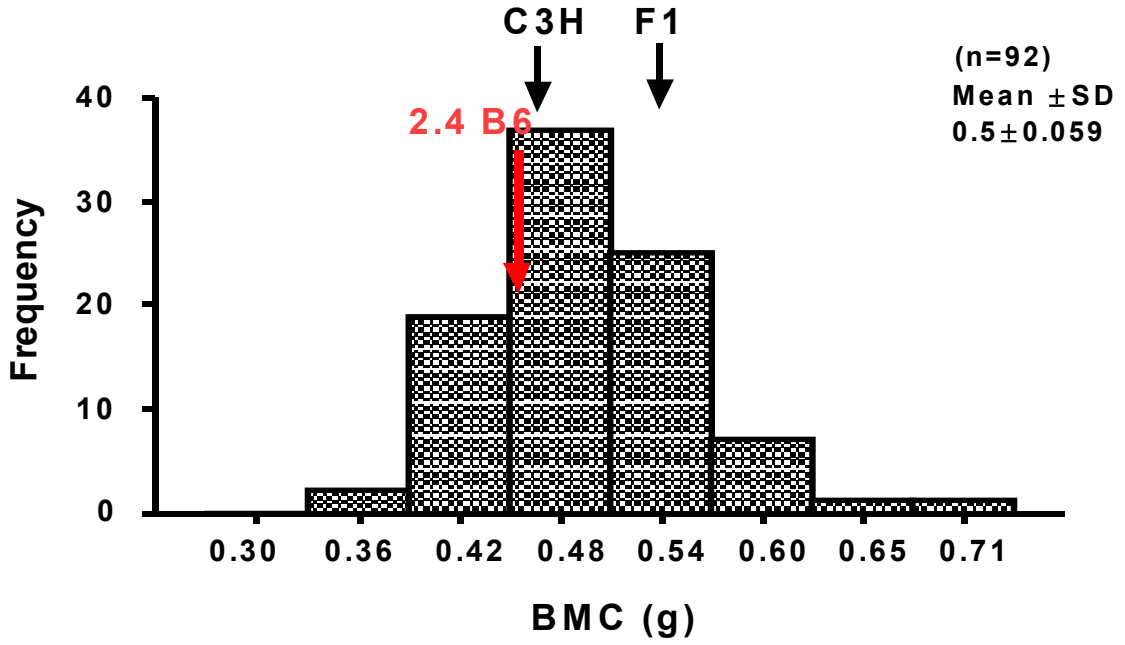

Figure 24. Frequency distribution of total body BMD phenotype in F2 female progeny (Line 2.4). The BMD data appears to be normally distributed; therefore, interval mapping could be used to identify QTLs affecting BMD. We have completed the phenotype and currently performing the genotyping of all F2 mice to identify the mutant locus.

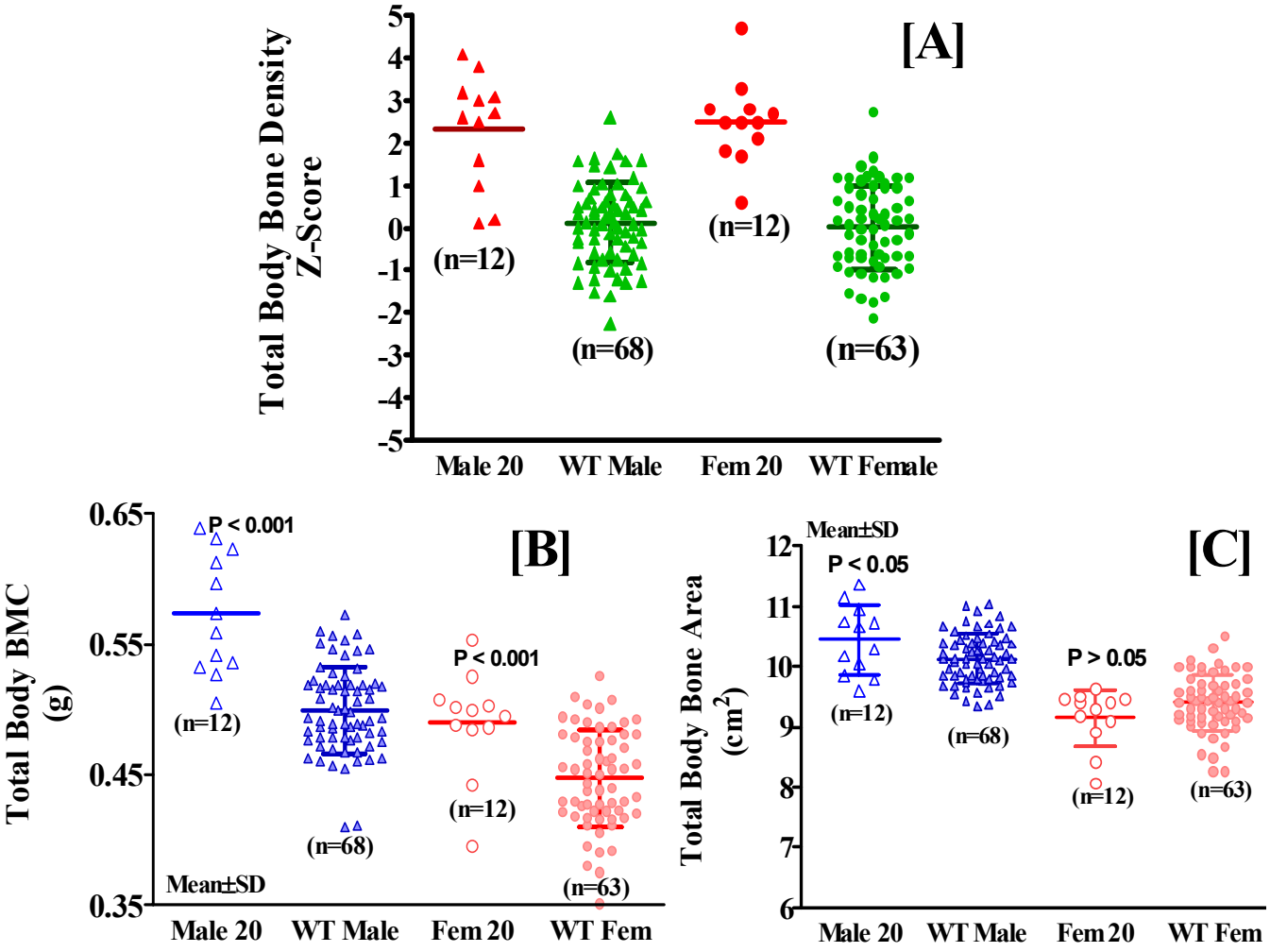

Figure 25. Generation of affected progeny for mutant mice B20.3E (referred as Line 20) identified previously in B6 recessive screen with high bone density. Figure A shows Z-scores for total body bone density, affected mice show >10% difference in bone density as compared to age and sex matched WT control mice. The increase in bone density was primarily due to higher total body bone mineral content (B) in females; in males, the bone area was also significantly higher as compared to wild type control male. The x-axis includes all IT progeny including the non-affected littermates. About 25% of the IT progeny could be classified as affected.

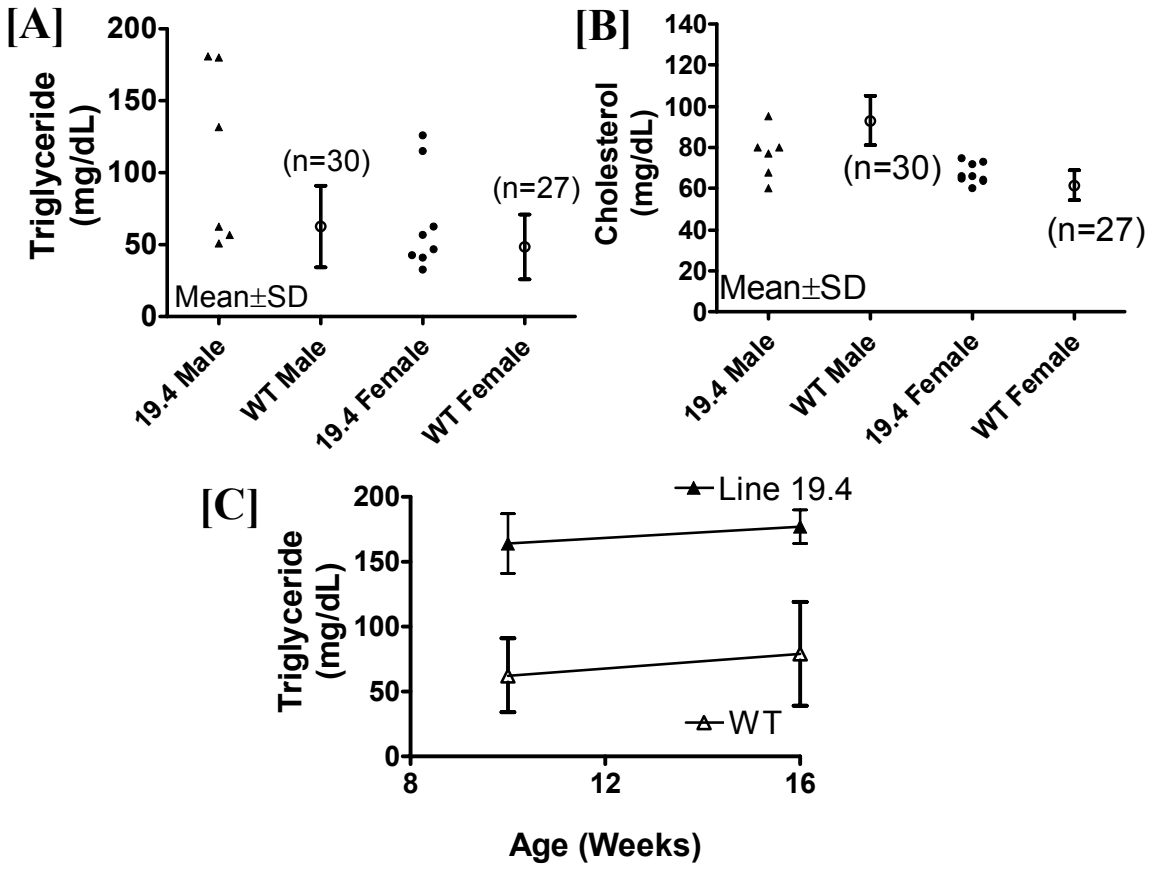

Figure 26. Lipid levels in progeny from mutant mice B19.4 identified previously in B6 recessive screen. We could only generate limited number of F3 mice and some mice appear to have elevated lipid levels. The lipid levels were elevated at both 10-week and 16-week age (C). However, the lipid levels in blood samples were analyzed in non-fasting conditions and could be affected by food intake. We are currently collecting fasting samples to confirm the phenotype.

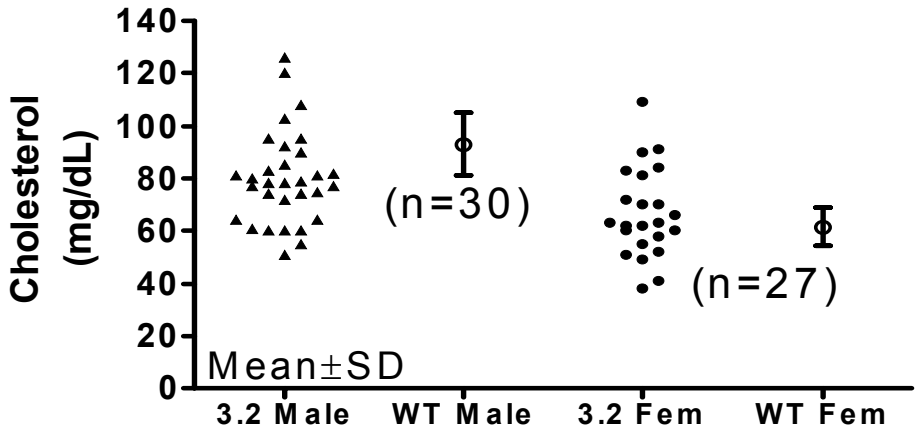

Figure 27. Total cholesterol levels in progeny from mutant mice B3.2 identified previously in B6 recessive screen. The cholesterol levels in some mice appear to be elevated, however, the lipid levels in blood samples were analyzed in non-fasting conditions and could be affected by food intake. We are currently collecting fasting samples to confirm the phenotype.

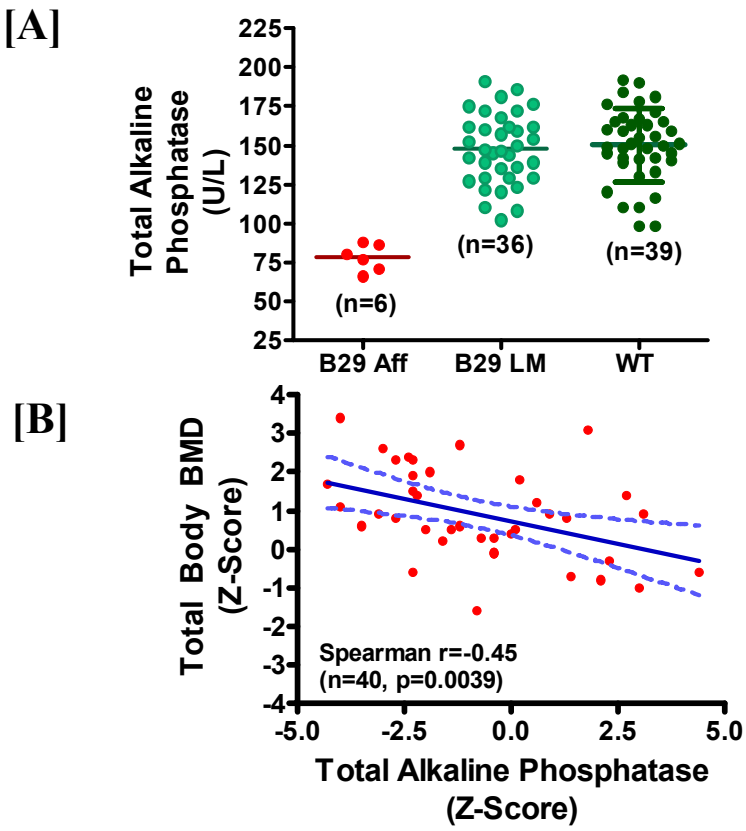

Figure 28. (A) Total alkaline phosphatase levels in serum from 10-week old progeny from B29.2 mutant (referred as Line 29) mice. The total alkaline phosphatase levels in mutant mice were 3 SD levels lower than WT control mice. Similar results were obtained with serum osteocalcin levels. (B) The bone marker levels negatively correlated with total body BMD. The data points include both male and female progeny from B29.

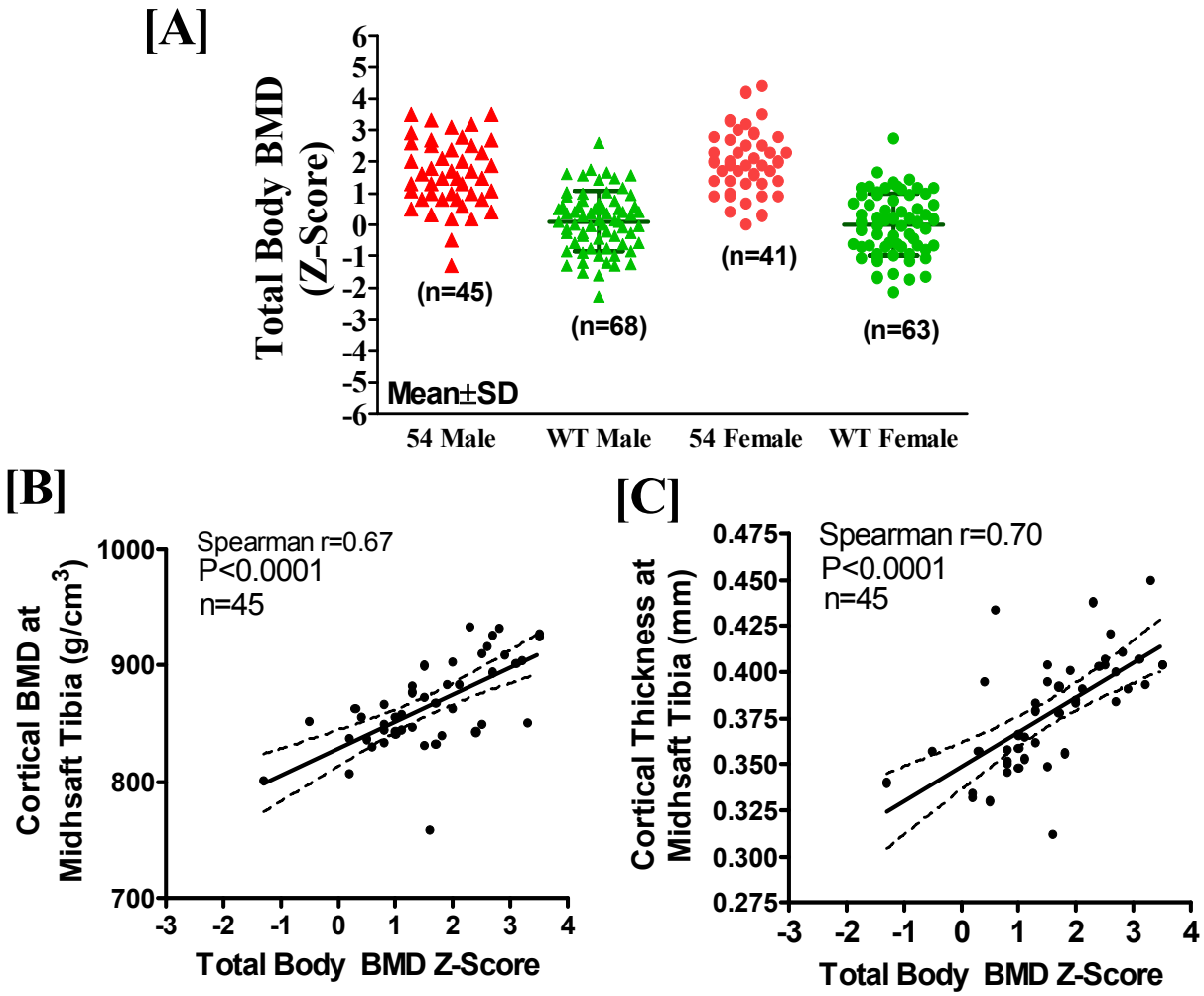

Figure 29. Z-scores calculated for total body BMD (A) measured by DEXA in 16-week old progeny from B54 male and female mice. The mean BMD Z-score (A) of all affected B54 male and female mice was +2.8 and mean BMC Z-score was +2.1. As expected, approximately 25% mice expressed high BMD phenotype. Interestingly, the total body BMD in B54 progeny correlated positively with volumetric bone density and cortical thickness measured by peripheral quantitative computed tomography (pQCT) at midshaft tibia.

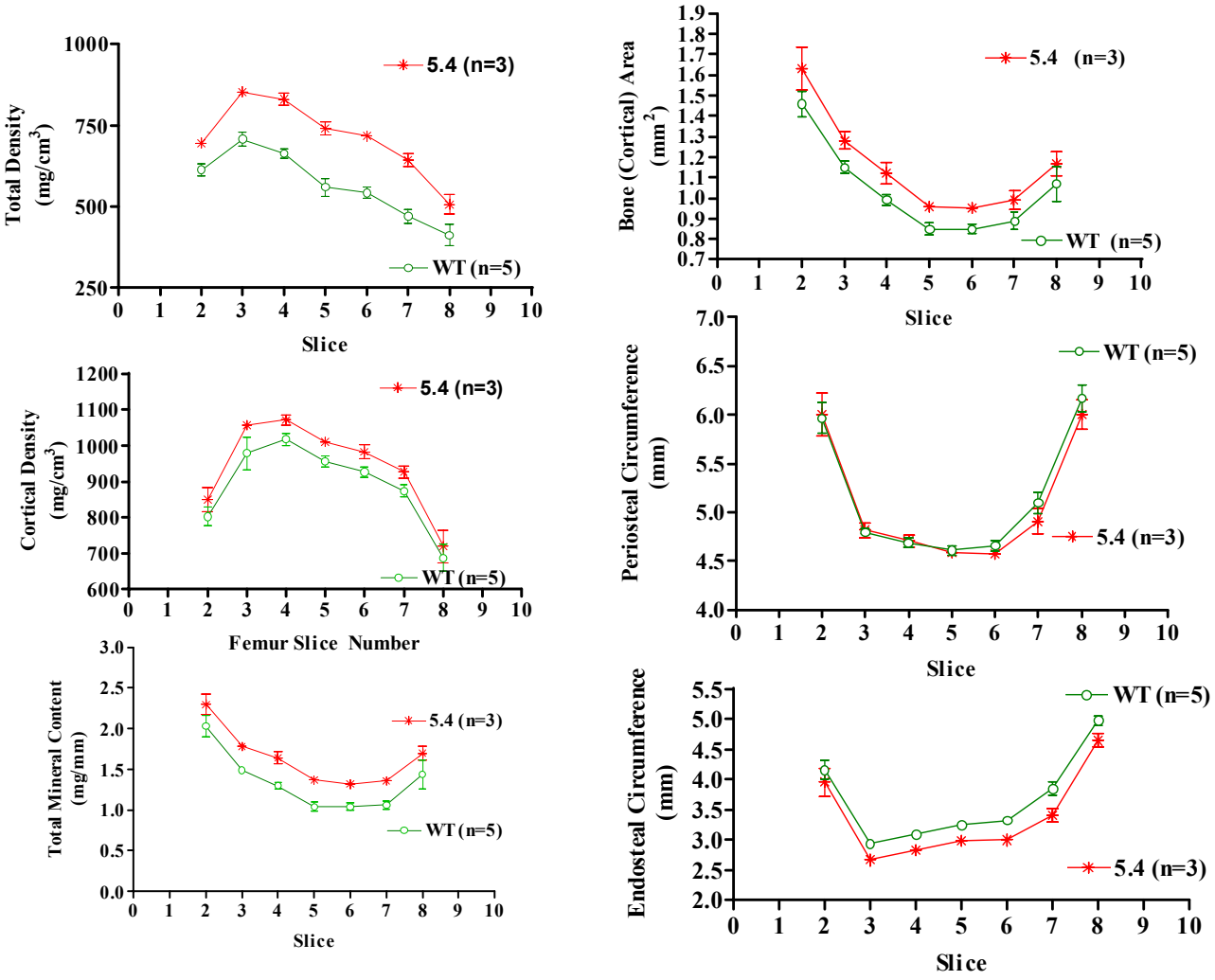

Figure 30. *Ex-vivo* bone area measurements in femur from high bone density mutant identified in B6 recessive screen (Line 5.4). The total bone density, cortical bone density, and total bone mineral content measured by pQCT were higher in 16-week old female progeny, as compared to WT B6 (IT). The increased bone density was associated with higher bone area, which appears to be due to lower endosteal circumference in affected 5.4 female mice. These data suggest that the phenotype can be explained by decreased bone resorption or increased bone formation at endocortical bone surface.

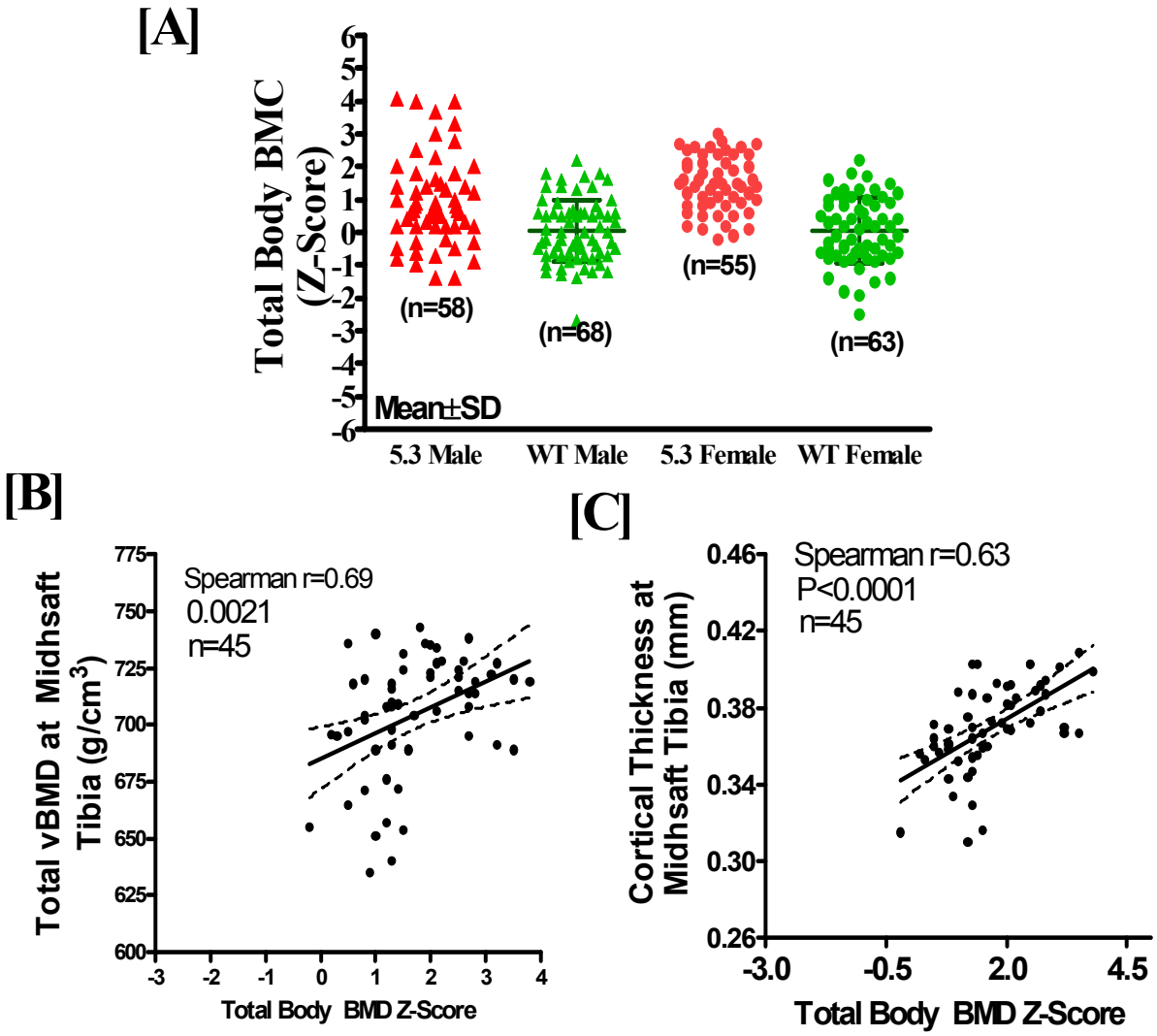

Figure 31. Z-scores calculated for total body BMD (A) measured by DEXA in 16-week old progeny from B5.3 male and female mice. The mean BMD Z-score (A) of all affected B5.3 male and female mice was +2.0. As observed in Line B5.4, the higher total body BMD correlated positively with volumetric bone density and cortical thickness measured by peripheral quantitative computed tomography (pQCT) at midshaft tibia.

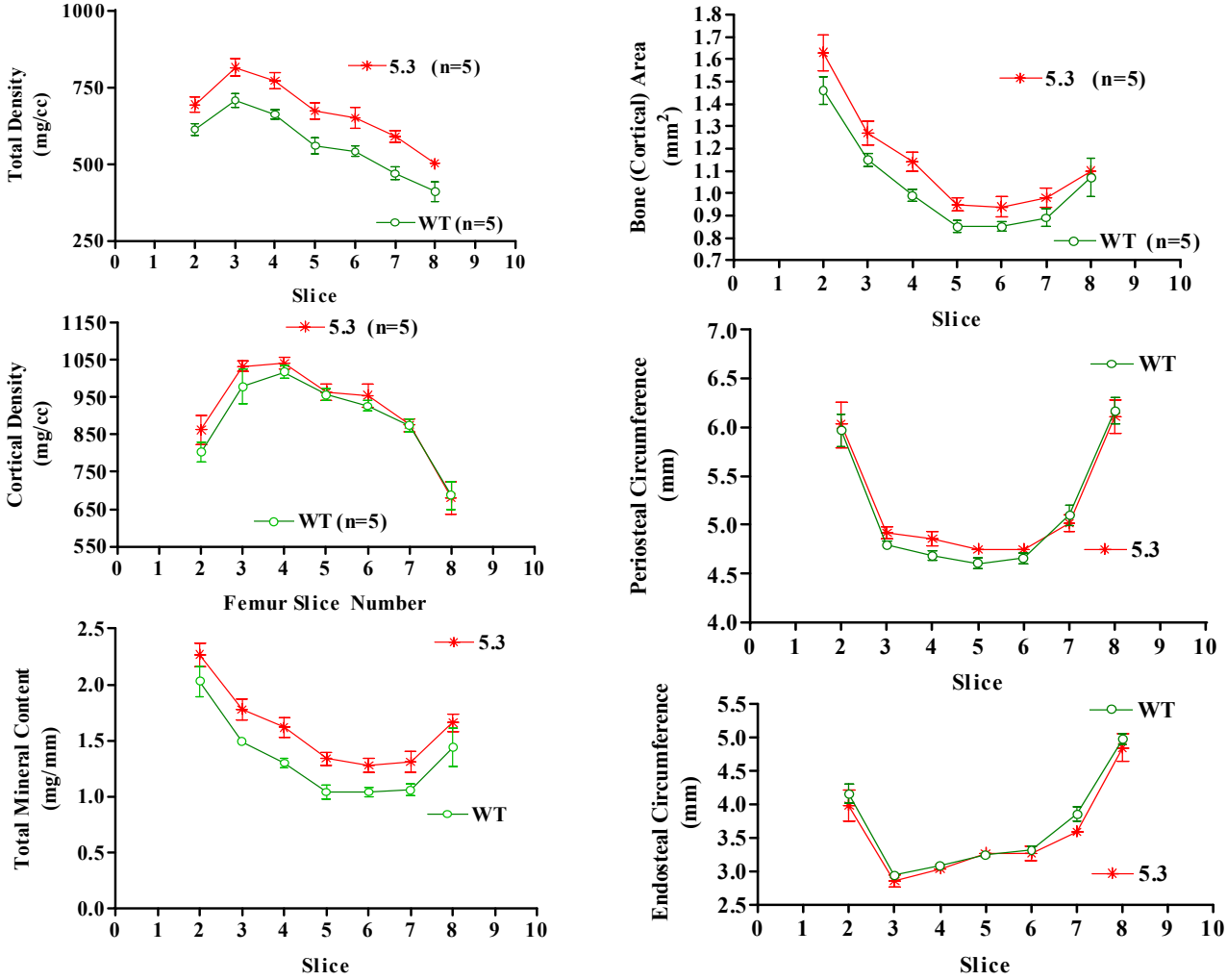

Figure 32. *Ex-vivo* bone area measurements in femur from high bone density mutant identified in B6 recessive screen (Line 5.3). The total bone density and total bone mineral content measured by pQCT were higher in 16-week old female progeny, as compared to WT B6 (IT). The increased bone density was associated with higher bone area. These data suggest that the phenotype can be explained by increased bone formation at periosteal bone surface.

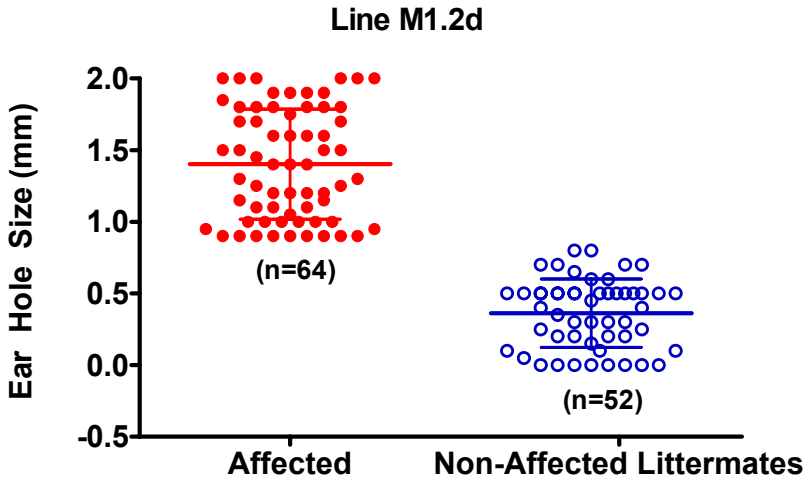

Figure 33. Phenodeviant with Slow Soft-Tissue Healing (M1.2d). Line M1.2d was identified in a dominant screen using MRL strain of mice; we have generated more than 100 progeny from the original mutant mice and data shows a slower rate of healing of a 2 mm hole punched in ear lobe. Error bars are Mean±SD.

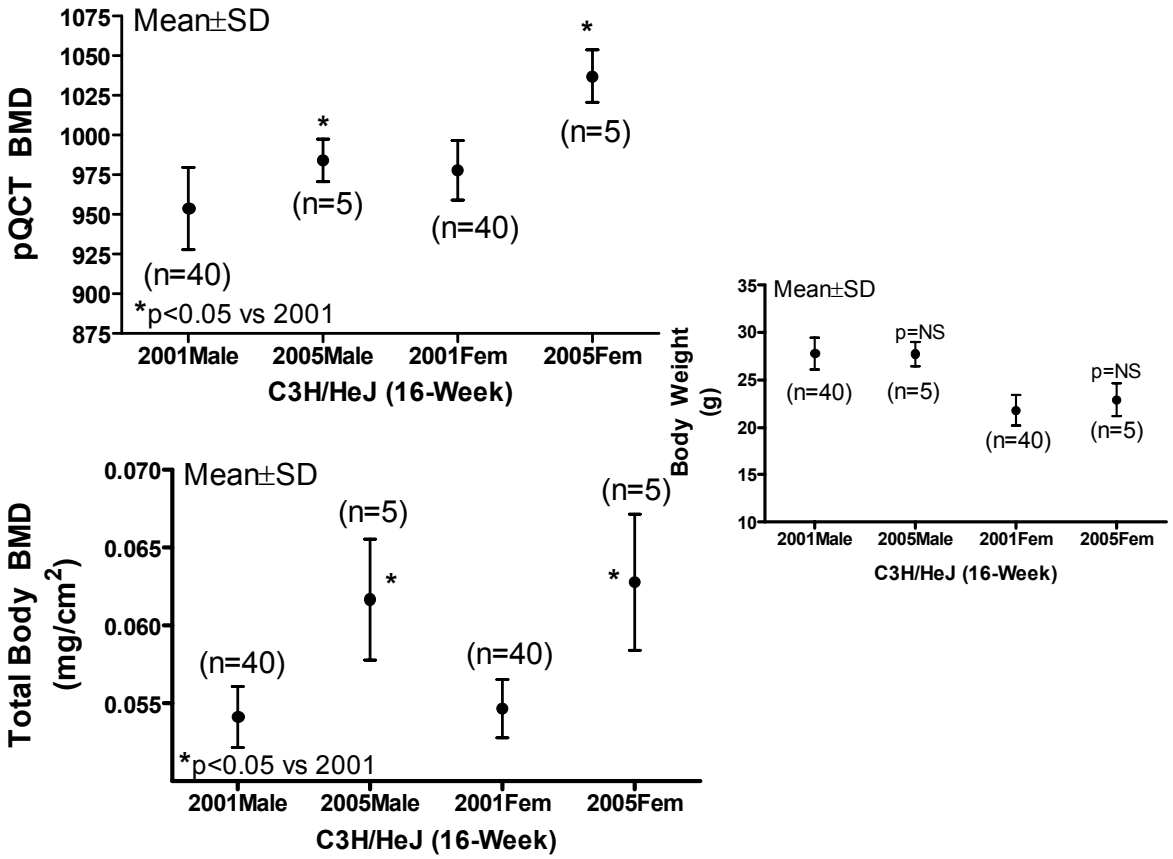

Figure 34. Shift in normal range values in C3H/HeJ strain of mice acquired in 2001 and those acquired in 2005. The body weights of both male and female were not affected, however, the total body bone density and volumetric bone density was significantly higher in mice obtained in 2005 from The Jackson Laboratory as compared to those obtained in 2001. This shift in bone density and other phenotype compromises the breeding of mutants that are in C3H/HeJ background. A similar comparison in C57BL/6J strain of mice did not show significant differences in BMD and body weights.

Key Research Accomplishments

- We have screened 118 F1 offspring from dominant screen for tissue regeneration, growth, and musculoskeletal phenotypes. We bred 10 MRL F1 mice to generate recessive lines and screened 24 F3 mice.

- We identified >30 phenodeviants in dominant and recessive screens.

- We confirmed >20 phenodeviants in repeat testing.

- We introduced >20 mice to progeny testing.

- We produced approximately 1400 mice by breeding phenodeviants identified in previous year screens and screened approximately 1200 mice generated from the inheritance test crosses.

- We have confirmed four B6 phenodeviants and one MRL phenodeviant in inheritance testing.

- We have performed extensive characterization of selected mutant lines in terms of histomorphometric and *in-vitro* analysis to identify cellular mechanisms causing skeletal phenotypes.

- We have performed three crosses between the mutant strain and another mapping strain for identifying chromosomal location of mutations.

- We have generated 466 F2 mice from intercrosses between mutant and wild type strains.

- We have genotyped >150 F2 mice using 40-60 informative markers.

- We have performed interval mapping and compared QTLs for mutant crosses with that of wild type mice.

- We have mapped chromosomal location of a mutant with high bone density phenotype (identified earlier in dominant screen) to a distal region of chromosome-4.

- We performed DNA microarray analysis of two phenodeviants to examine genome wide gene expression pattern in affected tissues from mutant mice and compared that with wild type control mice.

- In our preliminary analysis, we have identified approximately 50 genes or EST clones that are differentially expressed in mutant mice as compared to control mice.

Reportable outcomes

Abstract

1. Srivastava AK, Mohan S, Chest V, Wergedal JE & Baylink DJ. Mapping an ENU mutant with higher bone density reveals genetic locus on distal region of chromosome 4.

Plenary poster presentation in 27th Annual Meeting of American Society for Bone and Mineral Research, 2005..

2. Srivastava AK, Mohan S & Baylink DJ. An update on N-ethyl-N-nitrosourea (ENU) induced mutation screen for musculoskeletal phenotypes in mouse. Plenary poster presentation in 27th Annual Meeting of American Society for Bone and Mineral Research, 2005.

Manuscript

1. Srivastava AK, Kapur S, Mohan S, Yu H, Kapur S, Wergedal JE and Baylink DJ. Identification of novel genetic loci for bone size and mechanosensitivity in an ENU mutant exhibiting decreased bone size. J Bone Miner Res. 2005 Jun;20(6):1041-50. Epub 2004 Dec 27.

Conclusions

1. We injected two batches of MRL/MpJ males with ENU dose of 3 X 100 mg/kg to generate ENU founder males. We bred the ENU injected males in a breeding scheme to generate 119 F1 mice for dominant screening and 10 lines of recessive screening F3 progeny. We screened 118 mice for dominant mutation and 24 mice for recessive mutation. In addition, we have screened 107 mice to generate normative data. Thus, the total number of mice we have screened is 225, and therefore, we have exceeded our goals for first four objectives of the 'Specific Objective-1.'

2. We have bred >30 phenodeviants identified earlier for heritability testing and confirmed four new phenodeviants as inheritable mutations. We produced approximately 1400 mice in inheritance testing breeding and screened approximately 1200 mice. Therefore, we have achieved the fifth objective of 'Specific Objective-1' of repeat testing and confirming the inheritance of observed mutations. Furthermore, from the mice generated in inheritance-test crosses, we have done extensive characterization of mutant phenotype to explore cellular mechanism responsible for mutant phenotype; this was an additional progress from the proposed work.

3. We have tested expression of phenotype in a different strain of mice than the parent strain by breeding three ENU mutant mice with other strains of mice to generate 466 F1 and F2 mice. We have genotyped >150 F2 mice using 40-60 genome-wide informative markers to find out QTLs harboring mutant gene (s). We have completed mapping of a bone density mutant and identified that a distal locus on chromosome 4 could harbor the mutation. We fine mapped this locus and identified a 65-75 cM region on distal chromosome-4 that potentially harbors mutant locus. Therefore, we have met the 'Specific Objective-2.'

4. Finally, to identify the candidate gene in the chromosomal locus established for the bone size mutant mice, we performed DNA microarray analysis to investigate if the global gene expression pattern was altered in two mutant mice, Line 917M and M1.2d, as compared with wild type control mice. In our analysis, we have identified approximately 50 genes or EST that are differentially expressed in 917M mutant mice as compared to control mice. The Microarray data

from mutant M1.2d is currently being analyzed. In further studies, we will evaluate the sequence of these differentially expressed genes to identify mutant gene. The function of mutant gene will be determined using *in-vitro* studies. Therefore, we have completed all four objectives of 'Specific Objective-3.'

APPENDICES

Edderkaoui B, Baylink DJ, Beamer WG, Shultz K, Dunn N, Wergedal JE, Mohan S. (2005) CAST chromosome 1 QTL is complex and contains three BMD loci and one bone size locus: Evidence from subcongenic lines. Plenary Poster presentation at the 27th American Society for Bone and Mineral Research, Sept 23-27, Nashville, TN.

Edderkaoui B, Baylink DJ, Beamer WG, Wergedal JE, Dunn N, Shultz K and Mohan S. (2005) Multiple Genetic Loci From CAST/EiJ Chromosome 1 Affect vBMD Either Positively or Negatively in a C57BL/6J Background. J Bone Min Res 21(1):97-104.

Edderkaoui B, Baylink DJ, Shultz K, Beamer WG, Wergedal JE, Porte R, Chaudhuri A and Mohan S. (2006) Identification of Duffy Antigen/Receptor for Chemokine (DARC) as a Chromosome 1 BMD QTL Gene in Mice. 28th American Society for Bone and Mineral Research, September 15-19, Philadelphia, PA

Masinde GL, Li R, Nguyen B, Yu H, Srivastava AK, Edderkaoui B, Wergedal JE, Baylink DJ, Mohan S. (2005) New quantitative trait loci (QTL) that regulate wound healing in an intercross progeny from DBA/1J and 129X1/SvJ inbred strains of mice. Genomics. Funct Integr Genomics. 2005 Oct 6:1-7, (Epub).

Yu H, Mohan S, Masinde GL, Baylink DJ. (2005) Mapping the dominant wound healing and soft tissue regeneration QTL in MRL X CAST. Mammalian Genome. (In press)

Srivastava AK, Mohan S, Chest V, Wergedal JE and Baylink DJ. (2005) Mapping an ENU mutant with higher bone density reveals genetic locus on distal region of chromosome 4. Plenary poster presentation in 27th Annual Meeting of American Society for Bone and Mineral Research, Sept 23-27, Nashville, TN

Srivastava AK, Mohan S and Baylink DJ. (2005) An update on N-ethyl-N-nitrosourea (ENU) induced mutation screen for musculoskeletal phenotypes in mouse. Plenary poster presentation in 27th Annual Meeting of American Society for Bone and Mineral Research, Sept 23-27, Nashville, TN.

Srivastava AK, Kapur S, Mohan S, Yu H, Kapur S, Wergedal JE and Baylink DJ. (2004) Identification of novel genetic loci for bone size and mechanosensitivity in an ENU mutant exhibiting decreased bone size. J Bone Miner Res. Jun;20(6):1041-50. Epub Dec 27, 2004

Cast chromosome 1 QTL is complex and contains three BMD loci and one bone size locus: evidence from subcongenic lines

B. Edderkaoui[1], D. J. Baylink[2], W. G. Beamer[3], K. L. Shultz[3], N. Dunn[1], J. E. Wergedal[2], S. Mohan[2].
JLP VAM, Loma Linda, CA, USA[1], JLP VAMP and LLU, Loma Linda, CA, USA[2], Jackson Labs, Bar Harbor, MI, USA[3].

ABSTRACT

BMD is an important component of bone strength and a recognized predictor of risk for osteoporotic fracture. Elucidating the genetic basis for BMD variation could lead to identification of potential preventive measures against developing osteoporosis. Genome wide-linkage analysis using C57BL/6J(B6)-CAST/EiJ (CAST) intercross revealed the presence of quantitative trait locus (QTL) responsible for BMD variations in Chr 1. Our goal was to delineate the chromosome interval harboring this QTL by using subcongenic lines of mice. The B6.CAST-1T congenic line which carries the CAST segment covering the whole QTL region in Chr 1 was previously generated to confirm the effect of this QTL on femoral vBMD (Beamer et al., 2003). Ten subcongenic lines were generated after several backcrossings of the initial B6-CAST-1T congenic with the B6 mice. 16-week-old female mice were characterized. Three sublines carrying non-overlapping CAST segments showed significant change of femoral vBMD compared to B6 control mice. This provided evidence for the presence of 3 genes within the initial QTL capable of regulating BMD independently. Phenotypic characterization of the remaining sublines, which carried over-lapping regions, confirmed the presence of at least three loci (BMD1-1, BMD1-2 and BMD1-3) responsible for vBMD variation in Chr 1 QTL. Sublines carrying CAST segment that covered the first two loci (BMD1-1 and BMD1-2) showed significantly greater femur vBMD (5-12%) compared to B6. However, sublines carrying *cast* alleles within BMD1-3 locus showed significantly reduced femur vBMD compared to B6 control mice (6%). Correlation analysis showed that the femur vBMD phenotype had a strong negative correlation with endosteal perimeter ($r=-0.8$; $P=0.003$), and a strong positive correlation with cortical thickness among the ten sublines ($r=0.97$; $P<0.001$). These data provided evidence that the three genes in Chr 1 may influence the vBMD phenotype by affecting endocortical bone formation and/or bone resorption. In addition to the vBMD loci, the proximal region of BMD1-2 locus contains bone size (BS) QTL. The significantly greater periosteal in the two sublines covering this region was lost after adjustment for body weight (BW). In contrast, none of the vBMD QTL was affected by BW adjustment. In conclusion: (1) the initial vBMD QTL in Chr 1 is the result of three separate QTLs which affect vBMD both positively and negatively; (2)The three loci influence femur vBMD primarily by increasing or reducing the endosteal perimeter; (3) A genetic locus associated with both BW and BS phenotypes was found within the BMD QTL in Chr 1.

INTRODUCTION

Bone mineral density (BMD) is an important component of bone strength and measurement of BMD is a useful tool for determining one's risk for osteoporotic fracture. A number of studies have shown that BMD has a strong heritable component, ranging between 50-90% in humans and mice (1-3). Elucidating the genetic basis for BMD

variation could lead to identifying potential preventive measures that would lower the risk of developing osteoporosis.

In previous studies (1), four QTLs that contribute to femur volumetric bone mineral density (vBMD) were identified from the cross between C57BL/6J (B6), the low BMD mice, and CAST/EiJ (CAST), the high BMD mice. In the present study, we focused on Chr 1 for several reasons, including: 1) this QTL exhibits the highest LOD score in the B6 x CAST F2 intercross female progeny; and 2) the Chr 1 QTL has also been identified in other inbred mouse strain crosses such as B6 x C3H, B6 x DBA/2, and MRL/MpJ x SJL/J (2, 4, 5). Furthermore, a syntenic region in human chromosome 1q21-q43 carries a BMD QTL which has been reported in independent studies using human populations (6, 7).

In this study, we have used the B6.CAST-1T congenic line which encompasses the entire QTL region, to generate subcongenic lines which carry small CAST chromosomal segments from the QTL region in the B6 background. Characterization of the skeletal phenotype of the ten congenic sublines revealed evidence for the presence of three BMD loci within the QTL in Chr 1 (BMD1-1, BMD1-2, BMD1-3). While BMD1-1 and BMD1-2 had a positive effect, BMD1-3 had a negative effect on femoral vBMD phenotype. Furthermore, phenotypic analyses of subcongenic lines carrying overlapping regions suggested the presence of additional loci related to body weight in Chr 1. These data provided evidence for the complexity of the BMD QTL in Chr 1.

MATERIALS AND METHODS

Generation of subcongenic line of mice

Mice were produced and maintained at the animal research facilities of both The Jackson Laboratory (TJL) (Bar Harbor, ME) and at the Jerry L. Pettis VA Medical Center (LL) (Loma Linda, CA) under the standard conditions.

After several backcrosses of the B6.CAST-1T congenic strain, which carried the initial BMD QTL in Chr 1 with B6 mice, the N10F1 generation mice were intercrossed to obtain recombinations that yielded different regions of the QTL. Thirty-eight polymorphic markers were used to fine map the initial 1T QTL region (100-192Mb). Databases used to identify the polymorphic markers included the Mouse Genome Informatic database (http://www.informatics.jax.org/) and the NCBI database (www.ncbi.nlm.nih.gov).

Phenotype analyses

We analyzed 8-19 female mice from the B6 line and from each congenic subline at 16 weeks of age. Body weights were recorded at necropsy. Bones collected in LL were stored in 1 x PBS buffer supplemented with 0.05% sodium azide, while bones collected at TJL were stored in 95% ethanol until measured for bone parameters. Their lengths were measured with digital calipers (Stoelting, Wood Dale, IL, USA). Then, isolated femurs were assessed using the peripheral quantitative computed tomography (pQCT) system from Stratec XCT-RESEARCH (Norland Medical System, Fort Atkinson, WI, USA).

Statistical analyses

Different skeletal parameters were compared between the ten sublines newly generated and the B6 female mice at 16 weeks of age. Data are expressed as a percentage change from B6 and are mean + SEM, n=8-19. Subcongenic lines generated in LL were compared with B6 mice bred in LL, while subcongenic mice generated in TJL were compared with B6 bred in TJL (Body weights for LL-B6 and for TJL-B6 were 22.5 + 0.3 g and 23.5 + 0.5 g, respectively (Mean + SEM, P=0.11 for LL-B6 *versus* TJL-B6)). T-test was used to determine the significant difference between sublines and B6 control mice, while one-way ANOVA and Post-hoc (Newman-Keuls) tests were performed to compare the phenotype between the sublines.

RESULTS

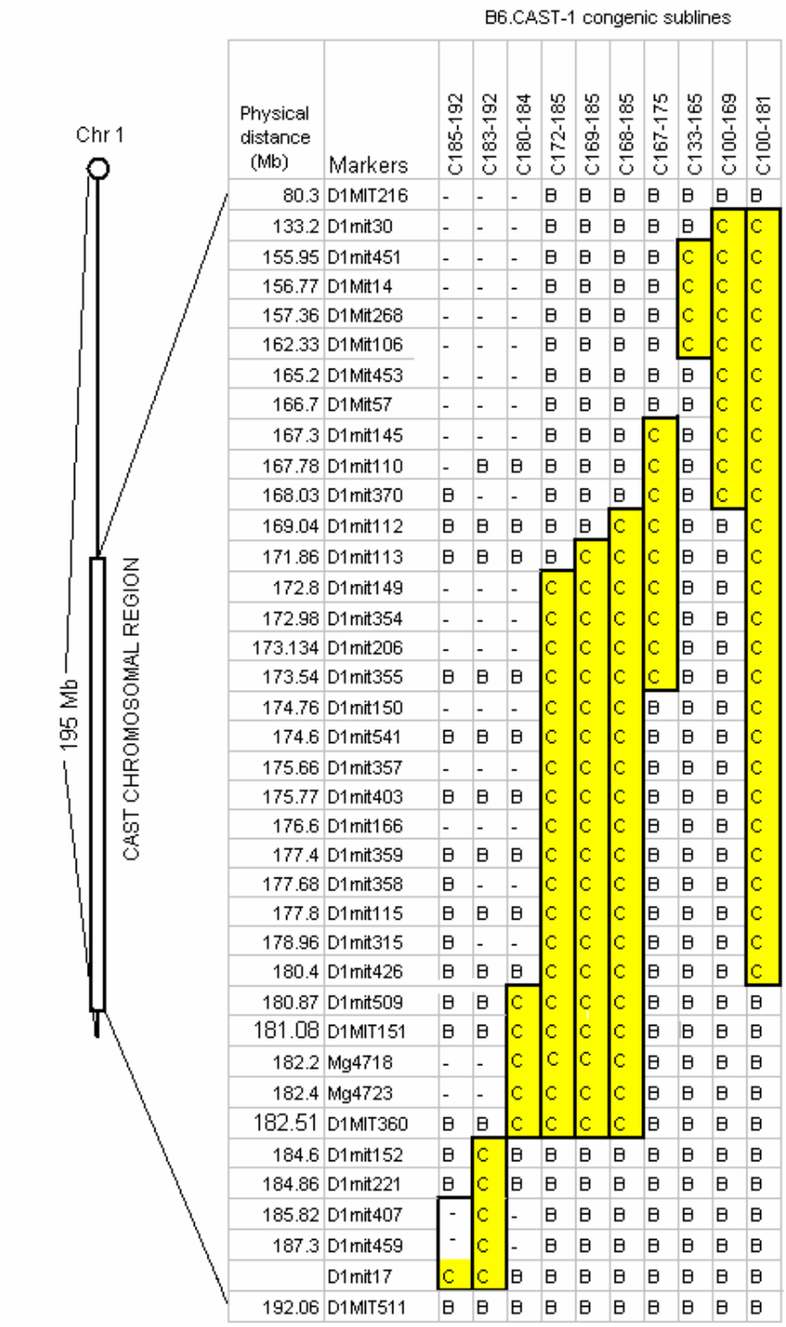

Physical distance (Mb)	Markers	C185-192	C183-192	C180-184	C172-185	C169-185	C168-185	C167-175	C133-165	C100-169	C100-181
80.3	D1MIT216	-	-	-	B	B	B	B	B	B	B
133.2	D1mit30	-	-	-	B	B	B	B	B	C	C
155.95	D1mit451	-	-	-	B	B	B	B	C	C	C
156.77	D1Mit14	-	-	-	B	B	B	B	C	C	C
157.36	D1Mit268	-	-	-	B	B	B	B	C	C	C
162.33	D1Mit106	-	-	-	B	B	B	B	C	C	C
165.2	D1Mit453	-	-	-	B	B	B	B	B	C	C
166.7	D1Mit57	-	-	-	B	B	B	B	B	C	C
167.3	D1mit145	-	-	-	B	B	B	C	B	C	C
167.78	D1mit110	-	B	B	B	B	B	C	B	C	C
168.03	D1mit370	B	-	-	B	B	B	C	B	C	C
169.04	D1mit112	B	B	B	B	B	C	C	B	B	C
171.86	D1mit113	B	B	B	B	C	C	C	B	B	C
172.8	D1mit149	-	-	-	C	C	C	C	B	B	C
172.98	D1mit354	-	-	-	C	C	C	C	B	B	C
173.134	D1mit206	-	-	-	C	C	C	C	B	B	C
173.54	D1mit355	B	B	B	C	C	C	C	B	B	C
174.76	D1mit150	-	-	-	C	C	C	B	B	B	C
174.6	D1mit541	B	B	B	C	C	C	B	B	B	C
175.66	D1mit357	-	-	-	C	C	C	B	B	B	C
175.77	D1mit403	B	B	B	C	C	C	B	B	B	C
176.6	D1mit166	-	-	-	C	C	C	B	B	B	C
177.4	D1mit359	B	B	B	C	C	C	B	B	B	C
177.68	D1mit358	B	-	-	C	C	C	B	B	B	C
177.8	D1mit115	B	B	B	C	C	C	B	B	B	C
178.96	D1mit315	B	-	-	C	C	C	B	B	B	C
180.4	D1mit426	B	B	B	C	C	C	B	B	B	C
180.87	D1mit509	B	B	C	C	C	C	B	B	B	B
181.08	D1MIT151	B	B	C	C	C	C	B	B	B	B
182.2	Mg4718	-	-	C	C	C	C	B	B	B	B
182.4	Mg4723	-	-	C	C	C	C	B	B	B	B
182.51	D1MIT360	B	B	C	C	C	C	B	B	B	B
184.6	D1mit152	B	C	B	B	B	B	B	B	B	B
184.86	D1mit221	B	C	B	B	B	B	B	B	B	B
185.82	D1mit407	-	C	-	B	B	B	B	B	B	B
187.3	D1mit459	-	C	-	B	B	B	B	B	B	B
	D1mit17	C	C	B	B	B	B	B	B	B	B
192.06	D1MIT511	B	B	B	B	B	B	B	B	B	B

Figure 1. The regions of CAST Chr 1 transferred from CAST mice onto B6 background, for the ten congenic sublines. The genotyping data for every marker are represented with "B" referring to homozygous b6/b6, "C" referring to cast/cast and "-" for data not available. The names of the subcongenic lines are at the top. We used a letter "C"

followed by the proximal and distal limits of cast alleles carried by the congenic sublines in megabases. The yellow squares denote the CAST chromosomal regions carried by each congenic subline. The polymorphic markers with their physical positions along Chr 1 are presented at the left.

Interpretation (1) Ten subcongenic lines were generated, each subline carrying a small CAST chromosomal region from the initial BMD QTL in Chr 1. (2) Sublines carrying CAST overlapping chromosomal regions will allow narrowing down the size of the QTL. (3) Phenotypic characterization of sublines carrying CAST non-overlapping regions will determine whether more than one gene in Chr 1 is involved in the BMD variation.

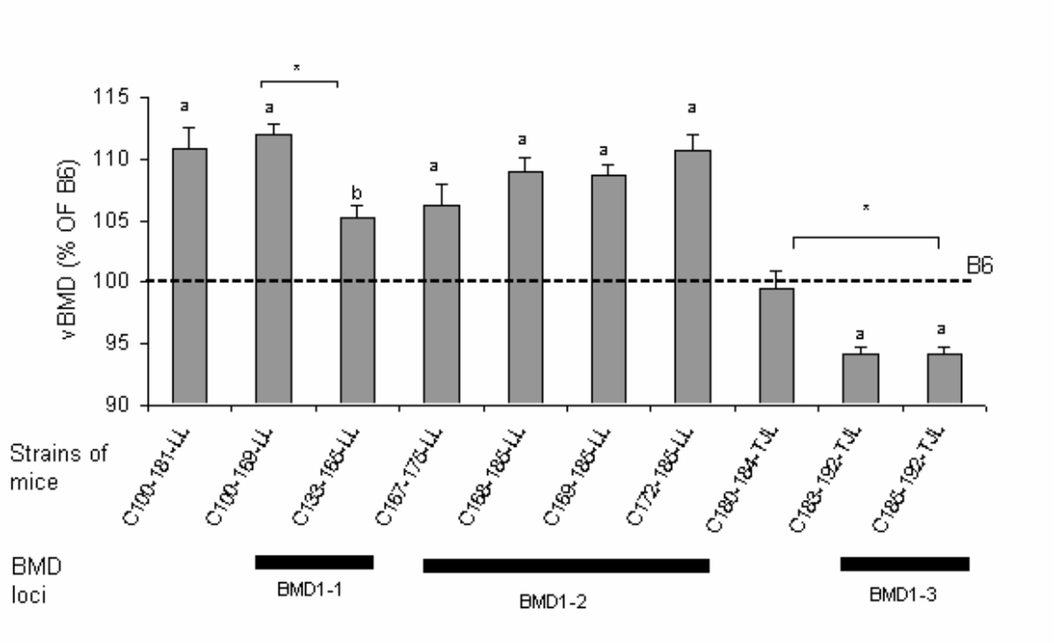

Figure 2. Mid-diaphysis femur vBMD from the ten subcongenic strains of mice. Individual sublines means were tested for significance by Student t-test. $^{a}P<0.005$, $^{b}P=0.01$, $^{c}0.01<P<0.05$. Comparison of the effect size between subcongenic lines was tested by ANOVA and Neuman-keuls post-hoc test. $^{*}P<0.01$. The effects identified with "^{a}" remained statistically significant after Bonferroni correction for multiple t-test comparisons was applied.

Interpretation: (1) Our finding that subcongenic lines C100-169, C172-185, and C185-192, which do not overlap in CAST chromosome segments, exhibited a significant change of femur vBMD compared to B6 control mice, provide clear evidence for the presence of three separate QTLs in Chr 1 (BMD1-1, BMD1-2, and BMD1-3) with independent effect on vBMD.
(2) In most congenic sublines the predominant effect of the transferred QTLs was to increase BMD. However, the two sublines C183-192 and C185-192, which carried CAST segments underlying BMD1-3 QTL, exhibited significantly reduced vBMD compared to

the B6 mice. These data demonstrate that cast alleles can affect BMD phenotype either positively or negatively.

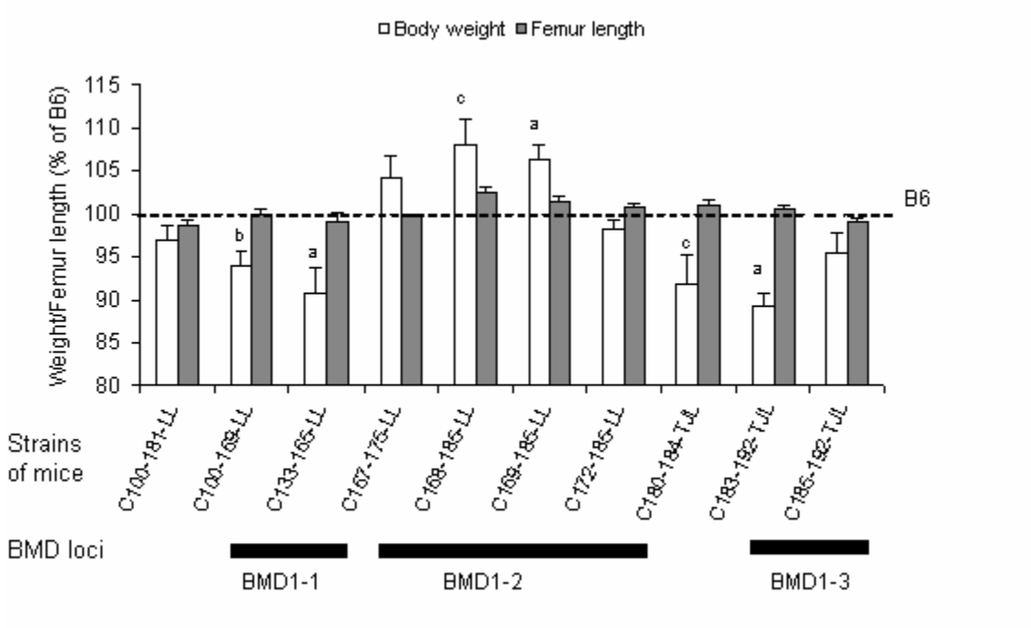

Figure 3. Body weight and femur length from the ten congenic sublines compared to B6 control mice. T-test was used to compare the mean values of each subline with B6 progenitors, $^{a}P<0.005$, $^{b}P=0.01$, $^{c}0.01<P<0.05$.

Interpretation: (1) Because CAST progenitor mice are considerably smaller than the B6 mice, we evaluated femur length and body weights of these congenic sublines to determine if these two phenotypes co-segregate with mid-diaphyseal vBMD.
(2) No significant changes in femur length were found among the ten sublines despite differences in body weight (BW).
(3) The finding that sublines C167-175, C168-185 and C169-185 showed significantly greater BW compared to B6 progenitors while C172-185 didn't show the BW phenotype narrowed down the size of BW locus to 169-172Mb from the centromere.
(4) Furthermore, evidence for the presence of additional loci associated with BW variation were provided by sublines C100-169 and C133-165 at 133-165 Mb and by C180-184 and C183-192 at 182.5-184.6 Mb (concluded from Fig. 1) showing the complexity of the initial BMD1 QTL.

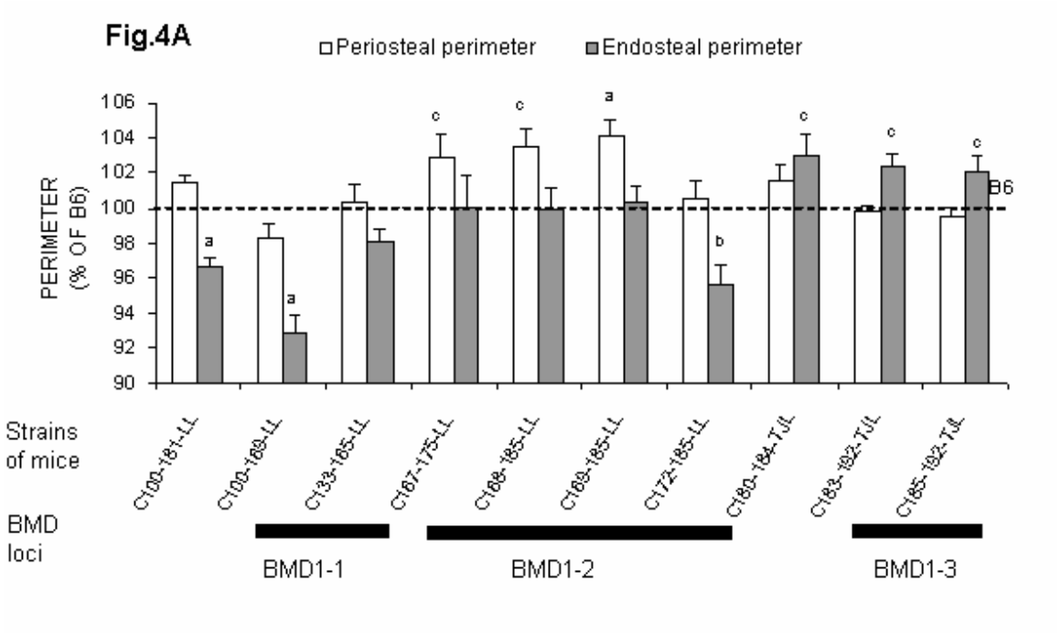

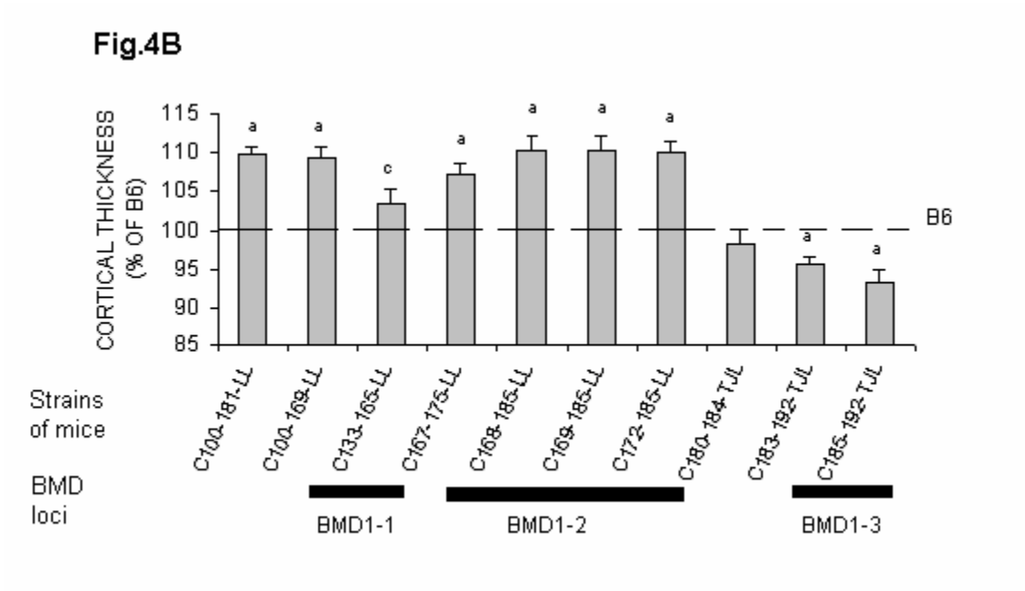

Figure 4. Mid-diaphysis femur data from periosteal, endosteal perimeters (Fig.4A) and cortical thickness (Fig. 4B) of the ten sublines. Individual sublines means were tested for significance by Student t-test. $^{a}p<0.005$, $^{b}p=0.01$, $^{c}0.01<p<0.05$.

Interpretation: (1) Sublines carrying either BMD1-1 or BMD1-2 loci exhibited a small endosteal perimeter (Endo.P.), which contributed to an increased cortical thickness (CT) and, consequently, increased femoral vBMD, while sublines carrying BMD1-3 showed a larger Endo. P., which contributed to a small CT and, consequently, led to a lower vBMD compared to the B6 control mice.

(2) A strong correlation was found between body weight and both PC and EC for sublines C167-175, C168-185, C169-185 (r=0.8-0.9, P<0.005), but not for the C172-185 subline, which carried overlapping CAST chromosomal segments. Furthermore, after adjustment for body weight, only C167-175 showed significant change in both PC and EC (data not shown), suggesting the presence of a genetic locus which most probably affects both body weight and bone size at 169-172 Mb.

Table 1. Correlation among various phenotypes from the ten congenic sublines tested.

	Crt.Thickness	Perios.P	Endos.P	Weight	Femur length
vBMD	**0.97**	0.26	**-0.80**	0.50	0.09
Crt.Thickness	1.00	0.43	**-0.67**	**0.62**	0.23
Perios.C	0.43	1.00	0.37	**0.77**	0.54
Endos.C	**-0.67**	0.37	1.00	-0.03	0.28
Weight	**0.62**	**0.77**	-0.03	1.00	0.45
Femur length	0.23	0.54	0.28	0.45	1.00

Crt.Thickness, refers to cortical thickness. Perio.P, refers to periosteal perimeter. Endo.P, refers to endosteal perimeter. Significant correlations are shown in bold (p<0.05, N=10). Values for all phenotypes were expressed as a percentage difference compared with B6 mice.

Interpretation (1) The overall correlation between body weight and vBMD among the 10 sublines was positive, but did not reach statistical significance. Moreover, the adjustment for BW or femur length did not affect the significance of femoral vBMD change (data not shown). This provided evidence that body weight is not responsible for the vBMD variation introduced by CAST donated segments.
(2)The vBMD variation among the sublines showed a strong negative correlation with Endo.P. and a positive correlation with CT. These data provide evidence that the three genes in Chr 1 may influence the BMD phenotype by affecting endocortical bone formation and/or bone resorption.

CONCLUSIONS

(1) The initial vBMD QTL in Chr 1 is the result of three separate genetic loci which affect vBMD either positively or negatively.
(2)The three loci influence femur vBMD primarily by increasing or reducing the endosteal perimeter.
(3) Three genetic loci associated with body weight phenotypes were found within the BMD QTL in Chr 1. At least one locus is associated with both body weight and bone size.
(4) The phenotypic and genotypic data from 10 subcongenic lines provide evidence for the complexity of the BMD QTL in Chr 1.

REFERENCES

1. Beamer WG, Shultz KL, Churchill GA, Frankel WN, Baylink DJ, Rosen CJ, Donahue LR 1999 Quantitative trait loci for bone density in C57BL/6J and CAST/EiJ inbred mice. Mamm Genome **10**:1043-9.
2. Beamer WG, Shultz KL, Donahue LR, Churchill GA, Sen S, Wergedal JR, Baylink DJ, Rosen CJ 2001 Quantitative trait loci for femoral and lumbar vertebral bone mineral density in C57BL/6J and C3H/HeJ inbred strains of mice. J Bone Miner Res **16**:1195-206.
3. Eisman JA 1999 Genetics of osteoporosis. Endocrine Reviews 20:788-804.
4. Klein RF, Carlos AS, Vartanian KA, Chambers VK, Turner EJ, Phillips TJ, Belknap JK, Orwoll ES 2001 Confirmation and fine mapping of chromosomal regions influencing peak bone mass in mice. J Bone Miner Res **16**:1953-61.
5. Masinde GL, Li X, Gu W, Wergedal J, Mohan S, Baylink DJ 2002 Quantitative trait loci for bone density in mice: the genes determining total skeletal density and femur density show little overlap in F2 mice. Calcif Tissue Int **71**:421-8.
6. Koller DL, Econs MJ, Morin PA, Christian JC, Hui SL, Parry P, Curran ME, Rodriguez LA, Conneally PM, Joslyn G, Peacock M, Johnston CC, Foroud T 2000 Genome screen for QTLs contributing to normal variation in bone mineral density and osteoporosis. J Clin Endocrinol Metab **85**:3116-20.
7. Ralston SH 2002 Genetic control of susceptibility to osteoporosis. J Clin Endocrinol Metab **87**:2460-6.

ACKNOWLEDGEMENTS

This work was supported by Assistance Award No. DAMD17-99-1-9571. The US Army Medical Research Acquisition Activity, 820 Chandler Street, Fort Detrick MD21702-5014, is the awarding and administering acquisition office. The information contained in this publication does not necessarily reflect the position or the policy of the Government and no official endorsement should be inferred.

Multiple Genetic Loci From CAST/EiJ Chromosome 1 Affect vBMD Either Positively or Negatively in a C57BL/6J Background

Bouchra Edderkaoui [1], David J. Baylink [1,2], Wesley G. Beamer [3], Jon E. Wergedal [1,2], Nancy R. Dunn [1], Kathryn L. Shultz [3] and Subburaman Mohan [1,2]

[1]Musculoskeletal Disease Center, Jerry L. Pettis Memorial VA Medical Center, Loma Linda, CA,USA

[2]Department of Medicine, Loma Linda University, Loma Linda, CA, USA

[3]The Jackson Laboratory, Bar Harbor, ME, USA

Running title: Complexity of BMD QTL in Chr 1

Funding Sources: Assistance Award DAMD17-99-1-9571

No. Words/Characters in Abstract and Ms: 5,646 wds /30,218 chr

No. of Figures: 5

Corresponding Author: Subburaman Mohan, Ph.D.

Musculoskeletal Disease Center

Jerry L. Pettis VA Medical Center

11201 Benton Street (151)

Loma Linda, CA 92357

Phone: 909 828 7084 ext 2932

Fax: 909 796 1680

Email: subburaman.mohan@med.va.gov

Conflict of Interest Statement:

All Authors have no conflict of interest.

MicroAbstract

Skeletal phenotype analyses of ten B6.CAST-1 congenic sublines of mice have revealed evidence for the presence of three closely linked QTLs in chromosome 1 (Chr 1) that influence femoral volumetric bone mineral density (vBMD) both positively and negatively.

Abstract

Introduction: Bone mineral density (BMD) is an important component of bone strength and a recognized predictor of risk for osteoporotic fracture. Our goal in this study was to fine map the chromosomal location of vBMD QTL in mouse distal Chr 1.

Materials and methods: After several backcrosses of the B6.CAST-1T congenic strain, which carried the initial BMD QTL in Chr 1 with B6 mice, the N10F1 generation mice were intercrossed to obtain recombinations that yielded different regions of the QTL. Thirty-eight polymorphic markers were used to fine map the initial 1T QTL region (100-192Mb). Different skeletal parameters were compared between the ten sublines and B6 female mice at 16 weeks of age. T-test was used to determine the significant difference between sublines and B6 control mice, while one-way ANOVA and Post-hoc (Newman-Keuls) tests were performed to compare the phenotype between the sublines.

Results: Significantly higher femur vBMD was found in sublines which carried *cast* alleles from 100-169 Mb and 172-185 Mb of the centromere compared to the B6 control mice (10-12%, $p<0.001$). However, sublines that carried *cast* alleles from 185-192 Mb showed significantly lower femur vBMD compared to the

control mice (-6%, $p<0.05$). Furthermore, femur vBMD phenotype showed a negative correlation with endosteal circumference ($r=-0.8$ and $p=0.003$), and a strong correlation with cortical thickness for combined data from the ten sublines ($r=0.97$, $p<0.001$). Moreover, a high correlation was found between body weight and both periosteal and endosteal circumferences for sublines carrying *cast* alleles from 167-175Mb, 168-185Mb, and 169-185Mb, while no significant correlation was found between these parameters for sublines carrying *cast* alleles from 172-185 Mb.

Conclusion: Genetic analysis using congenic sublines revealed that the initial BMD QTL on Chr 1 is a complex site with multiple loci affecting bone phenotypes, illustrating the value of the congenic approach in clearly identifying loci which control specific traits.

Key words: Congenic sublines of mice, bone mineral density, genetic loci, chromosome 1, femur

Introduction

Bone mineral density (BMD) is an important component of bone strength and measurement of BMD is a useful tool for determining one's risk for osteoporotic fracture. A number of studies have shown that BMD has a strong heritable component, ranging between 50-90% in humans and mice (1-3). Elucidating the genetic basis for BMD variation could lead to identifying potential preventive measures that would lower the risk of developing osteoporosis.

Most studies aimed at understanding the genetics of bone density have focused on population-based case control association studies of candidate genes known to be involved in bone metabolism. These include the vitamin D receptor (4-8), the type I collagen α1 gene (9,10), the type I collagen α2 gene (11), the estrogen receptor (4,9,11-13), insulin-like growth factor-I (14,15), and interleukin-6 (16,17). Positive and negative association results have been reported for each of these candidate genes, however whether or not any of these genes play a significant role in BMD variability in the general population remains a controversial subject (18-20). As an alternative approach to these association studies, genome-wide linkage screens for new genes underlying BMD variability have been launched both in humans (21-23) and in mice (1,2,24,25). Generally, genome-wide linkage scans are conducted by using panels of microsatellite markers spaced uniformly throughout the entire genome to identify quantitative trait loci (QTLs) affecting different phenotypes. In previous studies (1), four QTLs that contribute to femur volumetric bone mineral density (vBMD) were identified

from the cross between C57BL/6J (B6), the low BMD mice, and CAST/EiJ (CAST), the high BMD mice. In the present study, we focused on Chr 1 for several reasons, including: 1) this QTL exhibits the highest LOD score in the B6 x CAST F2 intercross female progeny; and 2) the Chr 1 QTL has also been identified in other inbred mouse strain crosses such as B6 x C3H, B6 x DBA/2, and MRL/MpJ x SJL/J (2, 26, 27). Furthermore, a syntenic region in human chromosome 1q21-q43 carries a BMD QTL which has been reported in independent studies using human populations (28, 29).

To gain more insight into the effect of the Chr 1 QTL on the BMD phenotype, we used a strategy that involved generation of congenic and subcongenic mice carrying small segments from the CAST Chr 1 QTL region. This strategy has been used successfully to narrow down the size of genetic loci responsible for several traits (30-34). Thus, we generated a B6.CAST-1T congenic strain encompassing the entire QTL region, followed by the construction of subcongenic lines which carry small CAST chromosomal segments from the QTL region in the B6 background. A large number of polymorphic markers were used to determine accurately the limit of CAST chromosomal region carried by each subline of mice. Characterization of the skeletal phenotype of the ten congenic sublines revealed evidence for the presence of three BMD loci within the QTL in Chr 1 (BMD1-1, BMD1-2, BMD1-3), which had not only a positive effect but also had a negative effect on femoral vBMD phenotype. Furthermore, phenotypic analyses of subcongenic lines

carrying overlapping regions suggested the presence of three loci related to body weight and overlap with the BMD loci. These data provided evidence for the complexity of the BMD QTL in Chr 1.

Materials And Methods

Mice

The study used two inbred strains of mice, B6 and CAST, which have been previously shown to differ widely in total femur BMD at 16 weeks of age (1). The rationale for selecting these two inbred strains of mice was based on the fact that these strains are highly polymorphic for genetic differences at more than 95% of their genomes (35). Mice were produced and maintained at the animal research facilities of both The Jackson Laboratory (TJL) (Bar Harbor, ME) and at the Jerry L. Pettis VA Medical Center (LL) (Loma Linda, CA) under the standard conditions of 14 h light, 10 h darkness, ambient temperature of 20^{o}C, and relative humidity of 40-60%. Mice in TJL facility were placed on National Institutes of Health (NIH)-31 Mouse/Rat Diet containing 6% fat, while mice in LL facility received Harlan Teklad Mouse/Rat Diet containing 4% fat. The animal work performed in this study has been approved by the institutional animal care and use committees at both The Jackson Laboratory and the Jerry L Pettis VA Medical Center.

Generation of congenic strains

Each congenic strain was developed by transfer of the small region of Chr 1 carrying *cast* alleles responsible for the difference in the vBMD phenotype into a

B6 background, as previously described by Shultz et al. (34). After the 10th back-cross, the N10F1 heterozygotes were intercrossed and N10F2 females and males homozygous for the transferred CAST Chr 1 segment were used to establish the first congenic strain (B6.CAST-1T) (34). This congenic line carried the CAST chromosomal region which covered the entire QTL region from 100-192 Mb. Additional crosses between the B6.CAST-1T congenic and the B6 progenitor produced new recombinations carrying smaller overlapping segments that were fixed in the ten congenic sublines reported herein. Each subline was genotyped using the polymorphic markers (Table 1) that encompass the initial Chr 1 vBMD QTL region.

Fine mapping:

Extraction of genomic DNA from tail snips was performed following the Gentra PurGene protocol (PUREGENE Tissue kit, Par#D-7000A). In order to fine map the BMD QTL in Chr 1 and to determine the limit of CAST chromosomal regions transferred onto the B6 background, we used 38 polymorphic markers located within the BMD QTL region that covers 60 cM in mouse Chr 1 (*D1mit216* to *D1mit511*). Table 1 represents the “mit” markers as well as the polymorphic markers newly identified in this work, with the approximate genetic distance from the centromere, in centimorgans (cM), from the MGI database and the physical distance from the centromere, in megabases (Mb), from the NCBI/ensembl database. We opted to follow the physical distance, which is more accurate than

existing genetic maps and does not depend on the frequency of recombination that can differ from one region to another.

Databases used to identify the polymorphic markers included the Mouse Genome Informatic database (http://www.informatics.jax.org/) and the NCBI database (www.ncbi.nlm.nih.gov). Thirty-six markers were found in the Jackson mouse database, while two markers were identified by screening CT-repeated sequences within the QTL region through the NCBI database. Then, the primers flanking the dinucleotide repeat sequences were designated and used for PCR analyses. Polymorphism was determined by checking the size differences of the repeated sequences between the B6 and CAST mice.

Primers newly designated in this study:

Mg4718-F: 5'-GCA TTT TGA TCC CTT ATA ATA CA-3'

Mg4718-R: 5'-GTG GAA GAC CCT TGA ATG G-3'

Mg4723-F: 5'-GCA TAG CCA ACA AAA GAA ATC TAA TG-3'

Mg4723-R: 5'-GCA GTG TAG CTC AGT GGT AGA TCA C-3'

Genotyping of individual mouse DNA was accomplished using two methods: (1) We amplified genomic regions of interest by polymerase chain reaction (PCR) using oligonucleotide primer pairs from Integrated DNA Technologies (Coralville, IA, USA). PCR products were separated by electrophoreses on 20-cm polyacrylamide gels, stained with ethidium bromide, and photographed under UV light. Photographs were scored twice and ambiguous genotypes were reamplified. (2) We also used fluorescently end-labeled primers to amplify genomic regions of interest. Using labeled primers, the sizes of the fluorescently-

labeled PCR products were directly determined by the ABI PRISM 377 GeneScan Analyzer. PCR products from B6, CAST and their F1 hybrids were used as standards to identify the mouse genotypes.

Phenotype analyses

Based on data from our previous studies that showed rapid acquisition of vBMD peaked at approximately 16 weeks, resulting in significant higher density values in the CAST females compared to the B6 females (1), we chose this time point as the age at which to measure our phenotypes. We analyzed 8-19 female mice from the B6 line and from each congenic subline at 16 weeks of age. Body weights were recorded at necropsy. Bones collected in LL were stored in 1 x PBS buffer supplemented with 0.05% sodium azide, while bones collected at TJL were stored in 95% ethanol until measured for bone parameters. Their lengths were measured with digital calipers (Stoelting, Wood Dale, IL, USA). Then, isolated femurs were assessed using the peripheral quantitative computed tomography (pQCT) system from Stratec XCT-RESEARCH (Norland Medical System, Fort Atkinson, WI, USA), operating at a resolution of 0.07 mm. The bone scans were analyzed with an outer threshold of 630 mg/cm^3 to determine bone area/total volume. This threshold was selected to yield areas values consistent with bone histomorphometric derived values. A second analysis was carried out with a threshold set at 230 mg/cm^3 to determine mineral content. Isolated femurs were scanned at nine locations symmetrically located around the midpoint, 11% of the femur length apart and covering the entire length. The vBMD was

calculated by dividing total mineral content by the associated total volume. Femur vBMD as well as periosteal circumference, endosteal circumference, and cortical thickness were evaluated at the mid-diaphysis region of the femurs (average of slices 4 and 5). Analyses of the scans were performed using manufacturer-supplied software program (Stratec Medizintechnik GMBH Bone Density Software, version 5.40C).

Statistical analyses

The measured parameters were expressed as the percentage of B6 control mice and used for comparison among different subcongenic lines. Bones collected from subcongenic lines generated in LL were compared with B6 mice bred in LL, while bones collected from sublines generated in TJL were compared with bones collected from B6 progenitor controls bred at TJL. Standard descriptive statistics were computed for all pQCT variables. Characteristics of each congenic subline were compared to the parental B6 progeny using student *t-test*, and differences were judged statistically significant when $p<0.05$. To further test the statistical significance, Bonferoni's correction for multiple comparisons was applied. Furthermore, the significance of differences between subcongenic lines was determined by ANOVA post-hoc testing using Newman-Keuls test (StatSoft, Inc. Tulsa, OK74104).

To test for body weight and femur length effect, statistical evaluation was undertaken using the JMP (SAS Institute Inc., Cary, NC) ANOVA software program for assessment of Linear Model regression analyses. The pQCT data were adjusted for effects, if any were detected, of body weight and femur length.

Differences between adjusted least squares means for B6 and each congenic subline were tested by Student's t-test, with significance declared when $p < 0.05$ was observed.

Results

To further narrow down the size of the major QTL in Chr 1 and allow for a successful BMD candidate gene screening, we generated a nested set of congenic sublines by transferring small segments from CAST Chr 1 BMD QTL into a B6 background. The sublines of mice that were genetically homozygous *cast/cast* at Chr 1 segments were homozygous for B6 at more than 99% of the remaining genome (34). Therefore, femoral vBMD variations observed within congenic sublines generated in this study were attributed to a CAST donated segment.

Figure 1 illustrates the ten congenic sublines that carry CAST chromosomal regions. Each subcongenic line is presented with a “C” letter referring to the *cast* allele, followed by the position (in megabases) of the two markers flanking the donated CAST segment. We designated the congenic subline B6.CAST-1$^{D1mit216\text{-}D1mit112}$ as C100-169 which indicates the approximate proximal and distal megabase limits known for the CAST chromosomal region. For this subline, we adopted 100Mb as the proximal limit of the CAST segment because we did not test markers between *D1mit216* (80.3 Mb) and *D1mit30* (133.2 Mb) to accurately determine the proximal limit of *cast* alleles. Congenic subline B6.CAST-1$^{D1mit30\text{-}D1mit453}$ carries *cast* alleles from the region 133.2-165.2Mb and was designated as

C133-165. All the remaining sublines were designated following the same nomenclature.

vBMD and other related bone parameters of the ten congenic sublines along with age- and gender-matched B6 mice were evaluated at the mid-diaphysis region of the femur using pQCT. Figure 2 shows the relative change in various phenotypes introduced by CAST donated regions compared with B6 control mice. All the sublines, which carried overlapping CAST segments from the region 100-185 Mb of the centromere, exhibited a significantly greater vBMD compared to the B6 mice, except subline C180-184 (Figure 2A). The vBMD change for various subcongenic lines were +12.0% for C100-169, +11.0% for C100-181, +5.0% for C133-165, +6.3% for C167-175, +9.0% for C168-185, +8.6% for C169-185, +10.6% for C172-185, and +0.5% for subline C180-184. When these data are superimposed on the genetic map shown in Figure 1, there is evidence for the presence of two separates genetic loci that control the vBMD variation; one located within 100-169 Mb (BMD1-1), and the second located within 172-175 Mb (BMD1-2). Furthermore, sublines C183-192 and C185-192, which carried overlapping CAST chromosomal regions at the distal region of Chr 1, showed a significant decrease of femoral vBMD compared to B6 mice (-6.0%), indicating the presence of a third locus with a negative effect on femur vBMD (BMD1-3).

Because CAST progenitor mice are considerably smaller than the B6 mice (-64% compared to B6 mice, data not shown), we evaluated the body weights of these congenic sublines to determine if a body weight phenotype co-segregates with mid-diaphyseal vBMD. Figure 2B shows that sublines carrying *cast* alleles from the BMD1-1 and BMD1-3 loci exhibited significantly smaller body weight compared to B6 (5-8%), while sublines which covered the BMD1-2 locus exhibited significantly greater body weight compared to B6 mice (6-8%). Furthermore, overall correlation (Table 2) between body weight and vBMD among the 10 sublines was positive (r=+0.5; p=0.12), but did not reach statistical significance. Moreover, the adjustment for body weight or femur length did not affect the significance of femoral vBMD change (data not shown). This provided evidence that body weight is not responsible for the vBMD variation introduced by CAST donated segments. Fig. 2B shows that there were no significant changes in femur length among the ten sublines.

In order to determine if the body weight difference in some of the congenic sublines can be explained on the basis of difference in litter sizes, we compared the average litter for the various sublines. We found no significant difference in the number of pups per litter for all the congenic sublines compared to B6 control mice (litter size average for LL-B6 was 4 $\pm$ 0.6 and for TJL-B6 was 6.26 $\pm$ 0.41. Thus the observed differences in body weight between congenic sublines and B6 control mice are genetically determined.

Other bone parameters such as endosteal circumference (EC), periosteal circumference (PC), and cortical thickness (CT), were analyzed to determine if other phenotypes co-segregated with the vBMD phenotype or could account for the changes in femoral vBMD. Sublines which carried *cast* alleles underlying BMD1-1 and BMD1-2 loci showed significantly smaller EC compared to B6 control mice; EC from C100-169 and C172-185 were 7% and 4% smaller than B6 mice, respectively. In contrast, the two sublines (C183-192 and C185-192) that covered the distal BMD locus (BMD1-3) showed a slight (2-4%) but significant increase in EC compared to the B6 control mice (Figure 2C). No significant difference in EC was found in sublines C167-175, C168-185, and C169-185, but after adjustment for body weight, C167-175 showed significantly smaller EC compared to the B6 (-3.0%, $p<0.05$). Among the ten subcongenic lines there was a significant negative correlation between the changes of vBMD and EC ($r=-0.67$, $p=0.024$).

With respect to PC, the sublines C167-175, C168-185, and C169-185 showed significantly greater PC (3-4%, Figure 2C). However, after adjustment for body weight and femur length, only PC from C167-175 and C100-181 sublines showed a significant difference compared to the B6 control mice. Thus, only C167-175 and C100-181 exhibited both an increase of PC and a decrease of adjusted EC compared with the B6 mice, which suggests the presence of a

genetic locus associated with body weight and bone size at 169-172 Mb from the centromere.

A change in vBMD can be explained on the basis of change in CT and/or material BMD. While sublines showing a higher vBMD exhibited significantly greater CT compared to the B6 mice (4-9%), sublines which showed reduced vBMD exhibited a reduced CT (4-6%) compared to the B6 control mice (Figure 2D), and when tested for correlation, a strong correlation was found between vBMD change and CT among the ten sublines (r=0.97; p=0.0001) (Table 2). Thus, a change in cortical thickness, rather than cortical material density properties, appears to mainly drive the QTL changes in vBMD observed in our congenic sublines.

Discussion

Comprehensive congenic coverage revealing multiple BMD loci in Chr 1

In this study, we demonstrate for the first time that the Chr 1 BMD QTL in a B6 x CAST intercross is the result of at least three separate genetic loci. The effect of the initial QTL on femoral vBMD was confirmed by the initial B6.CAST-1T congenic carrying a CAST chromosomal region that covered the initial QTL region (100-192 Mb). However, the critical question whether this QTL region consists of more than one locus could not be addressed due to the large size of the CAST chromosomal region. To address this question, ten B6.CAST-1 subcongenic lines carrying both overlapping and non overlapping CAST

segments from the whole QTL region, were generated to assess the effect of *cast* alleles on femoral vBMD.

Our finding that subcongenic lines C100-169, C172-185, and C185-192, which do not overlap in CAST chromosome segments (Figure 2), exhibited a significant change of femur vBMD, provided clear evidence for the presence of three separate QTLs in Chr 1 (BMD1-1, BMD1-2, and BMD1-3) with independent effect on vBMD. Congenic subline C133-165, which carried a CAST segment from 133-165Mb, also showed a significantly greater vBMD compared to B6, which confirmed the presence of BMD1-1 locus at 133-165 Mb. Interestingly, this region overlaps with the human syntenic region 1q21-q23 which was previously reported by Koller et al. (28) to be significantly associated with lumbar spine BMD. Furthermore, the presence of BMD1-2 was confirmed by four sublines, C166-175, C168-185, C169-185, and C172-185, which showed significantly greater femur vBMD compared to B6 control mice. Based on the finding that there was no significant difference in femur vBMD between the four sublines after Newman-keuls correction (P>0.05), and the finding that the four sublines carried an overlapping CAST chromosomal segment from 172-175 Mb, it can be concluded that BMD1-2 locus is present at 172-175 Mb.

Overall, in most congenic sublines the predominant effect of the transferred QTLs was to increase BMD. However, the two sublines C183-192 and C185-192, which carried CAST segments underlying BMD1-3 QTL, exhibited significantly

reduced vBMD compared to the B6 mice. These data showed that *cast* alleles can affect BMD phenotype both positively and negatively.

Previous studies establishing the initial Chr 1T congenic strains reported two BMD QTLs in Chr 1 for the B6.C3H-1T region (34). One QTL was found to reside in the proximal region (73-84Mb) of Chr 1. The second locus was located at the distal region where the initial BMD QTL from the B6 x CAST intercross was found (135-185Mb). Furthermore, a BMD QTL in this region has also been identified in other inbred mouse strain crosses such as MRL/MpJ x SJL/J and B6 x DBA (26,27). It remains to be determined whether Chr 1 BMD QTL in these other inbred strain crosses are also made up of multiple loci and if the genetic alleles that contribute to BMD variation in each of these BMD loci are same or different for the various inbred mouse strain crosses.

Interaction between multiple loci in Ch r1.

The femoral vBMD from subline C100-169 was significantly greater than that of subline C133-165 (p=0.001, ANOVA, Newman-Keuls test), which raised the possibility that there are two genes associated with BMD phenotype within BMD1-1 locus, with one located at 133-165Mb from the centromere, and the other locus located either upstream or downstream of the region 133-165 Mb. The two loci appeared to act together by increasing femur vBMD.

Furthermore, our findings that *cast* alleles in Chr 1 can have both positive and negative effects on BMD phenotype, explain why an additive effect was not observed from the congenic lines which covered more than one BMD locus in Chr 1, specifically, the initial B6.CAST-1T congenic that covered the whole QTL region. B6.CAST-1T exhibited an 8% increase of femoral vBMD compared to B6 mice (34), which is similar to BMD change from congenic sublines reported herein. A possible interaction between BMD1-3 and either BMD1-1 or BMD1-2 can happen if both loci use a common pathway to control the BMD phenotype, which may favor one locus on behalf of the other. As for C100-181 subline, which covered both BMD1-1 and BMD 1-2, it's not clear why it did not show an additive effect on BMD variation. There is evidence for multiple interactions between the different genetic loci in Chr 1 to control BMD phenotype. The analysis of these interactions may point to biological relationship among these genes. Therefore, the identification of these interactions is critical in order to understand the mechanisms that contribute to BMD variation.

Mechanisms that contribute to vBMD variation

While our main focus was on femoral vBMD, we have analyzed other phenotypes, which co-segregated with the vBMD phenotype in order to identify the mechanisms that contribute to BMD variation. In this regard, vBMD showed a strong negative correlation with EC and a positive correlation with CT among the sublines. Therefore, sublines carrying either BMD1-1 or BMD1-2 loci exhibited a small EC, which contributed to an increased CT and, consequently, increased

femoral vBMD (Figure 2), while sublines carrying BMD1-3 showed a larger EC, which contributed to a small CT and, consequently, led to a lower vBMD compared to B6 control mice (Figure 2). These data provide evidence that the three genes in Chr 1 may influence the BMD phenotype by affecting endocortical bone formation and/or bone resorption, which is in favor of our hypothesis that the three genetic loci in Chr 1 interact to influence BMD phenotype.

Presence of genetic loci related with body weight within the BMD QTL in Chr 1

A strong correlation was found between body weight and both PC and EC for sublines C167-175, C168-185, C169-185 (r=0.8-0.9, P<0.005), but not for C172-185 subline, which carried overlapping CAST chromosomal segments. Furthermore, after adjustment for body weight only C167-175 showed significant change in both PC and EC, suggesting the presence of a genetic locus which most probably affects both body weight and bone size at 169-172 Mb from the centromere (Fig.1). Furthermore, evidence for the presence of additional loci associated with body weight variation were provided by sublines C100-169 and C133-165 at the proximal region of BMD1 QTL (at 133-165 Mb) and by C180-184 and C183-192 at 182.5-184.6 Mb (concluded from Fig. 1) showing the complexity of the initial BMD1 QTL.

Potential candidate genes

There are number of potential candidate genes within the three QTLs identified in this study, which include transcription factors, growth factors,

mediators of cytokine signaling, metalloproteases, kinases, and phosphatases. The availability of various subcongenic lines of mice described in this study, which encompassed different BMD loci, will provide a valuable resource in our search for genes involved in BMD regulation. Currently, we are focused on screening for candidate genes related to femur vBMD within each of the genetic loci identified in Chr 1, using an approach similar to the one previously employed by Klein, et al. (36) to identify the lipoxygenase Alox15 as a negative regulator for BMD. When the candidate gene is found, the next step will be to test the effect of these genes on BMD variation in human populations using association study. The BMD candidate genes can be used for future diagnosis of patients who are susceptible to osteoporosis. Furthermore, the identity of candidate gene could lead to future development of protein or gene based therapy for treatment of bone disease.

Summary

The majors findings from the current studies are: (1) comprehensive and systematic congenic coverage revealed multiple vBMD loci in the distal portion of Chr 1, each locus is able to affect femoral vBMD independently in a B6 background; (2) skeletal phenotype analyses of these congenic sublines showed that these genetic loci in B6 background have not only a positive effect, but also a negative effect on vBMD phenotype; (3) The three loci affect vBMD phenotype by influencing mainly endocortical bone formation and/or bone resorption; (4) interactions between BMD loci in Chr 1 contribute in part to femoral vBMD

variation; and (5) At least three body weight/bone size loci are present within the major BMD QTL in Chr 1.

Acknowledgements

This work was supported by Assistance Award DAMD17-99-1-9571. The US Army Medical Research Acquisition Activity, 820 Chandler Street, Fort Detrick, MD 21702-5014, USA is the awarding and administering acquisition office. All work was performed in facilities provided by the Department of Veterans Affairs and the Jackson Laboratory (AR43618).

References

1. Beamer WG, Shultz KL, Churchill GA, Frankel WN, Baylink DJ, Rosen CJ, Donahue LR 1999 Quantitative trait loci for bone density in C57BL/6J and CAST/EiJ inbred mice. Mamm Genome **10**:1043-9.

2. Beamer WG, Shultz KL, Donahue LR, Churchill GA, Sen S, Wergedal JR, Baylink DJ, Rosen CJ 2001 Quantitative trait loci for femoral and lumbar vertebral bone mineral density in C57BL/6J and C3H/HeJ inbred strains of mice. J Bone Miner Res **16**:1195-206.

3. Eisman JA 1999 Genetics of osteoporosis. Endocrine Reviews **20**:788-804.

4. Brodowska A 2003 The influence of hormonal replacement therapy on bone density in postmenopausal women depending on polymorphism of vitamin D receptor (VDR) and estrogen receptor (ER) genes. Ann Acad Med Stetin **49**:111-30.

5. Cooper GS, Umbach DM 1996 Are vitamin D receptor polymorphisms associated with bone mineral density? A meta-analysis. J Bone Miner Res **11**:1841-9.

6. Morrison NA, Qi JC, Tokita A, Kelly PJ, Crofts L, Nguyen TV, Sambrook PN, Eisman JA 1994 Prediction of bone density from vitamin D receptor alleles. Nature **367**:284-7.

7. Peacock M, Hustmyer FG, Hui S, Johnston CC, Christian J 1995 Vitamin D receptor genotype and bone mineral density. Evidence conflicts on link. BMJ **311**:874-5, Erratum in: BMJ 1995 Nov 25;**311**:1439.

8. Seremak-Mrozikiewicz A, Drews K, Danska A, Spaczynski M, Opala T, Mrozikiewicz PM 2004 [Vitamin D receptor polymorphism in the group of postmenopausal women with low bone mineral density]. Ginekol Pol **75**:367-72.

9. Sapir-Koren R, Livshits G, Kobyliansky E 2003 Association and linkage disequilibrium analyses suggest genetic effects of estrogen receptor alpha and collagen IA1 genes on bone mineral density in Caucasian women. Calcif Tissue Int **72**:643-50.

10. Mezquita-Raya P, Munoz-Torres M, Alonso G, de Luna JD, Quesada JM, Dorado G, Luque-Recio F, Ruiz-Requena ME, Lopez-Rodriguez F, Escobar-Jimenez F. 2004 Susceptibility for postmenopausal osteoporosis: interaction between genetic, hormonal and lifestyle factors. Calcif Tissue Int. **75**:373-9.

11. Lei SF, Deng FY, Dvornyk V, Liu MY, Xiao SM, Jiang DK, Deng HW 2005 The (GT)(n) polymorphism and haplotype of the COL1A2 gene, but not the (AAAG)(n) polymorphism of the PTHR1 gene, are associated with bone mineral density in Chinese. Hum Genet. **116**:200-7.

12. Boot AM, van der Sluis IM, de Muinck Keizer-Schrama SM, van Meurs JB, Krenning EP, Pols HA, Uitterlinden AG 2004 Estrogen receptor alpha gene polymorphisms and bone mineral density in healthy children and young adults. Calcif Tissue Int **74**:495-500.

13. Sano M, Inoue S, Hosoi T, Ouchi Y, Emi M, Shiraki M, Orimo H 1995 Association of estrogen receptor dinucleotide repeat polymorphism with osteoporosis. Biochem Biophys Res Commun **217**:378-83.

14. Yakar S, Rosen CJ 2003 From mouse to man: redefining the role of insulin-like growth factor-I in the acquisition of bone mass. Exp Biol Med (Maywood) **228**:245-52.

15. Zhang M, Xuan S, Bouxsein ML, von Stechow D, Akeno N, Faugere MC, Malluche H, Zhao G, Rosen CJ, Efstratiadis A, Clemens TL 2002 Osteoblast-specific knockout of the insulin-like growth factor (IGF) receptor gene reveals an essential role of IGF signaling in bone matrix mineralization. J Biol Chem **277**:44005-12.

16. Ferrari SL, Karasik D, Liu J, Karamohamed S, Herbert AG, Cupples LA, Kiel DP 2004 Interactions of interleukin-6 promoter polymorphisms with dietary and lifestyle factors and their association with bone mass in men and women from the Framingham Osteoporosis Study. J Bone Miner Res **19**:552-9.

17. Murray RE, McGuigan F, Grant SF, Reid DM, Ralston SH 1997 Polymorphisms of the interleukin-6 gene are associated with bone mineral density. Bone **21**:89-92.

18. Econs MJ, Speer MC 1996 Genetic studies of complex diseases: let the reader beware. J Bone Miner Res **11**:1835-40.

19. Liu PY, Lu Y, Long JR, Xu FH, Shen H, Recker RR, Deng HW 2004 Common variants at the PCOL2 and Sp1 binding sites of the COL1A1 gene and

their interactive effect influence bone mineral density in Caucasians. J Med Genet **41**:752-7.

20. Morita A, Iki M, Dohi Y, Ikeda Y, Kagamimori S, Kagawa Y, Matsuzaki T, Yoneshima H, Marumo F 2004 Prediction of bone mineral density from vitamin D receptor polymorphisms is uncertain in representative samples of Japanese Women. The Japanese Population-based Osteoporosis (JPOS) Study. Int J Epidemiol **33**:979-88.

21. Devoto M, Shimoya K, Caminis J, Ott J, Tenenhouse A, Whyte MP, Sereda L, Hall S, Considine E, Williams CJ, Tromp G, Kuivaniemi H, Ala-Kokko L, Prockop DJ, Spotila LD 1998 First-stage autosomal genome screen in extended pedigrees suggests genes predisposing to low bone mineral density on chromosomes 1p, 2p and 4q. Eur J Hum Genet **6**:151-7.

22. Niu T, Chen C, Cordell H, Yang J, Wang B, Wang Z, Fang Z, Schork NJ, Rosen CJ, Xu X 1999 A genome-wide scan for loci linked to forearm bone mineral density. Hum Genet **104**:226-33.

23. Shen H, Zhang YY, Long JR, Xu FH, Liu YZ, Xiao P, Zhao LJ, Xiong DH, Liu YJ, Dvornyk V, Rocha-Sanchez S, Liu PY, Li JL, Conway T, Davies KM, Recker RR, Deng HW 2004 A genome-wide linkage scan for bone mineral density in an extended sample: evidence for linkage on 11q23 and Xq27. J Med Genet **41**:743-51.

24. Bouxsein ML, Uchiyama T, Rosen CJ, Shultz KL, Donahue LR, Turner CH, Sen S, Churchill GA, Muller R, Beamer WG 2004 Mapping quantitative trait

loci for vertebral trabecular bone volume fraction and microarchitecture in mice. J Bone Miner Res **19**:587-99.

25. Klein RF, Mitchell SR, Phillips TJ, Belknap JK, Orwoll ES 1998 Quantitative trait loci affecting peak bone mineral density in mice. J Bone Miner Res **13**:1648-56.

26. Klein RF, Carlos AS, Vartanian KA, Chambers VK, Turner EJ, Phillips TJ, Belknap JK, Orwoll ES 2001 Confirmation and fine mapping of chromosomal regions influencing peak bone mass in mice. J Bone Miner Res **16**:1953-61.

27. Masinde GL, Li X, Gu W, Wergedal J, Mohan S, Baylink DJ 2002 Quantitative trait loci for bone density in mice: the genes determining total skeletal density and femur density show little overlap in F2 mice. Calcif Tissue Int **71**:421-8.

28. Koller DL, Econs MJ, Morin PA, Christian JC, Hui SL, Parry P, Curran ME, Rodriguez LA, Conneally PM, Joslyn G, Peacock M, Johnston CC, Foroud T 2000 Genome screen for QTLs contributing to normal variation in bone mineral density and osteoporosis. J Clin Endocrinol Metab **85**:3116-20.

29. Ralston SH 2002 Genetic control of susceptibility to osteoporosis. J Clin Endocrinol Metab **87**:2460-6.

30. Christians JK, Keightley PD 2004 Fine mapping of a murine growth locus to a 1.4-cM region and resolution of linked QTL. Mamm Genome **15**:482-91.

31. Haag JD, Shepel LA, Kolman BD, Monson DM, Benton ME, Watts KT, Waller JL, Lopez-Guajardo CC, Samuelson DJ, Gould MN 2003 Congenic rats

reveal three independent Copenhagen alleles within the Mcs1 quantitative trait locus that confer resistance to mammary cancer. Cancer Res **63**:5808-12.

32. Garrett MR, Rapp JP 2002 Two closely linked interactive blood pressure QTL on rat chromosome 5 defined using congenic Dahl rats. Physiol Genomics **8**:81-6.

33. Kloting N, Wilke B, Kloting I 2004 Phenotypic and genetic analyses of subcongenic BB.SHR rat lines shorten the region on chromosome 4 bearing gene(s) for underlying facets of metabolic syndrome. Physiol Genomics **18**:325-30.

34. Shultz KL, Donahue LR, Bouxsein ML, Baylink DJ, Rosen CJ, Beamer WG 2003 Congenic strains of mice for verification and genetic decomposition of quantitative trait loci for femoral bone mineral density. J Bone Miner Res **18**:175-85.

35. Dietrich WF, Miller J, Steen R, Merchant MA, Damron-Boles D, Husain Z, Dredge R, Daly MJ, Ingalls KA, O'Connor TJ 1996 A comprehensive genetic map of the mouse genome. Nature **380**:149-52.

36. Klein RF, Allard J, Avnur Z, Nikolcheva T, Rotstein D, Carlos AS, Shea M, Waters RV, Belknap JK, Peltz G, Orwoll ES 2004 Regulation of bone mass in mice by the lipoxygenase gene Alox15. Science **303**:229-32.

Table 1. Genetic and Physical Positions Of Molecular Markers Used in this study

Marker name	Genetic position (cM)	Physical position (Mb)
D1mit216	49.7	77.00
D1mit30	70.0	133.20
D1mit451	81.6	155.95
D1mit14	81.6	156.77
D1mit268	83.4	157.36
D1mit106	85.0	162.33
D1Mit453	89.4	165.20
D1Mit57	87.8	166.70
D1mit145	89.0	167.30
D1mit110	88.1	167.78
D1mit370	88.3	168.03
D1mit112	91.3	169.04
D1mit113	93.3	171.86
D1mit149	94.2	172.80
D1mit354	95.8	172.98
D1mit206	95.8	173.13
D1mit355	97.0	173.54
D1mit150	100.0	174.76
D1mit541	97.7	174.60
D1mit357	99.8	175.66

D1mit403	100.0	175.77
D1MIT166	100.0	176.60
D1mit359	100.0	177.40
D1mit358	100.0	177.68
D1mit115	99.7	177.80
D1mit315	101.0	178.96
D1mit426	101.0	180.40
D1mit509	101.0	180.87
D1mit151	101.0	181.10
Mg4718	-	182.20
mg4723	-	182.40
D1mit360	101.2	182.50
D1mit152	101.5	184.60
D1mit221	102.0	184.86
D1mit407	101.5	185.82
D1mit459	102.0	187.30
D1mit17	106.3	-
D1mit511	109.6	192.06

"-" means that the distance is not available.

Table 2. Correlation among various phenotypes from the ten congenic sublines tested. Significant correlations are shown in bold (p<0.05, N=10). Values for all phenotypes were expressed as a percentage difference compared with B6 mice.

	Crt.Thickness	Perios.C	Endos.C	Weight	Femur length
vBMD	**0.97**	0.26	**-0.80**	0.50	0.09
Crt.Thickness	1.00	0.43	**-0.67**	0.62	0.23
Perios.C	0.43	1.00	0.37	**0.77**	0.54
Endos.C	**-0.67**	0.37	1.00	-0.03	0.28
Weight	**0.62**	**0.77**	-0.03	1.00	0.45
Femur length	0.23	0.54	0.28	0.45	1.00

Crt.Thickness, refers to cortical thickness. Perio.C, refers to periosteal circumference. Endo.C, refers to endosteal circumference.

Figure Legend

Figure 1. The regions of CAST Chr 1 transferred from CAST mice onto B6 background, for the ten congenic sublines. The genotyping data for every marker are represented with "B" referring to homozygous *b6/b6*, "C" referring to *cast/cast* and "-" for data not available. The names of the subcongenic lines are at the top. We used a letter "C" followed by the proximal and distal limits of *cast* alleles carried by the congenic sublines in megabases. The grey squares denote the CAST chromosomal regions carried by each congenic subline. The solid bars indicate the potential BMD QTLs and the open bar presents the QTL related with body weight and bone size traits. The polymorphic markers with their physical positions along Chr 1 are presented at the left. BMD loci are designated as BMD1-1, BMD1-2 for the second locus and BMD1-3 for the third locus.

Figure 2. Femoral and body weight data from the ten different subcongenic strains of mice. Data are expressed as a percentage change from B6 and are mean $\pm$ SEM, n=8-19. Subcongenic lines generated in LL were compared with B6 mice bred in LL, while subcongenic mice generated in TJL were compared with B6 bred in TJL (Body weights for LL-B6 and for TJL-B6 were 22.5 $\pm$ 0.3 g and 23.5 $\pm$ 0.5 g, respectively (Mean $\pm$ SEM, P=0.11 for LL-B6 *versus* TJL-B6)). The X axis represents the sublines characterized in this study. The identified BMD loci are indicated by solid bars underneath the names of the sublines. Figure 2A. Mid-diaphysis femur vBMD. Figure 2B. Body weight and femur length. Figure 2C. Mid-diaphysis femur periosteal circumference and endosteal circumference. Figure 2D. Mid-diaphysis cortical thickness. In each panel,

significant differences between B6 control mice and subcongenic lines are indicated by lowercase letters. [a]$p<0.005$, [b]$p=0.01$, [c]$0.01<p<0.05$ using t-test. The significant difference between subcongenic lines was indicated by asterisk for *$p<0.01$ using one-way ANOVA and Newman-Keuls test. Individual sublines means were tested for significance by Student t-test. Differences were judged statistically significant when $P<0.05$. Comparison of the effect size between subcongenic lines was tested by ANOVA and Neuman-keuls post-hoc test. If the conservative Bonferroni correction for multiple t-test comparisons is applied, those effects identified with [a] are still statistically significant. This includes all the vBMD effects and 8 of 9 cortical thickness effects.

Identification of Duffy Antigen/Receptor for Chemokine (DARC) as a Chromosome 1 BMD QTL Gene in Mice

Edderkaoui B[1], Baylink DJ[1], Schultz K[2], Beamer WG[2], Wergedal JE[1], Porte R[1], Chaudhuri A[3], and Mohan S[1]. [1]JLPVAMC, Loma Linda, CA, USA [2]Jackson Labs, Bar Harbor, ME,USA [3]NY Blood Ctr. NY,NY,USA

To identify the BMD QTL gene, we focused on the Chr1 QTL, as it has been identified in several different inbred strain mouse crosses and since a syntenic region in human Chr1 contains BMD QTL. We recently reported that Chr1 QTL contains three BMD loci (BMD1-1, 1-2 & 1-3), of which BMD1-2 QTL exhibited the highest LOD score (Edderkaoui et al., 2006). To narrow down the size of the BMD1-2 QTL region to permit candidate gene search, we generated additional congenic sublines C168-179 and C168-172, which carried the CAST/EiJ (CAST) chromosomal region underlying the BMD1-2 locus and between the BMD1-1 and 1-2 loci. Significantly higher (8.6%, $P<0.001$) femur vBMD was found in subline C168-179 compared with the C57BL/6J (B6) mice, while C168-172 did not show any difference with B6 progenitors ($P=0.78$). After superimposing the CAST chromosomal regions carried by all of the subcongenic lines, we have narrowed down the size of the BMD1-2 locus to 172-175 Mb in Chr1. In order to screen for potential BMD candidate genes, we compared the expression levels of 48 genes and ESTs located within the BMD1-2 region between the bones of B6 control mice and the two subcongenic lines and found only the Duffy (*Dfy*/DARC) gene, located at 173.26 Mb, showed a 6-fold higher expression in C168-179 subline ($P<0.001$), but not in the C168-172 subline, compared to the B6 control. We next sequenced the *Dfy* gene to determine the SNPs that might be the cause of the difference in *Dfy* expression between the B6 and the high BMD subcongenic mice. Of the 28 SNPs that distinguished the *Dfy* gene B6 from the CAST strain, 6 SNPs found in the coding region led to amino acid changes. The involvement of the *Dfy* protein in BMD variation was confirmed by Dfy-KO mice in a B6 background that exhibited a 5% increase ($P<0.001$) in femur vBMD compared to B6 mice. Because *Dfy* binds chemokines that regulate osteoclastogenesis, we tested the possibility that *Dfy* is involved in regulating formation of osteoclasts (Ocl). Treatment of non-adherent bone marrow cells (NABMC) derived from *Dfy* KO mice with RANKL and MCSF produced 50% less TRAP-positive Ocl *in vitro* compared to NABMC from wild type mice. Also, despite the increase of *Dfy* gene expression in C168-179, this subline showed a 70% decrease of Ocl compared to B6 mice. To determine if decreased Ocl formation in C168-179 line is due to reduced activity of Dfy protein caused by SNP-induced amino acid substitutions, we determined chemokine binding to NABMC and found 50% lower binding of ^{125}I-MCP-1 to NAMBC derived from congenic mice compared to B6 mice. Based on our findings, we conclude that the *Dfy* gene is a BMD QTL gene that regulates Ocl formation, bone resorption and thereby BMD.

New Quantitative Trait Loci (QTL) that Regulate Wound Healing in an Intercross Progeny from DBA/1J and 129X1/SvJ Inbred Strains of Mice.

Godfred L. Masinde[1*]; Runzhi Li[1*]; Bay Nguyen[1*]; Hongrun Yu[1]; Apurva Srivastiva[1,2] Bouchra Edderkaoui[1]; Jon Wergedal[1,2]; David J. Baylink[1, 2]; Subburaman Mohan[1-4]

[1] Musculoskeletal Disease Center, JL Pettis VA Medical Center, Loma Linda, CA 92357, USA

[2] Department of Medicine, Loma Linda University, Loma Linda, CA 92350

[3] Department of Biochemistry, Loma Linda University, Loma Linda, CA 92350

[4] Department of Physiology, Loma Linda University, Loma Linda, CA 92350

* These authors contributed equally to this article

Running title: New QTL for wound healing/regeneration in DBA X 129 F2 cross

Key Words: Wound healing; QTL; Mice; DBA X 129

Corresponding Author: Subburaman Mohan, PhD, Musculoskeletal Disease Center (151), Jerry L. Pettis Memorial Veterans Administration Medical Center, 11201 Benton Street, Loma Linda, CA 92357, Tel: (909)-825-7084 ext. 2932, FAX: (909)-796-1680, E-mail: Subburaman.Mohan@med.va.gov

Abstract

Wound healing/regeneration mouse models are few and studies performed have mainly utilized crosses between MRL/MPJ (a good healer) and SJL/J (a poor healer) or MRL/lpr (a good healer) and C57BL/6J (a poor healer). Wound healing is a complex trait with many genes involved in the expression of the phenotype. Based on data from previous studies that common and additional QTL were identified using different crosses of inbred strains of mice for various complex traits, we hypothesized that a new cross would identify common and additional QTL, unique modes of inheritance, and interacting loci, which are responsible for variation in susceptibility to fast wound healing. In this study, we crossed DBA/1J (DBA, a good healer) and 129/SvJ (129, a poor healer) and performed a genome-wide scan using 492 (DBA x 129) F_2 mice and 98 markers to identify QTL that regulate wound healing/regeneration. Four QTL on chromosomes 1, 4, 12 and 18 were identified which contributed towards wound healing in F2 mice and accounted for 17.1% of the phenotypic variation in ear punch healing. Surprisingly, locus interactions contributed to 55.7% of the phenotype variation in ear punch healing. In conclusion, we have identified novel QTL and shown that minor interacting loci contribute significantly to wound healing in DBA X 129 mice cross.

Introduction

Wound healing occurs in different stages, such as inflammation, fast wound healing, and remodeling stages (Lynch *et al*. 1991; Martin, 1997; Singer and Clark, 1999; Stocum, 1996), and is a complex process regulated by multiple genes (Clark *et al.* 1998; Masinde *et al.* 2001; McBrearty *et al.* 1998). Previous studies to identify genetic loci that regulate wound healing utilized crosses between MRL/lpr x C57BL/6J and MRL/MPJ x SJL/J (Masinde *et al.* 2001; McBrearty *et al.* 1998) strains of mice and identified over 20 QTL. Based on these and other past QTL studies involving different inbred mouse strain crosses, we hypothesized that a new cross not only would reveal common QTL that regulate wound healing/regeneration but may also reveal new QTL for wound healing. For example, in a similar complex trait such as bone mineral density (BMD), studies utilizing as many as six different mice crosses have revealed over 40 common and strain-specific QTL that potentially harbor BMD regulatory genes (Beamer *et al.* 1999; Beamer *et al.* 2001; Benes *et al.* 2000; Drake *et al.* 2001; Masinde *et al.* 2002; Klein *et al.* 1998; Koller *et al.* 2000; Shimizu *et al.* 1999). Our rationale for performing QTL studies in different inbred mouse strain crosses is based on the assumptions that: 1) identification of as many genetic variables as possible could facilitate a better understanding of genetic mechanisms that contribute to wound healing; and 2) the QTL data generated from various inbred strain crosses should be useful in the future identification of candidate genes by single nucleotide polymorphism haplotype analysis.

The main objective of the study was to identify common and additional QTL from a DBA/1J (DBA, good healer) X 129/SvJ (129, poor healer) F2 cross (intercross

between DBA X 129 F1 siblings). We chose these two strains based on the availability of their whole genome sequences from the Celera database, which would facilitate future identification of potential candidate genes. The results of our QTL studies using these crosses revealed: 1) new QTL that regulate wound healing/regeneration in the F2 progeny; and 2) several minor interacting loci that contribute significantly to wound healing.

Materials and Methods

Mice

The two inbred strains, DBA and 129, were purchased from the Jackson Laboratory (Bar Harbor, Maine) and maintained under 14:10 h light/dark cycles. DBA females were crossed to 129 males to produce the F1 progeny, which were then intercrossed to produce F2 progeny (492 mice). These inbred strains of mice were selected from our study of twenty different strains used for earlier ear regeneration studies (Li *et al.* 2001). Parental strains, F1 and F2 mice were sacrificed at 7 weeks of age and used for phenotypic and genotypic measurements. The mice were fed on a standard diet and kept under conditions as described in Masinde *et al.*, 2001. All of the animal procedures were approved by the Institutional Care and Use Committee of the Jerry L. Pettis VA Medical Center in Loma Linda, California.

Ear punch and measurement

Four hundred and ninety two (492) F2 progeny (male and female) mice were generated to conduct the study. A 2-mm through and through hole was made in three-

week old F2 mice in the lower cartilaginous part of each ear using a metal ear punch (Fisher Scientific, Pittsburgh, Catalog No. 01-337B). The hole diameter was measured using a 7X magnifier at days 3, 7, 15, 21, and 25 after ear punch (Masinde *et al*. 2002). The precision of hole measurement as determined by repeated measurement of the same hole 10 times was 2.4% (Masinde *et al*. 2001; Li *et al*. 2001b).

Genetic Analysis

The genetic analysis was performed as previously reported using 98 microsatellite markers (Masinde *et al*., 2001). In brief, 492 F2 progeny were sacrificed at 7 weeks of age and livers collected for isolation of DNA for genotyping. Genomic DNA was prepared from the liver of each F2 animal using a Wizard Genomic DNA kit (Promega, Madison, WI), as per the manufacturer's instructions. Polymerase Chain Reaction (PCR) primers were purchased from Invitrogen (Carlsbad, CA), to perform a genome wide scan of the F2 mice. PCR was performed using the True Allele mix [Applied Biosystems (CA)] according to the manufacturer's instructions. PCR products were resolved on 6% polyacrylamide gels (19:1 for acrylamide:bis), stained with ethidium bromide, and visualized by ChemiImager^{TM} 4400 Low Light Imaging System (Alpha Innotech Corporation, San Leandro, CA).

Statistical analysis

Genotype data was analyzed using a MapQTL (4.0) program (CPRO-DL), Wageningen, The Netherlands) (Stocum, 1996; Van Ooijen, 1999). MapQTL interval mapping was utilized for QTL mapping and the significance threshold LOD scores were

calculated using MapQTL permutation test (Beamer, *et al.* 1999; Masinde *et al.* 2001; Masinde *et al.* 2002). QTL with a LOD score $\geq$ 3.5 were considered significant while QTL with LOD score $\geq$ 2.7 were considered suggestive using a permutation test (Van Ooijen, 1999). The broad-sense of heritability was estimated by using variances obtained from parental strains, F1, and F2 mice, as previously described (Masinde *et al.* 2001; Masinde *et al*. 2002; Li *et al*. 2001b). QTL interactions were calculated with Map Manager QTX (Manly *et el.,* 2001).

Results

Phenotype distribution

Figure 1 shows healing of the ear punch hole in the parental strains DBA and 129, and their F1 progeny. In contrast to the anticipated intermediary healing between the two parental strains, F1 mice exhibited wound healing similar to or worse than the poor healer strain (129). The average healing in the F2 mice was similar to that of 129 mice.

Frequency distribution of the ear punch hole healing in F2 mice (Fig. 2) was not significantly different from the theoretical normal distribution. A majority of the F2 mice exhibited ear punch hole healing worse than the 129 (poor healer). Less than 5% of the F2 mice exhibited better healing than DBA.

QTL Analyses for wound healing phenotype

The results of genome-wide scan are presented in Table 1 and Figure 3. The genome-wide scan revealed two significant and two suggestive QTL for F2 mice on chromosomes 1, 4, 12, and 18 (Table 1, Figure 3). Total phenotypic variation explained

by the 4 QTL was 17.1% in the (DBA X 129) F2 cross. There were several minor locus to locus interactions that were not from the major QTL regions. For example, there are no QTL on chromosomes 13, 14, 15, and 19, and yet they harbor loci that may regulate wound healing through interactions (Table 2). Surprisingly, the interacting loci explain 55.7% of the phenotypic variation.

Comparison of QTL for wound healing in different crosses of F2 mice:

As shown in Table 3, the comparison of wound healing QTL so far has been carried out in three crosses: MRL/lpr x C57BL/6J (B6), MRL/MPJ x SJL/J, and DBA x 129. A study by McBrearty *et al*. in 1998 employing a MRL/lpr x B6 cross identified four QTL on chromosomes 8, 12, 13, and 15, with the highest LOD score varying from 2.1 to 2.4. A second study with the same cross identified QTL on chromosomes 4, 7, 8, 11, 12, 13, 15, 16, and 18, with the lowest LOD score found on chromosome 7 (1.1) and the highest LOD score on found chromosome 13 [(4.8) (Blankenhorn *et al*. 2003)].

MRL/MPJ x SJL/J cross yielded 10 QTL with the LOD score varying from 2.7 to 16.1, with the lowest LOD score on chromosome 13 (D13Mit228) and the highest on chromosome 9 (D9Mit270) (Table 3, Masinde *et al*. 2001). Four QTL were identified in the present study using the DBA X 129 mice. The contribution of different alleles generally fit a recessive type of inheritance with the exception that heterozygotes at locus D4Mit170 performed poorly, with unknown mode of inheritance (Table 4). The DBA X 129 cross had LOD scores ranging from 2.9 to 4.1 on chromosomes 1, 4, 12 and 18. Chromosome 1 had the highest LOD Score (4.1) and chromosome 12 had the lowest

[(2.9) (Table 1)]. Chromosome 4 QTL appears to be present in all three (MRL/MPJ x SJL/J, MRL/lpr x B6, and DBA x 129) crosses.

Discussion

In the present study using a cross between DBA and 129 mouse strains, the estimated heritability for wound healing was 66%. Three loci were contributed by the good healer DBA strain while only one locus was contributed by poor healer 129 strain. Interestingly, there were significant interactions between minor loci (loci with LOD scores of less than 2.7) from chromosomes with no QTL, as well as between chromosome 1 QTL and other minor loci. Individual QTL effect together with loci interactions contributed to 73% of variation in wound healing in the DBA X 129 intercross. In previous studies, we showed that heritability for wound healing was 88% using MRL/MPJ x SJL/J cross and 86% with a MRL/MPJ x DBA/J cross (Masinde *et al.* 2001; Li *et al*. 2001b). Thus, the variation in wound healing in different strains of mice is mainly determined genetically.

Rate of wound healing and mode of inheritance in DBA X 129 mice

Quantitative traits are typically due to small contributions by many genes, resulting in a phenotype (Blankenhorn *et al.* 2003). When the DBA was crossed with the 129, it was expected that an equal contribution in wound healing would be from both DBA and 129 inbred strains of mice. Consequently, the ear punch hole healing in F1 mice was expected to be intermediate between the DBA and 129 mice (Li *et al*. 2001b). However, the F1 mice showed a poorer healing capacity than the 129 mice (poor healer). These data suggest that the 129 parent may harbor a recessive gene(s) or interacting

genes that contribute to the decreased wound healing in the F1 mice compared to the anticipated intermediary healing between DBA and 129 parental strains. There is evidence from a previous study that the MRL/DBA cross resulted in the suppression of wound healing (Li *et al.* 2001b), although this suppression was not as pronounced as that observed in the DBA X 129 cross. The phenotype distribution in the F2 mice was skewed towards the poor healer as more of the F2 mice had mean healing rates less than the poor healer strain. This provides additional evidence for the presence of a recessive gene(s) or gene interactions contributed by both DBA and 129 mice that impede wound healing (Frankel, 1995).

QTL analysis for DBA X 129 F2 cross

More than 20 QTL have been identified thus far for wound healing phenotype from the 3 inbred strain crosses (Blankenhorn *et a*l. 2003; Masinde *et a*l. 2001; McBrearty *et al*. 1998). Surprisingly, only two of these QTL appear to be common based on their common chromosomal location, a finding similar to that reported for bone phenotype studies (Beamer *et al.* 1999; Beamer *et al.* 2001; Benes *et al.* 2000; Drake *et al.* 2001; Masinde *et al.* 2002; Klein *et al.* 1998; Koller *et al.* 2000; Shimizu *et al.* 1999). These data suggest that complex mechanisms may contribute to wound healing in different inbred strains of mice.

In the present study, we have shown that wound healing variation in a (DBA X 129) F2 cross has a high heritable component (66% heredity). However, the four identified QTL from the F2 mice only explained 17.1% of variation in the rate of wound healing/regeneration. There are a number of explanations for the low contribution by the

QTL identified in this study which include: 1) wound healing/regeneration is influenced by many genetic loci but only a few could be detected using this cross; and 2) epistatic interactions may play a major role in genes regulating wound healing/regeneration. Consistent with the later explanation, we found that the interactions between different loci contributed to more than 50% of the phenotypic variation. Several of these interactions however, occurred between minor loci not located in the identified QTL regions, which is in contrast to our earlier study using MRL X SJL, where most of the interacting loci were from chromosomes with major QTL (Masinde *et al*. 2001).

Potential Candidate Genes

We examined the chromosomal regions at DNA sequence level for the QTL we identified in this study, and found a number of potential candidate genes that may contribute to the observed variation in wound healing response in the DBA X 129 intercross. They include epherin receptor genes on chromosome 4, disintegrin and metalloprotease domain genes on chromosome 12, and protocadherin genes on chromosome 18.

Ephrin receptors are tyrosine kinases, and together with their ligands, the ephrins, are mediators of cell-cell communication. They are involved in the development and repairs of many tissues and organs such as nervous and cardiovascular systems (Goldshmit *et al.* 2004; Himanen and Nikolov 2003). Ephrin receptor genes Ephb2, Epha8 and Epha2 are located at positions of 135.72 Mb, 135.84 Mb and 140.21 Mb of chromosome 4, respectively, while the *earheal2* QTL peak is near a marker (D4Mit170)

at 137.50 Mb on this chromosome, thus raising the possibility that one or more of the three receptor genes could be *earheal2* QTL genes.

QTL *earheal3* on chromosome 12 is next to D12Mit118 at 86.93 Mb. Not far from this position are two disintegrin and metalloprotease domain genes at 78.28 Mb and 78.42 Mb, Adam4 and Adam21. Disintegrin and metalloproteases belong to matrix metalloproteinases, which facilitate release of growth factors from membranes and extracellular matrix and play a role in wound healing as well as in normal development (Rosenberg 2002). It has been shown that metalloproteinases MMP-2 and MMP-9 were up-regulated and their tissue inhibitors TIMP-2 and TIMP-3 were down-regulated in the super healer mouse strain MRL (Heber-Katz *et al.* 2004), raising the possibility that Adam4 and Adam21 could be *earheal3* QTL genes.

The chromosome 18 QTL *earheal4* is located between D18Mit12 (36.11 Mb) and D18Mit36 (46.76 Mb). Within this region are protocadherin 12 gene Pcdh12 (38.49 Mb), protocadherin alpha cluster genes Pcdha@ (37.15 Mb), protocadherin beta genes Pcdhb1 to Pcdhb22 (37.49 Mb – 37.74 Mb), and protocadherin gamma cluster genes Pcdhg@ (38.07 Mb). Cadherins and protocadherins mediate cell-cell contact and adhesion, which may be related to would healing (Down *et al.* 2005; Matsuyoshi *et al.* 1997; Medina *et al.* 2004). Future studies are needed to address if any of the above candidate genes are, in fact QTL genes from one or more loci.

In conclusion, the present study has revealed some novel QTL that regulate wound healing in a (DBA X 129) F2 cross. At the same time, we have evidence of minor loci playing a major role in the regulation of wound healing. In addition, the study reveals lack of overlap between QTL for wound healing in DBA X 129, MRL/lpr X B6, and

MRL/MPJ X SJL/J mice crosses, which suggests that different genes may regulate wound healing in different crosses.

Acknowledgements

Assistance Award #DAMDBA7-99-1-9571 supported this work. The U.S. Army Medical Research Acquisition Activity, 820 Chandler Street, Fort Detrick MD 21702-5014, is the awarding and administering acquisition office. The information contained in this publication does not necessarily reflect the position or policy of the Government and no official endorsement should be inferred. The authors wish to thank Heather Davidson and Melanie Hamilton-Ulland for their excellent technical support and the JL Pettis VA Medical Center for their support.

References

1. Beamer WG, Shultz KL, Churchill GA, Frankel WN, Baylink DJ, Rosen CJ and Donahue LR (1999) Quantitative trait loci for bone density in C57BL/6J and CAST/EiJ inbred mice. Mamm Genome 10: 1043-1049.

2. Beamer WG, Shultz KL, Donahue LR, Churchill GA, Sen S, Wergedal JR, Frankel WN, Baylink DJ, and Rosen CJ (2001) Quantitative trait loci for Femoral and Lumbar Vertebral Bone Mineral Density in C57BL/6J and C3H/HeJ inbred strains of mice. J Bone Min Res 16: 1195-1206.

3. Benes H, Weinstein RS, Zheng W, Thaden JJ, Jilka RL, Manolagas SC and Reis RJS (2000) Chromosomal mapping of osteopenia-associated quantitative trait loci using closely related mouse strains. J Bone Miner Res 15: 626-633.

4. Blankenhorn EP, Troutman S, Clark LD, Zhang X-M, Chen P, Heber-Katz E (2003) Sexually dimorphic genes regulate healing and regeneration in MRL mice. Mamm Genome, 14: 250-260.

5. Clark LD, Clark RK, Heber-Katz E (1998) A new murine model for mammalian wound repair and regeneration. Clin Immunol Immunopathol 88: 35-45.

6. Down M, Power M, Smith SI, Ralston K, Spanevello M, Burns GF, Boyd AW (2005) Cloning and expression of the large zebrafish protocadherin gene, Fat. Gene Expr Patterns. 5: 483-90.

7. Drake TA, Schadt E, Hannani K, Kabo JM, Krass K, Colinayo V, Greaser LE, Golden J, Lusis AJ. (2001) Genetic loci determining bone density in mice with diet-induced atherosclerosis. Physiol Genomics 5: 205-215.

8. Frankel W (1995) Taking stock of complex trait genetics in mice. Trends Genet. 11(12): 471-7.

9. Goldshmit Y, Galea MP, Wise G, Bartlett PF, Turnley AM (2004) Axonal regeneration and lack of astrocytic gliosis in EphA4-deficient mice. J Neurosci. 24: 10064-73.

10. Heber-Katz E, Leferovich JM, Bedelbaeva K, Gourevitch D (2004) Spallanzani's mouse: a model of restoration and regeneration. Curr Top Microbiol Immunol. 280: 165-89

11. Himanen JP, Nikolov DB (2003) Eph signaling: a structural view. Trends Neurosci. 26: 46-51.

12. Klein RF, Mitchell SR, Phillips TJ, Belknap, JK and Orwoll ES (1998) Quantitative trait loci affecting peak bone mineral density in mice. J. Bone Miner Res 13: 1657-9.

13. Koller DJ, Econs MJ, Morin, PA, Christian JC, Hui SL, Parry P, Curran ME, Rodriguez LA, Conneally PM, Joslyn G, Peacock M, Johnston CC and Foroud T (2000) Genome screen for QTL contributing to normal variation in bone mineral density and osteoporosis. J Clin Endocrin Metab 85: 3116-3120.

14. Li X, Gu W, Masinde G, Hamilton-Ulland M, Xu S, Mohan S, and Baylink DJ (2001) Genetic control of the rate of wound healing in mice. Heredity 86:668-74.

15. Li X, Gu W, Masinde G, Hamilton-Ulland M, Xu S, Mohan S and Baylink DJ (2001b) Genetic Control of the rate of Wound Healing in mice. J Hered 86: 1-7.

16. Lincoln SE, Daly MJ and Lander ES. Using MAPMAKER/QTL Version 1.1 (1993) A Tutorial and Reference Manual. Whitehead Institute for Biomedical Research Technical Report.

17. Lynch SE, Colvin BB, Antoniades HN (1991) Growth factors in wound healing. Single and synergistic effectiveness of partial thickness porcine skin wounds. J Clin. Invest 84: 640-6.

18. Manly, KF, Cudmore, Jr, RH, Meer, JM (2001) Map Manager QTX, cross platform software for genetic mapping. Mammalian Genome 12:930-932.

19. Martin P (1997) Wound healing-aiming for perfect skin regeneration. Science 276: 75-81.

20. Masinde GL, Li X, Gu W, Davidson H, Mohan S, and Baylink DJ (2001) Identification of wound healing/regeneration quantitative trait loci (QTL) at multiple time points that explain seventy percent of variance in (MRL/MpJ and SJL/J) mice F2 population. Genome Res 11:2027-33.

21. Masinde, G., Li X, Gu W, Wergedal J, Mohan S, and Baylink DJ (2002) Quantitative Trait Loci for Bone Density in Mice: the Genes Determining Total Skeletal Density and Femur Density Show Little Overlap in Same F2 Mice. Calcified Tissue International 71:421-8.

22. Matsuyoshi N, Imamura S (1997) Multiple cadherins are expressed in human fibroblasts. Biochem Biophys Res Commun. 235: 355-8.

23. McBrearty BA, Clark LD, Zhang XM, Blankenhorn EP, Heber- Katz E (1998) Genetic analysis of a mammalian wound-healing trait. Proc Natl Acad Sci 95: 11792-11797.

24. Medina A, Swain RK, Kuerner KM, Steinbeisser H (2004) Xenopus paraxial protocadherin has signaling functions and is involved in tissue separation. EMBO J. 23: 3249-58.

25. Rosenberg GA (2002) Matrix metalloproteinases in neuroinflammation. Glia. 39: 279-91.

26. Shimizu M, Higuchi K, Bennett B, Xia C., Tsuboyama T, Kasai S, Chiba T, Fujisawa H *et al.* (1999) Identification of peak bone mass QTL in a spontaneously osteoporotic mouse strain. Mamm Genome 10: 81-7.

27. Singer AJ and Clark RAF (1999) Cutaneous wound healing. The New England J Med 341: 738-746.

28. Stocum DL (1996) Tissue Restoration: approaches and prospects. Wound Rep. Reg 4: 3-15.

29. Van Ooijen JW and Maliepaard C (1996). MapQTLs (tm) version 4.0: Software for the calculation of QTLS positions on the genetic maps. CPRO-DLO, Wageningen, The Netherlands.

30. Van Ooijen JW (1999) LOD significance thresholds for QTL analysis in experimental populations of diploid species. Heredity 83: 613-624.

Figure Legend

Fig.1. Line graph of the ear punch hole diameter measured from day 0 to day 28 in the DBA and 129 parental strains, and their F1 progenies. DBA (a good healer) heals much faster than 129 (a poor healer), while F1 heals more poorly than the 129.

Fig.2. Normal distribution of wound healing phenotype for the combined male and female DBA X 129 F2 mice at 7 weeks of age. The bars show a frequency histogram for wound healing, while the line shows theoretical normal distribution. Mean values for DBA and 129, mice are shown by arrows.

Fig.3. Interval maps for chromosomes 1, 4, 12, and 18 shown to carry QTL for wound healing. The vertical axis shows the LOD scores while the horizontal axis shows the markers from centromeric end of each chromosome on the left extending towards telomeric end on the right.

Table 1. QTL for fast wound healing detected in DBA x 129 mice population (combined male and female) using MapQTL program.

QTL designation	Marker	Distance (cM)	LOD score	% phenotypic variance explained	Source
earheal1	D1Mit406	101.2	4.1	6.3	129
earheal2	D4Mit170	66.6	2.9	4.3	DBA
earheal3	D12Mit118	45.0	3.1	2.9	DBA
earheal4	D18Mit12	17.0	3.2	3.6	DBA
Total phenotypic variance explained (%)			**17.1**		

Table 2: (DBA X 129) F2 mice genotype locus/locus interaction using Map Manager QTX program

Locus 1	Locus 2	P-value	% Expl.
D1Mit159	D11Mit71	0.001	6.0
D1Mit159	D11Mit151	0.001	6.3
D1Mit159	D11Mit231	0.001	6.0
D1Mit406*	D8Mit292	0.001	7.7
D4Mit268	D8Mit45	0.001	5.5
D13Mit78	D19Mit72	0.001	6.7
D14Mit263	D19Mit72	0.001	5.4
D15Mit6	D19Mit72	0.001	5.9
D15Mit16	D18Mit36	0.001	6.2
Total			55.7

* Represents significant QTL.

Table 3: Comparison of QTL for Fast Wound Healing in different F2-mice populations

MRLxB6 (Blankenhorn *et al.,* 2003)			MRLxSJL (Masinde *et al*., 2001)			DBAx129 (This study)		
Peak marker	Distance (cM)	LOD	Peak marker	Distance (cM)	LOD	Peak marker	Distance (cM)	LOD
D8Mit211 (heal1)	49.0	4.1	D1Mit334 (sth1)	49.2	7.1	D1Mit406	101.2	4.1
D13Mit117 (heal2)	19.0	3.3	D3Mit217 (sth2)	43.7	5.4	**D4Mit170**	66.6	2.9
D13Mit144 (heal3)	48.0	3.2	D4Mit214 (sth3)	21.9	6.1	D12Mit118	45.0	3.1
D13Mit245 (heal7)	30.0	4.8	**D4Mit31 (sth4)**	50.3	6.5	D18Mit12	17.0	3.2
D4Mit13 (heal8)	71.0	3.0	D6Mit261 (sth5)	29.5	4.1			
D11Mit213 (heal10)	55.0	2.4	D7Mit220 (sth6)	38.3	4.8			
			D7Mit12 (sth7)	62.3	4.3			
			D9Mit207 (sth8)	31.7	14.2			
			D9Mit270 (sth9)	41.5	16.1			
			D13Mit228 (sth10)	45.9	2.7			

Common QTL shown in bold.

Table 4. Single locus genotype value for wound healing QTL in DBA x 129 F2 mice

Genotype	Hole Size (mm)	N	P	Mode of action
D1Mit406				
b/b	0.945± 0.27	57	0.0003	
b/a	1.103± 0.24	146	0.8957	Recessive for 'b' allele (129 allele)
a/a	1.108± 0.27	71	0.0011	
D4Mit170				
b/b	1.055± 0.27	120	0.0544	
b/a	1.112± 0.25	235	0.0010	Unclear mode of inheritance
a/a	1.011± 0.28	120	0.2120	
D12Mit118				
b/b	1.091± 0.25	95	0.4904	
b/a	1.070± 0.25	226	0.1730	Recessive for 'a' allele (DBA allele)
a/a	1.027± 0.29	116	0.0858	
D18Mit12				
b/b	1.133± 0.24	83	0.2122	
b/a	1.093± 0.27	232	0.0040	Recessive for 'a' allele (DBA allele)
a/a	1.003± 0.26	107	0.0050	

Hole size values are Mean ± SD; N: Number of observations; P: probability value obtained from T-test and vertically listed as b/b vs. b/a, b/a vs. a/a, and a/a vs. b/b. Genotypes: 'a' represents DBA mouse strain, 'b' for 129-mouse strain.

Incorporating Mouse Genome
Mammalian Genome
Genes and Phenotypes

Mapping the dominant wound healing and soft tissue regeneration QTL in MRL × CAST

Hongrun Yu,[1] Subburaman Mohan,[1–3] Godfred L. Masinde,[1,2] David J. Baylink[1,2]

[1]Musculoskeletal Disease Center, Jerry L. Pettis Memorial VA Medical Center, Loma Linda, California 92357, USA
[2]Department of Medicine, Loma Linda University, Loma Linda, California 92350, USA
[3]Departments of Biochemistry and Physiology, Loma Linda University, Loma Linda, California 92350, USA

Received: ■ / *Accepted:* ■

Abstract

We have used a mouse ear punch model and the QTL (quantitative trait loci) mapping technique to identify genes that are responsible for soft tissue regeneration. In the early studies, we have identified several QTL and have shown that the inheritance of ear healing was additive in one cross (MRL × SJL), and recessive in another cross (DBA × 129). Because CAST mice are genetically distinct and have a different genetic background, CAST would facilitate the identification of common and novel QTL when crossed with common inbred lines. We made a cross between super healer MRL and poor healer CAST and collected ear punch phenotype and marker genotype data from F_2. Ear punch healing exhibited a dominant mode of inheritance in this cross. There were three main QTL on Chromosomes 4, 9, and 17, and two suggestive QTL on Chromosomes 1 (new) and 7. Taken together, these QTL accounted for about 29% of total F_2 variance of MRL × CAST. Compared with another study with the same cross, we found a totally different set of QTL. Two QTL interactions were identified by a full QTL model: Chromosomes 4×17 and 9×17; the latter reached to a statistical level at $p < 0.05$. These interactions explained about 4% of the F_2 phenotypic variance. We conclude that soft tissue regeneration is controlled by multiple genes and locus vs. locus interactions.

This work was supported by Assistance Award No. DAMD17-99-1-9571. The U.S. Army Medical Research Acquisition Activity, Fort Detrick, MD, is the awarding and administering acquisition office. The information contained in this publication does not necessarily reflect the position or policy of the U.S. Government and no official endorsement should be inferred.

Correspondence to: Subburaman Mohan, Musculoskeletal Disease Center (151), Jerry L. Pettis Memorial VA Medical Center, 11201 Benton Street, Loma Linda, CA 92357, USA; E-mail: Subburaman.Mohan@med.va.gov

Ear punch in mice has been used to study wound healing and soft tissue regeneration. A wide range of variations exists in the healing rate of ear hole closure among mouse inbred strains (Li et al. 2001). The MRL/MpJ mouse and a progenitor strain, LG/J, heal four times faster than other strains such as Balb/cByJ and SJL/J. In addition, it was found recently that only MRL/MpJ could heal completely and without scarring (Clark et al. 1998; Heber-Katz 1999).

The mouse ear hole healing rate is highly inheritable, with a heritability of 86% (Li et al. 2001). Over the last few years, several QTL (quantitative trait loci) mapping studies have been conducted to identify mouse wound healing and soft tissue regeneration genes (Blankenhorn et al. 2003; Heber-Katz et al. 2004a; Masinde et al. 2001; McBrearty et al. 1998). These studies used crosses between super healer MRL/MpJ (MRL) and poor healer strains such as C57BL/6 (B6), CAST/Ei (CAST), and SJL/J (SJL). More recently, we also used another cross, DBA/1J (DBA) × 129X1/SvJ (129), where DBA served as a better healer (Masinde et al. 2005). These studies identified several QTL for wound healing and soft tissue regeneration. In addition, it was found that the mode of inheritance was different in different crosses. For example, the inheritance of ear healing was additive in MRL × SJL (Masinde et al. 2001), while it was recessive in DBA × 129 (Masinde et al. 2005).

The common laboratory mice are *Mus musculus*, which is a species with four subspecies, including *domesticus* and *castaneus* (Silver 1995). In the past, inbred lines that were used in soft tissue QTL mapping, such as B6, MRL, and SJL, were all predominantly derived from *domesticus* (Herber-Katz et al. 2004a; Wade et al. 2002). The *castaneus* mice are genetically distinct from these other strains. Thus, we hypothesize that the different genetic backgrounds in crosses between *castaneus* and common inbred lines would facilitate the identification of common and

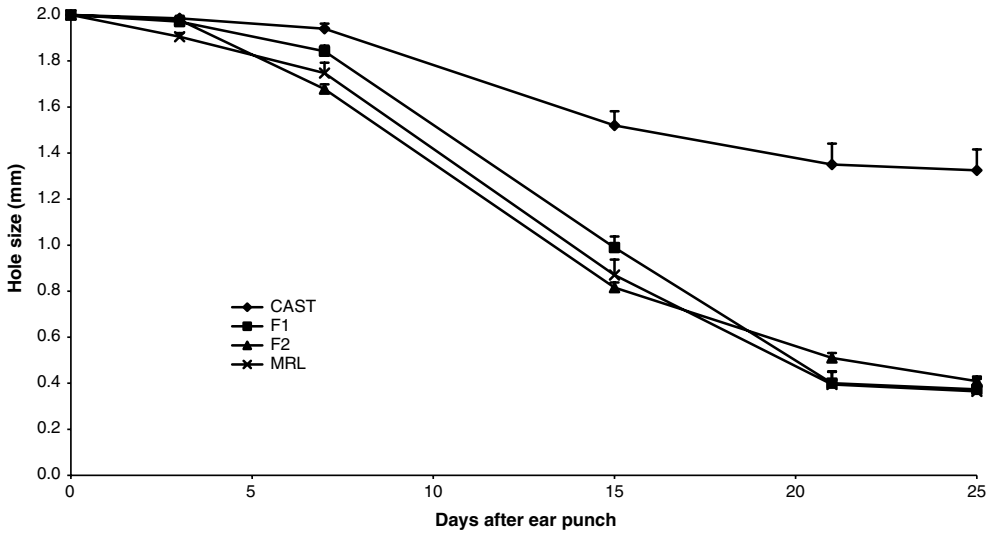

Fig. 1. Line graphs of the wound healing rates measured at different time points after ear punch for the cross of MRL × CAST. Data values are presented as means + SE.

novel QTL. The objectives of the current study were to identify these QTL and to elucidate the mode of inheritance in a cross between super healer MRL and a poor healing inbred line of *castaneus*, CAST/Ei (CAST).

Materials and methods

Mice. Inbred mouse strains MRL/MpJ (MRL) and CAST/Ei (CAST) were obtained from the Jackson Laboratory (Bar Harbor, ME). The animals were housed at the Animal Research Facility, J.L. Pettis Veterans Administration Memorial Medical Center. Housing and breeding conditions were described previously (Li et al. 2001, 2002; Masinde et al. 2001, 2002). The experimental protocols were in compliance with the established animal welfare regulations and approved by the animal research committee of J.L. Pettis VA Memorial Medical Center. MRL × CAST cross was made. The number of MRL × CAST F_2 mice was 328 (171 females and 157 males).

Genotyping and phenotyping. Ear punch closure measurements and the method of genotyping were described previously (Li et al. 2001; Masinde et al. 2001, 2005). Ear punch closure measurements were made at days 3, 7, 15, 21, and 25 after the punch was made. As previously shown (Masinde et al. 2001), healing plateaued at day 25 and therefore we did not perform further measurements beyond that time point. Eighty-six markers were genotyped for the F_2 of MRL × CAST. The average distance between markers was 17 cM. Thirty-three percent (33%) of intermarker distances was greater than 20 cM. However, none of these were in regions of the QTL identified in this study.

Data analysis. Standard statistical analysis, such as correlation and analysis of variance (ANOVA), was done on the phenotypes using STATISTICA (StatSoft, Inc, Tulsa, OK). Genotype data were analyzed using both MapQTL v5.0 (Van Ooijien 2004) and Pseudomarker (Sen and Churchill 2001; Srivastava et al. 2004). MapQTL's interval mapping option was used. Logarithm of the odds (LOD) thresholds for suggestive significance and significance were obtained by MapQTL's permutation test option. MapQTL provides both individual thresholds per linkage group and the genome-wide threshold. The former was used as our significant criteria. In general, we used a LOD score of 2 as a cutoff for suggestive evidence of linkage. Permutation tests indicated that a LOD score of 2 had an average $p < 0.1$ per linkage group. A LOD score of 3, shown in permutation tests as equivalent to $p = 0.01$, was considered evidence of significant linkage. Because there could be high level of kurtosis and skewness in the data distribution for some of the ear-healing phenotypes, MapQTL's nonparametric Kruskal-Wallis option was also used. For this analysis, $p < 0.005$ was used as cutoff for suggestive evidence of linkage when it was used alone. In Pseudomarker, the ''mainscan'' function was used for genome-wide scan. ''Pairscan'' and ''fitqtl'' were used to determine significance and amount of F_2 variance of the interactions between QTL on different chromosomal positions.

Results

Ear punch healing phenotype. Compared with MRL, CAST is a poor healer (Fig. 1). Significant difference at $p < 0.01$ in healing between CAST and

Table 1. Average hole size at different time points after ear punch in the cross between MRL and CAST

		CAST	*F_1*	*F_2*[a]	*MRL*
Day 15	Number of animals	10	26	318	10
×	Hole size (mm)	1.52	0.99^{A}	0.82^{Ab}	0.87^{A}
	Standard deviation	0.19	0.25	0.40	0.21
	Skewness	−0.12	1.21	0.30	−0.05
Day 21	Number of animals	10	26	302	10
	Hole size (mm)	1.35	0.40^{A}	0.51^{A}	0.40^{A}
	Standard deviation	0.29	0.25	0.37	0.18
	Skewness	0.09	0.61	0.73	−1.15
Day 25	Number of animals	10	26	304	10
	Hole size (mm)	1.33	0.37^{A}	0.41^{A}	0.37^{A}
	Standard deviation	0.29	0.26	0.36	0.17
	Skewness	0.16	0.43	0.93	−0.93

Note: Upper-case letters A, B, and C indicate a significant difference at $p < 0.01$ from CAST, F_1, F_2, respectively; Lower-case letters indicate the same at $p < 0.05$.
[a]A total of 328 F_2 mice were ear-punched. Because of missing data, the actual numbers at different time points of measurement varied.

MRL started at day 15 (Table 1). However, the F_1 of MRL × CAST healed almost at the same rate as MRL (Fig. 1). There was no significant difference between the F_1 and MRL (Table 1). In other words, ear punch healing exhibited a dominant mode of inheritance in MRL × CAST. The average healing rate of F_2 was similar to that of F_1. There was also no significant difference in healing rates between males and females in the F_2 (data not shown).

Correlation analysis indicated that the ear-healing measurements at different time points were all significantly correlated, with $r > 0.81$ (e.g., $r = 0.95$, $p < 0.05$ for day 21 vs. day 25). In the F_2, we have also collected data for body weight at day 49, when the mice were sacrificed. Healing showed no significant correlation with body weight at day 49.

QTL identified. QTL with suggestive significant LOD scores above 2 were identified on Chromosomes 1, 4, 7, 9, and 17 (Table 2). Among these, only Chromosomes 4, 9, and 17 had LOD scores over 3, the significant threshold equivalent to $p < 0.01$. The total amount of F_2 variance explained by these QTL averaged among the days 15, 21, and 25 phenotypes were approximately 29%. We have performed a separate analysis to determine the role of gender in QTL mapping for soft tissue regeneration. The results with gender as a covariate were similar to those without gender in the analysis. Thus, contrary to the findings of Blankenhorn et al. (2003), gender was not a major factor in our study.

Marker *D4Mit170* on Chromosome 4 at 66.6 cM had associated peaks with significant LOD scores for the ear punch phenotype at all time points (Table 2). The LOD score was 3.85 at day 15, 3.38 at day 21, and 3.16 at day 25. This QTL is confirmed by another marker nearby, *D4Mit203*. Chromosome 9 has the longest QTL, ranging from 26 to 61 cM, as indicated by either LOD scores greater than 2 or significant Kruskal-Wallis test statistics at $p < 0.005$. By examining the alleles of this QTL, one can see both MRL and CAST served as the source of better healing alleles. Chromosome 17 had the highest LOD score, 5.13, and the highest Kruskal-Wallis test statistic, 16.9 ($p < 0.0005$), associated with marker *D17Mit51*. Unlike QTL on other chromosomes, where super healer MRL contributed better healing alleles, poor healer CAST contributed this QTL on Chromosome 17. The LOD scores of this QTL were higher for the later measurements than the early measurements, with day 25 having the highest LOD scores (Fig. 2).

As shown for the total healing phenotype in Fig. 1, individual QTL represented by peak markers also showed a dominant mode of inheritance for better healing alleles (Fig. 3). For example, for markers *D4Mit170* and *D9Mit355* of the Chromosomes 4 and 9 QTL, homozygotes and heterozygotes for better healing allele from MRL were not significantly different from each other in the healing rate as expressed by the ear hole size but were significantly different from the homozygotes for poorer healing allele from CAST. The same thing is true for better healing allele from CAST for the Chromosome 17 QTL as represented by marker *D17Mit51*; the heterozygotes were not statistically different from CAST homozygotes but were statistically different from poorer healing MRL homozygotes.

QTL interactions. We have performed genome-wide ''pairscan'' in the Pseudomarker analysis to detect QTL interactions. Only two interactions with significant LOD score for the full-effect model were found: 4 × 17 and 9 × 17 (Table 3). These two interactions occurred between the Chromosomes 4 and 9 QTL and the Chromosome 17 QTL. LOD score for the 9 × 17 interaction was higher than that of 4 × 17

Table 2. Identified QTL regions for soft tissue repair and regeneration in MRL × CAST F_2.

Chrom	*Associated marker*	*Position (cM)*	*Phenotype*	*LOD Score*[a]	*K*[b]	*p*[c]	*Variance explained (%)*	*Healer allele*
1	*D1Mit64*	5	Day 15	2.13	7.9	0.05	5.7	MRL
4	*D4Mit203*	60	Day 15	**3.85**	9.8	0.01	6.9	MRL
4	*D4Mit170*	66.6	Day 15	**3.85**	**14.7**	0.001	6.9	MRL
4	*D4Mit170*	66.6	Day 21	**3.38**	**14.6**	0.001	6.6	MRL
4	*D4Mit170*	66.6	Day 25	**3.16**	**11.4**	0.005	6.4	MRL
7	*D7Mit98*	53.3	Day 15	2.31	7	0.05	4.9	MRL
7	*D7Mit98*	53.3	Day 25	2.21	6.4	0.05	4.6	MRL
9	*D9Mit129*	26	Day 15	1.76	**11.6**	0.005	2.8	MRL
9	*D9Mit129*	26	Day 21	2.22	**18.2**	0.0005	3.7	MRL
9	*D9Mit129*	26	Day 25	1.98	**13.4**	0.005	4.3	MRL
9	*D9Mit198*	49	Day 15	2.02	**10.8**	0.005	3.1	CAST
9	*D9Mit198*	49	Day 21	2.75	**14.5**	0.001	6.5	CAST
9	*D9Mit198*	49	Day 25	**3.26**	**15.6**	0.0005	9.8	CAST
9	*D9Mit355*	53	Day 15	**3.27**	**14.2**	0.001	5.5	MRL
9	*D9Mit355*	53	Day 21	**3.01**	**13.4**	0.005	5.3	MRL
9	*D9Mit355*	53	Day 25	**3.1**	**12.4**	0.005	5.5	MRL
9	*D9Mit347*	56	Day 15	2.43	7.1	0.05	6.2	MRL
9	*D9Mit347*	56	Day 21	**3.01**	**11.6**	0.005	5.3	MRL
9	*D9Mit347*	56	Day 25	**3.1**	**10.8**	0.005	5.5	MRL
9	*D9Mit350*	61	Day 15	2.3	7	0.05	3.5	CAST
17	*D17Mit51*	22.9	Day 15	2.66	7	0.05	4.2	CAST
17	*D17Mit51*	22.9	Day 21	**4.3**	**12.5**	0.005	6.9	CAST
17	*D17Mit51*	22.9	Day 25	**5.13**	**16.9**	0.0005	8.3	CAST
17	*D17Mit10*	24.5	Day 21	**3.9**	**11.6**	0.005	6.7	CAST
17	*D17Mit10*	24.5	Day 25	**4.49**	**13.9**	0.005	7.8	CAST
17	*D17Mit180*	29.4	Day 21	**3.02**	6.5	0.05	5.7	CAST
17	*D17Mit180*	29.4	Day 25	**3.42**	9.2	0.05	7	CAST
17	*D17Mit39*	45.3	Day 15	2.11	5.9	0.05	3.7	CAST

[a]Bold font indicates LOD score above 3.
[b]*K*: the Kruskal-Wallis test statistics. Bold font indicates $p < 0.01$.
[c]*p*: *p* value for the Kruskal-Wallis test statistics.

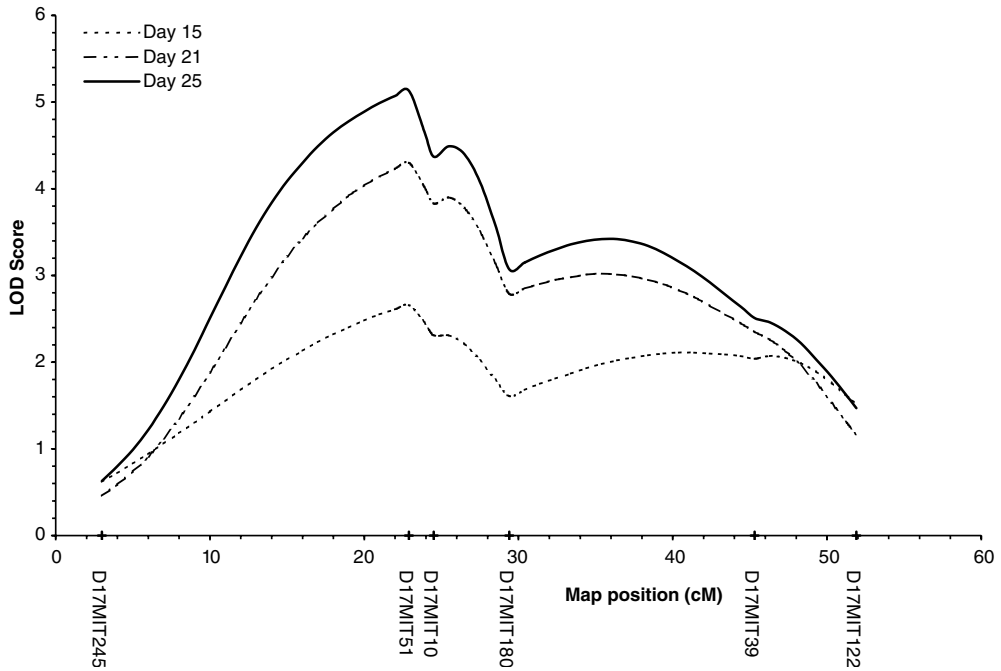

Fig. 2. Chromosome 17 QTL map for soft tissue regeneration in the cross of MRL × CAST obtained from MapQTL using the interval mapping option. Ear hole size measurements at day 15, 21, and 25 served as phenotypes.

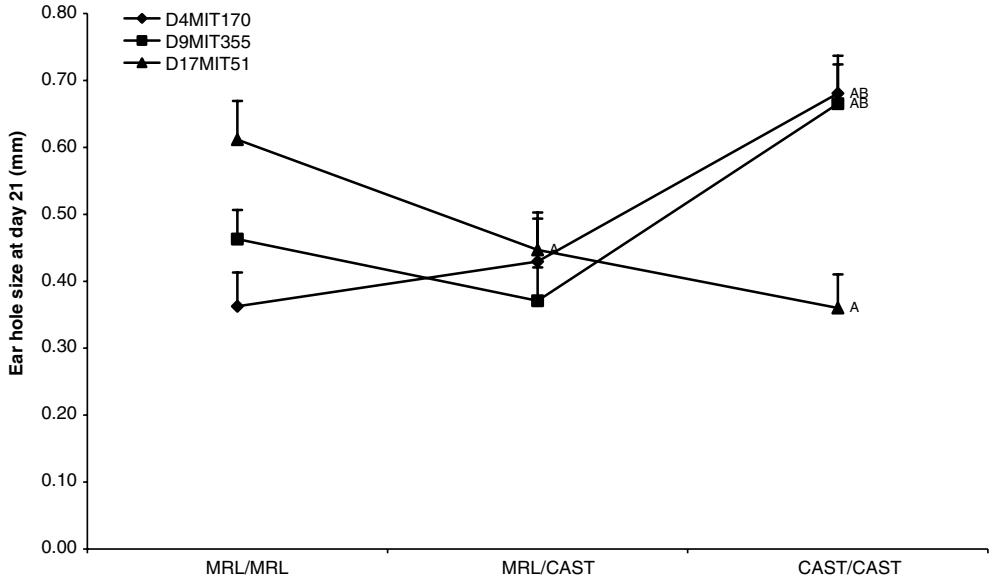

Fig. 3. Effect on the ear healing rate by different marker genotypes for the soft tissue regeneration QTL on Chromosomes 4, 9, and 17. Data values are presented as means + SE. Letters A and B indicate a significant difference at $p < 0.05$ from MRL/MRL and MRL/CAST, respectively.

(2.39 vs. 0.88). Analysis using Pseudomarker's "fitqtl" function determined that 4 × 17 and 9 × 17 interactions accounted for about 1% and 3% of the F_2 variance, respectively.

We have used genotype combinations of the markers located at chromosomal positions where interactions occurred to determine the phenotypic effect of QTL interactions. Because MRL contributed Chromosomes 4 and 9 QTL (represented by *D4Mit170* and *D9Mit355*) and CAST contributed Chromosome 17 QTL (represented by *D17Mit51*), genotype combination MRL/MRL × CAST/CAST had the best healing and the smallest hole sizes in both 4 × 17 and 9 × 17 interactions (ear hole size = 0.34 mm and 0.32 mm, respectively). In 4 × 17 interaction, genotype combination CAST/CAST × MRL/CAST had better healing than CAST/CAST × CAST/CAST (0.54 mm vs. 0.76 mm). Genotype combination MRL/CAST × MRL/CAST had better healing than MRL/CAST × CAST/CAST (0.38 mm vs. 0.48 mm) in 9 × 17 interaction. These numbers may have caused the significant interactions.

Discussion

Dominant inheritance. One interesting phenomenon we found was the mode of inheritance for the ear healing rate in different genetic backgrounds. For example, it was an additive inheritance in the cross of MRL × SJL (Masinde et al. 2001), whereas in the current study with MRL × CAST, it was a complete dominance, even though one parent was in common in both crosses. In another cross, DBA × 129 (Masinde et al. 2005), it was shown that both F_1 and F_2 had no significant differences with poor healer 129, while better healer DBA displayed a significant difference from all three groups. Thus, the DBA × 129 cross showed a recessive inheritance pattern. Therefore, ear healing exhibits a complex pattern of inheritance in different genetic backgrounds. We speculate that this may have resulted from the interactions between mouse genomes when different inbred strains are intercrossed.

Comparison with other studies. Table 4 compares the QTL identified in this study to all other QTL published thus far in the literature. When compared with another study using the same cross (MRL × CAST), we found that Chromosome 17 QTL appeared in both studies, with CAST as the contributing parent, thus validating this important QTL. However, when we examine other QTL, it is puzzling that the two studies had entirely different sets of QTL. In our study, we had QTL on Chromosomes 4, 7, and 9, which were also detected in the other

Table 3. List of significant genetic interactions between different chrompsornal regions in F2 of MRL × CAST

Chrom	*cM1*	*CM2*	*LOD full*	*LOD int*	*p value*	*LOD Q1*	*p value*	*LOD Q2*	*p value*
4 × 17	70	20	7.72	0.88	0.3975	3.88	0.0001	3.11	0.0008
9 × 17	50	20	9.06	2.39	0.0266	4.06	0.0001	2.94	0.00111

Note: Threshold for significant full effect (LOD full) was 7.63. Threshold for significant interaction effect (LOD int) was 4.93. LOD Q1 and Q2 indicate LOD scores for main effect of the two chromosomal regions.

Table 4. Comparison of this study with other QTL studies using different crosses for soft tissue regeneration

Chrom position[a] (cM)		*Associated marker*	*QTL names*	*Source*
MRL × CAST (this study)				
1	5	*D1Mit64*		MRL
4	**60 – 66.6**	***D4Mit170***	**Earheal2/Heal8/Sth4?**	**MRL**
7	**53.3**	***D7Mit98***	**Sth7?**	**MRL**
9	**26**	***D9Mit129***	**Sth8**	**MRL**
9	**49 – 61**	***D9Mit355***	**Sth9?**	**Both**
17	**22.9 – 45.3**	***D17Mit51***	**Heal13**	**CAST**
MRL × CAST (Heber-Katz et al. 2004a)				
11	58 – 70	*D11Mit213*	Heal10	MRL
13	10	*D13Mit16*	Heal2	MRL
13	35	*D13Mit13*	Heal7	MRL
14	12	*D14Mit201*	Heal12	CAST
17	**44**	***D17Mit93***	**Heal13**	**CAST**
MRL × B6 (McBrearty et al. 1998, Blankenhorn et al. 2003)				
4	**66 – 71**	***D4Mit13***	**Heal8**	**MRL**
7	26 – 52	*D7Mit85*	Heal6	MRL
8	49 – 68	*D8Mit211*	Heal1	B6
11	55 – 61	*D11Mit213*	Heal10	MRL
12	52	*D12Mit132*	Heal5	MRL
13	9 – 19	*D13Mit116*	Heal2	MRL
13	30 – 35	*D13Mit245*	Heal7	MRL
13	48 – 60	*D13Mit144*	Heal3	MRL
15	**48 – 56**	***D15Mit224***	**Heal4**	**MRL**
16	4 – 20	*D16Mit122*	Heal11	Both
18	30 – 44	*D18Mit33*	Heal9	B6
MRL × SJL (Masinde et al. 2001)				
1	49.2	*D1Mit334*	Sth1	MRL
3	43.7	*D3Mit217*	Sth2	MRL
4	21.9	*D4Mit214*	Sth3	MRL
4	**50.3**	***D4Mit31***	**Sth4**	**MRL**
6	29.5	*D6Mit261*	Sth5	MRL
7	38.3	*D7Mit220*	Sth6	SJL
7	**62.3**	***D7Mit12***	**Sth7**	**SJL**
9	**31.7**	***D9Mit207***	**Sth8**	**MRL**
9	**41.5**	***D9Mit270***	**Sth9**	**MRL**
13	45.9	*D13Mit228*	Sth10	MRL
DBA × 129 (Masinde et al. 2005)				
1	101.2	*D1Mit406*	Earheal1	129
4	**66.6**	***D4Mit170***	**Earheal2**	**DBA**
12	45	*D12Mit118*	Earheal3	DBA
18	17	*D18Mit12*	Earheal4	DBA

[a]A number indicates a single peak around that position, while a range indicates the range containing a series of peaks. Bold font indicates presence of Common QTL in multiple crosses.

crosses such as MRL × B6, MRL × SJL, and DBA × 129. However, they were totally absent in the other study (Heber-Katz et al. 2004a). One explanation is the random sampling nature of QTL studies. The chance of detecting the same QTL is small when the sample sizes are small. We used only 328 F_2 mice; 301 were used in the Herber-Katz (2004a) study. There are many factors in determining the sample size required to identify the same QTL. For example, a study to detect, with 50% of power, an additive QTL with allele effect of 0.25 and a LOD threshold of 4.3 would require at least 524 F_2 individuals (Darvasi 1998).

We also tried to match the QTL identified in our study with those in other studies. Among the six QTL identified, five appeared to be the same as identified by others (Table 4). The QTL on Chromosome 7 is in the same region as *Sth7*. However, in our study, this QTL was contributed by MRL, while SJL contributed the better healing allele of *Sth7*. The Chromosome 9 QTL in the 49–61-cM region appeared to be the same as *Sth9*. However, both parental strains contributed better healing alleles (Table 2), although at different chromosomal positions within the QTL. The presence of separate QTL is unlikely in such a short chromosomal region of only 4 cM. Additional markers need to be genotyped to resolve this contradiction. QTL at 5 cM on Chromosome 1 (marker *D1Mit64*) was not previously identified, although this was significant with only suggestive evidence (Table 2).

Many QTL exist in multiple crosses. One example is the QTL on Chromosome 4 (Tables 2 and 4). It was identified as *Heal8* in the MRL × B6 cross, associated with markers *D4Mit13* at 71 cM (Blankenhorn et al. 2003) and *D4Mit148* at 66.7 cM (Heber-Katz et al. 2004b). We think that it might be the same as *Sth4*, which was associated with marker *D4Mit31* at 50.3 cM (Masinde et al. 2001). Recently, it was found as *Earheal2* in DBA × 129, with the better healing allele contributed by DBA (Masinde et al. 2005). We now show that two markers at positions 60 and 66.6 cM were also associated with peaks of significant LOD scores, thus validating all other studies. The rationale of using genetically distinct inbred lines in QTL mapping is to assure the detection of common and novel QTL in diverse genetic backgrounds. This point has been demonstrated by the identification of this Chromosome 4 QTL. The fact that it has been also detected in three different studies implies that this is a very important QTL for soft tissue regeneration.

In summary, our group has identified QTL for soft tissue regeneration across Chromosomes 1, 3, 4, 6, 7, 9, 12, 13, 17, 18, and 19 (Table 4) (this study; Masinde et al. 2001, 2005). Another group has identified QTL on Chromosomes 4, 7, 8, 11, 12, 13, 14, 15, 16, 17, and 18 (McBrearty et al. 1998; Blankenhorn et al. 2003; Heber-Katz et al. 2004b). We were not able to confirm QTL *Heal1* on Chromosome 8, *Heal10* on Chromosome 11, *Heal12* on Chromosome 14, *Heal 4* on Chromosome 15, *Heal11* on Chromosome 16, which were all identified by the other group. There are so far no QTL detected on Chromosomes 2, 5, 10, and X.

Acknowledgments

The authors thank Heather Davidson and Courtney Kruse for their technical assistance and the J.L. Pettis VA Medical Center for its support.

References

1. Blankenhorn EP, Troutman S, Clark LD, Zhang XM, Chen P, et al. (2003) Sexually dimorphic genes regulate healing and regeneration in MRL mice. Mamm Genome 14, 250–260
2. Clark LD, Clark RK, Heber-Katz E (1998) A new murine model for mammalian wound repair and regeneration. Clin Immunol Immunopathol 88, 35–45
3. Darvasi A (1998) Experimental strategies for the genetic dissection of complex traits in animal models. Nat Genet 18, 19–24
4. Heber-Katz E (1999) The regenerating mouse ear. Semin Cell Dev Biol 10, 415–419
5. Heber-Katz E, Chen P, Clark L, Zhang XM, Troutman S, et al. (2004a) Regeneration in MRL mice: further genetic loci controlling the ear hole closure trait using MRL and M.m. Castaneus mice. Wound Repair Regen 12, 384–392
6. Heber-Katz E, Leferovich JM, Bedelbaeva K, Gourevitch D (2004b) Spallanzani's mouse: a model of restoration and regeneration. Curr Top Microbiol Immunol 280, 165–189
7. Li X, Gu W, Masinde G, Hamilton-Ulland M, Xu S, et al. (2001) Genetic control of the rate of wound healing in mice. Heredity 86, 668–674
8. Li X, Masinde G, Gu W, Wergedal J, Hamilton-Ulland M, et al. (2002) Chromosomal regions harboring genes for the work to femur failure in mice. Funct Integr Genomics 1, 367–374
9. Masinde GL, Li X, Gu W, Davidson H, Mohan S, et al. (2001) Identification of wound healing/regeneration quantitative trait loci (QTL) at multiple time points that explain seventy percent of variance in (MRL/MpJ and SJL/J) mice F2 population. Genome Res 11, 2027–2033
10. Masinde GL, Li X, Gu W, Wergedal J, Mohan S, et al. (2002) Quantitative trait loci for bone density in mice: the genes determining total skeletal density and femur density show little overlap in F2 mice. Calcif Tissue Int 71, 421–428
11. Masinde GL, Li R, Nguyen B, Srivastiva A, Edderkaoui B, et al. (2005) New quantitative trait loci (QTL) that regulate wound healing in DBA/129 F2 mice Cross. Funct Integr Genomics X, XXX–XXX
12. McBrearty BA, Clark LD, Zhang XM, Blankenhorn EP, Heber-Katz E (1998) Genetic analysis of a mammalian wound-healing trait. Proc Natl Acad Sci USA 95, 11792–11797
13. Sen S, Churchill GA (2001) A statistical framework for quantitative trait mapping. Genetics 159, 371–387
14. Silver LM (1995) *Mouse Genetics* (New York: Oxford University Press)
15. Srivastava AK, Kapur S, Mohan S, Yu H, Kapur S, et al. (2005) Identification of novel genetic loci for bone size and mechanosensitivity in an ENU mutant exhibiting decreased bone size. J Bone Miner Res 20, 1041–1050
16. Van Ooijen JW (2004) MapQTL® *5, Software for the mapping of quantitative trait loci in experimental populations* (Wageningen, Netherlands: Kyazma B.B.)
17. Wade CM, Kulbokas EJ 3rd, Kirby AW, Zody MC, Mullikin JC, et al. (2002) The mosaic structure of variation in the laboratory mouse genome. Nature 420, 574–578

Mapping an ENU mutant with high bone density reveals a major locus on distal region of chromosome 4

Srivastava AK, Mohan S, Chest V, Wergedal JE & Baylink DJ
Musculoskeletal Disease Center, Jerry L Pettis Veterans Medical Center, Loma Linda, CA 92357, and, Department of Medicine, Loma Linda University, Loma Linda, CA, 92354

Using ENU mutagenesis approach to reveal gene function, we have identified a mutant with increased bone density in a dominant screen in C57BL/6J (B6) mice. Data from 16-week old progeny produced (total number of pups n=102) from this mutant mice showed that mean total body bone mineral density (BMD) was 9-13% higher ($p<0.001$, n=45) and total body bone mineral content (BMC) was 10-14% higher ($p<0.01$), as compared to age and sex matched wild type (WT) controls. The total body bone area was not significantly affected. In addition to bone density, the lean body mass determined by DEXA was 8-17% higher in mutant progeny. Volumetric bone density measured in tibia and femur by pQCT was 4-7% higher at midshaft region, as compared to WT mice. To determine the chromosomal location of the ENU mutation, we bred mutant B6 mice with C3H/HeJ (C3H) mice in an intercross breeding to generate 137 B6C3H F2 mice for a low-resolution (using 66 markers) QTL mapping. Body weight adjusted total body bone density and total body bone mineral content determined by DEXA were used as phenotypes. Data from female (n=67) and male (n=70) C3HB6 F2 mice were combined for QTL analysis. Interval mapping of BMD indicated a major peak with LOD score of 8.1 (genome wide significance value $p<0.00001$) on Chr 4 (70 cM). Similarly, interval mapping of BMC trait indicated a major peak with LOD score of 4.6 ($p=0.000024$) on Chr 4 (55 cM). In conclusion, we report identification and characterization of an ENU mutant with approximately 10% higher bone density, and QTL mapping of mutant mice indicates locus on distal Chr 4 that regulates bone density. Further studies on positional cloning will reveal the mutant gene that contributes to higher bone density in mutant B6 mice.

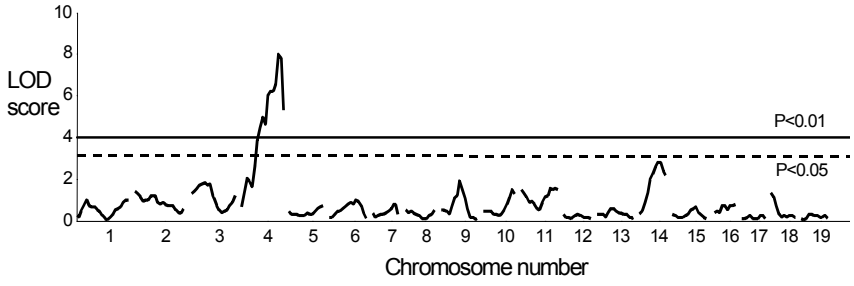

An update on N-Ethyl-N-nitrosourea (ENU) induced mutation screen for musculoskeletal phenotypes in mouse

Srivastava AK, Mohan S & Baylink DJ
JLP VAMC and LLU, Loma Linda, CA, 92354

Chemical mutagenesis followed by screening for abnormal phenotypes in the mouse holds great promise as a method for revealing gene function. Earlier, we have described a mouse N-ethyl-N-nitrosourea (ENU) mutagenesis program incorporating a genome-wide screen of one-generation dominant (F1) as well as three-generation recessive (F3) recessive mutations affecting musculoskeletal disorders in mouse model. Abnormal phenotypes are identified as ±2-3SD units different from control mice. The mutant mice were progeny tested to determine whether their abnormality is inheritable with a bimodal segregation of offspring in expected 1:1 or 1:3 Mendelian ratios, in dominant and recessive screens, respectively. We have screened approximately 2000 F1 and F3 mice. We observed more than 60 quantitative phenodeviants in primary screen, confirmed more than 30 phenodeviants in secondary screen, and tested approximately 30 phenodeviants for inheritable phenotypes. So far six musculoskeletal phenodeviants have been confirmed in multiple litters and are currently undergoing positional cloning.

Mutant Mouse ID	Genetic Screen	Major Phenotype	# Affected Mice (# of Progeny Screened)
917	Dominant	10-13% Lower total body bone area in males, females not affected	68 (165)
12137	Dominant	11-12% Higher Total Body Bone Density (BMD) and 12-14% Higher Bone Mineral Content (BMC)	56 (132)
12184	Dominant	11-14% Higher BMD, 15-20% Higher Trabecular BMD at Proximal Femur & Lumbar Vertebrae	45 (102)
B24	Recessive	13-14% Higher BMD and 14-15% Higher BMC	29 (86)
B29	Recessive	20-30% Low Bone Markers and 8-10% Higher Total Body BMD	6 (30)
B54	Recessive	9-14% Higher BMD, 14% Higher BMC	26 (85)

We have identified chromosomal location of a bone size mutant (ID 917) to a proximal region (12 cM) of chromosome 4. A high bone density mutant (ID12184) shows major locus on distal Chr 4 that regulates bone density. In conclusion, this program has identified mutants with significant differences in BMD, BMC and bone size, which would facilitate future discovery of major gene(s) that regulate BMD and other relevant skeletal phenotypes. In addition, the larger phenotypic variations in the mutant mice compared to QTL effects (~5%) and the availability of mutant mice for phenotypic characterization and gene expression without the need to develop congenic mice would increase the efficiency of gene identification process.

Identification of novel genetic loci for bone size and mechanosensitivity in an ENU mutant exhibiting decreased bone size

Apurva K. Srivastava[1,2], Sanjay Kapur[1], Suburaman Mohan[1,2,3], Hongrun Yu[1], Sonia Kapur[1], Jon Wergedal[1,2] & David J. Baylink[1,2,3]

[1]Musculoskeletal Disease Center, Jerry L. Pettis Veterans Administration Medical Center, Loma Linda, CA 92357

[2]Department of Medicine, Loma Linda University, Loma Linda, CA, 92354

[3]Department of Biochemistry, Loma Linda University, Loma Linda, CA, 92354

Running Title: Mapping ENU mutation with decreased bone size

Corresponding author: Suburaman Mohan, PhD
Musculoskeletal Disease Center,
Jerry L. Pettis Veterans Administration Medical Center,
Loma Linda, CA 92357
E-Mail: suburaman.mohan@med.va.gov
Phone: (909) 825 7084 ext. 2932
Fax: (909) 796 1680

Microabstract
Using a dominant ENU mutagenesis screen in C57BL/6J (B6) mice to reveal gene function, we have identified a mutant, 917M, with a reduced bone size phenotype, which is expressed only in males. We show that mutation results in osteoblasts with reduced proliferation, increased apoptosis, and an impaired response to mechanosensitivity. The mutation is mapped to a novel locus (LOD score of 7.9 at 10.5 cM) on chromosome 4.

Abstract
Introduction: Using a dominant ENU mutagenesis screen in C57BL/6J (B6) mice to reveal gene function, we have identified a mutant, 917M, with a reduced bone size phenotype, which is expressed only in males. In this report, we show the chromosomal location of this mutation using linkage analysis and cellular characterization of the mutant phenotype.
Materials and Methods: The mutant mouse was bred to wild type B6 to produce progeny for characterization of the bone size phenotype. Periosteal osteoblasts isolated from the tibia and femur of mutant and wild type mice were studied for proliferation, differentiation, and apoptosis potential. To determine the chromosomal location of the mutation, a low-resolution linkage map was established by completing a genome-wide scan in B6C3H F2 male mice generated from intercross breeding of mutant mice.
Results and Conclusion: Mutant progeny (16-weeks old) displayed a total body bone area that was 10-13% lower and periosteal circumference 5-8% lower at the femur and tibia midshaft compared to wild type B6 mice. Periosteal osteoblasts from mutant mice showed 17-27% reduced cell proliferation and 23% increased apoptosis compared to wild type controls. In addition, osteoblasts from mutant mice show an impaired response to shear stress-induced proliferation rate, an *in-vitro* model for mechanical loading. Interval mapping in B6C3H F2 males (n=69) indicated two major loci affecting bone size on Chr 1 at 45 cM (LOD 4.9) and Chr 4 at 10.5 cM (LOD 7.9, genome wide $p<0.01$). Interval mapping using body weight as covariate revealed only one significant interval at Chr 4 (LOD 6.8). Alleles of the Chr 4 interval inherited from the B6 mutant strain contribute to a significantly lower bone size than those inherited from C3H. A pair-wise interaction analysis showed evidence for a significant interaction between loci on Chr 1 with the Chr 4 QTL. The 917M locus on Chr 4 appears to be novel because it does not correspond with those loci previously associated with bone size on Chr 4 in B6 and C3H/HeJ mice or other crosses.

Key words: point mutation, ethyl-N-nitrosourea, bone size, quantitative trait loci, inbred

mice

Introduction

The use of chemical (ethyl N-nitrosourea, ENU) mutagenesis has provided an opportunity to develop and expand the repertoire of mutants affecting several disease models [1-5] for gene function studies. Phenotype-driven approaches have gained substantial attention in recent years due to their focus on mutagenesis procedures that emphasize recovery of new phenotypes relevant to clinical diseases without an assumption about the nature of the underlying genes or biological pathways involved. A major advantage of the large-scale ENU mutagenesis method is that each locus is randomly mutated and mutations are expected to result in non-lethal phenotypes and altered protein function instead of complete abrogation, thereby increasing the opportunity to identify mutants that are informative for that locus. This approach has recently produced variants that mimic phenotypes commonly seen in humans in the clinical setting.[6-8]

Earlier, we established an ENU screen in mice for mutations affecting musculoskeletal and growth related phenotypes [9] in an effort to improve our understanding of the genetic basis of osteoporotic disease. Genetic factors contributing to osteoporosis involve material properties such as bone mineral content and structural components such as size, shape and three-dimensional structure. Therefore, our ENU screen consisted of an assessment of screens for bone density, bone mineral content, bone area, radiographs, and serum biochemistry in 10- and 16-week old mice. Inheritance testing of mice with abnormal phenotypes has confirmed the presence of several robustly inherited mutant phenotypes, including those affecting body weight, bone density, bone size, and bone

markers. One of the ENU mutants (named 917M) confirmed in the ENU screen had a reduced bone size phenotype identified in a dominant screen in C57BL/6J (B6) mice. Three of the main parameters that assess bone size, specifically total body bone area, total body bone mineral content, and bone perimeter (periosteal circumference) at the midshaft tibia and femur, were all significantly lower in affected mice, implying that the affected genes might play a role in bone size regulation. In addition, the differences in bone size were expressed only in the male progeny from the 917M mice.[10] The main aims of this study were to further characterize affected cell types and to identify the mutant locus affecting decreased bone size in 917M mouse.

Our efforts on the cell type characterization was primarily focused on periosteal cells from long bones for the following reasons: 1) bone size is dependent on periosteal expansion mediated by increased bone formation and/or by decreased bone resorption;[11,12] and 2) important factors that regulate bone size such as sex hormones and exercise influence periosteal expansion by increasing periosteal bone formation and/or by decreasing periosteal bone resorption.[13,14]

Material & Methods

Generation of Mutant Progeny

Mice were maintained and used in accordance with protocols established by the Institutional Animal Care and Use Committee of this facility. Generation and dominant screening of progeny from ENU injected B6 male mice has been described previously

(9). The 917M male mouse was identified in the dominant screen with a low total body bone area and bone mineral content (22% low as compared to wild type control) phenotype measured by DEXA instrument (PIXImus, Lunar Corporation, Madison, WI). The 917M male was first bred with 2-3 wild type (WT) B6 female mice to produce approximately 20 first generation progeny. We determined the tibia midshaft bone area in these progeny by in-vivo pQCT, which showed approximately 8% lower periosteal circumference in male progeny as compared to age and sex matched wild type control mice. Since animals were not genotyped at this stage, phenotype distribution was the only means for differentiating the mutants from their unaffected littermates. To avoid potential breeding of an un-affected progeny due to classification errors in distinguishing mutants, we bred only extreme scoring mice with WT female B6 mice for generating 2nd and 3rd generation of progeny and excluded those mice that were on the borderline of our criteria to define mutants as described earlier.[9]

Screening of Mutant Progeny

Bone size was measured using the DEXA instrument, which reports bone size in area measurements per units of centimeter square. In addition, bone size was also measured at the midshaft tibia using pQCT as described earlier.[9,15] Body weight was used to normalize all size traits in the mutant progenies as described earlier.[9] Baseline data on WT B6 mice were collected from approximately 50-80 male and female control mice, DEXA and pQCT were performed when animals were 10 and 16 weeks of age (age varied by ±2 days).

Isolation of Periosteal Osteoblasts from Long Bones of Mutant Mice

The periosteal osteoblasts were isolated from the femur and tibiae of wild type and 917M mutant B6 male and female mice and were propagated in culture. The 10-week-old mice were euthanized using carbon dioxide, femur and tibia dissected out and soft tissue removed with minimum scraping of the bones. These bones were then used for isolation of periosteal cells by collagenase (1mg/ml inDMEM, Cellgro, Cat. No 50-013-PB,) digestion for 90 minutes at 37^{o}C. Cells were plated at a density of 100,000 cells/well in 6-well tissue culture plates and grown to confluence in 10% FBS/DMEM/antibiotics. Periosteal osteoblasts at passage 2-3 were used to study cell proliferation, differentiation and apoptosis. Alkaline phosphatase (ALP) staining was used to confirm the presence of osteoblasts. Cells isolated in identical manner from age and sex matched wild type B6 mice were used as control.

In-vitro Proliferation, Differentiation, and Apoptosis of Periosteal Osteoblasts from Mutant Mice

Basal cell proliferation was studied by two assays: 1) CyQuant-GR cell proliferation assay kit (Molecular Probes Inc., OR); and 2) [^{3}H]-thymidine incorporation into cell DNA. Briefly, osteoblast cells were incubated for 24 h in serum free media and [^{3}H]-thymidine (1.5 μCi/ml) was added during the final 6 h of the incubation. Cell differentiation was measured by observing changes in the specific activity of alkaline phosphatase using PNPP as substrate (16). Caspase activities were measured by Homogeneous Caspase Assay kit (Roche Diagnostics, IN) to determine the rate of apoptosis. Briefly, the assay was based on the ability of activated caspases to cleave a

fluorogenic peptide containing caspases specific cleavage site, consequently releasing the fluorogenic molecule Rhodamine. The flurogenic tetrapeptide used in this assay is substrate for caspases 2, 3, 6, 7, 8, 9 and 10. Apoptosis was also analyzed by flow cytometry using Annexin-V conjugated to FITC-labeled dUTP to label apoptotic cells and a FACScan flow cytometer (Becton Dickinson, San Jose, CA, U.S.A.) to identify fluorescent labeled cells. The percentage of cells that underwent apoptosis was determined after electronic subtraction of signal due to background fluorescence, which was determined using cells incubated with FITC-labeled dUTP, but without terminal deoxynucleotidyl transferase. A minimum of 5000 cells were analyzed.

Fluid flow shear stress as in-vitro model of mechanical loading

Periosteal osteoblasts isolated from wild type B6 mice and ENU mutant male and female mice were plated on glass slides (75 x 38 mm) at 5 x 10^4 cells/slide in DMEM containing 10% bovine calf serum. After the cultures became ~80% confluent, the cells were serum-deprived for 24 hours and subjected to shear stress as previously described.[16] Briefly, slides containing osteoblast cells were placed in a chamber inside the Cytodyne flow loop apparatus (San Diego, CA), which is under constant hydrostatic pressure, exposing the cells to the steady laminar fluid flow and a well-defined fluid shear stress of 20 dynes/cm^2 for 30 minutes. The system was always maintained at 37°C and the medium was continuously bubbled with 5% CO_2-95% air. The static controls were performed on cells grown in identical conditions but were not exposed to the shear stress.

Genetic analysis

Genomic DNA was isolated from tail clips using mouse DNAeasy kits (Qiagen). DNA samples were quantified and the quality was determined by measuring their absorbance at 260 nm and 280 nm. A genome-wide genotyping scan using 60 microsatellite markers (Invitrogen, CA) was undertaken using the ABI Linkage Mapping Set 2. PCR reactions and running conditions allowed from 5-6 microsatellite markers to be multiplexed in a single electrophoretic lane. The pooled products were analyzed for fragment size on ABI Model 3100 DNA Analyzer and Genescan software was used to size alleles (Applied Biosystems). Allele calls and edits were done using Genotyper software (Applied Biosystems) and exported as tab-delimited tables. Preliminary analysis involved using 4 markers on chromosomes 1, 2, 4, and three markers for each of the rest of the autosomes. Subsequent analysis involved 10-12 additional markers for chromosomes 1 and 4.

Statistical analyses

The total body bone areas obtained from DEXA were normalized for body weight as described earlier [10]. The Z-scores were calculated using formula: Z-score=(Bone Area of Progeny – Mean Bone Area of Control Male mice)/SD of Bone Area of Control Male mice (n=40-80). Results from cell culture experiments are shown as mean ±SEM. The statistical significance of the differences between groups was determined by 2-way ANOVA, using gender and phenotype as variables, interaction between sex and phenotype variable were calculated to indicate that males are more affected than females. A p-values of <0.05 was considered for significant interactions.

Genotype data were initially analyzed using a MAPQTL (5.0) program (Kyazma B.V., Wageningen, Netherlands). MAPQTL interval mapping was used for QTL mapping and the LOD score significance thresholds were calculated using 1000 permutation test.[17] Since body weight is strong predictor of bone size traits, we used multivariate analysis with body weight as the covariant to perform interval mapping using the Pseudomarker (obtained from www.jax.org/research/churchill) MAINSCAN program written for the MATLAB (Mathworks Inc., Natick, MA, USA) programming environment. This allows us to delineate the bone size trait from growth related QTLs. To study genome-wide interactions between QTLs, we used the Pseudomarker PAIRSCAN algorithm.[17] This program analyzes not only the phenotypic effect of each marker or marker interval taken singly (MAINSCAN) but also the phenotypic effects of pairs of markers or intervals taken jointly (PAIRSCAN) for their effects on the trait. The PAIRSCAN allows a genome-wide search for epistasis. For PAIRSCAN, we tested the combined (or full model) effects on the trait of a marker pair, which reflects the main effects of both markers plus their interaction. The threshold for genome-wide error was set at 5%, which was estimated by a 500 permutation test carried out on the F2 data. When the combined effect of the marker pair was significant, then their interaction was tested at a significance level of $p<0.05$ as described earlier.[17]

Results

Bone Size Phenotype in 917M Mice

We generated about 120 male and 120 female progeny from the original affected 917M male identified in the dominant screening. The bone size phenotypes, which included

total body bone area and bone area at the tibia midshaft, were determined at 10-and 16-weeks of age in all inherited progeny. Data described below for distinguishing mutant progeny was taken from 16-week old mice because we observed a lower variation and a higher difference between 917M and WT mice at this age. We used total body bone area (cm^2) phenotype and -2.0SD units as the cut-off to classify a mutant from the unaffected littermates. Among males, approximately 42% mice were classified as affected 917M (with reduced bone size) and 58% were similar to WT, whereas females were largely unaffected (approximately5%showed the low total body bone area phenotype as shown in Figure-1). Both male and female progeny from 917M showed normal distribution for the low bone area trait indicating that about 2.5% of the female could fall below 2SD cut-off range. Based on these data the phenotype was mainly expressed in males and the observed ratio of mutants (approximately 0.8:1) in males was close to the 1:1 inheritance ratio expected for dominant Mendelian traits. The bone size trait was not sex-linked (X-linked) based on the inheritance of affected males from wild type females. The total bone area expressed as Z-score is shown in Figure-1. The mean Z-scores for bone area and body weight adjusted bone area for affected 917M mice were -3.3±0.8 and -3.1±1.0, respectively. The distribution of phenotype in affected, non-affected, and wild type male mice is shown in Figure-2. The total bone area in affected 917M male progeny was 10-13% ($p<0.001$) lower as compared to unaffected 917M littermates or WT B6 males. The body weight adjusted area was about 9-10% ($p<0.001$) lower in the affected917M mice as compared to unaffected littermates or WT B6 males. The average total bone area of affected 917M male mice (8.80±0.35 cm^2) was significantly ($p<0.01$) lower than the female littermates (9.25±0.58 cm^2), which was similar to WT B6 females (9.36±0.45

cm^2, p=NS vs female littermates). The mean total body BMD (DEXA) in the 917M mice (0.0483±0.0032 mg/cm^2) was similar to WT B6 males (0.0488±0.0026 mg/cm^2). The periosteal circumference and other bone size parameters measured *in-vivo* at the midshaft tibia (mean of three slices at 1.0 mm apart) are shown in Table-1. Figure-3 shows bone size data on excised femur and tibia from 917M (n=3) and WT control (n=5) mice measured by pQCT at 9 slices covering entire length of the bone. The femur or tibia length was not different in 917M mice as compared to WT B6 control mice. The averaged total area was 10-15% lower, periosteal circumference was 4-8% lower (Figure-3), and endosteal circumference was 6-11% lower in both femur and tibia as compared to WT mice.

In-vitro Cell Proliferation & Differentiation Potential of Periosteal Osteoblasts from 917M Mice

The basal proliferation potential of 917M osteoblasts analyzed by CyQuant assay showed a 17% decrease ($p<0.05$) (2608 ± 370 fluorescence units vs 3138 ± 371 for controls) in proliferation in 917M mice as compared to the wild type. Similarly, [^{3}H]-thymidine incorporation assay showed a 27% decrease proliferation rate in 917M males, as shown in Figure-4. The 2-way ANOVA revealed that osteoblasts from affected 917M mice had significantly reduced proliferation (p-value <0.001 for interaction), whereas, proliferation rate was not altered in cells from female littermates (Figure-4) of 917M mice. No significant differences in the specific activity of alkaline phosphatase were observed between cells from WT (6.6 ± 0.9 mU/mg protein) and 917M mice (6.8 ± 0.8 mU/mg protein) indicating 917M and wild-type osteoblasts had the same differentiation potential.

Increased Apoptosis of Periosteal Osteoblasts from 917M Mice

Caspases activity in periosteal osteoblasts from 917M affected male mice showed a 23% increase, whereas, cells from female 917M littermates did not show significant differences in the Caspase activity as compared to those from WT (Figure-4), as shown by 2-way ANOVA with a sex-phenotype interaction p-value of 0.0431. This indicates a Caspase dependent increase in apoptosis of osteoblast cells from 917M. FACS of periosteal osteoblasts from 917M mice indicated a higher (18.7%) number of apoptotic cells from 917M male mice as compared to those from WT (13.3%) (details not shown). There were no significant differences in total apoptosis in cells isolated from female littermates of 917M mice in FACS analysis.

Reduced Mechanosensitivity of periosteal osteoblast from 917M mice

The application of a 30-min steady flow shear stress at 20 dynes/cm^2 on WT osteoblasts consistently caused a 60-80% (p<0.01) increase in the [^{3}H]-thymidine incorporation compared to the control cells not subjected to shear stress (Figure-6). In contrast, the shear stress-stimulated increase in proliferation was only 5% (of control) in cells from the 917M mice. The 2-way ANOVA reveals that in control mice, sex has no significant differences in response to stress (p-value 0.3345), whereas in 917M littermates, the affected 917M mice has significantly reduced response to shear stress (p-value <0.0001 for interaction).

Linkage analyses for bone size traits in 917M B6C3H F2 mice

A total of 129 B6C3H F2 mice were generated from three 917M male mice. Male and female mice were mapped separately. The bone area of male F1 and F2 mice is shown in Figure-7. The mean bone area in 917M B6C3H F1 male mice (Figure-7) was 8-12% lower ($p<0.01$ by ANOVA) as compared to WT B6C3H F1 male mice, which shows that the low bone area phenotype was expressed in C3H background. Similarly, the bone area in 917M B6C3H F2 male mice (Figure-7) was significantly lower as compared to WT B6C3H F2 male mice. The body weight adjusted bone area of F2 males (n=69) generated from both 917M and wild type B6 mice was normally distributed. The results from whole-genome linkage analysis using total bone area showed evidence for linkage at loci on Chr 1 (LOD score 4.9 at 45 cM) and Chr 4 (LOD score 7.9 at 10.5 cM) as shown in Figure-8. The LOD scores for Chr 1 and Chr 4 QTLs were 3.4 ($p>0.05$) and 6.8 ($p<0.01$), respectively, when body weight was used as a covariant (data analyzed using Pseudomarker program). The LOD scores for Chr 4 QTL for femur bone area, periosteal circumference, and endosteal circumference when body weight was used as covariant were, 6.2 ($p<0.01$), 9.1 ($p<0.01$), 5.6 ($p<0.01$), respectively. Genome wide linkage analysis of B6C3H F2 females (n=60) generated from 917M B6 male did not show any significant QTL (data not shown).

Interval mapping using eight additional marker (total of 11 markers) for Chr 4 and bone size traits revealed peak interval on proximal Chrs 4 at 10.5 cM with a LOD scores 4.0-8.2 (genome-wide error rate of $p < 0.05$) as shown in Figure-9. However, the peak interval for periosteal circumference was shifted to 50 cM with LOD score of 6.6

(genome-wide error rate of $p < 0.01$). Bone size QTLs on Chr 4 explained 38-42% of the phenotypic variance in bone area of F2 male mice. Alleles in the Chr 4 interval that are inherited from the B6 parental strain contribute to a significantly lower bone area than do alleles inherited from C3H (Figure-10). Alleles of Chr 1 interval that contribute to low bone area are for genotype C3H /C3H.

Linkage analyses for bone size in wild type B6C3H F2 mice

A whole-genome linkage search for loci affecting the body size traits (total body bone area and total bone area and periosteal circumference at midshaft tibia) in WT B6C3H F2 male (n=92) and female (n=85) did not reveal any suggestive or significant QTLs. A suggestive QTL for total bone area was observed on Chr 14 (LOD score 4.7 at 5 cM) when body weight was used as a covariate (data not shown).

QTL-QTL Interactions for total body bone area trait

Two loci show interactions when the genotype at one locus influences the effect of the other locus. Table-2 shows genome-wide significant interactions observed in B6C3H F2 mice for total body bone area. The interaction involving Chr 1 and Chr 4 was noteworthy because Chr 1 locus was the only other locus that was associated with any significant QTL observed for bone size. The combined variance explained by the two interactive QTL on Chr 1 and Chr 4 was 60% of the F2 population (calculated separately by Pseudomarker Fit QTL algorithm). Other significant interactions were noticed between 10cM and 80 cM region of the Chr 4. Both Chr 1 and Chr 4 harbor loci known to regulate bone density and bone biomechanical properties phenotypes. A significant

interaction between these loci would suggest a complex interaction between genes that regulate skeletal phenotypes or suggest the presence of modifying loci influencing bone area trait.

Discussion

Bone size is an independent determinant of the bone strength.[18,19] Therefore, the identification of genes regulating bone size should reveal important determinants for fracture risk. Previous studies have utilized bone size differences in the inbred strain of mice to identify QTLs that regulate bone size, geometry, and biomechanical properties.[20-26] We use a complementary phenotype-driven mutagenesis approach to reveal a locus that regulates bone size. The major advantage of this approach is that any locus identified in this study presumably represents one gene in contrast to QTLs identified by linkage studies, which is likely to represent multiple genes at each locus. Thus, positional cloning of the gene identified by the ENU mutagenesis approach is potentially easier.

The data presented in this study demonstrates that the point mutation generated by ENU results in decreased bone size at multiple anatomical sites including decreased perimeter at the midshaft tibia and femur (without affecting the length) in the mutants as compared to the wild type mice. The phenotype was expressed in males with a dominant mode of inheritance. The potential mechanism whereby bone size could be genetically regulated includes factors affecting periosteal apposition or resorption.[11,12] Our data on the *in-vitro*

cell culture of osteoblasts suggest that a decrease in bone size could be attributed to an overall decrease in mature osteoblast cell numbers due to: 1) a decreased cell proliferation rate; 2) increased apoptosis; or 3) a combination of both these factors. It could be inferred that the ENU mutation shifts the balance between undifferentiated and differentiated cells by decreasing the proliferation of immature cells and promoting apoptosis of more mature osteoblasts without affecting the differentiation potential and activity. Further studies will be required to explore the molecular basis of these differences in osteoblasts derived from mutant versus WT mice.

The finding that mutation affects only males is consistent with the outcomes of linkage studies [20, 21] that have implicated a variety of gender-specific chromosomal regions (and presumably genes) that regulate bone size in mice and humans.[26] There are different mechanisms in males and females for periosteal bone expansion leading to sex differences in bone size and geometry, which in part may explain the lower risk in males against age-related fracture incidences in humans.[27,28] In B6 mice, the bone size differences between males and females appear after puberty.[29] Our data (details not shown) on WT B6 male (n=40-60) and female mice (n=40-60) shows that total body bone area is 12.9%, 11.5% and 8.5% higher ($p<0.0001$) in males as compared to females at 6-, 10-, and 16-weeks, respectively. In 917M male mice, the total bone area is 0.3% and 4.9% lower at 10-weeks and 16-weeks, respectively, as compared to female littermates, indicating that mutation is affecting a sex-related disparity in bone size. Two main factors, sex steroids and mechanical loading, have been proposed as important regulators of periosteal apposition (and presumably bone size) differences between males

and females. Animal studies offer evidence for a positive effect of androgens and a negative effect of estrogens on periosteal bone formation rates. Thus, if the sex difference in bone size is due to androgen/estrogen action as some animal studies suggest,[30] this lends us to speculate that the mutation identified in this study may mediate the effects of androgen/estrogen on bone size. Another finding that points toward the probable involvement of sex hormones is our data on a loss of stimulatory effect of mechanical stress on osteoblast proliferation in mutant mice. Mechanical force induces the expression of a variety of genes in the periosteum [31] with a rapid transformation of quiescent periosteal surfaces to those on which bone formation occurs. In addition, it has been recently shown that the estrogen receptor (ER) is essential [32] for mediating the stimulatory effects of mechanical stress, thus an impaired response to mechanical stimuli would indicate the involvement of the ER pathway. Further studies are needed to confirm whether or not the mutant gene is responsive to sex hormones and mechanical loading.

To localize ENU mutation, we used low-resolution linkage mapping covering the whole genome with markers spaced at intervals of ~21 cM. Use of multivariate analysis with body weight as a covariate for bone size traits provides a more accurate assessment of bone size QTL(s), which otherwise could be confounded by growth related QTLs. Interestingly, we identified only one strong candidate interval on proximal Chr 4 that modulates bone size. No other chromosomal interval has a LOD score remotely as high as proximal Chr 4. All bone size traits mapped to Chr 4 to confirm specificity of this QTL, although peak interval for one bone size trait, periosteal circumference at the tibia

midshaft (data on periosteal circumference is shown in Figure-9), appear to be located at slightly distal region. It remains to be verified if the two peaks represent two distinct QTL. As one would expect in point mutations, the locus identified on Chr 4 accounts for as much as a 40% of the phenotypic variance of all bone size traits, which is in contrast to approximately 5-15% variance explained in QTL studies employing these two strains of mice.

Although our data on linkage analysis emphasizes a single interval where mutation could be located (on Chr 4), there are differences in bone size between C3H and B6 mapping strains reflecting allelic variation at a variety of QTLs governing bone size and geometry. Thus, it is possible that the presence of these naturally segregating allelic variations will result in the appearance of QTL (background) confounding the search for a unique QTL that could be attributed to ENU mutation. Our finding of a single QTL is likely due to two factors: 1) magnitude of the phenotype caused by mutation (as evident in Figure-7); and 2) robustness of the phenotype expressed in the background of C3H (mapping) strain of mice. As our data demonstrates, the effect of the mutant phenotypes is larger than most of the published bone size QTLs.[20-25] Our strategy to employ a low-resolution map with a small sample size was designed to reduce the power to detect background QTL, as shown in case of a WT control population (Figure-9). Under these conditions, a QTL would arise only if a mutation occurred that significantly altered the phenotype distribution in the F2 population, which is the case in F2s generated from ENU mutant mice.

Several lines of evidence support our view that the locus on Chr 4 harbors a mutation. First, the alleles on the Chr 4 interval inherited from the B6 mutant strain contribute to a significantly lower bone area (including periosteal circumference) than alleles inherited from C3H, which is not the case with the QTL observed on Chr 1. Second, we did not observe any significant or suggestive QTL on Chr 4 in interval mapping of the F2 population generated from the wild type B6 mice. Additionally, previous linkage studies using male mice [20,21] have not identified any locus on Chr 4 that regulates bone size. Although a linkage study [22] using the C3H and B6 strains of mice has shown a strong QTL (LOD score 16-21) on Chr 4 for biomechanical properties of femur, this locus, however, was identified in female mice and was located between 70-90 cM region. Based on these observations, the QTL identified in this study represents a distinct linkage finding. One approach commonly used to identify mutant genes in an ENU induced mutant mice is based on sequencing of a positional candidate gene. The potential candidate genes include those genes that regulate osteoblast activity, apoptosis, responsive elements to sex hormones and those involved in mechanosensors such as, gated ion channel. In this regard, potential candidate genes found on chromosome 4 region are calb1 (calbindin), igfbpl1 (insulin-like growth factor binding protein-like 1), Casp8ap2 (caspase 8 associated protein 2), Gabrr1 & Gabrr2 (gamma-aminobutyric acid receptor, subunit), Cga (glycoprotein hormones, alpha subunit), Rragd (ras-related GTP binding D), Il11ra1 (interleukin 11 receptor, alpha chain 1) and Musk (muscle, skeletal, receptor tyrosine kinase). However, the QTL region identified in this study that regulates bone size represent a fairly large region, which encompasses many more important genes other than mentioned above that can contribute to the bone size phenotype. Therefore, in

future studies, we propose to utilize differential display of genes in 917M vs. WT mice using microarray to identify key genes from chromosome 4 QTL region that can be selected for sequencing to locate the point mutation(s).

We have also discovered several suggestive and significant interactions between QTL on Chr 4 with other loci on Chr 1 and 2. The locus on Chr 1 is in the proximity of QTLs identified in earlier linkage studies, [33-35] indicating a wide-range of plietropic effects across diverse phenotypes of bone density, size, and biomechanical properties. The interaction with the Chr 1 loci was particularly significant because it may indicate that the main effect of the Chr 1 locus (which had a suggestive LOD score of 4.9) was primarily due to interaction effects with loci on Chr 4. This was evident in a very high (60%) variance (of F2 population) explained by the interaction effects of these two loci together. Our finding on these interactions highlights the degree to which the phenotypes of bone density and bone size are under the control of common genetic factors.

In conclusion, we have provided evidence that the decrease in bone size observed in ENU mutant male mice could be due to a mutation in gene regulating osteoblast function in terms of proliferation, apoptosis, and response to mechanical stimulus. In addition, linkage analysis indicates that the point mutation is located on a novel allele of Chr 4 because no mouse or human linkage study has described QTL in a corresponding position. Finally, this report demonstrates for the first time the effectiveness of employing phenotype-driven ENU mutagenesis in the investigation of genetics of osteoporosis. It also illustrates the utility of the ENU mutagenesis approach for

generating models for use in genetic studies of osteoporosis where conventional knockout could be lethal.

Acknowledgments

This work was supported by the Army Assistance Award No. DAMD17-99-1-9571. The US Army Medical Research Acquisition Activity (Fort Detrick, MD) 21702-5014 is the awarding and administering acquisition office for the DAMD award. The information contained in this publication does not necessarily reflect the position or the policy of the Government, and no official endorsement should be inferred. All work was performed in facilities provided by the Department of Veterans Affairs. The authors' would like to thank Darcie Nagel, TaMarrah Oliver, Valerie Chest, and Cynthia Ganda for their expert technical assistance.

References

1. Nolan PM, Peters J, Strivens M, Rogers D, Hagan J, Spurr N, Gray IC, Vizor L, Brooker D, Whitehill E, Washbourne R, Hough T, Greenaway S, Hewitt M, Liu X, McCormack S, Pickford K, Selley R, Wells C, Tymowska-Lalanne Z, Roby P, Glenister P, Thornton C, Thaung C, Stevenson JA, Arkell R, Mburu P, Hardisty R, Kiernan A, Erven A, Steel KP, Voegeling S, Guenet JL, Nickols C, Sadri R, Nasse M, Isaacs A, Davies K, Browne M, Fisher EM, Martin J, Rastan S, Brown SD, Hunter J 2000 A systematic, genome-wide, phenotype-driven mutagenesis programme for gene function studies in the mouse. Nat Genet **25**(4)**:**440-3.
2. Herron BJ, Lu W, Rao C, Liu S, Peters H, Bronson RT, Justice MJ, McDonald JD, Beier DR 2002 Efficient generation and mapping of recessive developmental mutations using ENU mutagenesis. Nat Genet **30**(2)**:**185-9.
3. Nolan PM, Peters J, Vizor L, Strivens M, Washbourne R, Hough T, Wells C, Glenister P, Thornton C, Martin J, Fisher E, Rogers D, Hagan J, Reavill C, Gray I, Wood J, Spurr N, Browne M, Rastan S, Hunter J, Brown SD 2000 Implementation of a large-scale ENU mutagenesis program: towards increasing the mouse mutant resource. Mammalian Genome **11**(7)**:**500-6.
4. Rathkolb B, Decker T, Fuchs E, Soewarto D, Fella C, Heffner S, Pargent W, Wanke R, Balling R, Hrabe de Angelis M, Kolb HJ, Wolf E 2000 The clinical-chemical screen in the Munich ENU Mouse Mutagenesis Project: screening for clinically relevant phenotypes. Mammalian Genome 11(7):543-6.

5. Thaung C, West K, Clark BJ, McKie L, Morgan JE, Arnold K, Nolan PM, Peters J, Hunter AJ, Brown SD, Jackson IJ, Cross SH 2002 Novel ENU-induced eye mutations in the mouse: models for human eye disease. Human Molecular Genetics 11(7):755-67.
6. Toye AA, Moir L, Hugill A, Bentley L, Quarterman J, Mijat V, Hough T, Goldsworthy M, Haynes A, Hunter AJ, Browne M, Spurr N, Cox RD 2004 A new mouse model of type 2 diabetes, produced by N-ethyl-nitrosourea mutagenesis, is the result of a missense mutation in the glucokinase gene. Diabetes 53(6):1577-83.
7. Meyer CW, Korthaus D, Jagla W, Cornali E, Grosse J, Fuchs H, Klingenspor M, Roemheld S, Tschop M, Heldmaier G, De Angelis MH, Nehls M 2004 A novel missense mutation in the mouse growth hormone gene causes semidominant dwarfism, hyperghrelinemia, and obesity. Endocrinology 145(5):2531-41.
8. Inoue M, Sakuraba Y, Motegi H, Kubota N, Toki H, Matsui J, Toyoda Y, Miwa I, Terauchi Y, Kadowaki T, Shigeyama Y, Kasuga M, Adachi T, Fujimoto N, Matsumoto R, Tsuchihashi K, Kagami T, Inoue A, Kaneda H, Ishijima J, Masuya H, Suzuki T, Wakana S, Gondo Y, Minowa O, Shiroishi T, Noda T 2004 A series of maturity onset diabetes of the young, type 2 (MODY2) mouse models generated by a large-scale ENU mutagenesis program. Hum Mol Genet 13(11):1147-57.
9. Srivastava AK, Mohan S, Wergedal JE, Baylink DJ 2003 A genome-wide screening of N-ethyl-N-nitrosourea mutagenized mice for musculoskeletal phenotypes. Bone 33(2):179-91.

10. Srivastava AK, Mohan S, Wergedal JE, & Baylink DJ 2003 An ENU Mutant Mouse Characterized by the Combination of a Decrease in Bone Size and Increase in Fat Mass with Evidence of Gender Difference. 25th Annual Meeting of American Society for Bone and Mineral Research, Program and Abstracts, J Bone Miner Res 18(1), pS176.
11. Orwoll E, Orwoll S, Kohama S, Evans G, Turner R 2002 Periosteal bone formation and resorption are both active at the femoral neck: Mechanisms for change in bone size. J Bone Miner Res 17:S1;S300.
12. Seeman E 2003 Periosteal bone formation--a neglected determinant of bone strength. N Engl J Med 349(4):320-3.
13. Lanyon L, Armstrong V, Ong D, Zaman G, Price J 2004 Is estrogen receptor alpha key to controlling bones' resistance to fracture? J Endocrinol 182(2):183-91.
14. Tobias JH 2003 At the crossroads of skeletal responses to estrogen and exercise. Trends Endocrinol Metab 14(10):441-3.
15. Schmidt C, Priemel M, Kohler T, Weusten A, Muller R, Amling M, Eckstein F 2003 Precision and accuracy of peripheral quantitative computed tomography (pQCT) in the mouse skeleton compared with histology and microcomputed tomography (microCT). J Bone Miner Res 18(8):1486-96.
16. Kapur S, Baylink DJ, Lau KH 2003 Fluid flow shear stress stimulates human osteoblast proliferation and differentiation through multiple interacting and competing signal transduction pathways. Bone 32(3):241-51.

17. Sugiyama F, Churchill GA, Higgins DC, Johns C, Makaritsis KP, Gavras H, Paigen B 2001 Concordance of murine quantitative trait loci for salt-induced hypertension with rat and human loci. Genomics 71:70-77.
18. Seeman E 2001 Sexual dimorphism in skeletal size, density, and strength. J Clin Endocrinol Metab 86:4576-4584.
19. Seeman E, Duan Y, Fong C, Edmonds J 2001 Fracture site-specific deficits in bone size and volumetric density in men with spine or hip fractures. J Bone Miner Res 16(1):120-7.
20. Klein R, Turner R, Skinner L, Vartanian K, Serang M, Carlos A, Shea M, Belknap J, Orwoll E 2002 Mapping quantitative trait loci that influence femoral cross sectional area in mice. J Bone Miner Res 17:1752-1760.
21. Christians JK, Bingham VK, Oliver FK, Heath TT, Keightley PD 2003 Characterization of a QTL affecting skeletal size in mice. Mamm Genome 14(3):175-83.
22. Koller DL, Schriefer J, Sun Q, Shultz KL, Donahue LR, Rosen CJ, Foroud T, Beamer WG, Turner CH 2003 Genetic effects for femoral biomechanics, structure, and density in C57BL/6J and C3H/HeJ inbred mouse strains. J Bone Miner Res 18(10):1758-65.
23. Turner CH, Sun Q, Schriefer J, Pitner N, Price R, Bouxsein ML, Rosen CJ, Donahue LR, Shultz KL, Beamer WG 2003 Congenic mice reveal sex-specific genetic regulation of femoral structure and strength. Calcif Tissue Int 73(3):297-303.

24. Dohmoto A, Shimizu K, Asada Y, Maeda T 2002 Quantitative trait loci on chromosomes 10 and 11 influencing mandible size of SMXA RI mouse strains. J Dent Res 81(7):501-4.

25. Koller DL, Liu G, Econs MJ, Hui SL, Morin PA, Joslyn G, Rodriguez LA, Conneally PM, Christian JC, Johnston CC Jr, Foroud T, Peacock M 2001 Genome screen for quantitative trait loci underlying normal variation in femoral structure. J Bone Miner Res 16:985-991.

26. Deng HW, Shen H, Xu FH, Deng H, Conway T, Liu YJ, Liu YZ, Li JL, Huang QY, Davies KM, Recker RR 2003 Several genomic regions potentially containing QTLs for bone size variation were identified in a whole-genome linkage scan. Am J Med Genet 119A(2):121-31.

27. Duan Y, Turner CH, Kim BT, Seeman E 2001 Sexual dimorphism in vertebral fragility is more the result of gender differences in age-related bone gain than bone loss. J Bone Miner Res 16(12):2267-75.

28. Orwoll ES, Belknap JK, Klein RF 2001 Gender specificity in the genetic determinants of peak bone mass. J Bone Miner Res 16(11):1962-71.

29. Richman C, Stepan K, Miyakoshi N, Srivastava AK, Beamer WG, Donahue LR, Rosen CJ, Wergedal JE, Baylink DJ & Mohan S. 2000 Postnatal and pubertal skeletal changes contribute predominantly to the differences in peak bone density between C3H/HeJ and C57BL/6J mice. J Bone & Miner Res, 16(2):386-397.

30. Orwoll ES 2001 Androgens: Basic biology and clinical implication. Calcif Tissue Int 69:185-188.

31. Matsumoto T, Nakayama K, Kodama Y, Fuse H, Nakamura T, Fukumoto S 1998 Effect of mechanical unloading and reloading on periosteal bone formation and gene expression in tail-suspended rapidly growing rats. Bone 22(5 Suppl):89S-93S.

32. Jessop HL, Suswillo RF, Rawlinson SC, Zaman G, Lee K, Das-Gupta V, Pitsillides AA, Lanyon LE 2004 Osteoblast-like cells from estrogen receptor alpha knockout mice have deficient respones to mechanical strain. J Bone Miner Res 19(6):938-46.

33. Beamer WG, Shultz KL, Donahue LR, Churchill GA, Sen S, Wergedal JR, Baylink DJ, Rosen CJ 2001 Quantitative trait loci for femoral and lumbar vertebral bone mineral density in C57BL/6J and C3H/HeJ inbred strains of mice. J Bone Miner Res 16(7):1195-206.

34. Beamer WG, Shultz KL, Churchill GA, Frankel WN, Baylink DJ, Rosen CJ, Donahue LR 1999 Quantitative trait loci for bone density in C57BL/6J and CAST/EiJ inbred mice. Mamm Genome 10(11):1043-9.

35. Masinde GL, Wergedal J, Davidson H, Mohan S, Li R, Li X, Baylink DJ 2003 Quantitative trait loci for periosteal circumference (PC): identification of single loci and epistatic effects in F2 MRL/SJL mice. Bone 32(5):554-60.

Table-1. Differences in bone size parameters at tibia midshaft in affected 917M progeny as compared to non-affected littermates.

Phenotype	10-Week*	p-value	16-Week*	p-Value
Total Bone Area	-8.8%	<0.001	-9.3%	<0.001
Total BMC	-9.7%	<0.001	-10.4%	<0.001
Cortical Area	-7.3%	<0.001	-8.9%	<0.001
Periosteal Circumference	-4.4%	<0.01	-4.7%	<0.001
Endosteal Circumference	-6.6%	<0.001	-5.5%	<0.001

*Values represents difference in size phenotypes at midshaft tibia in mutant mice (n=52) as compared to littermates (n=72) or WT B6 male mice

Table-2. List of suggestive and significant marker pair showing interaction from genome-wide analysis of bone area in 917M B6C3H F2 males.

Chr. Pairs Q1 × Q2	cM Q1	cM Q2	LOD full	LOD int	p-value (Interaction)	LOD Q1	p-value	LOD Q2	p-value
1 × 1	5	40	9.31	5.02	0.0001	3.49	0.0003	0.00	0.9975
1 × 2	45	95	8.78	3.06	0.0070	1.32	0.0481	5.38	0.0000
1 × 4	90	10	12.32	3.18	0.0054	7.62	0.0000	1.16	0.0686
4 × 4	10	80	12.22	3.69	0.0019	0.56	0.2748	7.86	0.0000

Threshold for significant full effects (LODfull) was LOD 8.9 (when combined effects of marker pair were significant at $p<0.05$) and threshold for suggestive interaction was LOD 8.7 ($p<0.1$). Threshold for significant interaction (LODint) was LOD 5.6 and threshold for suggestive interaction was LOD 5.1 ($p<0.1$). Q1 and Q2 indicate locus 1 and 2. LODQ1 and LODQ2 indicate LOD score for main effect of locus 1 and locus 2. The cM1 and cM2 indicate centi-Morgan position of locus 1 and locus 2.

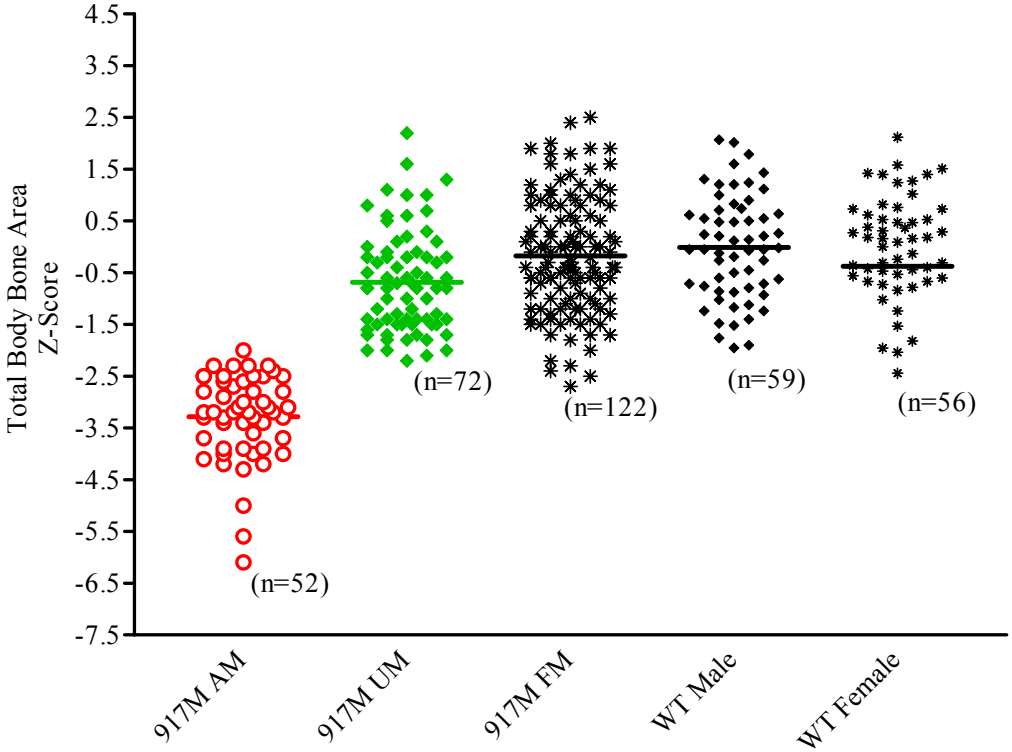
Total Body Bone Area
Z-Score
4.5
3.5
2.5
1.5
0.5
-0.5
-1.5
-2.5
-3.5
-4.5
-5.5
-6.5
-7.5
(n=52)
(n=72)
(n=122)
(n=59)
(n=56)
917M AM
917M UM
917M FM
WT Male
WT Female

Figure-1

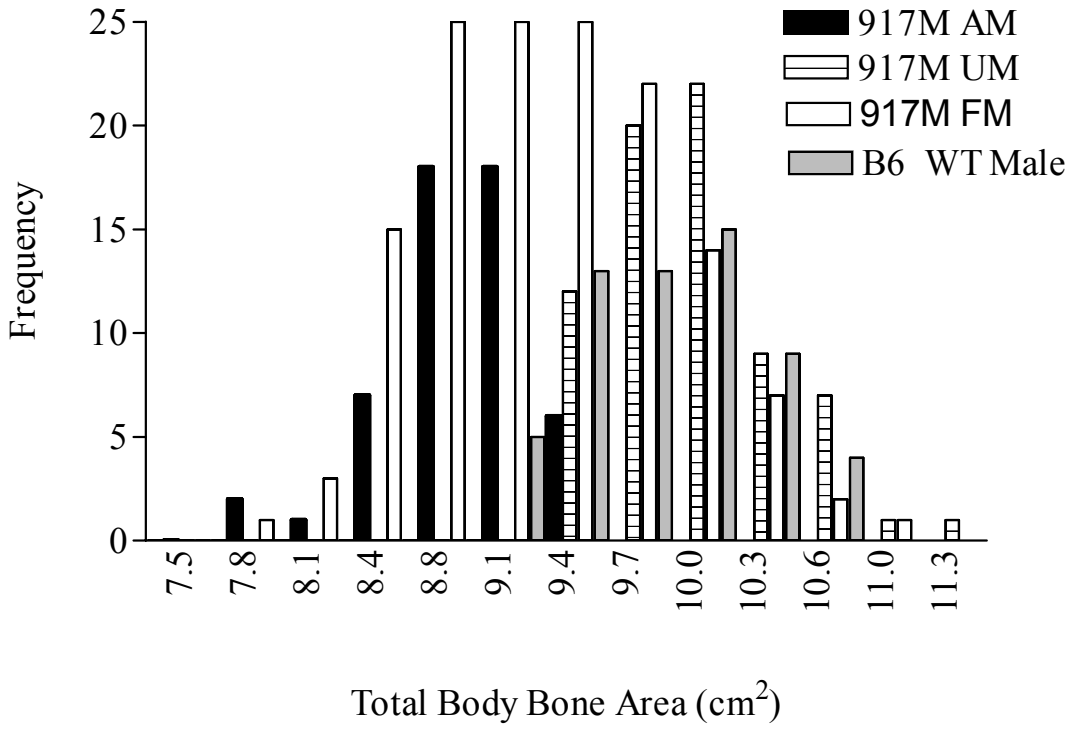
917M AM
917M UM
917M FM
B6 WT Male
Frequency
25
20
15
10
5
0
7.5
7.8
8.1
8.4
8.8
9.1
9.4
9.7
10.0
10.3
10.6
11.0
11.3
Total Body Bone Area (cm2)

Figure-2

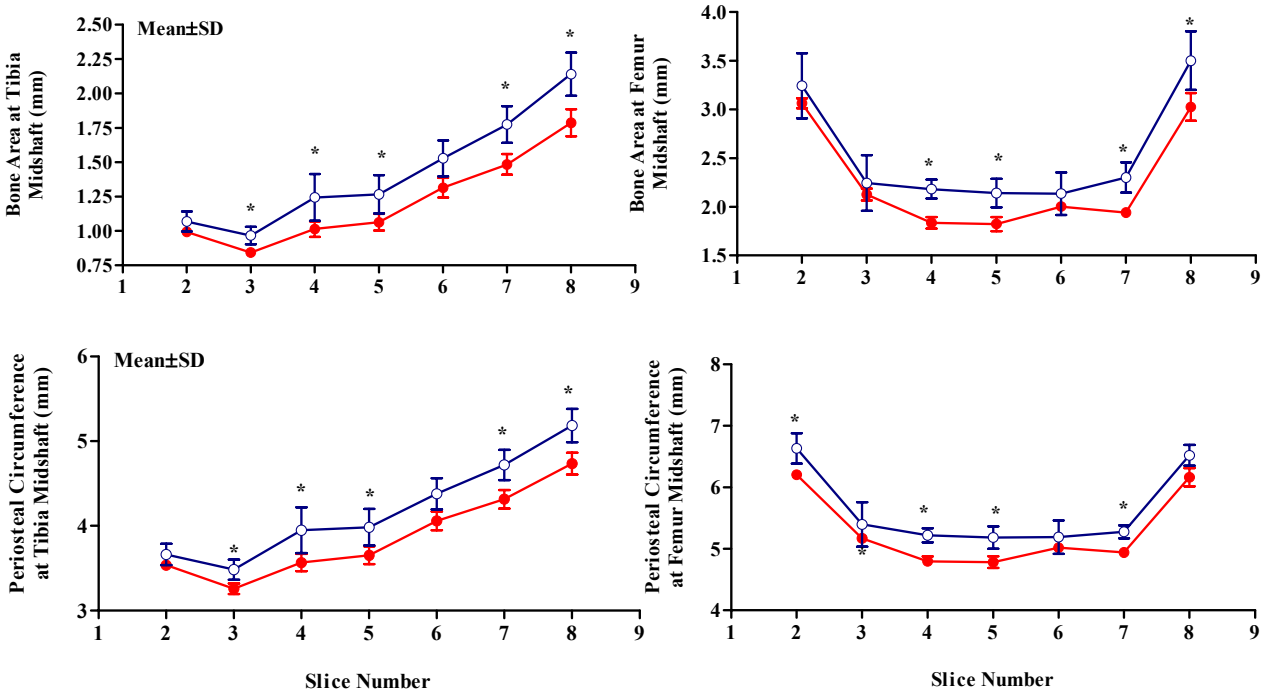
Mean±SD
Bone Area at Tibia Midshaft (mm)
Bone Area at Femur Midshaft (mm)
Periosteal Circumference at Tibia Midshaft (mm)
Periosteal Circumference at Femur Midshaft (mm)
Slice Number
Slice Number

Figure-3

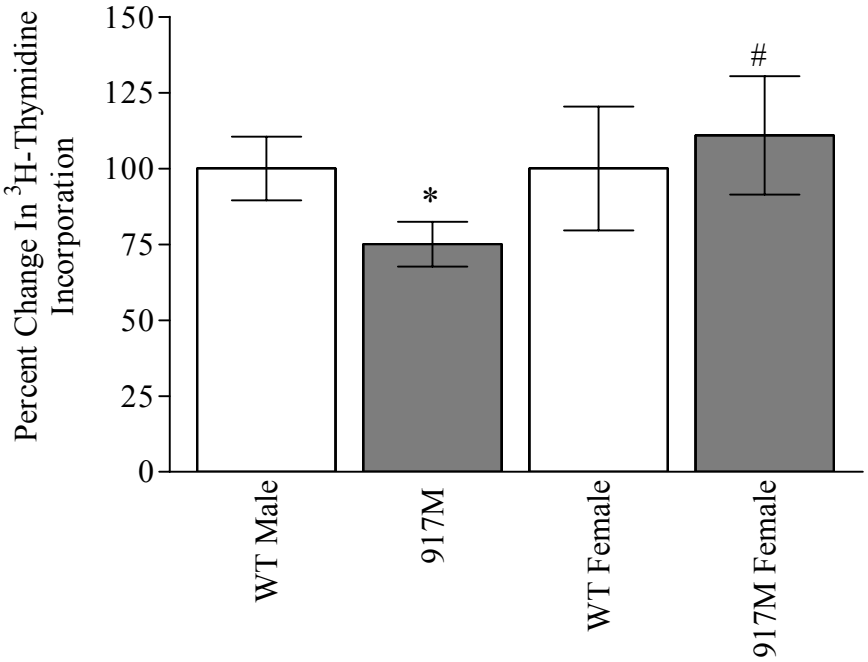
Percent Change In ^{3}H-Thymidine Incorporation
150
125
100
75
50
25
0
*
#
WT Male
917M
WT Female
917M Female

Figure-4

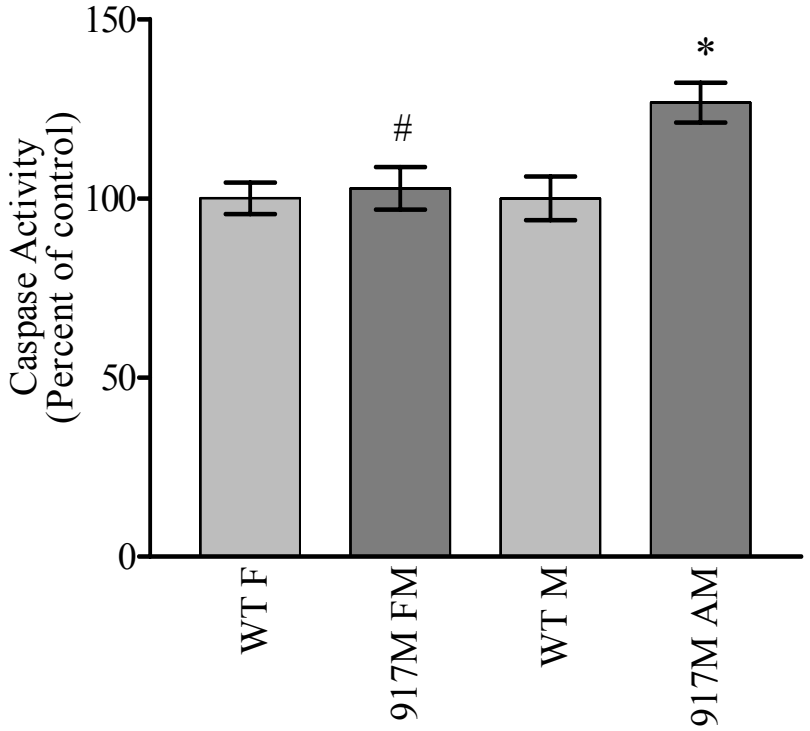
150
100
50
0
Caspase Activity
(Percent of control)
#
*
WT F
917M FM
WT M
917M AM

Figure-5

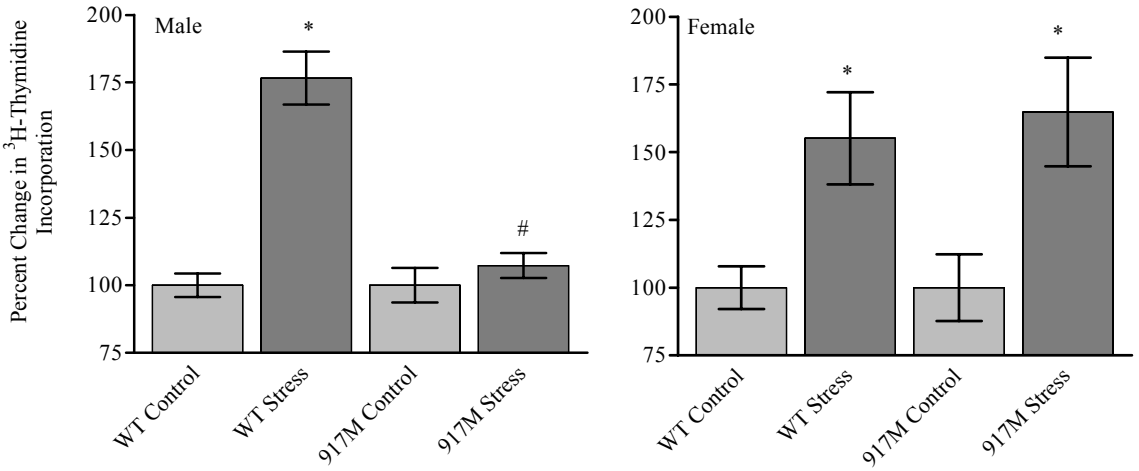
Percent Change in ^{3}H-Thymidine Incorporation
Male
Female
200
175
150
125
100
75
*
#
WT Control
WT Stress
917M Control
917M Stress

Figure-6

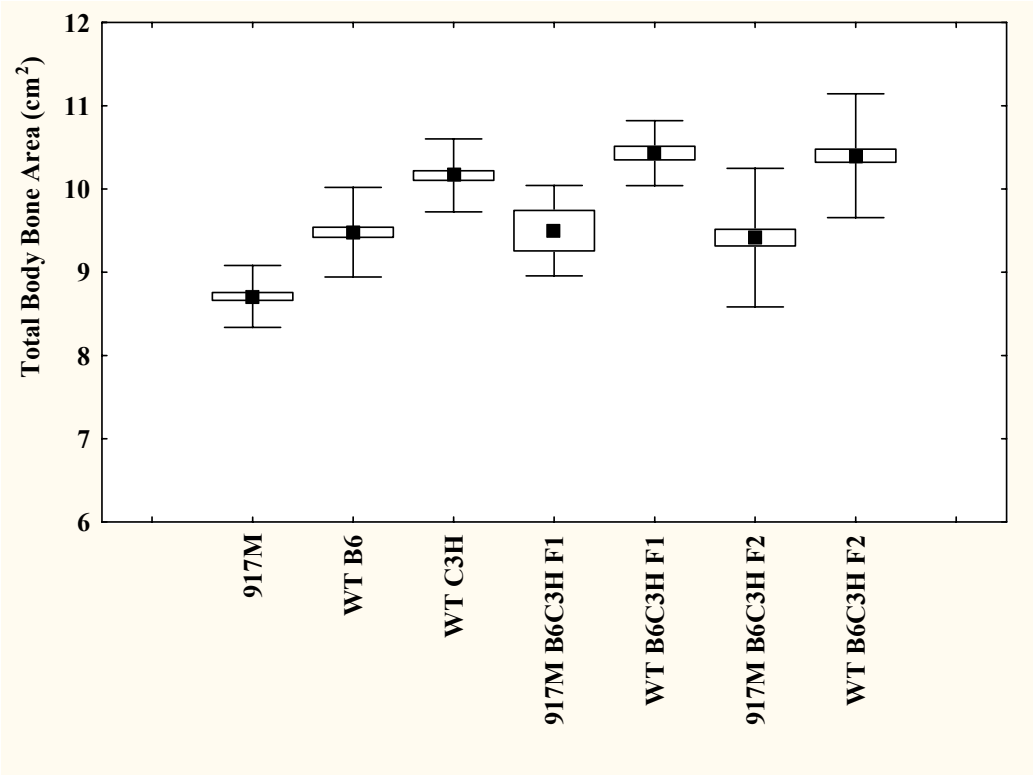
Total Body Bone Area (cm2)
12
11
10
9
8
7
6
917M
WT B6
WT C3H
917M B6C3H F1
WT B6C3H F1
917M B6C3H F2
WT B6C3H F2

Figure-7

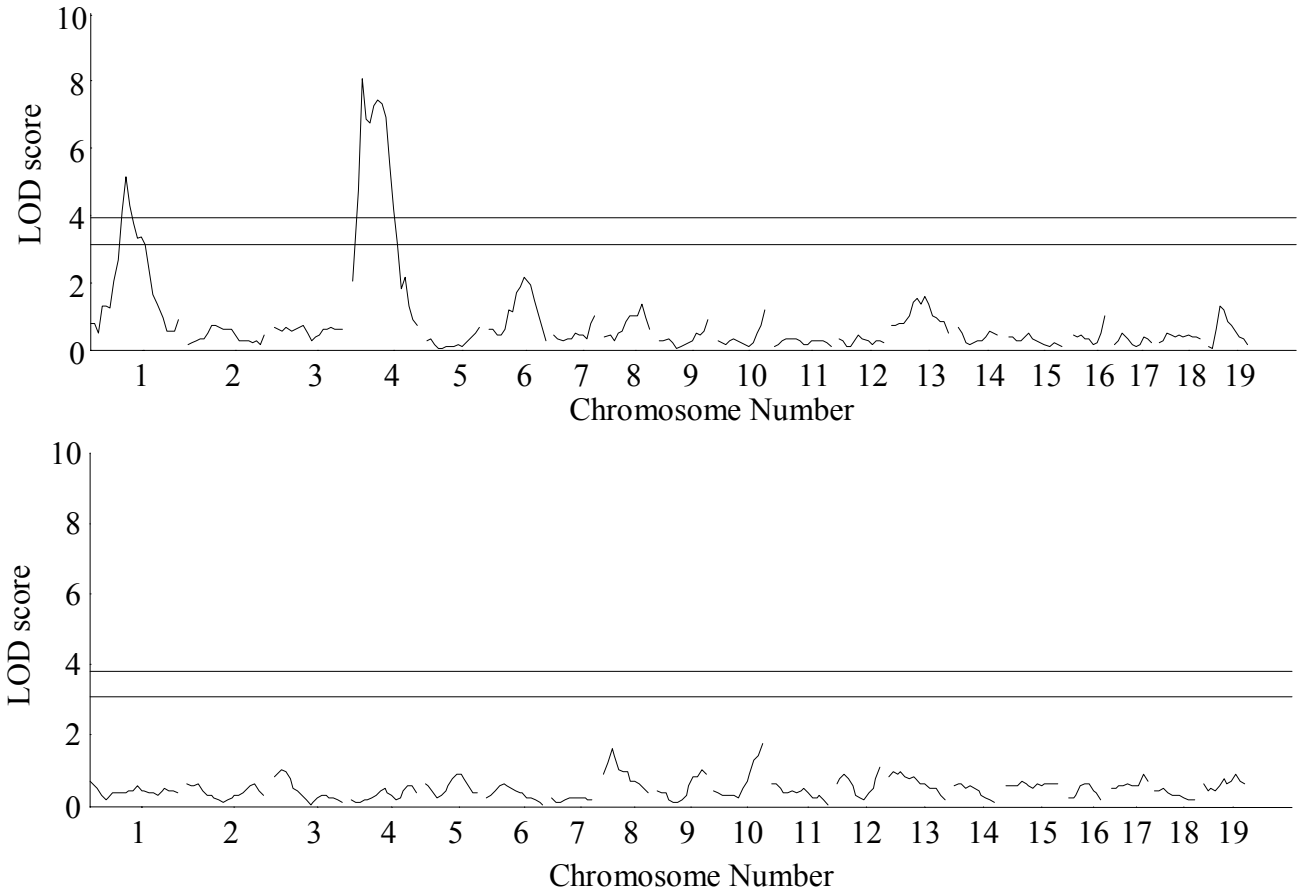
LOD score
10
8
6
4
2
0
1 2 3 4 5 6 7 8 9 10 11 12 13 14 15 16 17 18 19
Chromosome Number
LOD score
10
8
6
4
2
0
1 2 3 4 5 6 7 8 9 10 11 12 13 14 15 16 17 18 19
Chromosome Number

Figure-8.

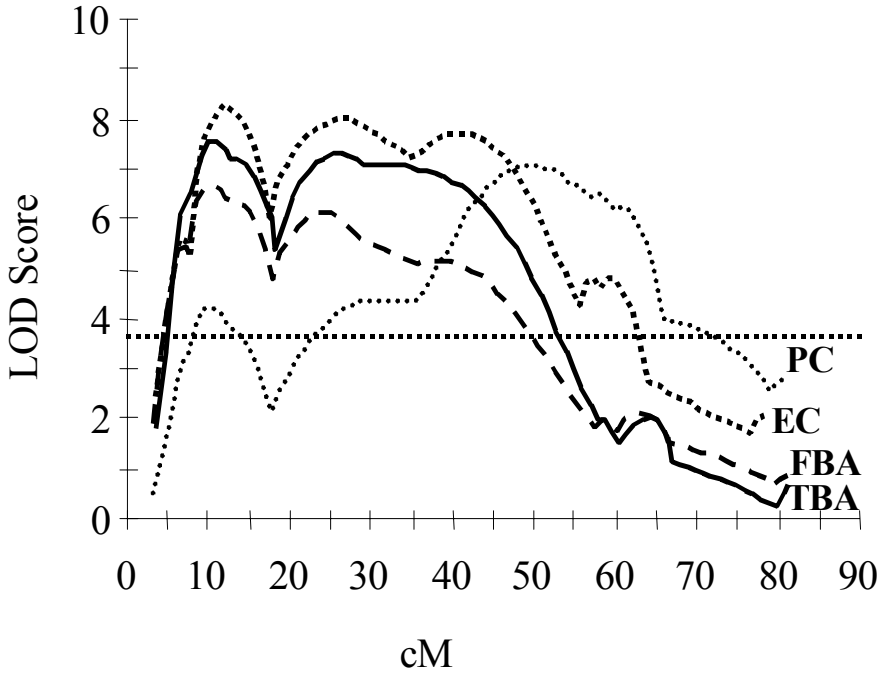

Figure-9

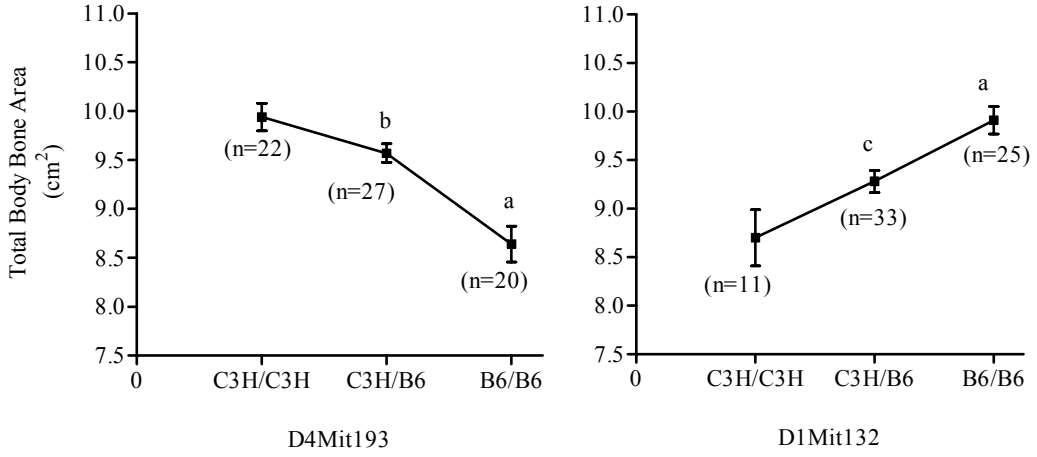
Total Body Bone Area (cm2)
11.0
10.5
10.0
9.5
9.0
8.5
8.0
7.5
0
C3H/C3H
C3H/B6
B6/B6
(n=22)
b
(n=27)
a
(n=20)
D4Mit193
(n=11)
c
(n=33)
a
(n=25)
D1Mit132

Figure-10.

Figure Legends

Figure-1: Z-scores calculated for total body bone area measured by DEXA in 16-week old progeny from 917M mice. The average Z-score of all affected 917M male mice was –3.45 and that of non-affected male and female littermates were, -0.69 and –0.55, respectively. (Z-scores indicates differences in total body bone area in terms of SD units from control mice, n=60). 917M AM= 917M affected male, 917M UM=917M Unaffected male littermates, 917M FM= 917M Female littermates, WT=Wild type.

Figure-2: Frequency histogram of total bone area (measured by DEXA) phenotype measured in 16-week old 917M affected mice (917M AM n=52), 917M un-affected littermates (917M UM, n=72), 917M female littermates (917M FM, n=122) and wild type B6 males (WT B6, n=59). The mean total bone area of the affected 917M AM progeny (8.80 cm^2) was 11.7% lower ($p<0.0001$) as compared to 917M UM (9.96 cm^2) and 13.4% lower compared to WT mice (10.16 cm^2). Female littermates showed normal distribution and were largely unaffected by the mutation.

Figure-3: Ex-vivo bone area measured by pQCT in tibia (left panel) and femur (right panel) of 16-week old 917M male mice. Nine slices covering entire length of the bone (slices 1 & 9 were excluded due to large variation) were scanned. Bone areas of affected 917M male mice (solid circles) were consistently lower over the entire length of tibia and femur as shown with age and sex matched type WT mice (open circles). *$p<0.05$ *vs* WT.

Figure-4: Basal proliferation rate of periosteal osteoblasts isolated from femur and tibia of 10-week-old B6 wild type and 917M male (n=3) and female mice (n=3). Equal number of cells was seeded at a density of 2000 cells/well in a 96 well plate and grown in presence of 10%FCS for 48 hours. The differences between groups were analyzed by 2-way ANOVA (overall $p<0.0001$). *$p<0.05$ for interaction between differences in proliferation and gender. #$p>0.05$.

Figure-5: Caspase activity in periosteal osteoblasts isolated from 917M male and wild type mice were grown under serum-depleted conditions for 48 hours. WT F=wild type females, 917M FM=female littermates of 917M, WT M=wild type male mice, 917M AM=Affected 917M male mice. *$p<0.05$ for interaction between differences in proliferation and gender calculated by 2-way ANOVA. #$p>0.05$.

Figure-6: Reduced mechanosensitivity of osteoblasts isolated from 917M mice measured by [^{3}H]-thymidine incorporation in periosteal osteoblasts from normal and 917M male and female mice subjected to 30-minute steady fluid flow shear strain. The 2-way ANOVA shows that in control mice, sex has no significant differences in response to stress (p-value 0.3345), whereas in 917M littermates, the affected 917M mice has significantly reduced response to shear stress (p-value <0.0001 for interaction). *$p<0.001$ vs. control, #$p>0.05$ vs. control.

Figure-7: Total body bone area of 10-week old 917M (n=62), wild type (WT) B6 males (n=58), WT C3H males (n=82), 917M B6C3H F1 male hybrids (n=5), WT B6C3H F1

male hybrids (n=16), WT B6C3HF2 male hybrids (n=69), and 917M B6C3H male F2 mice (n=92). The box represents Mean±SEM and error bars represent SD. Bone area in 917M, 917M B6C3H F1 hybrids and 917M B6C3H F2 males were significantly ($p<0.05$ by ANOVA) lower than the WTB6, WT B6C3H F1 and WT B6C3H F2 hybrids.

Figure-8. Genome wide main QTL(s) associated with total body bone area (DXA) in 10-week old intercrossed B6C3H F2 males (n=69) generated from 917M mice. The bottom plot shows QTLs associated with total body bone area in wild type C3HB6 F2 males (n=92). The horizontal lines indicate genome-wide error levels of $p<0.01$ and $p<0.05$. Chromosome 4 harbors a locus that significantly affects total bone size in F2 male mice generated from 917M; the bottom plot shows that this locus was absent in F2 males from WT mice.

Figure-9. LOD scores of multiple bone size phenotypes for chromosome 4. Dashed horizontal line indicates significance threshold level used at $p<0.05$ for genome wide significance. PC- Periosteal circumference (pQCT), EC-Endosteal circumference (pQCT), FBA-Femur bone area (DXA), TBA-Total bone area (DXA).

Figure-10. The main effects of genetic alleles on the mean total body bone area for markers D4Mit193 (LOD score 6.74) and D1Mit132 (LOD score 3.4). Allele of the Chr 4 interval that was inherited from the B6 parental strain (917M mutant strain) contribute to a significantly lower bone area than do alleles inherited from C3H. Data are presented as mean±SEM and number of animals for each group is indicated in

parentheses. a=p<0.001 *vs* C3H/C3H, b=p<0.01 *vs* B6/B6 and p>0.05 vs C3H/C3H, and c=p<0.05 *vs* C3H/C3H and B6/B6 by ANOVA.